Dissertation

submitted to the
Combined Faculties for the Natural Sciences and for Mathematics
of the Ruperto-Carola University of Heidelberg, Germany
for the degree of
Doctor of Natural Sciences

presented by
Diplom-Physicist: Christian Mühlinghaus
born in: Mannheim, Germany
Oral examination: 02.07.2008

The principles of growth and isotopic fractionation of stalagmites - A numerical model to reconstruct temperature and precipitation records from stalagmites grown under disequilibrium conditions

Referees:
Prof. Dr. Augusto Mangini
Prof. Dr. Werner Aeschbach-Hertig

Abstract

Speleothems and stalagmites in particular are frequently used as archives of paleoclimate. Their growth, isotopic carbon and oxygen profiles and the possibility of an exact dating provide time series in a high temporal resolution. However, the interpretation of these profiles is difficult since the isotopic signal in stalagmites underlies several influences outside and inside the cave.
In this study the basic principles of stalagmite growth and isotopic enrichment under equilibrium and disequilibrium conditions in dependence on climate related parameters are described quantitatively using numerical models. In a final step these basics are used to develop a combined model, which enables the reconstruction of temperature and drip interval records from isotopic profiles of kinetically grown stalagmites. In contrast to former models, which have been limited in their application to samples developed under equilibrium conditions, this model is able to cope with kinetically grown samples and hence extends the number of stalagmites, which might be investigated. Furthermore the model exceeds the results of former models by yielding drip intervals in addition to temperature records. The model is applied to two stalagmites from Southern Chile and reveals first temperature and drip interval records obtained by stalagmites from extremely low latitudes.
The study was carried out in the framework of the daphne Forschergruppe in Heidelberg.

Speläotheme, und speziell Stalagmiten, werden aufgrund ihrer genauen Datierbarkeit sowie der hochaufgelösten Kohlen- und Sauerstoff Isotopenprofile häufig als Archive des Paläoklimas genutzt. Die Interpretation dieser Profile ist jedoch schwierig, da das Signal diversen Einflüssen sowohl außerhalb als auch innerhalb der Höhle unterliegt.
In dieser Arbeit werden die Grundlagen des Stalagmitenwachstums sowie der isotopischen Anreicherung unter Gleichgewichts- und Ungleichgewichtsbedingungen in Abhängigkeit von klimarelevanten Parametern mit Hilfe numerischer Modelle beschrieben. Basierend darauf wird ein kombiniertes Modell entwickelt, welches die Rekonstruktion von Temperatur und Tropfabständen anhand kinetisch gebildeten Stalagmiten ermöglicht. Im Gegensatz zu früheren Modellen, welche auf die Verwendung von unter Gleichgewichtsbedingungen entstandenen Proben beschränkt waren, ermöglicht dieses Modell auch die Interpretation kinetisch gebildeter Stalagmiten. Neben einer Temperaturbestimmmung ist so zusätzlich die Bestimmung des Tropfabstands möglich. Das Modell wurde auf zwei Stalagmiten aus Süd-Chile angewendet und liefert die ersten Temperatur- und Tropfabstands-Zeitreihen aus Stalagmiten extrem südlicher Breiten.
Diese Arbeit wurde im Rahmen der daphne Forschergruppe in Heidelberg durchgeführt.

Contents

Chapter 1

Introduction

1.1 Motivation and intention

Climate. An issue which nowadays is more present than ever. But do we understand climate, its mechanisms and the driving forces behind? An idea of the answer of this question might be found in the past, which reveals information on climate in order to understand what is happening now and in the future. Two important climate parameters are temperature and precipitation, which are essential for life and culture. To investigate these two parameters archives are needed, which are able to preserve climate information of the past over a long period and last long enough to be used by scientists today. The Earth offers many possibilities like ice cores, tree rings, pollen records, sediments or speleothems. All these archives have their advantages and disadvantages regarding the global distribution, climate information storage, easy access and transport of samples, precise dating techniques or the understanding of the mechanisms occurring in these archives and according to their interaction with climate.

In this work the focus lies on speleothems and stalagmites in particular. These archives are found in many caves all over the world providing a good coverage of the Earth's land masses. Stalagmites grow very slowly with growth rates ranging around 80 μm per year and are able to outlast periods of several thousand years due to their protected location, which is not exposed to environmental stresses like erosion for instance. A stalagmite is fed by drip water, from which calcite is precipitated in annual layers comparable to tree rings. This calcite saves information in form of carbon and oxygen isotope proxies and trace elements like uranium, magnesium and others. The long lasting growth and storage of climate related proxies predestine stalagmites as an archive for climate.

The most important data sets, which can be obtained from stalagmites are information on the growth rate and the isotopic profiles of rare carbon and oxygen isotopes contained in the precipitated calcite. Profiles of the isotopes can be found both along the vertical growth axis of the stalagmite and along individual growth layers.

In general stalagmites can develop under two kind of conditions: (i) the development under equilibrium conditions and (ii) the development under disequilibrium conditions. Thereby the terms "equilibrium" and "disequilibrium" refer to the condition prevailing during the fractionation and precipitation of calcite. In the early years of stalagmite research mainly samples which developed under equilibrium conditions were used for analysis and interpretation, since the extraction of temperature records from the oxygen isotope profile is based on the well known temperature dependence of fractionation under equilibrium. However, these samples do not provide any information about rainfall. By contrast stalagmites, which show fractionation under disequilibrium contain both, the information about temperature and about precipitation. Thus, these samples came into focus of research during the last years. However, the extraction of temperature and precipitation from these stalagmites is complicated and can not be performed in the same manner as for stalagmites growing under equilibrium condi-

tions.

The intention of this work is to describe the mechanisms of stalagmite growth and isotopic fractionation occurring under disequilibrium conditions in a theoretical way in order to understand the underlying processes. In addition analytical and numerical models are developed to mimic these natural processes in stalagmites and in reverse to extract information about the past climate in form of a temperature and rainfall record from the provided data sets of a stalagmite.

All calculations and models of this work are written and compiled using the program MATLAB®.

1.2 Stalagmite development

The development of speleothems can be described best by tracking a water droplet on its way from the atmosphere down through the soil and the underlying bedrock. This development is bound to specific conditions of the surrounding environment, which will be explained in the following section and Fig 1.2.1.

A drop of a bulk of rainwater is equilibrated with the surrounding atmosphere with respect to CO_2 and has therefore a typical CO_2 partial pressure of approximately $p^{atm}_{CO_2}$ = 380ppm (McDermott, 2004). When the drop hits the ground it percolates down through a soil layer, which can vary in thickness and CO_2 partial pressure depending on erosion and vegetation processes. The drop enters this soil zone and starts to equilibrate with the surrounding CO_2, which is in general much higher than the CO_2 partial pressure of the atmosphere. Depending on the type of vegetation and its activity this pressure has annual and long-term variations, however, a typical pressure is in the range of $p^{soil}_{CO_2}$ = 5000 – 35000ppm (McDermott, 2004). The CO_2 enriched drop enters the calcite bedrock through fissures and small cracks. Due to its high amount of CO_2 the drop starts to dissolve calcite from the surrounding limestone until the solution is saturated. Here two extreme cases can be distinguished: (i) the solution is still in contact with the atmosphere of the soil zone in form of air bubbles, for instance. In this case the additional CO_2 reservoir causes an increased calcite dissolution and thus a higher calcium content of the solution. (ii) In the second case the solution is completely isolated from the soil atmosphere and dissolve only as much calcite until it is saturated. Thus, the dissolved amount of calcite is much smaller than in case (i). In natural systems a combination of these two cases occurs and mixing processes make it difficult to determine the exact amount of calcite dissolved from the limestone in the solution.

However, even solutions, which are already saturated with respect to calcite can dissolve more calcite if they are mixed. This is due to the non-linear correlation between CO_2 concentration in the solution and the calcite solubility. Thus, two saturated solutions with different CO_2 partial pressures can dissolve additional calcite, if they were mixed. This process is called mixing corrosion and is illustrated in Fig. 1.2.2.

After percolating through the bedrock the drop enters the cave, drips from the ceiling and hits the cave's floor. Depending on ventilation and exchange processes the atmosphere in caves is approximately on the same p_{CO_2} level as the external atmosphere or slightly enriched, if the cave is closed and lacks ventilation. However, this value is in general much lower than the partial pressure of the soil and thus the drop, even if seasonal variations are taken into account. The gradient of p_{CO_2} between the drop and the cave air causes an conversion of bicarbonate (HCO_3^-) into CO_2 within the solution. Depending on diffusion processes and thus on form and thickness of the solution layer CO_2 starts to degas from the solution and calcite ($CaCO_3$) precipitates. A stalagmite is formed.

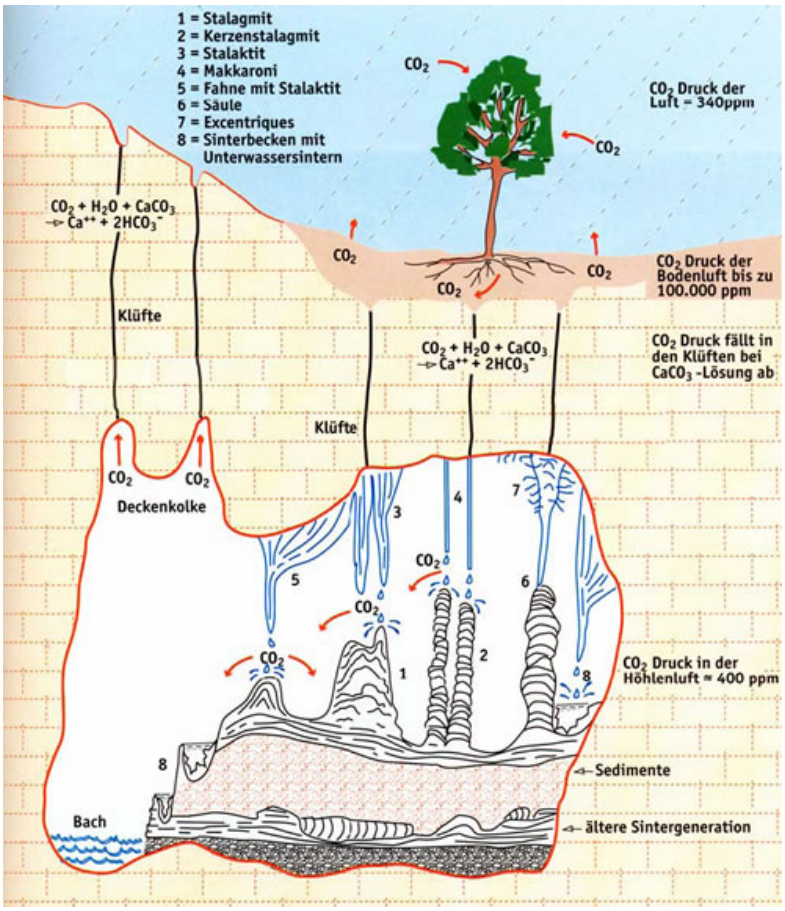

Figure 1.2.1: *From Kempe (1997). Development of caves and speleothems in natural karst systems. See text for details.*

The precipitation of calcite is driven by three mechanisms (Plummer et al., 1978; Usdowski, 1982): (i) surface reactions , (ii) laminar diffusion of involved species and (iii) conversion of bicarbonate into carbon dioxide. Due to the thin solution layer diffusion processes occur fast as well as surface reactions on top of the stalagmite. In comparison the temperature dependent conversion of bicarbonate into carbon dioxide is slow and is therefore the limiting factor for the carbonate precipitation rate (Dreybrodt et al., 1996, 1997).

The chemical processes, which occur in the soil, bedrock and cave zone are summarised in the following boxes. First processes occurring in the soil zone are described, in particular reactions between the percolating water the carbon dioxide content of the surrounding soil.

Chemical processes in the H_2O – CO_2 – system

Dissolution of gaseous carbon dioxide:

$$CO_2^{gaseous} \rightleftharpoons CO_2^{liquid}. \tag{1.2.1}$$

Reaction of the dissolved carbon dioxide with water (In the following $CO_2 \triangleq CO_2^{liquid}$):

$$CO_2 + H_2O \rightleftharpoons H_2CO_3. \tag{1.2.2}$$

Fast dissociation of carbon acid into hydrogen and bicarbonate:

$$H_2CO_3 \rightleftharpoons H^+ + HCO_3^-. \tag{1.2.3}$$

Since the typical pH value of karst systems is around 7.5 a further dissociation of bicarbonate can be neglected, which would need a pH value of greater than 8.3.
Furthermore water dissociates partially according to:

$$H_2O \rightleftharpoons H^+ + OH^-. \tag{1.2.4}$$

When the solution enters the bedrock zone, calcite is dissolved. This process is described in the following box.

Chemical processes in the H_2O – CO_2 – $CaCO_3$ – system

Dissolution of calcium carbonate:

$$Ca^{2+} + CO_3^{2-} + H^+ \rightleftharpoons Ca^{2+} + HCO_3^-. \tag{1.2.5}$$

Reaction of calcium carbonate with carbon acid:

$$CaCO_3 + H_2CO_3 \rightleftharpoons Ca^{2+} + 2HCO_3^-. \tag{1.2.6}$$

Dissolution of calcium carbonate in water (double dissociation):

$$CaCO_3 + H_2O \rightleftharpoons Ca^{2+} + HCO_3^- + OH^-. \tag{1.2.7}$$

These reactions can be summarised to the following net-reaction:

$$\boldsymbol{CaCO_3 + H_2O + CO_2 \rightleftharpoons 2\left(HCO_3^-\right) + Ca^{2+}.} \tag{1.2.8}$$

From the net-reaction 1.2.8 follows that the ability of the solution to dissolve calcite is limited to the existing amount of carbon dioxide. In the reverse process of precipitation

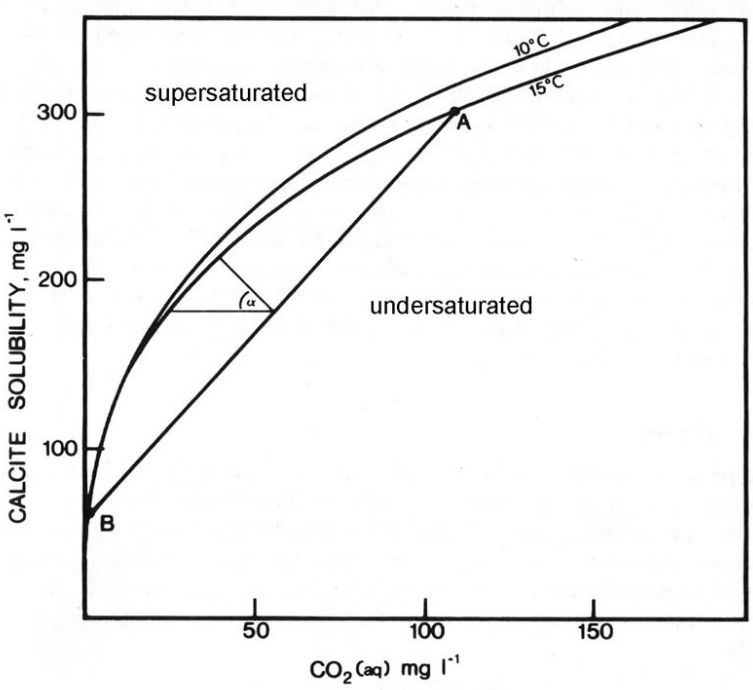

Figure 1.2.2: *Two with respect to calcite saturated solutions A and B are undersatured if they were mixed. This process is called mixing corrosion. Figure modified from Dreybrodt (1988).*

the number of calcite molecules precipitated from the solution must be equal to the number of carbon dioxide molecules released from the solution.

In general the water supply of a stalagmite is seasonal driven. During summer most of the rain penetrating the soil above the cave is removed due to evapo-transpiration processes. However, some water is stored in the deep soil or the carbonate host rock containing a high amount of organic material. With the winter rainfall this stored summer water is washed throughout the soil to the cave and calcite is precipitated on top of the stalagmite. The organic material manifests in small dark brown layers and indicates in general limited water supply. If on the other hand water supply is high the stalagmite grows faster and the precipitated calcite exhibits a whitish colour. However, local cave features or calcite crystallization processes can influence the appearance of these layers as well.

From the thickness of the precipitated calcite layers the corresponding growth rates of a stalagmite can be determined. This has been the subject of both experimental studies by analysing annual lamination patterns (Baker and Smart, 1995; Dreybrodt et al., 1996, 1997; Baker et al., 1998) and theoretical ones (Buhmann and Dreybrodt, 1985b,a). These studies show that growth rate as well as the outer shape of stalagmites depends on external parameters like cave temperature, drip interval and the CO_2 partial pressure of

the cave air and the soil zone, which in turn are related to the current climate conditions. Hence, a change of growth rates or the radius of stalagmites reflects variations of climate.

Besides growth also the isotopic composition of speleothems has been studied on stalagmites from all parts of the world (Bar-Matthews et al., 2000; Burns et al., 2001; Neff et al., 2001; Harmon et al., 1978; Spötl and Mangini, 2002). Thereby precisely dated oxygen and carbon isotope records are analysed to derive paleoclimate information. However, their interpretation is difficult, since δ^{13}C and δ^{18}O can be influenced by a variety of parameters. In general, one has to distinguish between effects occurring apart the stalagmite (e.g. outside the cave) and effects occurring on top of the stalagmite. Effects outside the cave influence the isotopic composition of the drip water and were investigated in several publications (δ^{18}O : ice volume changes, amount effect, evaporation in the vadose zone; δ^{13}C : proportions of C3 versus C4 plants, atmospheric ^{13}C variations (Goede, 1994; Desmarchelier et al., 2000; Harmon et al., 2004)), but are not the focus of this study.

1.3 Preliminary model remarks

In every model presented in this study several parameters are used. Some of them are directly related to climate, some describe the surrounding environment of the cave and others are idealized model parameters. In this section all parameters appearing in this work are described shortly in an hierarchical order regarding their dependencies.

0^{th} stage parameters

Parameters of the 0^{th} stage depend on external conditions only (e.g. climate, cave environment). This stage includes the following set of parameters:

Drip interval d The water supply of stalagmites is one of the most important factors for stalagmite growth. In general, a stalagmite is fed by drops falling from the cave's ceiling, whereas the drip interval is defined as the time between two impinging drops. Instead of the drip interval the water supply is sometimes given in drip rates, which is defined as the reciprocal value of the drip interval. Obviously the drip interval depends on the size of the drop volume V, which is assumed to be constant. Although the water feeding the stalagmite originates in general from rainfall, in most cases drip intervals might not directly be related to the amount of rainfall above the cave. Evapotranspiration, soil or aquifer processes in the bedrock cause the drip interval to reflect the amount of precipitation qualitatively but generally not quantitatively.

Temperature T Another important factor is the temperature prevailing in the cave. Therefore all temperature values used in this thesis describe the temperature of the cave air unless otherwise stated. This temperature is relatively constant during the seasons and reflects the mean annual temperature outside the cave (McDermott, 2004). In general temperature is given in centigrade degree [T_c, °C], but sometimes in Kelvin [T_k, K] as well. The conversion between these two scales is: $T_k = T_c + 273,15$. Unless otherwise stated, temperature in centigrade is used.

CO_2 partial pressures p_{CO_2} The partial pressure of carbon dioxide both of the air in the soil zone and the cave has a significant influence on stalagmite processes. In the soil zone the abundance, type and productivity of plants a well as the soil type determines the amount of CO_2 which, in turn, determines the amount of solved calcite in the solution. In the cave the CO_2 partial pressure of the air affects the degassing of CO_2 from the solution layer. In general there is a large gradient between the CO_2 partial pressures of the soil zone and the cave air resulting in a fast degassing of CO_2 from the solution layer on top of the stalagmite. However, the value of p_{CO_2} both of the soil zone and the cave air can vary during a seasonal cycle. This is due to the missing activity of the vegetation during winter month (soil zone) or ventilation processes in the cave air.

Isotopic composition of the drip water $\delta^{13}C$, $\delta^{18}O$ The isotopic composition of the precipitated calcite on top of the stalagmite depends strongly on the isotopes contained in the feeding drip water, which are determined by external, climatic parameters. The δ^{13}C value is influenced by the atmospheric amount of CO_2, the abundance, type and productivity of plants, such as a change from C3 to C4 plants and the type and thickness of the overlying soil. The oxygen isotopes δ^{18}O of the drip water depend on meteoric effects like the amount effect or the continental effect as well as changes of temperature and precipitation above the cave. All these effects occur apart the stalagmite (outside the cave or in the soil zone) and are not investigated in this study. Unless otherwise stated the isotopic composition of the drip water is set as $\delta^{13}C = -10‰$ (VDPD) and $\delta^{18}O = -10‰$ (VSMOW) respectively.

Mixing coefficient ϕ The water supply of a stalagmite has a huge impact on its growth and development. Drops falling from the cave's ceiling hit the stalagmite and establish a thin film on its top. If a new drop hits this existing solution layer mixing processes between the two solutions occur, which are described by the mixing coefficient ϕ. This coefficient depends on the height of fall of the drop and the surface texture of the stalagmite's top. A drop falling a long distance has a high potential and so finally kinetic energy, which might results in a rather splashing mixing process in comparison to drops falling only short distances. However, the influence of the height of fall and the surface texture on top of the stalagmite on the mixing process are not investigated in this work. In general the mixing coefficient must be seen as a pure model parameter, however, the explanation described above is a good physical approach.

Buffer parameter b The isotopic composition of δ^{18}O in the precipitated calcite depends on the buffering effect of the huge water reservoir of the solution layer. Due to hydration and hydroxylation reactions the oxygen isotopes in bicarbonate might change significantly. The influence of these reactions is described by the buffer parameter b. A system which is completely buffered by the exchange reactions is equivalent to calcite precipitation under equilibrium conditions. If by contrast buffer processes are neglected the enrichment of δ^{18}O becomes maximal. This is the case of purely kinetic fractionation. In natural systems the buffer parameter lies somewhere in-between these values. However, b can hardly be calculated from chemical reactions. Therefore is it approximated by a linear interpolation between the two border cases of equilibrium and disequilibrium fractionation.

1st stage parameters

The next set of parameters in the hierarchical order are variables which depend on parameters of the 0th stage only. Dependencies are listed in the brackets after the corresponding symbol.

Equilibrated calcium concentration $[Ca^{2+}_{eq}](p_{CO_2}, T)$ The calcium concentration of a solution in equilibrium with the surrounding atmosphere is determined by the partial pressure of CO_2 and the temperature. There are two important regions, where the solution can equilibrate with the surrounding air: (i) the soil zone and (ii) the cave zone. Due to the higher p_{CO_2} of the soil zone the calcium concentration of the drip water $[Ca^{2+}]_{soil}$ is in general much higher than the concentration of the solution in equilibrium with the cave air $[Ca^{2+}]_{cave}$. Due to an inhibiting effect during the precipitation of calcite from the solution in the cave the calcium concentration in equilibrium with the cave air needs to be multiplied by a factor $\frac{1}{\sqrt{0.8}}$ (Dreybrodt, 1999; Kaufmann, 2003). This concentration is called the apparent concentration $[Ca^{2+}]_{app}$. The difference between $[Ca^{2+}]_{soil}$ and $[Ca^{2+}]_{app}$ determines the calcium excess concentration $[Ca^{2+}]_{ex}$.

Kinetic constant $\alpha(T, \delta)$ The kinetic constant describes the relationship between the deposition rate of calcite and the calcium excess concentration in the solution in a specific range. In this range the correlation between the deposition rate and the calcium excess can be approximated linearly, whereas α is the slope of this fit. However, α is not a constant, but depends on temperature and the thickness of the solution layer δ on top of the stalagmite (Baker et al., 1998; Buhmann and Dreybrodt, 1985b).

Fractionation factors $\alpha_i(T)$ There are several fractionation factors used during the calculation of δ^{13}C and δ^{18}O . For carbon the most important species are bicarbonate, carbon dioxide and calcium carbonate, whereas for oxygen water plays a major role. The temperature dependent fractionation factors between these species are:

Carbon

$\epsilon^{13}_{HCO_3^- \rightarrow CaCO_3}$ ($HCO_3^- \rightarrow CaCO_3$)

$\epsilon^{13}_{HCO_3^- \rightarrow CO_2}$ ($HCO_3^- \rightarrow CO_2$)

Oxygen

$\epsilon^{18}_{HCO_3^- \rightarrow CO_2}$ ($HCO_3^- \rightarrow CO_2$)

$\epsilon^{18}_{HCO_3^- \rightarrow CaCO_3}$ ($HCO_3^- \rightarrow CaCO_3$)

$\epsilon^{18}_{HCO_3^- \rightarrow H_2O}$ ($HCO_3^- \rightarrow H_2O$)

$\epsilon^{18}_{H_2O \rightarrow CaCO_3}$ ($H_2O \rightarrow CaCO_3$)

Constant parameters

Some parameters used in the models are kept constant due to their small variability or to simplify and accelerate calculations.

Drop volume V The volume of a drop hitting a stalagmite depends on the type and texture of the cave's ceiling. A drop detaching from a stalactite might have a smaller drop volume than drops released from a rather plain ceiling due to adhesion forces. To simplify this problem a fixed drop volume of $V = 10^{-7}m^3 = 0,1ml$ is assumed as suggested by Dreybrodt (1988).

Solution layer thickness δ Impinging drops establish a thin solution film on top of the stalagmite. The thickness of this film decreases with increasing distance from the stalagmite's centre due to gravitational effects. It also determines the influence of CO_2 mass transport processes occurring in the solution and thus the degassing rate of CO_2. Dreybrodt (1988) measured the thickness of this layer and suggested a fixed layer thickness of $\delta = 0,1mm$ to simplify further calculations.

Humidity of the cave air The humidity of the cave air is the driving force for the evaporation of water from the solution layer on top of the stalagmite. Thus, a low humidity would cause a high evaporation of preferably light H_2O^{16} molecules from the water film resulting in an isotopic enrichment of the heavier oxygen isotopes ^{18}O in the solution layer. However, most of the caves show a very high humidity of up to 99 % (McDermott, 2004). This allows to neglect evaporation effects in the cave environment of many caves.

0^{th} stage parameters			
Parameter	Symbol	Unit	Range
Drip interval	d	[s]	0 – 3600
Cave temperature	T	[°C]	0 – 20
Soil partial CO_2 pressure	p_{CO_2}	[ppm]	0 – 40000
Isotopic value of the drip water	$\delta^{13}C_{drop}$	[‰]	-20 – -10
Isotopic value of the drip water	$\delta^{18}O_{drop}$	[‰]	-15 – -5
Mixing coefficient	ϕ	-	0 – 1
Buffer parameter	b	-	0 – 1

1^{st} stage parameters			
Parameter	Symbol	Unit	Range
Calcium concentration	$[Ca^{2+}]_{eq}$	[mmol/l]	0 – 3,5
Kinetic constant	α	[m/s]	$(4 – 30)\times10^{-8}$
Fractionation factors	α_i	-	around 1

Constant parameters			
Parameter	Symbol	Unit	Range
Drop volume	V	[m^3]	10^{-7}
Layer thickness	δ	[m]	10^{-4}
Cave humidity	-	[%]	≈ 100

Table 1.3.1: *Ranges of the parameters used in the models.*

1.4 Model types

To investigate the dependencies of growth and isotopic fractionation processes in stalagmites analytical and numerical models have been developed. Generally two types of models can be distinguished: (i) Forward models, which calculate *climate proxies* (such as growth, shape or isotopic compositions) from given *climatic boundary conditions* (such as drip interval, temperature, p_{CO_2}). And (ii) models, which reverse the forward models to calculate *climatic boundary conditions* from *climate proxies* (reverse models).
This section gives a short overview of the models introduced in this work and their purpose in form of a short description including the input and output parameters.

Note, that all models dealing with isotopes are developed on the assumption of disequilibrium fractionation processes during the precipitation of calcite. However, processes occurring under equilibrium conditions can be obtained as a border case of disequilibrium processes. This will be shown later on.

1.4.1 Forward models

The forward models calculate climate proxies from given climatic boundary conditions. The notation is: **Model name** Input parameters → Output parameters.

Growth models

Exponential ansatz $d, T, \phi, p_{CO_2}^{soil/cave} \rightarrow$ Growth and shape
This model was developed by Dreybrodt (1988) and extended by Mühlinghaus et al. (2007). For given boundary conditions the growth along the growth axis of a stalagmite and the resulting shape can be calculated. However, the temporal development of the solution on top of the stalagmite is not included. Growth is assumed to decrease exponentially with increasing distance from the growth axis.

Gaussian ansatz $d, T, \phi, p_{CO_2}^{soil/cave} \rightarrow$ Growth and shape
This growth model was recently published by Romanov et al. (2008) and describes the temporal movement of the solution on top of the stalagmite. The iteratively calculated growth is approximated by a Gaussian function.

Multi-box-model In comparison to the growth model by Dreybrodt (1988) this multi-box-model is able to calculate the so far missing time-place link of the solution and is therefore suitable for both growth and isotopic composition calculations.

Growth $d, T, \phi, p_{CO_2}^{soil/cave} \rightarrow$ Growth and shape
Growth is calculated in each box and thus the resulting shape can be determined.

Isotopes along growth axis $d, T, \phi, p_{CO_2}^{soil/cave} \rightarrow \delta^{13}C$, $\delta^{18}O$
The isotopic composition of carbon and oxygen in the precipitated calcite is calculated along the growth axis of a stalagmite.

Isotopes along growth layer $d, T, \phi, p_{CO_2}^{soil/cave} \rightarrow \delta^{13}\mathrm{C}$, $\delta^{18}\mathrm{O}$
The isotopic composition of carbon and oxygen in the precipitated calcite is calculated along an individual growth layers of a stalagmite.

1.4.2 Reverse models

The reverse models are based on the inversion of the forward models and calculate climatic boundary conditions from given climate proxies and can be seen as the inversion of the forward models. Note, that all reverse models (except CSM) yield no clear result, if they are used individually.

AGE model Growth along growth axis $\rightarrow d, T, \phi, p_{CO_2}^{soil/cave}$
The reverse model of the growth model calculates one climatic parameter in dependence on all others using the growth rate calculated from the age-depth relation.

AXIS model

δ^{13}**C** $\delta^{13}\mathrm{C}$ along the growth axis $\rightarrow d, T, \phi, p_{CO_2}^{soil/cave}$
Based on the calculation of the innermost box of the isotope multi-box-model this model extracts one climatic parameter in dependence on all others.

δ^{18}**O** $\delta^{18}\mathrm{O}$ along the growth axis $\rightarrow d, T, \phi, b, p_{CO_2}^{soil/cave}$
Based on the calculation of the innermost box of the isotope multi-box-model this model extracts one climatic parameter in dependence on all others.

LAYER model

δ^{13}**C** $\delta^{13}\mathrm{C}$ along an individual growth layer $\rightarrow d, T, \phi, p_{CO_2}^{soil/cave}$
The reverse model of the isotope multi-box-model uses the isotopic enrichment to determine one parameter in dependence on all others.

δ^{18}**O** $\delta^{18}\mathrm{O}$ along an individual growth layer $\rightarrow d, T, \phi, b, p_{CO_2}^{soil/cave}$
The reverse model of the isotope multi-box-model uses the isotopic enrichment to determine one parameter in dependence on all others.

BUFFER model $\delta^{13}\mathrm{C}$ and $\delta^{18}\mathrm{O}$ along an individual growth layer $\rightarrow b$
This model uses Hendy-Test data sets to calculate the buffering effect of the water reservoir on bicarbonate in the solution on top of the stalagmite in a simplified way.

Combined stalagmite model/CSM Growth and isotopic profiles, $\delta^{13}C_{drop}$, $T^* \rightarrow T$, d, p_{CO_2}, $\delta^{18}O_{drop}$, ϕ
This model combines all reverse models in order to reconstruct temperature and drip interval records from kinetically grown stalagmites. It uses the age-depth relation, isotopic profiles and needs an estimation of the mean value of the isotopic

carbon composition of the drip water. To connect the floating temperature record, a temperature T^* at any time during the growth period has to be estimated. In addition to the obtained temporal records of temperature and drip interval, averaged values of the partial pressure of the soil, of the oxygen composition of the drip water and of the mixing coefficient are obtained.

Chapter 2

Basics

2.1 Species in the system

In the system of dissolved inorganic carbon (DIC) the concentration of bicarbonate dominates at a pH value of pH = 8, which is typical for karst systems (Mook and de Vriess, 2000). Within a temperature range of 1 to 20 °C bicarbonate amounts approximately 95 % of the DIC (see Fig. 2.1.1). In this case the concentration of the dissolved inorganic carbon is well approximated by the concentration of bicarbonate.

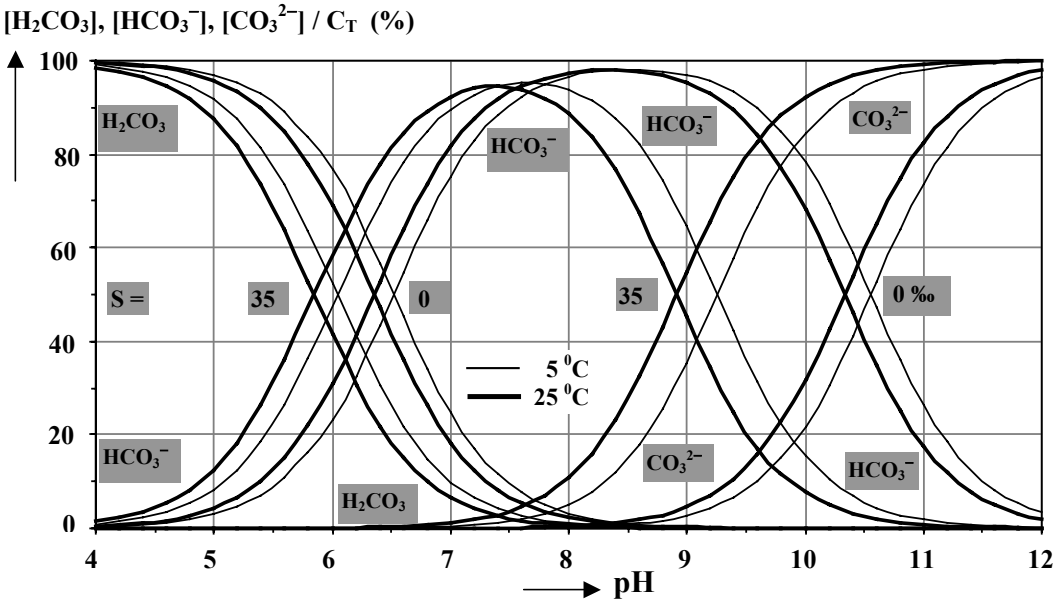

Figure 2.1.1: *The composition of dissolved inorganic carbon. Captured from Mook and de Vriess (2000)*

Based on the reactions occurring in the H_2O – CO_2 – $CaCO_3$ – system (see section 1.2) the concentrations of the involved species and their dependence on temperature and p_{CO_2} of the solution can be calculated. According to Dreybrodt (1988); Buhmann and Dreybrodt (1985b,a) and Kaufmann (2003) the concentration of the species in a solution, which is in equilibrium with the surrounding temperature and CO_2 partial pressure can be determined to:

$$[Ca^{2+}]_{eq} = \sqrt[3]{\frac{K_1\ K_C\ K_H}{4\ K_2\ \gamma_{Ca^{2+}}\ \gamma^2_{HCO_3^{2+}}}\ p_{CO_2}} \tag{2.1.1}$$

$$[HCO_3^-] = \frac{K_H\ K_1}{\gamma_H\ \gamma_{HCO_3}\ [H^+]}\ p_{CO_2} \tag{2.1.2}$$

$$[H^+] = \sqrt[3]{\frac{K_1^2\ K_2\ K_H^2\ \gamma_{Ca}}{2\ K_C\ \gamma_H \gamma_{HCO_3}}\ (p_{CO_2})^2} \tag{2.1.3}$$

$$[OH^-] = \frac{K_W}{\gamma_{OH^-}\ \gamma_H\ [H^+]}. \tag{2.1.4}$$

Concentrations are marked by squared brackets. The mass action constants K_i used for the reactions occurring in this system and the calculation of these concentrations are given according to Dreybrodt (1988); Buhmann and Dreybrodt (1985b,a):

$$K_0 = \frac{K_5}{K_6} \tag{2.1.5}$$

$$K_1 = 10^{-356.3094 - 0.06091964\ T_k + \frac{21834.37}{T_k} + 126.8339\ \log T_k - \frac{1684915}{T_k^2}} \tag{2.1.6}$$

$$K_2 = 10^{-107.8871 - 0.03252849\ T_k + \frac{5151.79}{T_k} + 38.92561\ \log T_k - \frac{563713.9}{T_k^2}} \tag{2.1.7}$$

$$K_5 = 1.707 \times 10^{-4} \tag{2.1.8}$$

$$K_6 = 10^{-356.3094 + \frac{21834.37}{T_k} - 0.060919964\ TK + 126.8339\ \log T_k - \frac{1684915}{T_k^2}} \tag{2.1.9}$$

$$K_C = 10^{-171.9065 - 0.077993\ T_k + \frac{2839.319}{T_k} + 71.595\ \log T_k} \tag{2.1.10}$$

$$K_H = 10^{108.3865 + 0.01985076\ T_k - \frac{6919.53}{T_k} - 40.45154\ \log T_k + \frac{669365}{T_k^2}} \tag{2.1.11}$$

$$K_W = 10^{22.801 - \frac{4787.3}{T_k} - 0.010365\ TK - 7.1321\ \log T_k}. \tag{2.1.12}$$

Note that temperature is given in Kelvin. The concentration of the i-th species is related to its activity (marked by rounded brackets) by the ion activity coefficient γ_i (Garrels and Christ, 1965; Dreybrodt, 1988):

$$(i) = \gamma_i [i]. \tag{2.1.13}$$

The activity coefficient is calculated using the extended Debye-Hückel equation:

$$\log \gamma_i = -A z_i^2 \frac{\sqrt{I}}{1 + B a_i \sqrt{I}} \tag{2.1.14}$$

with the constants A and B, the ionic strength I, the ionic radius a_i and the charge z_i of the corresponding species. Values for the activity coefficients are given by Dreybrodt (1988):

$$\gamma_H = 10^{\frac{-A\sqrt{I}}{1+B9\sqrt{I}}} \tag{2.1.15}$$

$$\gamma_{Ca} = 10^{\frac{-A4\sqrt{I}}{1+B5\sqrt{I}}} \tag{2.1.16}$$

$$\gamma_{HCO} = 10^{\frac{-A\sqrt{I}}{1+B5.4\sqrt{I}}} \tag{2.1.17}$$

$$\gamma_{OH} = 10^{\frac{-A\sqrt{I}}{1+B3.5\sqrt{I}}} \tag{2.1.18}$$

$$\tag{2.1.19}$$

using the temperature dependent constants A and B:

$$A = 0.48809 + 8.074 \times 10^{-4}T \tag{2.1.20}$$

$$B = 0.3241 + 1.600 \times 10^{-4}T. \tag{2.1.21}$$

The ionic strength I can sufficiently be approximated by:

$$I = 3[Ca^{2+}]_{eq}. \tag{2.1.22}$$

For uncharged species such as CO_2 the activity coefficients can be approximated by (Plummer and Mackenzie, 1974):

$$\gamma_{CO_2} = 1. \tag{2.1.23}$$

The two most important concentrations, used in the models, are the concentration of calcium and bicarbonate. Due to electro neutrality the amount of bicarbonate must be twice the amount of calcium in the solution. This can be seen in Fig. 2.1.2, which illustrates the calcium and bicarbonate concentration in dependence on temperature and CO_2 partial pressure.

The figure shows, that the concentration of both calcium and bicarbonate increase with increasing CO_2 partial pressure. This can be explained by Eq. 1.2.8, since a higher partial pressure of CO_2 drives the reaction from left to right and thus causes an increased amount of calcium and bicarbonate in the solution. With increasing temperature the concentrations decrease slightly. As expected the concentration of bicarbonate shows the same characteristics as calcium but with an increased concentration by a factor of two.

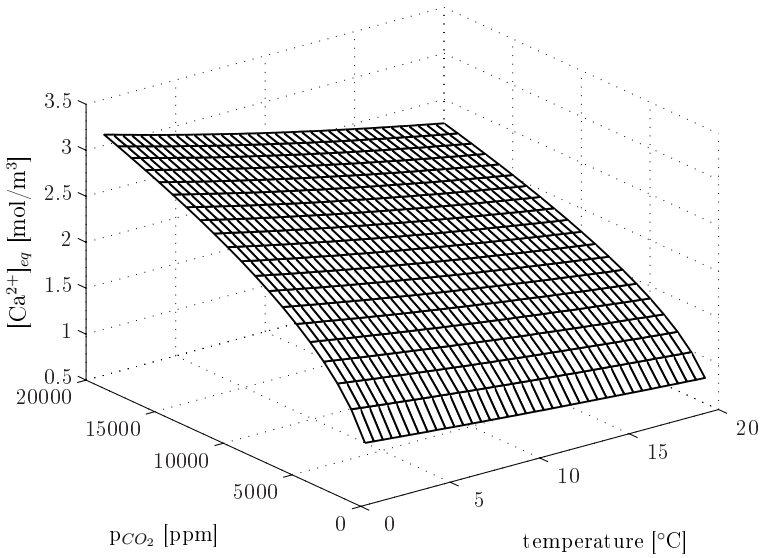

(a) *Calcium concentration of the solution*

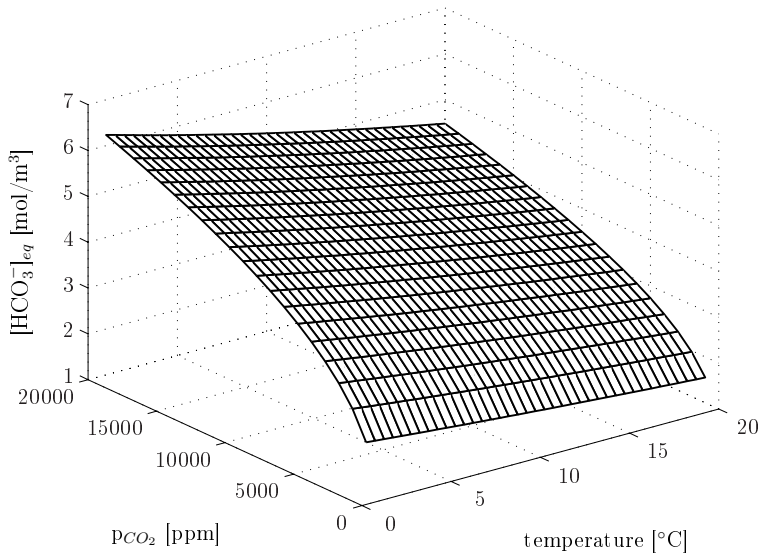

(b) *Bicarbonate concentration of the solution*

Figure 2.1.2: *Concentrations of calcium (a) and bicarbonate (b) in dependence of temperature and CO_2 partial pressure.*

2.2 The kinetics of the CO_2 – H_2O – $CaCO_3$ reaction

The precipitation of calcite is driven by the conversion of bicarbonate into carbon dioxide in the solution on top of the stalagmite. In addition also diffusion processes and surface reactions influence the process of precipitation, but proceed in comparison to the chemical conversion on much shorter time scales and can therefore be neglected in further considerations.

To calculate growth and the isotopic enrichment during calcite precipitation under disequilibrium conditions the temporal development of bicarbonate needs to be known. Due to electro neutrality the decrease of bicarbonate in the solution with time must be equal to the loss of calcium. The decrease of calcium has been determined by Buhmann and Dreybrodt (1985b,a) and follows an exponential decrease:

$$[Ca^{2+}](t) = [Ca^{2+}]e^{-\frac{\alpha t}{\delta}} \tag{2.2.1}$$

with the temperature dependent kinetic constant α and the film thickness δ. The kinetic constant is approximated according to Baker et al. (1998) by[1]:

$$\alpha(T) = 1,188 \times 10^{-11}T^3 - 1,29 \times 10^{-11}T^2 + 7,875 \times 10^{-9}T + 4,844 \times 10^{-8}. \tag{2.2.2}$$

In the following the decrease of bicarbonate is derived and compared to the results for calcium.

To calculate the time dependent decrease of bicarbonate theoretically the following chemical reaction occurring in the CO_2 – H_2O – $CaCO_3$ system must be used to start with:

$$H_2O + CO_2 \underset{k^-}{\overset{k^+}{\rightleftharpoons}} HCO_3^- + H^+. \tag{2.2.3}$$

The conversion process of this reaction depends on the pH value of the solution and is slowest in the region of pH $\approx$ 7.5, which is typical for karst water. The kinetics of reaction 2.2.1 leads to a time dependent rate equation for bicarbonate:

$$\frac{d[HCO_3^-]}{dt} = k^+ [CO_2] - k^- [HCO_3^-]. \tag{2.2.4}$$

Integrating this differential equation from t_0 to t yields for the temporal development of bicarbonate:

$$[HCO_3^-](t) = \frac{k^+ [CO_2]}{k^-} + \left([HCO_3^-](t_0) - \frac{k^+ [CO_2]}{k^-} \right) e^{-k^- (t-t_0)} \tag{2.2.5}$$

with the rate constants:

[1]The kinetic constant α was approximated by digitizing an α versus T figure (Baker et al., 1998) and a 3rd order polynomial fit.

$$k^+ = k_1^+ + k_2^+ [OH^-], \tag{2.2.6}$$

$$k^- = k_a [H^+] + k_2^- \tag{2.2.7}$$

and

$$k_a = \frac{k_1^- \gamma_H \gamma_{HCO_3^-}}{K_1(1+K_0)}, \tag{2.2.8}$$

$$k_1^- = 10^{13.558 - \frac{3617.1}{T_k}}, \tag{2.2.9}$$

$$k_1^+ = 10^{329.850 - 110.54 \log T_k - \frac{17265.4}{T_k}}, \tag{2.2.10}$$

$$k_2^- = 10^{14.09 - \frac{5308}{T_k}}, \tag{2.2.11}$$

$$k_2^+ = 10^{13.635 - \frac{2985}{T_k}}. \tag{2.2.12}$$

The exponential time constant $1/k^-$ of Eq. 2.2.5 depends strongly on the surrounding CO_2 pressure and temperature. The range of $1/k^-$ as a function of temperature is confined by two curves resulting from the extreme partial pressures of CO_2 in the soil (35000 ppm) and in the cave (400 ppm), respectively (see figure 2.2.1). For a solution that is highly supersaturated, we expect the time constant close to $1/k_{soil}^-$ ranging between 150 – 700 seconds, for temperatures between 0 to 20 °C, since most of the calcite precipitates during this early stage. This is shown by the lower curve. For a solution with less supersaturation the decay is slower, which is represented by the uppermost line in Fig. 2.2.1.

A comparison of $1/k^-$ with the exponential time constant of calcium, shows that the time constant of calcium is close to the time constant of bicarbonate for a highly supersaturated solution (dotted line in Fig. 2.2.1). This drives a fast degassing of CO_2, which favours the precipitation under disequilibrium conditions. For a temperature range between 0 and 20 °C the time constant of calcite ranges between 300 and 2000 seconds comparable to natural drip intervals[2]. In the following the exponential time constant δ/α is used to describe the decrease of bicarbonate in the solution:

$$\begin{aligned} [HCO_3^-](t) &= [HCO_3^-]_{cave} + \left([HCO_3^-]_{soil} - [HCO_3^-]_{cave}\right) e^{-\frac{\alpha t}{\delta}} \\ &= [HCO_3^-]_{cave} + [HCO_3^-]_{ex} e^{-\frac{\alpha t}{\delta}}. \end{aligned} \tag{2.2.13}$$

The indices *soil*/*cave* represent the surroundings under which the solution was equilibrated. The index *ex* indicates the excess amount of bicarbonate in the solution.

[2]Note, that the temperature dependence of the calculated time constant in Fig. 2.2.1 depends not linearly on the CO_2 partial pressure.

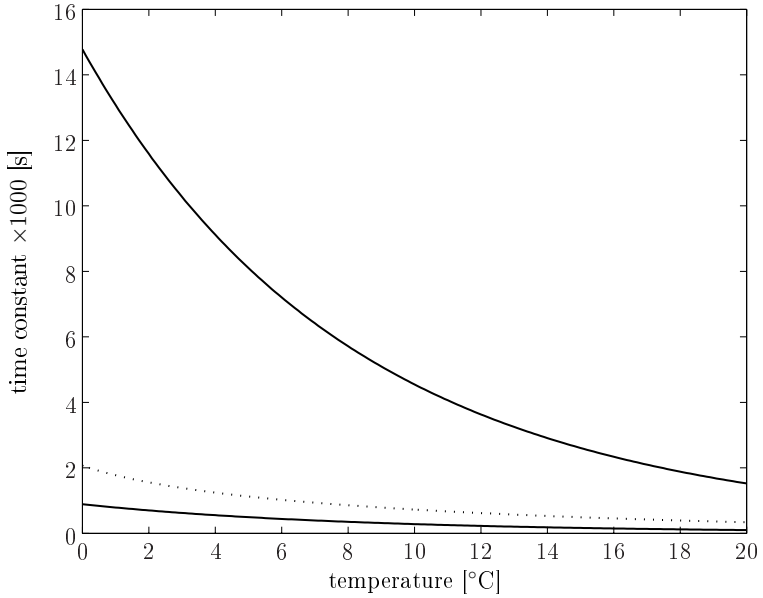

Figure 2.2.1: *Temperature dependence of the time constant describing the exponential decrease of bicarbonate. The lower curve was calculated for a typical p_{CO_2} of the soil zone of 35000 ppm. The uppermost line shows the time constant under cave conditions with a partial CO_2 pressure of 400 ppm. The approximated time constant of calcium (dotted line) is close to the lower curve due to fast degassing of CO_2*

2.3 Mixing processes

Mixing processes occur, if a drop dripping from the cave's ceiling impinges at the existing solution layer on top of the stalagmite. To describe this process in a mathematical way a mixing coefficient ϕ ($\phi \in [0;1]$) is introduced. Assuming an equal volume of two solutions A and B as well as of the mixed solution C, the mixing coefficient ϕ gives the percentage of solution B mixing with $(1-\phi)$ percent of solution A:

$$C = (1-\phi)A + \phi B. \tag{2.3.1}$$

By postulating a volume of the mixed solution C equal to the volume of the initial solutions A and B the overflow D of the mixing process is defined by

$$D = \phi A + (1-\phi)B = A + B - C. \tag{2.3.2}$$

This process is illustrated in figure 2.3.1.

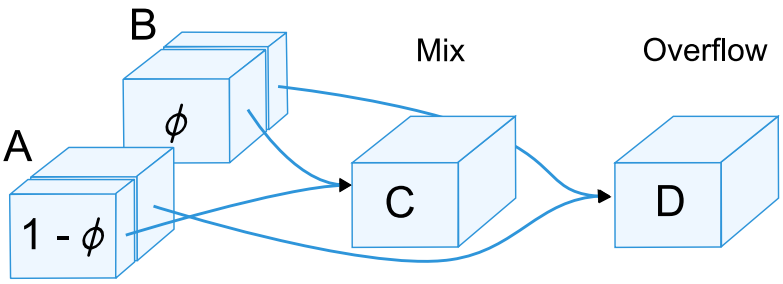

Figure 2.3.1: *Mixing process of two solutions A and B. To illustrate this process the mixed parts of the two solutions are graphically separated ($(1-\phi)A$, ϕB). Since the volume of the mixed solution C must be equal to the volume of one of the source solutions an overflow solution D must emerge.*

To apply the mixing process to the concentrations of the impinging drop and the existing solution layer, the temporal development of the involved concentrations need to be known. In the following the mixing of two bicarbonate concentrations are exemplified. According to equation 2.2.13 the temporal development of bicarbonate is:

$$[HCO_3^-](t) = [HCO_3^-]_{cave} + \left([HCO_3^-]_{soil} - [HCO_3^-]_{cave}\right) e^{-\frac{\alpha t}{\delta}} \tag{2.3.3}$$

A solution layer on top the stalagmite with an initial bicarbonate concentration of $[HCO_3^-](0)$ decreases during one drip interval to $[HCO_3^-](d)$ (Eq. 2.2.13). After one drip interval a new drop with the bicarbonate concentration of $[HCO_3^-]_{soil}$ hits the solution layer and mixes according to Eq. 2.3.1:

$$[HCO_3^-](1,0) = (1-\phi)[HCO_3^-](d) + \phi[HCO_3^-]_{soil}. \tag{2.3.4}$$

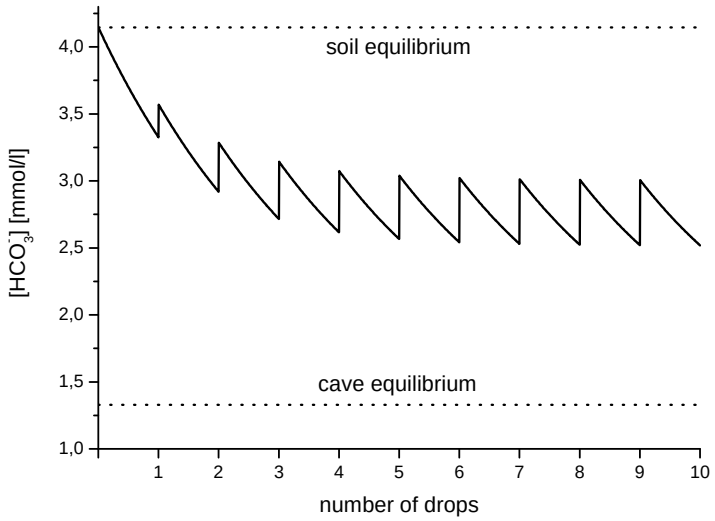

Figure 2.3.2: *Temporal development of the concentration of bicarbonate in the solution for* $d = 250s$, $T = 10°C$,$p_{CO_2} = 10000ppm$ *and* $\phi = 0,3$. *The horizontal dotted lines represent the concentrations in equilibrium with the soil and the cave air. The mixed solution already approaches an equilibrium like state after a few drops.*

The first variable of $[HCO_3^-](1,0)$ indicates the number of impinged drops (1) and the second parameter (0) the elapsed time after the mixing process. From this initial concentration of the mixed solution the concentration decreases again (see Fig. 2.3.2):

$$[HCO_3^-](1,t) = [HCO_3^-](1,0)f(t) \tag{2.3.5}$$

with

$$f(t) = e^{-\frac{\alpha t}{\delta}}. \tag{2.3.6}$$

Iterating this mixing process yields for the bicarbonate concentration after n drops[3] (Mühlinghaus et al., 2007):

$$[HCO_3^-](n,0) = [HCO_3^-]_{cave} + \lambda(n, f(d))[HCO_3^-]_{ex} \tag{2.3.7}$$

with

$$\lambda(n, f(d)) = ((1-\phi)\, f(d))^n + \phi \sum_{k=0}^{n-1} ((1-\phi)\, f(d))^k, \quad n > 0, \tag{2.3.8}$$

By using the function $f(t)$ Eq. 2.3.8 is kept in a general way. If mixing of concentrations with different kinds of decrease are investigated the corresponding decrease functions $f(t)$ must be used. In the case of calcium and bicarbonate $f(t)$ is given by Eq. 2.3.6 and the factor λ depends on the mixing coefficient, temperature, the drip interval and the

[3]See Appendix B.1 for derivation.

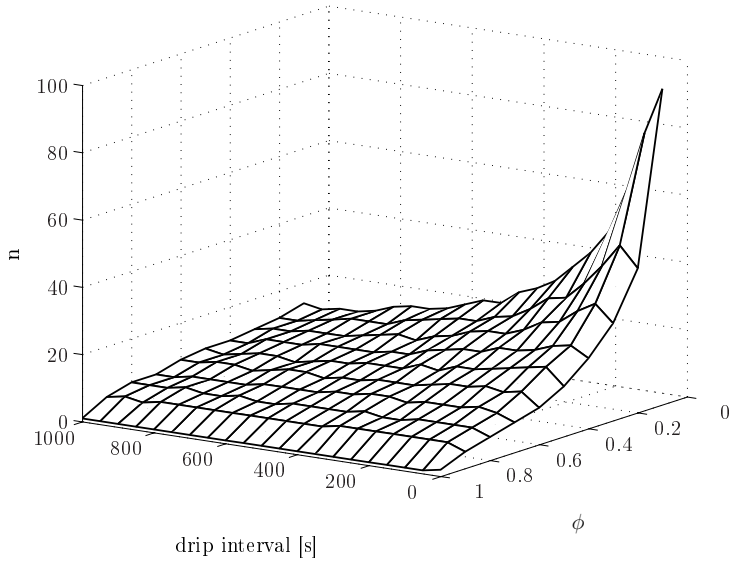

Figure 2.3.3: *Number of drops needed to establish an equilibrium of the concentration in the solution.*

number of drops n impinged at the solution layer. The factor λ reaches an equilibrium like state within the range of natural parameters after at most 100 drops. Figure 2.3.3 shows that the number of drops n, which are needed to establish a quasi equilibrium, exceeds about 40 only for low mixing coefficients paired with short drip intervals. λ itself can reach down to 0.2 for low mixing coefficients and large drip intervals.

Besides mixing of bicarbonate concentrations also the mixing of their isotope ratios need to be considered, which are needed for the calculation of isotopic profiles. Two solutions with the initial isotope ratios R_A and R_B and the corresponding δ values δ_A and δ_B mix according to:

$$\delta_{mix} = (1 - \phi)\delta_A + \phi\delta_B. \tag{2.3.9}$$

This yields for the mixed isotope ratios (see Mühlinghaus (2006)):

$$R_{mix} = (1 - \phi)R_A + \phi R_B. \tag{2.3.10}$$

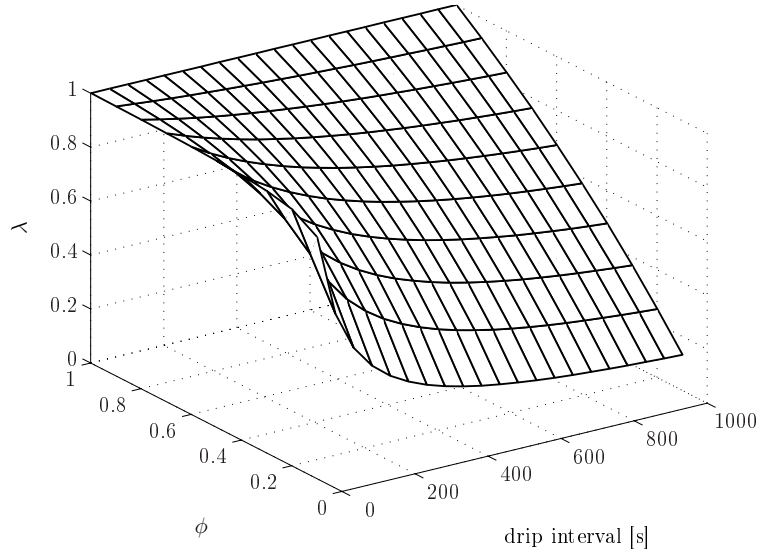

Figure 2.3.4: *λ factor describing the mixing process in dependence on drip interval and mixing coefficient. If no mixing occurs (ϕ=1), λ becomes equal to 1. If only small parts of the impinging drop mix with the existing solution layer, λ can decrease down to 0,2.*

2.4 Fractionation processes

During the degassing of CO_2 and precipitation of $CaCO_3$ from the solution isotopic fractionation processes occur. To understand the dependencies of these processes on temperature, the dependence of the used fractionation factors on temperature needs to be known. In this section the basics of fractionation processes are discussed and fractionation factors from literature are listed and compared.

2.4.1 Fractionation and standards

The natural abundance of stable isotopes is given in isotope ratios R. These ratios are defined as:

$$R = \frac{\text{abundance of rare isotope}}{\text{abundance of abundant isotope}}. \tag{2.4.1}$$

In this work stable carbon and oxygen isotopes and their isotope ratios are studied:

$$\begin{aligned} R^{13} &= \frac{^{13}C}{^{12}C} \\ R^{18} &= \frac{^{18}O}{^{16}O}. \end{aligned} \tag{2.4.2}$$

For reasons of clarity this ratio is in general expressed as the deviation in permil from a standard value R_{std}:

$$\delta = \left(\frac{R_{sample}}{R_{std}} - 1 \right) \times 1000 \tag{2.4.3}$$

with the standards Vienna Peedee belemnite and Vienna Standard Mean Ocean Water (Mook and de Vriess, 2000)

$$\begin{aligned} R_{std}^{VPDB}(^{13}C) &= 0,0112372 \\ R_{std}^{VPDB}(^{18}O) &= 0,0020672 \\ R_{std}^{VSMOW}(^{18}O) &= 0,0020052. \end{aligned} \tag{2.4.4}$$

During chemical reactions or phase transitions the isotope ratios of the involved species change due to the different molecular weight of the isotopes. If transitions occur in a closed system, this process is reversible and the change of the isotope ratio from state i to j is described by the temperature dependent fractionation factor $\alpha_{i\rightarrow j}$[4]:

$$\alpha_{i\rightarrow j} = \frac{R_j}{R_i}. \tag{2.4.5}$$

[4]In literature fractionation factors from state i to state j are often denoted as α_{j-i}, $\alpha_{j/i}$ or $\alpha_i(j)$. However, for reasons of clarity an arrow-notation is used here.

To describe the transition from state i to j in a more illustrative way the change of the isotope ratio is expressed in permil (see δ-notation). If the δ values of the states i and j are given as δ_i and δ_j and ϵ is introduced as the deviation of α from 1 in permil ($\epsilon = (\alpha - 1)1000$), the change can be described as follows:

$$\begin{aligned}
\delta_{i\to j} &= \delta_j - \delta_i \\
&= \left(\frac{R_j}{R_{std}} - 1\right) 1000 - \left(\frac{R_i}{R_{std}} - 1\right) 1000 \\
&= \left(\frac{\alpha_{i\to j} R_i}{R_{std}} - 1\right) 1000 - \left(\frac{R_i}{R_{std}} - 1\right) 1000 \\
&= \frac{R_i}{R_{std}} (\alpha_{i\to j} - 1)1000 \\
&\approx (\alpha_{i\to j} - 1)1000. \\
&= \epsilon_{i\to j}.
\end{aligned} \tag{2.4.6}$$

In the last step the ratio R_i/R_{std} is neglected since the factor 1000 dominates this term. Using the Taylor series for $\ln(x)$:

$$\ln(x) = (x-1) - \frac{(x-1)^2}{2} + ... \tag{2.4.7}$$

Eq. 2.4.6 can be expressed as:

$$\begin{aligned}
\delta_{i\to j} &\approx (\alpha_{i\to j} - 1)1000 \\
&= \epsilon_{i\to j} \\
&\approx 1000 \ln(\alpha_{i\to j}).
\end{aligned} \tag{2.4.8}$$

The last expression is frequently used in literature for the fractionation factor.

2.4.2 Fractionation factors of carbon and oxygen

In the following subsection fractionation factors for carbon and oxygen between species contained in the H_2O – CO_2 – $CaCO_3$ system are listed. These factors span different temperature ranges and are either determined experimentally (exp), theoretically (theo) or result from combinations of several experimental data (sum) (see Tables 2.4.1 and 2.4.2). The characteristics of the different fractionation factors is shown in Figs. 2.4.1 and 2.4.2.

However, the measurement or calculation of individual fractionation factors is complicated and can not be performed directly in some cases. Thus, a theoretical detour needs to be taken. To obtain the unknown factors individual fractionation factors are connected in such a way, that the initial species and final species of this factor-chain

Formula	T-Range [°C]	Method	Reference
$^{(a)}CO_2^g \rightarrow CO_2^{aq}$			
$^{(1)}\epsilon = (0.0041 \pm 0.0005)(T_k - 273.15) - (1.18 \pm 0.01)$	0 – 60	exp/theo	Vogel et al. (1970)
$^{(2)}\epsilon = \frac{6300}{T_k^2} - 0.91$		sum	Deines et al. (1974)
$^{(3)}\epsilon = -\frac{373 \pm 70}{T_k} + (0.19 \pm 0.23)$	0 – 150	exp	Mook et al. (1974)
$^{(4)}\epsilon = (0.0049 \pm 0.0015)(T_k - 273.15) - (1.31 \pm 0.05)$	5 – 25	exp	Zhang et al. (1995)
$^{(b)}HCO_3^- \rightarrow CO_2^g$			
$^{(1)}\epsilon = (0.109 \pm 0.005)(T_k - 273.15) - (10.56 \pm 0.16)$	20 – 60	exp	Emrich et al. (1970)
$^{(2)}\epsilon = -\frac{1099000}{T_k^2} + 4.54$		sum	Deines et al. (1974)
$^{(3)}\epsilon = -\frac{9483 \pm 220}{T_k} + (23.89 \pm 0.75)$	0 – 150	exp	Mook et al. (1974)
$^{(4)}\epsilon = -8.27 \pm 0.30$	25	exp	Turner (1982)
$^{(5)}\epsilon = (0.100 \pm 0.001)(T_k - 273.15) - (10.71 \pm 0.10)$	25 – 40	exp	Lesniak and Sakai (1989)
$^{(6)}\epsilon = (0.1141 \pm 0.0028)(T_k - 273.15) - (10.78 \pm 0.04)$	5 – 25	exp	Zhang et al. (1995)
$^{(c)}HCO_3^- \rightarrow CO_2^{aq}$			
$^{(1)}\epsilon = -\frac{9866 \pm 230}{T_k} + (24.12 \pm 0.78)$	0 – 150	exp	Mook et al. (1974)
$^{(d)}HCO_3^- \rightarrow CaCO_3$			
$^{(1)}\epsilon = 0.9 \pm 0.2$	25	exp	Rubinson and Clayton (1969)
$^{(2)}\epsilon = (0.035 \pm 0.013)(T_k - 273.15) + (1.15 \pm 0.35)$	20 – 60	exp	Emrich et al. (1970) corrected
$^{(3)}\epsilon = -\frac{4232}{T_k} + 15.10$	0 – 40	exp	Mook and de Vriess (2000)
$^{(e)}CaCO_3 \rightarrow CO_2^g$			
$^{(1)}\epsilon = -\frac{2988000}{T_k^2} + \frac{7666.3}{T_k} - 2.4612$	0 – 550	theo	Bottinga (1968)
$^{(2)}\epsilon = (0.063 \pm 0.008)(T_k - 273.15) - (11.43 \pm 0.24)$	20 – 60	exp	Emrich et al. (1970) corrected
$^{(3)}\epsilon = -\frac{1194000}{T_k^2} + 3.63$		sum	Deines et al. (1974)
$^{(4)}\epsilon = (0.12 \pm 0.01)(T_k - 273.15) - (11.98 \pm 0.13)$	10 – 40	exp	Romanek et al. (1992)

Table 2.4.1: *Carbon fractionation factors in* [‰] *from literature.*

Formula	T-Range [°C]	Method	Reference
$^{(a)}CO_2^g \rightarrow CO_2^{aq}$			
$^{(1)}\epsilon = -\frac{160515}{T_k^2} + \frac{1441.76}{T_k} - 1.9585$	0 – 60	sum	Thorstenson and Parkhurst (2004)
$^{(b)}H_2O \rightarrow CO_2^{aq}$			
$^{(1)}\epsilon = \frac{16600}{T_k} - 15.69$	-2 – 85	exp	O'Neil and Adami (1969)
$^{(2a)}\epsilon = (1.0412 - 1) \times 1000$	25	sum	Friedman and O'Neil (1977) mean out of 10 values
$^{(2b)}\epsilon = (1.0396 - 1) \times 1000$	25	theo	Usdowski and Hoefs (1993)
$^{(3)}\epsilon = \frac{17604}{T_k} - 17.93$	10 – 60	exp	Brenninkmeijer et al. (1983)
$^{(4)}\epsilon = -\frac{181115}{T_k^2} + \frac{19435.96}{T_k} - 21.9285$	0 – 100	sum	Thorstenson and Parkhurst (2004)
$^{(5)}\epsilon = \frac{2520000 \pm 30000}{T_k^2} + (12.12 \pm 0.33)$	15 – 40	exp	Beck et al. (2005)
$^{(c)}HCO_3^- \rightarrow H_2O$			
$^{(1)}\epsilon = -\frac{2920000 \pm 70000}{T_k^2} + (2.66 \pm 0.18)$	25 – 45	exp	Halas and Wolacewicz (1982)
$^{(2)}\epsilon = \left(\frac{1}{1.0346} - 1\right) \times 1000$	25	theo	Usdowski and Hoefs (1993)
$^{(3)}\epsilon = -\frac{2660000 \pm 50000}{T_k^2} - (1.18 \pm 0.52)$	15 – 40	exp	Beck (2004)
$^{(4)}\epsilon = -\frac{2590000 \pm 0}{T_k^2} - (1.89 \pm 0.04)$	15 – 40	exp	Beck et al. (2005)
$^{(d)}H_2O \rightarrow CaCO_3$			
$^{(1)}\epsilon = \frac{2780000}{T_k^2} - 3.39$	0 – 500	exp	O'Neil et al. (1969)
$^{(2)}\epsilon = \frac{2780000}{T_k^2} - 2.89$		sum	Friedman and O'Neil (1977)
$^{(3)}\epsilon = \frac{18030}{T_k} - 32.42$	10 – 40	exp	Kim and O'Neil (1997)
$^{(4)}\epsilon = \frac{19668}{T_k} - 37.32$	0 – 40	sum	Mook and de Vriess (2000)
$^{(e)}CaCO_3 \rightarrow CO_2^g$			
$^{(1)}\epsilon = -\frac{1803400}{T_k^2} + \frac{10611}{T_k} - 3.2798$	0 – 550	theo	Bottinga (1968)

Table 2.4.2: *Oxygen fractionation factors in* [‰] *from literature.*

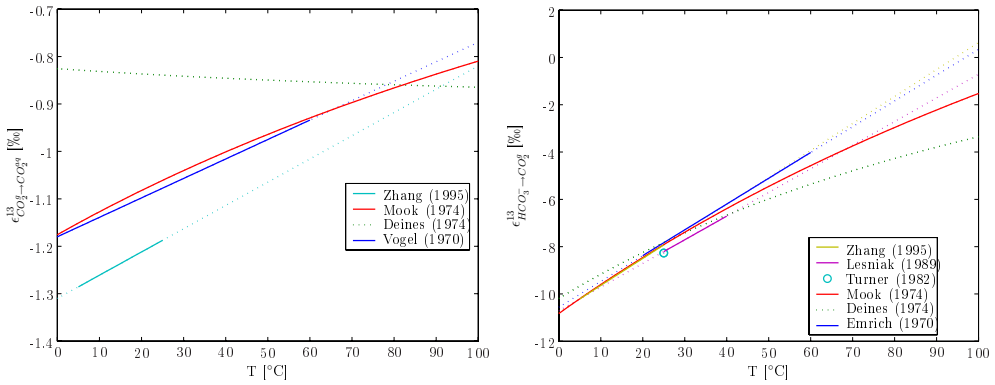

(a) $CO_2^g \rightarrow CO_2^{aq}$

(b) $HCO_3^- \rightarrow CO_2^g$

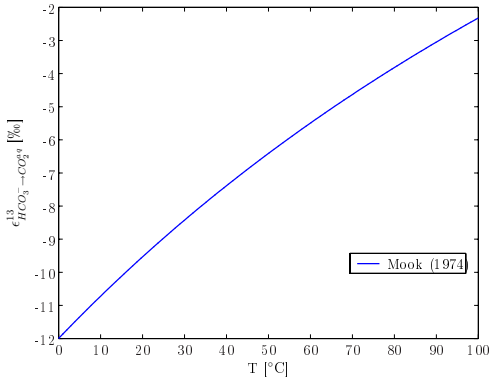

(c) $HCO_3^- \rightarrow CO_2^{aq}$

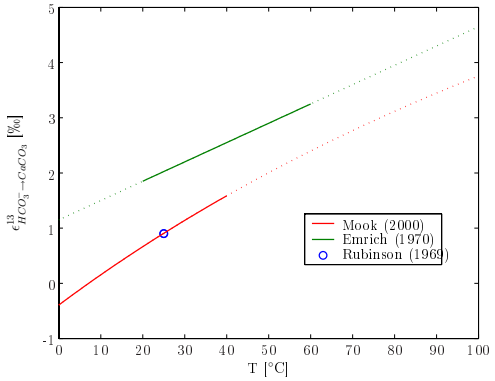

(d) $HCO_3^- \rightarrow CaCO_3$

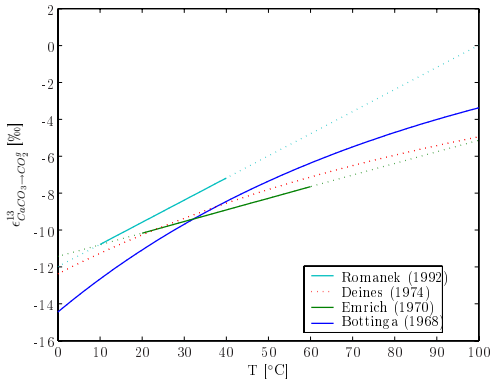

(e) $CaCO_3 \rightarrow CO_2^g$

Figure 2.4.1: *Fractionation factors for carbon between different species. The data are taken from literature (see Table 2.4.1). The dotted lines represent extrapolated values according to the given equation for temperatures between 0 and 100°C, whereas the solid lines represent the temperature range, wherein fractionation factors have been determined.*

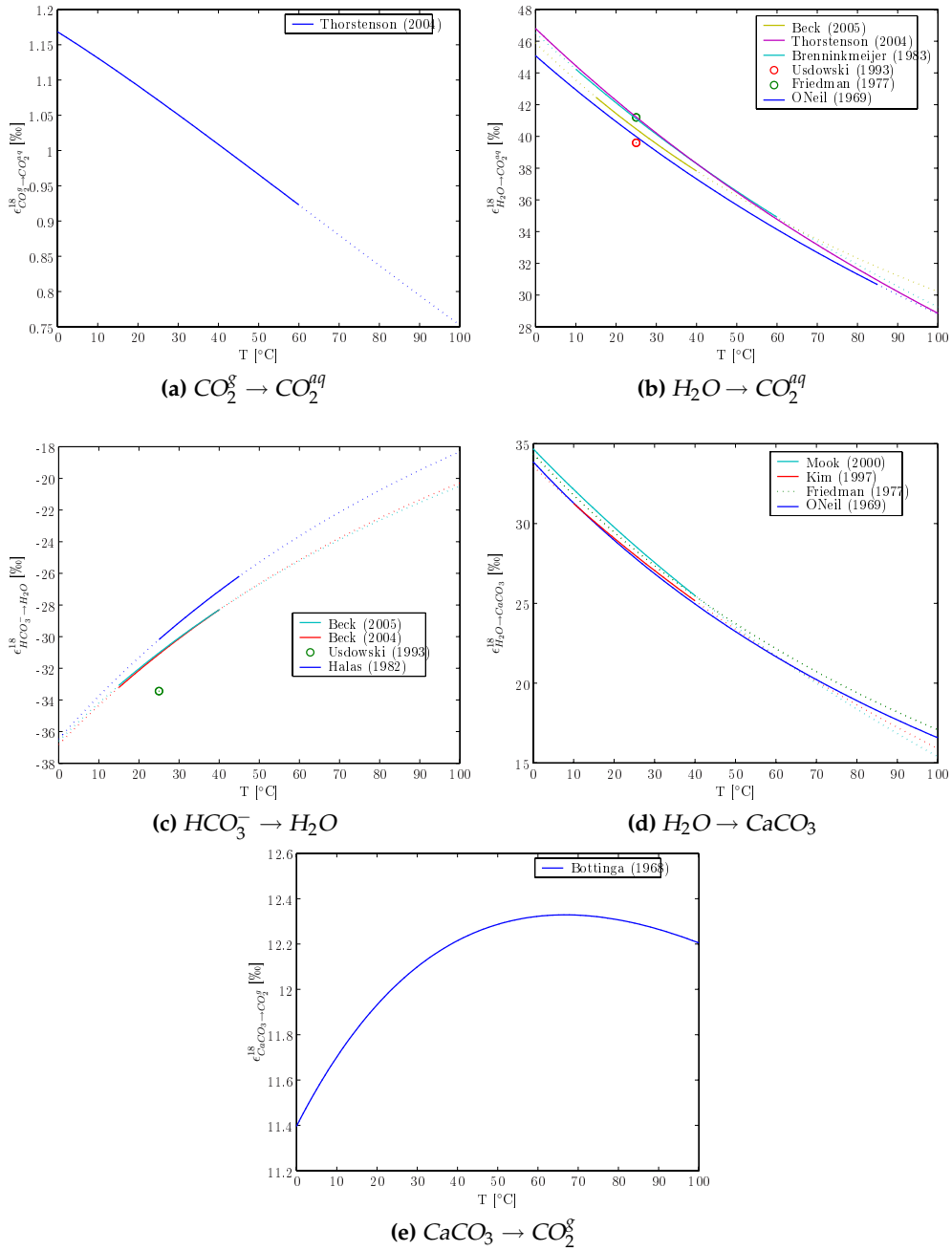

(a) $CO_2^g \rightarrow CO_2^{aq}$ **(b)** $H_2O \rightarrow CO_2^{aq}$

(c) $HCO_3^- \rightarrow H_2O$ **(d)** $H_2O \rightarrow CaCO_3$

(e) $CaCO_3 \rightarrow CO_2^g$

Figure 2.4.2: *Fractionation factors for oxygen between different species. The data are taken from literature (see Table 2.4.2). The dotted lines represent extrapolated values according to the given equation for temperatures between 0 and 100°C, whereas the solid lines represent the temperature range, wherein fractionation factors have been determined.*

match to the needed transition. According to Eq. 2.4.8 the isotopic change from state i to state k via state j can be written as:

$$1000 \ln \alpha_{i\to k} = \delta_{i\to k} = \delta_{i\to j} + \delta_{j\to k} = 1000 \ln \left(\alpha_{i\to j}\alpha_{j\to k}\right) \tag{2.4.9}$$

or between states l and n via state m

$$1000 \ln \alpha_{l\to n} = \delta_{l\to n} = \delta_{l\to m} - \delta_{n\to m} = 1000 \ln \left(\frac{\alpha_{l\to m}}{\alpha_{n\to m}}\right). \tag{2.4.10}$$

From this it follows for the connected fractionation factors:

$$\alpha_{i\to k} = \alpha_{i\to j}\alpha_{j\to k} \tag{2.4.11}$$

or

$$\alpha_{l\to n} = \frac{\alpha_{l\to m}}{\alpha_{n\to m}}. \tag{2.4.12}$$

Thus, the transition between two states can be described either by an additive δ-notation or a multiplicative α-notation. Knowing this, the individual fractionation factors between species which can not be measured directly can be determined.

2.4.3 Fractionation factors used in the models

There is a large number of fractionation factors for transitions between some species contained in the system, however, only few are relevant for the usage in the models. This is due to the fact that most of the factors are only determined for a specific temperature range, which needs to be appropriate for natural cave systems.

For carbon the fractionation factors between bicarbonate and carbon dioxide and calcium carbonate respectively are needed. According to Mühlinghaus et al. (2007) the following fractionation factors are used (Mook et al., 1974; Mook and de Vriess, 2000):

$$\begin{aligned} \epsilon^{13}_{HCO_3^-\to CO_2^g} &= -\frac{9483 \pm 220}{T_k} + (23.89 \pm 0.75) \\ \epsilon^{13}_{HCO_3^-\to CaCO_3} &= -\frac{4232}{T_k} + 15.10. \end{aligned} \tag{2.4.13}$$

For the fractionation of oxygen an additional fractionation factor is needed, that is the fractionation between bicarbonate and water. However, since there are no direct measurements of some of these factors, they need to be constructed as described in the previous section. The fractionation between bicarbonate and water is according to Beck et al. (2005):

$$\epsilon_{HCO_3^-\to H_2O} = -\frac{2590000 \pm 0}{T_k^2} - (1.89 \pm 0.04). \tag{2.4.14}$$

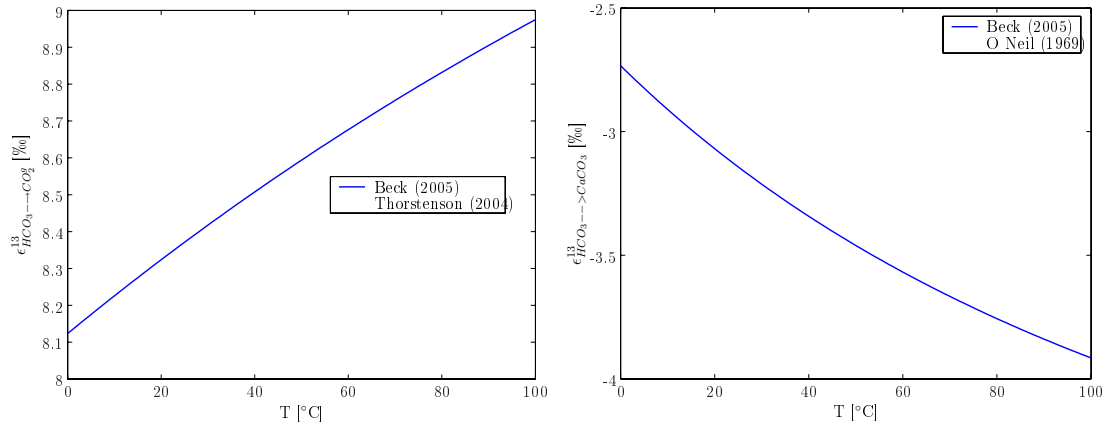

(a) $HCO_3^- \rightarrow CO_2$ **(b)** $HCO_3^- \rightarrow CaCO_3$

Figure 2.4.3: *Constructed fractionation factors for oxygen between different species used in the models.*

The fractionation between bicarbonate and gaseous carbon dioxide is given as:

$$\begin{aligned}\epsilon^{18}_{HCO_3^- \rightarrow CO_2^g} &= \epsilon^{18}_{HCO_3^- \rightarrow H_2O} + \epsilon^{18}_{H_2O^- \rightarrow CO_2^{aq}} - \epsilon^{18}_{CO_2^{aq} \rightarrow CO_2^g} \\ &= -\frac{2590000 \pm 0}{T_k^2} - (1.89 \pm 0.04) \\ &+ \frac{2520000 \pm 30000}{T_k^2} + (12.12 \pm 0.33) \\ &+ \frac{160515}{T_k^2} + \frac{1441.76}{T_k} - 1.9585.\end{aligned} \tag{2.4.15}$$

Values are taken from Beck et al. (2005); Thorstenson and Parkhurst (2004). The fractionation between bicarbonate and calcium carbonate is constructed as follows:

$$\begin{aligned}\epsilon_{HCO_3^- \rightarrow CaCO_3} &= \epsilon_{HCO_3^- \rightarrow H_2O} + \epsilon_{H_2O^- \rightarrow CaCO_3} \\ &= -\frac{2590000 \pm 0}{T_k^2} - (1.89 \pm 0.04) + \frac{2780000}{T_k^2} - 3.39.\end{aligned} \tag{2.4.16}$$

Values are taken from Beck et al. (2005); O'Neil et al. (1969). The temperature dependence of these two factors are shown in Figs. 2.4.3.

Note, that the selection of fractionation factors for the models is a crucial point, since their influence on the isotopic enrichment of the precipitated calcite is significant. For oxygen the temperature dependence of the factors of the relevant transitions show only a small variability regarding their trend and absolute values. However, carbon fractionation factors differ for some transitions. In the following the carbon factors of the

relevant transitions are chosen regarding their temperature range or in accordance to earlier publications (Mühlinghaus et al., 2007).

Chapter 3

Forward Models

3.1 Growth model

Growth and morphology of stalagmites are the properties, which catch a researcher's eye first. Thus, it is not surprising that the first mathematical models were developed to reconstruct growth and shape of stalagmites to investigate their change under varying external conditions. This was carried out in the late 80's by Dreybrodt (1988) and improved 15 years later by Kaufmann (2003). However, the basic idea still remains. The underlying concept is the iterative calculation of individual growth layers until a stalagmite shape establishes, which does not change in form but only in height (equilibrium shape). Due to crystal growth mechanisms the growth is perpendicular to the underlying surface and is maximal at the apex of the stalagmite. With increasing distance from the centre growth decreases. Applying this decreasing growth to different points along the growth layer a new layer is formed, which acts as the starting point of the next layer. In the first models growth was assumed to decrease exponentially from the apex to the flanks. However, this assumption is a guess and has no physical background.

A recent publication of Romanov et al. (2008), who used the flow velocity of the solution layer on top of the stalagmite to calculate the calcite deposition iteratively from the apex to the flanks. This results in a Gaussian decrease of the growth with increasing distance from the centre in comparison to the exponential decrease of the first models. In this section a general description of the growth model is given first followed by results achieved with the exponential and the Gaussian ansatz. In addition the mixing coefficient is built in the existing growth models. By taking mixing effects between the impinging drops and the existing solution layer into account, the existing models are improved in order to describe growth and shape of stalagmites in a more realistic way.

The shape of a stalagmite is determined by the iterative calculation of individual growth layers until an equilibrium shape is established. To determine the development of growth layers two information are needed: (i) the growth at the apex of the stalagmite, where growth is maximal, since the amount of calcium in the solution and so calcite deposition is maximal. (ii) the decrease of growth from the apex along the growth layer to the flanks of the stalagmite. This is a crucial point of the growth model. To keep the following theory in a general way a function $f(l)$ is used to describe the decreasing growth, which depends on the distance l from the apex and is characterized by a monotonically decrease.

The growth at the apex is determined by the deposition rate F. The correlation between calcium excess and deposition rate follows in a first approach a linear trend for calcium concentrations of $[Ca^{2+}] \leq [Ca^{2+}]_{eq}$ (Buhmann and Dreybrodt, 1985b,a; Baker et al., 1998). In this region F can be approximated by:

$$F = \alpha \left([Ca^{2+}]_{soil} - [Ca^{2+}]_{app} \right). \tag{3.1.1}$$

Thereby the deposition rate F is given in $[\frac{mol}{m^2 s}]$, the calcium concentrations in $[\frac{mol}{m^3}]$ and

the constant of proportionality α in $[\frac{m}{s}]$[1]. The apparent calcium concentration $[Ca^{2+}]_{app}$ is related to the equilibrium calcium concentration by $[Ca^{2+}]_{app} = \frac{[Ca^{2+}]_{eq}}{\sqrt{0.8}}$ due to an inhibiting effect during the precipitation of calcite (Dreybrodt, 1999; Kaufmann, 2003). To convert the deposition rate F $[\frac{mol}{m^2 s}]$ into a growth G $[m]$ it has to be multiplied by the quotient of molar mass and molar density of calcite:

$$G = \frac{m_{calcite}}{\rho_{calcite}} F = \frac{m_{calcite}}{\rho_{calcite}} \alpha \left([Ca^{2+}]_{soil} - [Ca^{2+}]_{app} \right). \tag{3.1.2}$$

During one drip interval the excess concentration of the solution changes due to calcite precipitation according to section 2.2:

$$\begin{aligned} [Ca^{2+}]_{ex}(t) &= \left([Ca^{2+}]_{soil} - [Ca^{2+}]_{app} \right) e^{-\frac{\alpha t}{\delta}} \\ &= [Ca^{2+}]^0_{ex} e^{-\frac{\alpha t}{\delta}}. \end{aligned} \tag{3.1.3}$$

Due to mixing processes between the impinging drop and the existing solution layer (see section 2.3) this concentration reaches an equilibrium like state after a sufficient number of drops n and can be calculated according to Eq. 2.3.7:

$$[Ca^{2+}]^n_{ex}(t) = [Ca^{2+}]^0_{ex} \lambda(n,d) e^{-\frac{\alpha t}{\delta}}. \tag{3.1.4}$$

$[Ca^{2+}]^0_{ex}$ represents the initial calcium excess concentration of the drop. To obtain the mean growth during one drip interval the equilibrated calcium concentration is inserted in Eq. 3.1.2 and the resulting equation is averaged over one drip interval. This yields for the growth in $[m]$ using $m_{calcite} = 0,10009 \frac{kg}{mol}$ and $\rho_{calcite} = 2689 \frac{kg}{m^3}$:

$$\begin{aligned} G_0 &= 37.222 \times 10^{-6} [Ca^{2+}]^0_{ex} \lambda(n,d) \alpha \int_0^d e^{-\frac{\alpha t}{\delta}} dt \\ &= 37.222 \times 10^{-6} [Ca^{2+}]^0_{ex} \lambda(n,d) \delta \left(1 - e^{-\frac{\alpha d}{\delta}} \right) \end{aligned} \tag{3.1.5}$$

and the growth rate in $[m/s]$:

$$W_0 = 37.222 \times 10^{-6} \frac{[Ca^{2+}]^0_{ex} \lambda(n,d) \delta}{d} \left(1 - e^{-\frac{\alpha d}{\delta}} \right). \tag{3.1.6}$$

The dependence of growth rate W_0 on drip interval, temperature and mixing coefficient is shown in Fig. 3.1.1. The number of drops is sufficient ($n \approx 100$) to fulfil the condition of equilibrated calcium excess concentration. An in- or decreased CO_2 partial pressure difference between the soil and the cave zone does not influence the characteristic of the dependencies on the other parameters, though, a quantitative change is observed. If the difference in CO_2 decreases, growth is reduced, especially for short drip intervals and vice versa.

[1] Note, that α is also known as the kinetic constant.

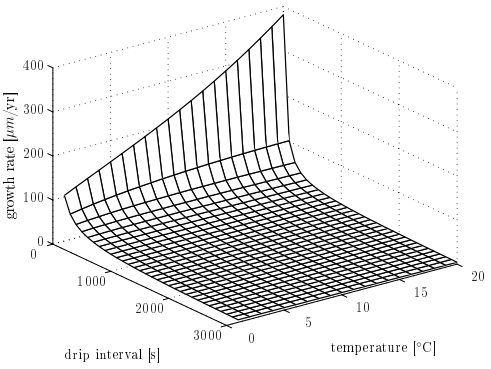

(a) *Growth rate for ϕ = 0,1*

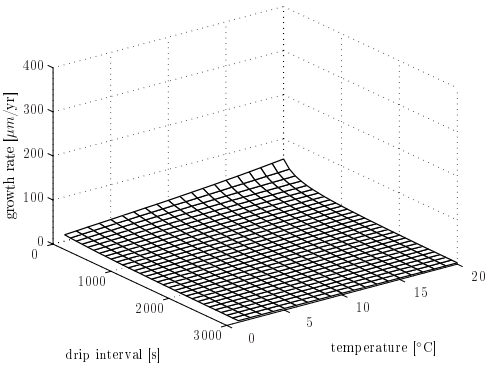

(b) *Growth rate for p_{CO_2} = 1000ppm*

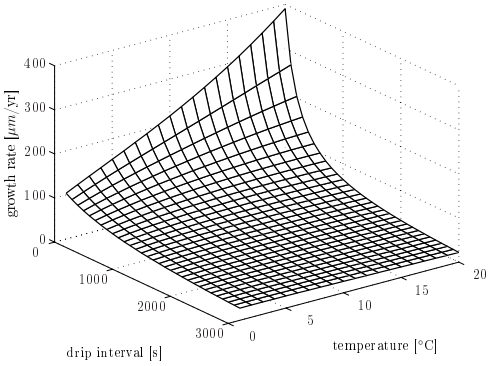

(c) *Growth rate for ϕ = 0,5*

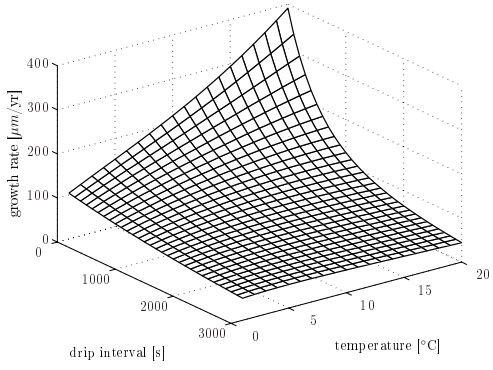

(d) *Growth rate for ϕ = 1,0*

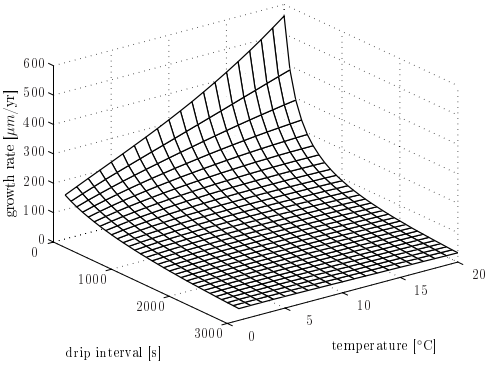

(e) *Growth rate for p_{CO_2} = 20000ppm*

Figure 3.1.1: *Dependencies of growth rate on drip interval, temperature, mixing coefficient and CO_2 partial pressure of the soil. The figures on the left hand side ((a), (c) and (d)) show the growth rate in $\mu m/yr$ for a change in the mixing coefficient for a p_{CO_2} value of the soil of 10000ppm. The figures on the right hand side ((b), (c) and (e)) are calculated for a fixed mixing coefficient of $\phi = 0,5$ and varying p_{CO_2} values. Lines are drawn every 100s and every degree centigrade. Note, that the scale of the z-axis is changed in Fig. (e).*

For short drip intervals ($d \rightarrow 0$) the growth rate becomes independent on the mixing coefficient ϕ and depends on temperature and the amount of supersaturation only. For high temperatures the degassing of CO_2 accelerates and more calcium carbonate precipitates. Thus, growth rate increases with increasing temperatures. With increasing drip interval this temperature dependence is attenuated and the influence of ϕ increases. For low mixing coefficients the growth rate decreases fast with increasing drip interval to a minimum value, whereas for high ϕ this decrease is much slower. This is due to an extended residence time of the solution at low mixing coefficients, which causes that the CO_2 partial pressure of the solution is almost in equilibrium with the surrounding cave air. For high mixing coefficients most parts of the solution are replaced by the drop and thus, growth rate increases.

To model the shape of a stalagmite not only growth at the apex must be known, but also apart the apex, along a growth layer. This growth layer is mathematically described by a polygon and consists of individual connected segments. The segment between two points of the polygon $\vec{P}_{i-1}$ and $\vec{P}_i$ has the length Δl_i. By adding up the segments the length l_i of the polygon at the point $\vec{P}_i$ can be calculated:

$$l_i = \sum_{j=1}^{i} \Delta l_j. \tag{3.1.7}$$

This is illustrated in Fig. 3.1.2. The growth is maximal at the apex of the stalagmite and decreases along the growth layer to the flanks. To keep the decrease of G_0 in a general way it is described by the function $f(l_i)$, which depends on the length l_i between the apex and the point $\vec{P}_i$ and is characterised by a monotonic decrease. This yields for the growth at point $\vec{P}_i$:

$$\vec{G}(l_i) = G_0 f(l_i)\vec{e}. \tag{3.1.8}$$

Due to the crystal structure of the existing growth layer, the deposited calcite and thus the direction of growth is always perpendicular to the underlying surface. This is mathematically described by the normal unit vector $\vec{e}$, which is orthogonal to the surface $\overrightarrow{P^{i-1}_{old} P^{i}_{old}}$.

The growth layer is technically implemented by a polygon, whereas growth at each point $\vec{P}_i$ is defined by Eq. 3.1.8. The resulting calculation of the coordinates of each point of the new polygon can be deduced geometrically from Fig. 3.1.2 and yields for point $\vec{P}^i_{new}$:

$$\vec{P}^i_{new} = \vec{P}^i_{old} + \vec{G}(l_i) \tag{3.1.9}$$

with the boundary condition:

$$\vec{e} \cdot \left(\vec{P}^i_{old} - \vec{P}^{i-1}_{old} \right) = 0. \tag{3.1.10}$$

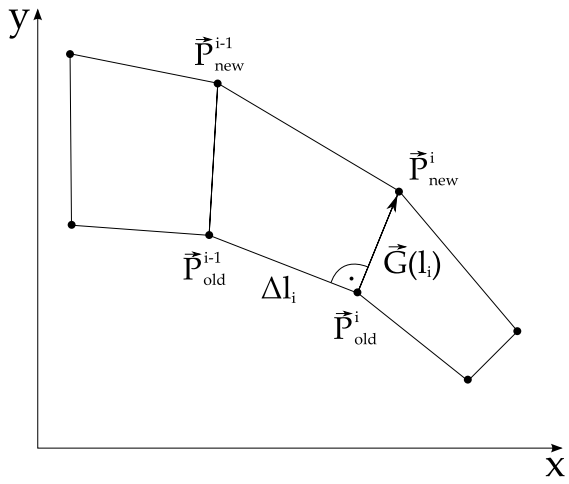

Figure 3.1.2: *An individual growth layer can mathematically be described by a polygon. Due to the crystal structure the growth direction is perpendicular to the underlying surface. By applying the individual growth to each point of the polygon a new layer or polygon respectively is established.*

This yields for the vector $\vec{e}$:

$$\vec{e} = \frac{1}{\Delta l_i} \begin{pmatrix} y^{i-1}_{old} - y^{i}_{old} \\ x^{i}_{old} - x^{i-1}_{old} \end{pmatrix}. \tag{3.1.11}$$

Combining Eq. 3.1.8, 3.1.9 and 3.1.11 yields for the new polygon point $\vec{P}^{i}_{new}$:

$$\begin{pmatrix} x \\ y \end{pmatrix}^{i}_{new} = \begin{pmatrix} x \\ y \end{pmatrix}^{i}_{old} + \frac{G_0 f(l_i)}{\Delta l_i} \begin{pmatrix} y^{i-1}_{old} - y^{i}_{old} \\ x^{i}_{old} - x^{i-1}_{old} \end{pmatrix} \tag{3.1.12}$$

Performing this calculation on each point of the old polygon yields a new polygon, which represents the growth layer established under the given boundary conditions. For constant boundary conditions an equilibrium shape is reached after a sufficient time of growth and the shape of the stalagmite is only shifted vertically without changing its form. According to Dreybrodt (1988) the height needed to obtain the equilibrium shape is at most four times the radius, however, boundary conditions must not change.

The radius R of a stalagmite, which has achieved an equilibrium shape, can be deduced using the following assumption: by mass conservation the amount of calcite deposited during one drip interval d must be equal to the loss of calcium from the solution on top of the stalagmite during this time. The input flux F_{in} of the drop in [mol/s] is given by the amount of calcium per drip interval:

$$F_{in} = \frac{V[Ca^{2+}]_{drop}}{d}. \tag{3.1.13}$$

The output flux F_{out} lost by the solution is given as the mean deposition rate during one drip interval times the area, where calcite has been precipitated. Assuming a planar stalagmite at the top this area is given by $A = \pi R^2$:

$$F_{out} = \overline{F(d)}A \tag{3.1.14}$$

with the mean deposition rate $\overline{F(d)}$:

$$\begin{aligned}\overline{F(d)} &= \frac{1}{d}\int_0^d \alpha[Ca^{2+}]_{sol}e^{-\frac{\alpha t}{\delta}}dt \\ &= \frac{[Ca^{2+}]_{sol}\delta}{d}\left(1-e^{-\frac{\alpha d}{\delta}}\right).\end{aligned} \tag{3.1.15}$$

In equilibrium F_{in} must be equal to F_{out} and the equilibrium radius R can be derived as follows:

$$R = \sqrt{\frac{V[Ca^{2+}]_{drop}}{\pi[Ca^{2+}]_{sol}\delta\left(1-e^{-\frac{\alpha d}{\delta}}\right)}} \tag{3.1.16}$$

with the calcium excess concentration of the drop $[Ca^{2+}]_{drop} = [Ca^{2+}]^0_{ex}$ and the solution $[Ca^{2+}]_{sol}$. If mixing effects are neglected, the calcium excess of the solution is equal to the one of the drop and is given as: $[Ca^{2+}]_{sol} = [Ca^{2+}]^0_{ex}$. Thus the radius becomes independent of calcium concentration:

$$R_0 = \sqrt{\frac{V}{\pi\ \delta\ \left(1-e^{-\frac{\alpha d}{\delta}}\right)}}. \tag{3.1.17}$$

If mixing effects were taken into account the calcium concentration of the solution is according to Eq. 3.1.4: $[Ca^{2+}]_{sol} = \lambda[Ca^{2+}]^0_{ex}$ and the radius changes to:

$$\begin{aligned}R_{mix} &= \sqrt{\frac{V}{\pi\ \delta\ \lambda\left(1-e^{-\frac{\alpha d}{\delta}}\right)}} \\ &= \frac{R_0}{\sqrt{\lambda}}.\end{aligned} \tag{3.1.18}$$

Note, R_{mix} is larger than R_0 (see Fig. 3.1.3), but still independent of the calcium excess concentration. If mixing processes are neglected the mixing coefficient is $\phi = 1$ and the radius R_{mix} becomes equal to R_0. Thus R_0 can be described as border case of R_{mix}, which is therefore used in the following as a more general description of the equilibrium radius.

In natural systems also radii occur, which are smaller than the minimal radius calculated by the ansatz of Dreybrodt (1988). For instance, caves in Romania show radii of

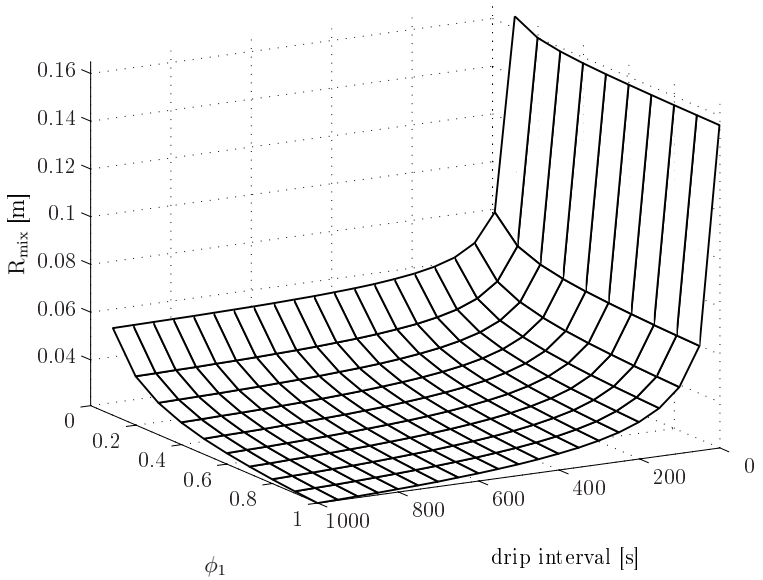

Figure 3.1.3: *Dependence of the equilibrium radius on mixing coefficient and drip interval for n = 100 and fixed temperature T = 10°C. The radius increases for low mixing coefficients compared to the case of no mixing ($\phi = 1$).*

down to 1 cm (Constantin, 2008). However, the minimal radius calculated by Eq. 3.1.16 for very long drip intervals is given as:

$$\begin{aligned} R_{min} &= \sqrt{\frac{V}{\pi\delta}} \\ &\approx 1,8cm. \end{aligned} \tag{3.1.19}$$

However, this calculation is based on the assumption of a rather flat top of the stalagmite, which is not observed for natural stalagmites. Assuming not a flat, but a rounded top of the stalagmite, the equilibrium radius decreases. This is illustrated in Fig. 3.1.4. The area, where calcite is deposited is given as A. Assuming natural stalagmites with very small radii this area might be better approximated by a part of a spherical area rather than a planar circular area. Thus, the new radius of the stalagmite is calculated as follows: By putting the area A with radius R_c upon a sphere in such an order, that it covers half of the sphere, the radius R_s of the sphere is given as[2]:

$$\begin{aligned} \pi R_c^2 &= \frac{4\pi R_s^2}{2} \\ R_s &= \sqrt{\frac{R_c^2}{2}}. \end{aligned} \tag{3.1.20}$$

[2]The indices indicate the assumption of a circular area (c) and a spherical area (s).

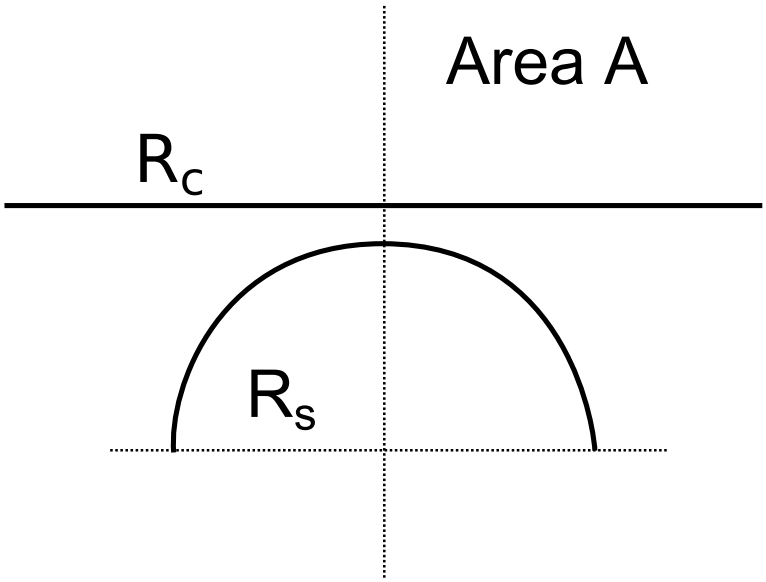

Figure 3.1.4: *Approximation of the top of the stalagmite at a two dimensional point of view. The vertical dotted line represents the growth axis of the stalagmite. Calcite is precipitated upon area A. If a circular area is assumed, the resulting radius is R_c, if a spherical are is assumed, the radius shrinks to R_s.*

This yields a smaller equilibrium radius of approximately $R_s = 1,26cm$, which is still too large compared to the smallest stalagmites observed, but it approaches their range in a much better way, than the former approximation does.

3.1.1 Exponential approximation

In the first models the monotonic decrease of the growth G from the apex to the flanks of a stalagmite is described by a decreasing exponential function $f(l_i)$. This function is used in the models developed by Dreybrodt (1988) and Kaufmann (2003), whereas the exponential ansatz depends on the length of the polygon describing the growth layer and the equilibrium radius of the stalagmite:

$$f(l_i) = e^{-\frac{l_i}{R}}. \tag{3.1.21}$$

However, this is an arbitrary assumption with no physical basis.

3.1.2 Gaussian approximation

In a recent publication Romanov et al. (2008) calculated the growth of stalagmites in an improved way. In this new model the movement of the solution along the stalagmite was determined by taking gravitational and frictional effects into account. The iterative calculation performed in this model allows to determine the time space correlation of

the solution on a physical basis. The calcium concentration of the solution decreases during the movement of the solution from the apex to the flanks and thus growth at any point of the polygon can be calculated. This computationally intensive procedure is approximated by a Gaussian function:

$$f(l_i) = e^{-\frac{l_i^2 \pi}{4R_g^2}}, \tag{3.1.22}$$

with the radius R_g:

$$R_g = \sqrt{\frac{V}{\pi \alpha d}} \tag{3.1.23}$$

Note, that R_g corresponds to the equilibrium radius of the exponential model in the high flow regime ($d \ll \delta/\alpha$).
However, there is a slight deviation between the shape obtained by using this fitted function and the real shape obtained by using the actual solution movement process (see Romanov et al. (2008)). Since this model is based on the iterative calculation of calcite precipitation from small solution parcels along the growth layer, the mixing coefficient can not be included in the same manner as for the exponential ansatz. This would be an improvement to a more realistic description of natural stalagmites. In this study the mixing coefficient is not included in the radius of the Gaussian model, but in its maximal growth, which is calculated in analogy to the growth of the exponential model.

3.1.3 Results and discussion

Using the exponential and Gaussian approximations for the decrease of growth from the apex to the flanks of a stalagmite, the morphology of a stalagmite can be modelled in dependence of 0^{th} stage parameters. To accelerate calculations growth is multiplied by a factor of 1000. This is reasonable, which shows a comparison of two model runs, whereas in the first run real growth and in the second one increased growth is used. As it can be seen in Fig. 3.1.5 the shape of these two runs shows no significant difference.

In the following the change in shape during the variation of 0^{th} stage parameters is investigated, whereas the range of these parameters is chosen in order to reflect the wide range of natural conditions in caves (see Table 3.1.1).
Generally Fig. 3.1.6 shows, that the shape calculated by the Gaussian model reaches equilibrium in a much shorter time-scale than the exponential model and reveals a rather flattened top at the apex of the stalagmite. This has already been shown by Romanov et al. (2008) and was emphasized as the major improvement of the model. Thus, the Gaussian model reveals a much more differentiated shape and the individual growth stages can be more easily detected due to an improved sensitivity to external changes. The exponential model on the other hand needs more time to reach equilibrium and is characterized by a declined surface at the apex. Due to overlapping growth stages the shape becomes smoother.

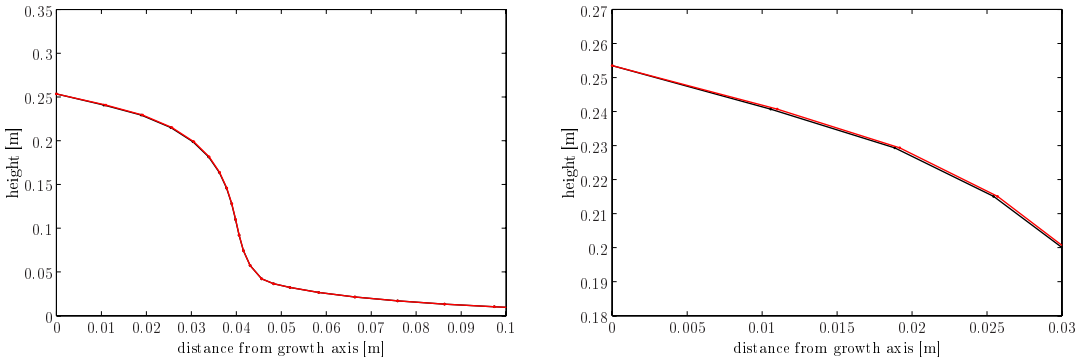

(a) *Growth comparison* **(b)** *Zoom*

Figure 3.1.5: *Comparison of two model runs for fixed boundary conditions, but different growth rates. The black lined shape is calculated for* $d = 200s$, $T_c = 5°C$ *and* $\phi = 1$. *In this case approximately* 150×10^6 *calculations are needed to obtain the final shape of the stalagmite. The red line indicates the morphology of a stalagmite, which was calculated using the same boundary conditions as in the first case, but with an accelerated growth by a factor of 1000. Thus much less calculations are needed to obtain an equilibrium shape. Both results are almost equal, however the accelerated growth (red line) shows a slight, but insignificant deviation of the shape at the top. Thus the accelerated growth is used for all upcoming model runs to save computing time.*

stage	drip interval [s]	temperature [°C]	ϕ	p_{CO_2} [ppm]	duration [years]
1	100	10	0,5	10000	
2	500	10	0,5	10000	
3	250	10	0,5	10000	
4	250	1	0,5	10000	
5	250	20	0,5	10000	1000
6	250	10	0,1	10000	
7	250	10	1,0	10000	
8	250	10	0,5	5000	
9	250	10	0,5	20000	

Table 3.1.1: *Values of the parameters used in the different growth stages of the models.*

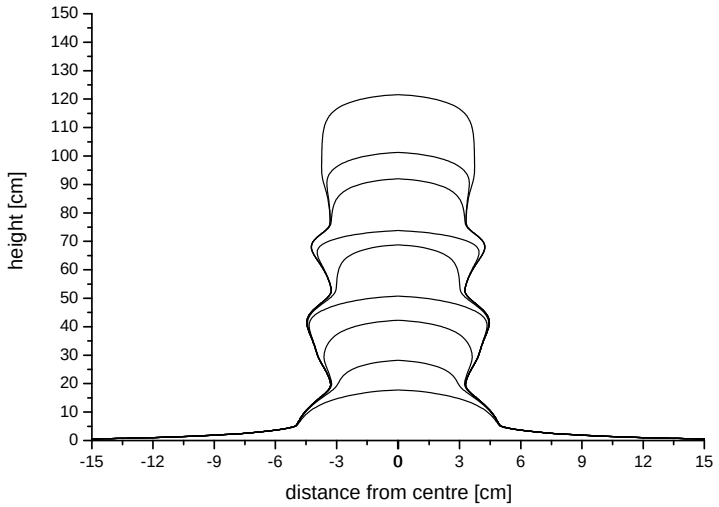

(a) *Exponential growth model*

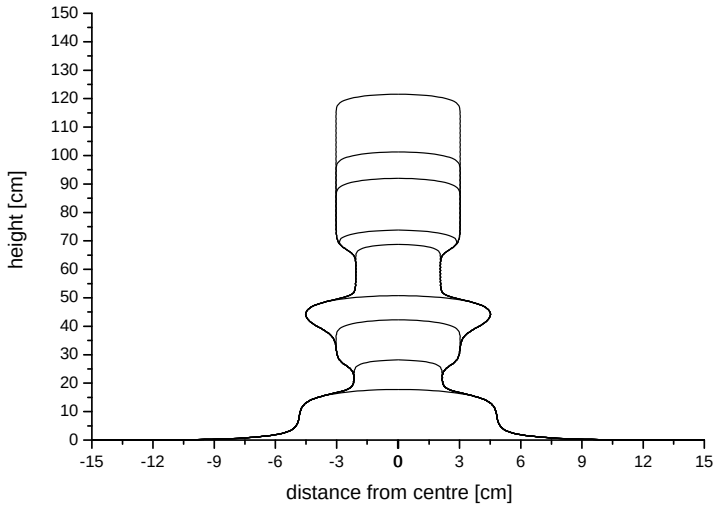

(b) *Gaussian growth model*

Figure 3.1.6: *Growth calculated by the model using the exponential ansatz (a) and the Gaussian ansatz (b) for varying boundary conditions. Lines are drawn every 1000 years. The different stages of growth are enumerated from stage 1 starting at the bottom of the stalagmite up to stage 9 at the top. For boundary conditions see Table 3.1.1.*

Another difference of the models is the influence of the mixing coefficient on the radius. The exponential model includes this dependence, whereas the Gaussian model does not. Thus, only the equilibrium radius and so the shape of the models during stage 7 with a mixing coefficient of $\phi = 1$ can be compared. In the following the influence of the parameters on the shape are discussed.

Variation of drip interval - stage 1 – 3 A variation of the drip interval influences the growth at the apex as well as the radius of the stalagmite. With increasing drip intervals the solution on top of the stalagmite is fed with less drops resulting in a reduced growth and smaller radius (stage 2). If the drip interval decreases the solution gains a higher calcium concentration and growth increases. In this high flow regime the radius increases as well. This change of the shape is well shown by the Gaussian model due to its short response time.

Variation of temperature - stage 4 – 5 If temperature varies the amount of calcite in the solution does not change. However, a variation influences growth and radius of the stalagmite. If growth increases at the apex for higher temperatures (stage 5) due to a faster chemical reaction between bicarbonate and carbon dioxide, the radius must decrease to obey mass conservation. If on the other hand temperatures are lowered, growth decreases, but the radius increases for the same reason. Again, this change can be well observed at the Gaussian model whereas the shape of the exponential model becomes blurred.

Variation of the mixing coefficient - stage 6 – 7 A variation of the mixing coefficient influences the two models in different ways due to different dependencies. The equilibrium radius of the exponential model depends on the mixing coefficient, whereas the radius of the Gaussian model is independent of the mixing coefficient. Thus, the Gaussian model shows only a variation of growth with changing mixing coefficient. This change - seen in both models - can be explained as follows: For a small mixing coefficient, the solution on top of the stalagmite is fed with only small parts of the impinging drop. If in addition drip intervals are long enough, the calcium concentration even approaches the value in equilibrium with the cave air. This results in small growth rates, since only sparse calcite can be deposited. If the mixing coefficient is large the solution on top of the stalagmite is replaced by the impinging drop and the maximal amount of calcite can be deposited resulting in an increased growth. For the exponential model the mixing coefficient influences the radius as well. For small ϕ the radius is enlarged, whereas a large mixing coefficient diminishes the radius.

Variation of the CO_2 partial pressure of the soil - stage 8 – 9 A variation of the partial pressure of the soil influences the amount of calcite excess in the solution, which can be precipitated, but has no influence on the radius. If more calcite is dissolved due to a higher p_{CO_2} of the soil, the more calcite can be deposited and growth increases. The smaller the CO_2 pressure of the soils, the less calcite is dissolved resulting in less growth or even no deposition or dissolution of prior precipitated

calcite on top of the stalagmite. This, however, can only happen, if the cave air has an higher CO_2 partial pressure than the soil, which is unlikely for most of the cave systems. Apparently the radius seems to increase for the exponential model with increasing p_{CO_2}. This increase is not attributed to the changing p_{CO_2}, but to the change of the mixing coefficient from stage 7 to 8 due to the slow achievement of the equilibrium shape.

Although the Gaussian model is based on the calculation of the solution flow on a physical basis, the results appear compared to the exponential model rather unrealistic. This is, for instance, manifested in the time the shape needs to establish an equilibrium shape. In case of the Gaussian model this time is short compared to the exponential model, which leads to a much more sensitive reaction on changes of external parameters, which is rarely observed for natural stalagmites.

Note
Theoretically the calculation of the stalagmite's shape is performed as explained above, however this causes technical problems. Using Eq. 3.1.12 the points of the polygon depart from each other with ongoing calculations. This is due to the inclined stalagmite surface and the fact that growth is perpendicular to the underlying surface. This would result in a shape with a very low resolution at the apex and a high resolution at the flanks. To overcome this problem two critical lengths Δl_{min}, Δl_{max} are introduced, which define the possible range of Δl_i. If Δl_i becomes larger than this range an extra point is interpolated between the current and the previous point and is added to the polygon. On the other hand, if Δl_i falls below the defined range the current point is removed from the polygon. This is illustrated in Figs. 3.1.7(c) and (d).

Another possibility to overcome the problem is to fix the distance Δl_i between two points. This yields in comparison to the previous method equidistant points resulting in a smoother shape. This is illustrated in Fig. 3.1.7(b). Using vector addition the new point $\vec{P}^i_{new}$ is given as:

$$\vec{P}^i_{new} = \vec{P}^{i-1}_{new} + \Delta l_i \frac{\vec{P}^i_{tmp} - \vec{P}^{i-1}_{new}}{\left|\vec{P}^i_{tmp} - \vec{P}^{i-1}_{new}\right|} \tag{3.1.24}$$

$$\begin{pmatrix} x \\ y \end{pmatrix}^i_{new} = \begin{pmatrix} x \\ y \end{pmatrix}^{i-1}_{new} + \Delta l_i \frac{\begin{pmatrix} x^i_{tmp} - x^{i-1}_{new} \\ y^i_{tmp} - y^{i-1}_{new} \end{pmatrix}}{\sqrt{\left(x^i_{tmp} - x^{i-1}_{new}\right)^2 + \left(y^i_{tmp} - y^{i-1}_{new}\right)^2}} \tag{3.1.25}$$

whereas $\vec{P}^i_{tmp}$ is given as:

$$\begin{pmatrix} x \\ y \end{pmatrix}^i_{tmp} = \begin{pmatrix} x \\ y \end{pmatrix}^i_{old} + \frac{G_0 f(l_i)}{\Delta l_i} \begin{pmatrix} y^{i-1}_{old} - y^i_{old} \\ x^i_{old} - x^{i-1}_{old} \end{pmatrix}. \tag{3.1.26}$$

This procedure simplifies the calculation of a smooth shape and avoids the uncertainties occurring by adding or removing points from the polygon as it was done before.

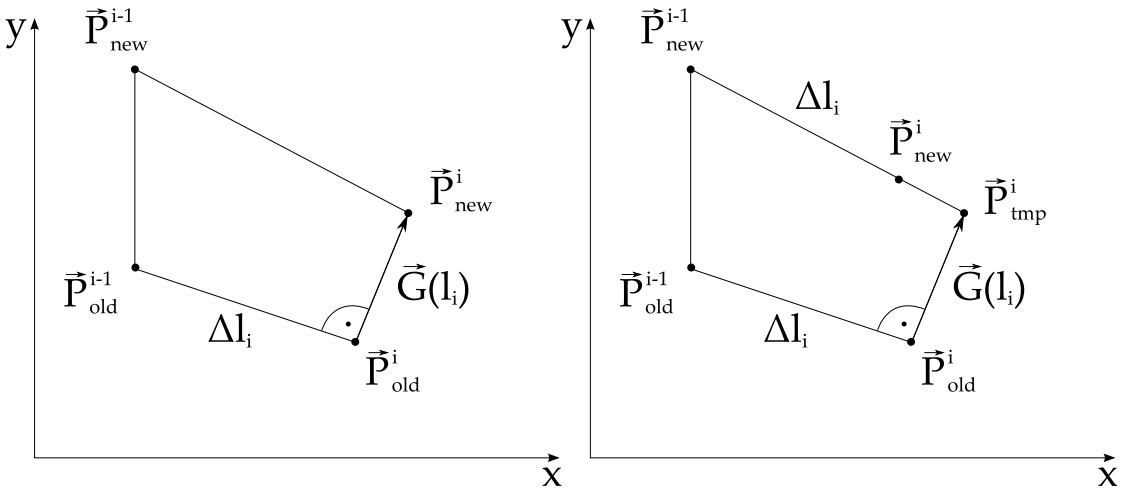

(a) *Theoretical polygon* **(b)** *Technical polygon*

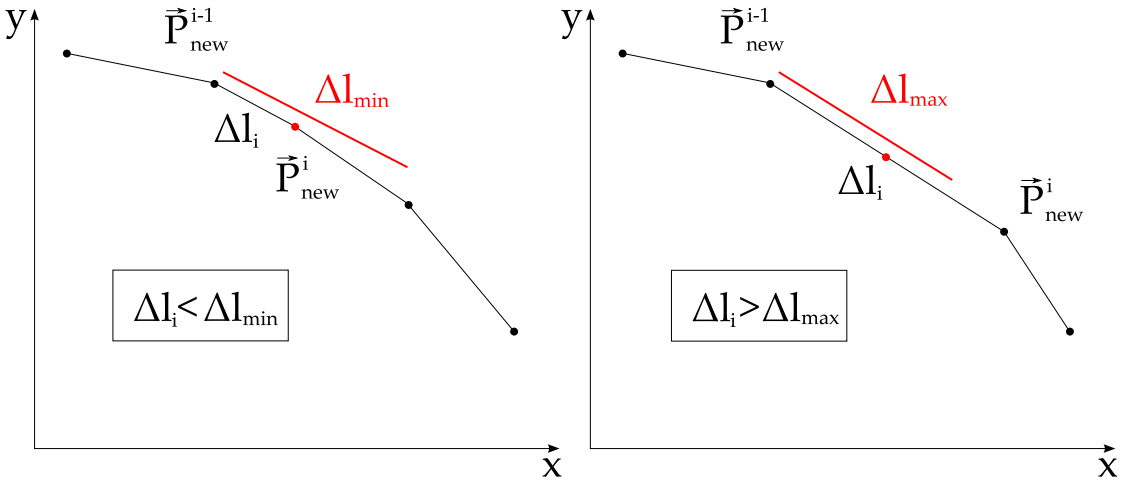

(c) *Removal of a polygon point* **(d)** *Addition of a polygon point*

Figure 3.1.7: *Fig. (a) illustrates the theoretical calculation of a polygon. Due to crystal growth mechanism the polygon points depart from each other. In a first program version this problem was solved by removing a polygon point, if Δl_i falls below the minimal value Δl_{min} (c) or adding a polygon point, if Δl_i exceeds the maximum value Δl_{max} (d). The removed and added points are marked red. In a second program version the distance between two polygon points is kept constant at a value Δl_i. This is illustrated in Fig. (b).*

3.2 Carbon isotope model

The fractionation of stable carbon isotopes occurs during the degassing of CO_2 and precipitation of $CaCO_3$ from the solution on top of the stalagmite. To determine the isotopic composition of the precipitated calcite the fractionation between bicarbonate, which amounts approximately 95 % of the dissolved inorganic calcite, and calcium cabonate is investigated. During this process the stable carbon isotopes ^{12}C and ^{13}C are fractionated, which is expressed by a change in $\delta^{13}C_{CaCO_3}$ in $[‰]$[3].

$$\delta^{13}C = \left(\frac{\alpha^{13}_{HCO_3^- \rightarrow CaCO_3} R_{HCO_3^-}}{R_{std}} - 1 \right) \times 1000. \tag{3.2.1}$$

Hereby the isotope ratio of the DIC was approximated by the isotope ratio of bicarbonate as described in section 2.1.

3.2.1 Fractionation under equilibrium conditions

Under equilibrium conditions the isotope ratio of bicarbonate in the solution does not change due to fractionation processes with time and thus the $\delta^{13}C$ value of the precipitated calcite can be calculated according to Eq. 3.2.1. Since the fractionation factor depends on temperature only, the $\delta^{13}C$ of the precipitated calcite shows a temperature dependence as well. Fractionation in equilibrium occurs favourably in caves with low temperatures and high water supply or small drip intervals respectively.

However, several studies on stalagmites and synthetic carbonates have shown that kinetic fractionation effects occurring during the precipitation of calcite can not be neglected and may even play a major role in affecting the isotopic composition of speleothems (Fantidis and Ehhalt, 1970; Harmon et al., 1979; Usdowski et al., 1979; Wiedner et al., 2007). In addition, a recent publication (Mickler et al., 2006) provided a data set including over 120 samples, whereas 71 % indicate calcite precipitation under disequilibrium conditions[4].

3.2.2 Fractionation under disequilibrium conditions

Fractionation of $\delta^{13}C$ under disequilibrium conditions occurs at higher temperatures and when water supply is limited causing long drip intervals. In this case the isotope ratio of bicarbonate in the solution changes with time since ^{12}C molecules are favourably removed from the solution. Thus, the bicarbonate of the solution and so the precipitated calcite enrich in heavy carbon isotopes. Assuming an irreversible Rayleigh fractionation process during the degassing of carbon dioxide and the precipitation of

[3] In the following $\delta^{13}C_{CaCO_3}$ is written as $\delta^{13}C$ unless otherwise stated.

[4] Note, that Mickler determined the correlation between $\delta^{18}O$ and $\delta^{13}C$ along the growth axis and followed kinetic fractionation from highly correlated samples. This, however, is no obligatory criterion for fractionation under disequilibrium conditions.

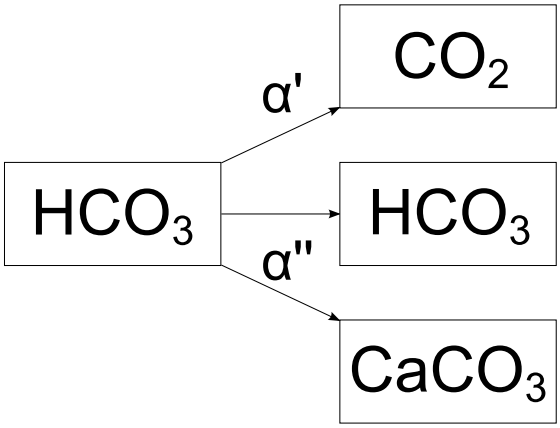

Figure 3.2.1: *The carbon fractionation is described by a Rayleigh process between the species bicarbonate, carbon dioxide and calcium carbonate. The corresponding fractionation factors α can be found in Table 2.4.1.*

calcite, respectively, (see Fig. 3.2.1, Salomons and Mook (1986)) the change of the isotope ratio of bicarbonate can be calculated:

$$R_{HCO_3^-}(t) = R_{HCO_3^-}(0)\ \left(\frac{[HCO_3^-](t)}{[HCO_3^-](0)}\right)^{\overline{\alpha^{13}}-1} \tag{3.2.2}$$

with the combined fractionation factor $\overline{\alpha^{13}} = \frac{\alpha^{13}_{HCO_3^- \rightarrow CaCO_3} + \alpha^{13}_{HCO_3^- \rightarrow CO_2^g}}{2}$ (see Table 2.4.1 for fractionation factors). $R^{13}_{HCO_3^-}(0)$ and $[HCO_3^-](0)$ represent the isotope ratio and concentration of bicarbonate at the time $t = 0$. The isotope ratio of bicarbonate depends strongly on the temporal development of the concentration of bicarbonate, which in turn also depends on mixing processes between the impinging drop and the existing solution layer (Mühlinghaus et al., 2007). The bicarbonate concentration of the solution and thus its isotope ratio changes with time until an equilibrium like state is established. The temporal progression of the mixing process is described in Fig. 3.2.2. At point A the initial solution contains the bicarbonate concentration $\left[HCO_3^-\right]_A$ with an isotope ratio of R_A. During one drip interval d the concentration changes after Eq. 2.2.13 and the isotope ratio after Eq. 3.2.2. A new drop with the concentration $\left[HCO_3^-\right]_{drop}$ and the isotope ratio R_{drop} hits the stalagmite and mixes according to section 2.3:

$$X_{mix} = (1 - \phi)\, X_1 + \phi X_2, \tag{3.2.3}$$

whereas X_1 denotes the concentration or the isotope ratio of bicarbonate in the solution and X_2 the one of the drop. This process is repeated until an equilibrium is established, whereas $\left[HCO_3^-\right]_B$ and R_B act as the new initial values. The iterative process can mathematically be derived by the calculation of several subsequent mixing steps in order to simplify the resulting equation (a proof is given in the Appendix B.1).

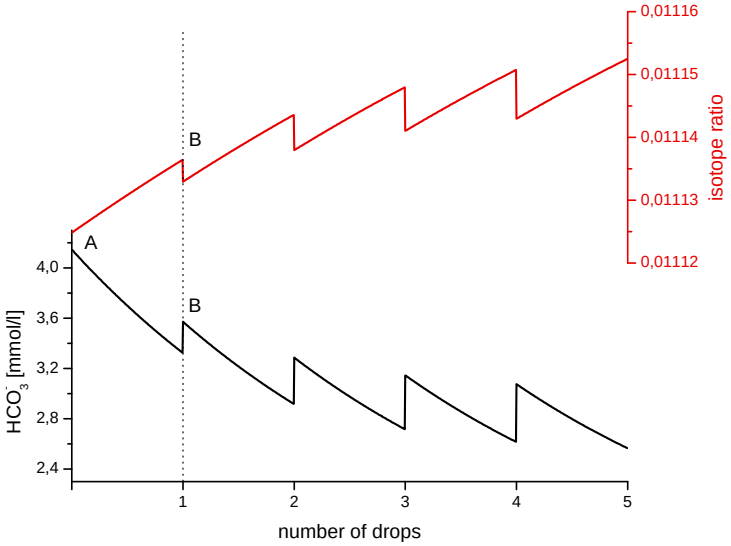

Figure 3.2.2: *Mixing process of the concentration (black) and the isotope ratio (red) of bicarbonate for d=250s, T=10°C, p_{CO_2}=10000ppm and $\phi = 0,3$. See text for details.*

Using Eqs. 2.2.13, 3.2.2 and 3.2.3 yields for the isotope ratio after n drops:

$$R_{HCO_3^-}(n) = \zeta(d, T, \phi, n)\ R_{drop} \tag{3.2.4}$$

with

$$\begin{aligned}\zeta =& (1-\phi)^n \prod_{k=0}^{n-1} \left(\frac{[HCO_3^-](k,d)}{[HCO_3^-](k,0)} \right)^{\overline{\epsilon^{13}}} \\ &+ \phi \sum_{k=0}^{n-1} (1-\phi)^k \prod_{m=n-k}^{n-1} \left(\frac{[HCO_3^-](m,d)}{[HCO_3^-](m,0)} \right)^{\overline{\epsilon^{13}}},\end{aligned} \tag{3.2.5}$$

using $\overline{\epsilon^{13}} = \overline{\alpha^{13}} - 1$. After establishing an equilibrium like state the isotope ratio of bicarbonate is averaged over one drip interval d to obtain the mean isotope ratio during one drip interval (Salomons and Mook, 1986; Mühlinghaus et al., 2007). Together with Eqs. 3.2.1 and 3.2.4 the mean isotope ratio of the precipitated calcite and thus δ^{13}C can be calculated:

$$\delta^{13}C = f_c(\delta^{13}C_{drop} + 1000) - 1000. \tag{3.2.6}$$

with the factor f_c given as:

$$
\begin{aligned}
f_c =& \alpha_2^{13} \frac{1}{\overline{\alpha^{13}}} \frac{\left(\frac{[HCO_3^-](n,d)}{[HCO_3^-](n,0)}\right)^{\overline{\alpha^{13}}} - 1}{\frac{[HCO_3^-](n,d)}{[HCO_3^-](n,0)} - 1} \\
& \times \left((1-\phi)^n \prod_{k=0}^{n-1} \left(\frac{[HCO_3^-](k,d)}{[HCO_3^-](k,0)}\right)^{\overline{\epsilon^{13}}} \right. \\
& \left. + \phi \sum_{k=0}^{n-1} (1-\phi)^k \prod_{m=n-k}^{n-1} \left(\frac{[HCO_3^-](m,d)}{[HCO_3^-](m,0)}\right)^{\overline{\epsilon^{13}}} \right).
\end{aligned} \tag{3.2.7}
$$

Hereby the factor f_c includes mixing processes between the impinging drop and the solution layer, the averaging of the isotope ratio of bicarbonate over one drip interval as well as the fractionation between bicarbonate and precipitated calcite. f_c depends on the drip interval, temperature, the mixing coefficient and the number of drops ($f_c(d, T, \phi, n)$).

3.2.3 Results and discussion

For a sufficient number of drops ($n > 100$) the dependence of δ^{13}C on 0^{th} stage parameters is shown in Fig. 3.2.3. For a constant mixing coefficient $\phi = 0,5$ and $p_{CO_2} = 10000ppm$ δ^{13}C increases with increasing drip interval approaching asymptotically an upper limit. This characteristic can be explained by the extended residence time on top of the stalagmite for long drip intervals resulting in increased CO_2 degassing until the partial CO_2 pressure of the solution layer approaches the value of the surrounding cave air. This in turn enriches the precipitated calcite.

With increasing temperature the drip interval, which is needed to achieve the upper limit of δ^{13}C , becomes shorter and the value of this limit slightly decreases. The faster change of δ^{13}C at high temperatures is due to an increased inner energy of the molecules in the solution, resulting in a reduced time for the conversion of bicarbonate in carbon dioxide and thus an accelerated CO_2 degassing compared to the degassing at low temperatures. For the same reason δ^{13}C increases slightly with increasing temperatures at short drip intervals.
This characteristic of δ^{13}C is also maintained while varying the mixing coefficient ϕ. For a low mixing coefficient only a small amount of the new drop mixes with the existing solution (Fig. 3.2.3d). This results in an longer effective residence time of the water film on top of the stalagmite and thus a higher enrichment of the precipitated δ^{13}C. For high mixing coefficients the residence time of the solution is shortest, which yields a lower enrichment of δ^{13}C.
If soil p_{CO_2} is lowered ($p_{CO_2} = 1000ppm$, Fig. 3.2.3b) the time needed to approach a constant value of δ^{13}C at fixed boundary conditions is reduced, since the gradient

between soil and cave p_{CO_2} is lowered and p_{CO_2} of the solution approaches the value of the surrounding cave air. However, the characteristics of δ^{13}C remains.

It is remarkable that the temperature gradient of δ^{13}C changes from $\frac{\partial \delta^{13}C}{\partial T}\Big|_{d\to 0} > 0$ at small drip intervals to $\frac{\partial \delta^{13}C}{\partial T}\Big|_{d\to\infty} < 0$ at long drip intervals, whereas the drip interval where $\frac{\partial \delta^{13}C}{\partial T}\Big|_{d} = 0$ increases with increasing mixing coefficients. This originates from the following[5]: The factor f_c consists roughly spoken of two factors $f_c^{(1)} = \alpha_2^{13}\frac{1}{\alpha^{13}}\frac{\left(\frac{[HCO_3^-](n,d)}{[HCO_3^-](n,0)}\right)^{\overline{\alpha^{13}}}-1}{\frac{[HCO_3^-](n,d)}{[HCO_3^-](n,0)}-1}$ and $f_c^{(2)}$, which contains the rounded brackets of Eq. 3.2.7. $f_c^{(1)}$ shows a low dependence on the drip interval and increases monotonously with increasing temperature. The characteristics of factor $f_c^{(2)}$ show a strong dependence on the drip interval in such a way that it increases for short drip intervals, but decreases for long drip intervals (after a short increase at low temperatures). This change of the characteristic of $f_c^{(2)}$ is amplified for low mixing coefficients. For small ϕ values the effective residence time of the solution increases, which is similar to a longer drip interval. Thus, in the range of short drip intervals, the factor $f_c^{(1)}$ dominates, whereas for long drip intervals the characteristic of $f_c^{(2)}$ is maintained.

For short drip intervals the isotopic composition of δ^{13}C precipitated under disequilibrium approaches the composition of δ^{13}C under equilibrium conditions[6]:

$$\delta^{13}C_{eq} = \lim_{d\to 0} \delta^{13}C_{de}. \tag{3.2.8}$$

Thus, fractionation under equilibrium conditions can be described as a border case of the more general fractionation under disequilibrium conditions.

[5]Since the δ^{13}C values of the precipitated calcite are correlated linearly to the fractionation factor f_c the following explanation is valid for $\delta^{13}C$ too, however it is more obvious by looking at f_c instead of $\delta^{13}C$.

[6]A proof is given in the Appendix B.1.

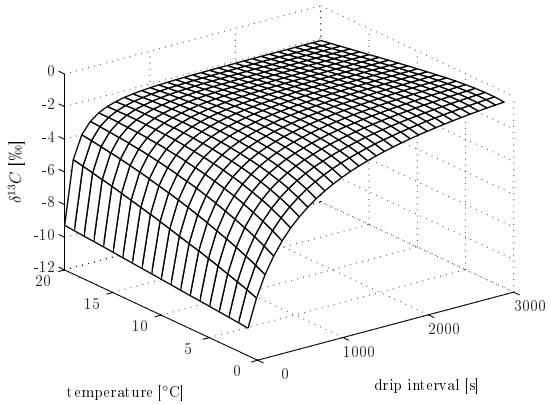

(a) $\phi = 0,1$

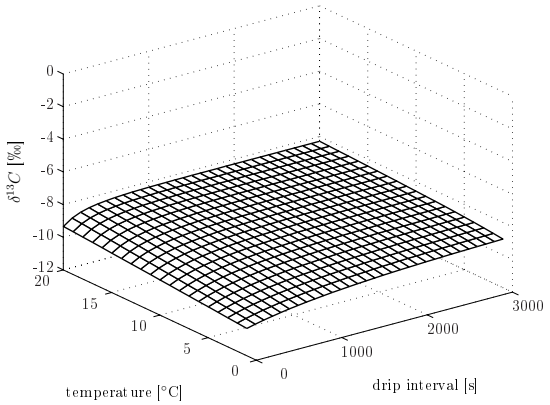

(b) $p_{CO_2} = 1000ppm$

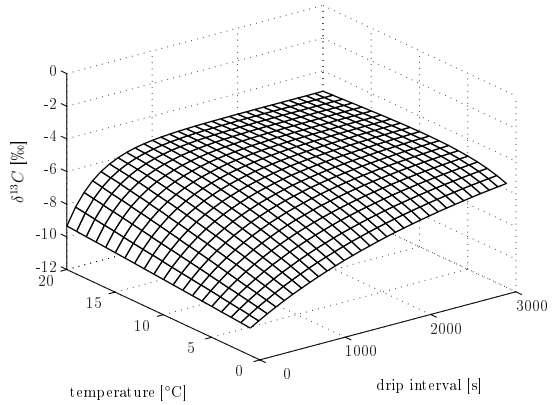

(c) $\phi = 0,5$

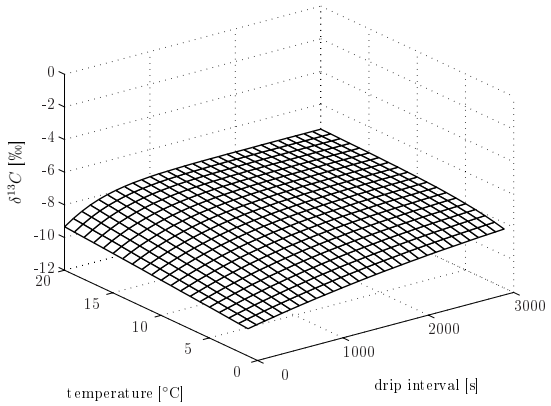

(d) $\phi = 1,0$

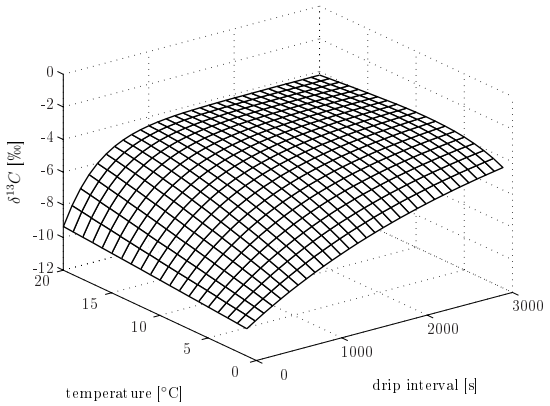

(e) $p_{CO_2} = 20000ppm$

Figure 3.2.3: *The figure shows the enrichment of $\delta^{13}C$ under varying boundary conditions. The figures on the left hand side ((a), (c) and (d)) show the enrichment for a change in the mixing coefficient for a p_{CO_2} value of the soil of 10000ppm. The figures on the right hand side ((b), (c) and (e)) are calculated for a fixed mixing coefficient of $\phi = 0,5$ and varying p_{CO_2} values. Lines are drawn every 100s and every degree centigrade.*

3.3 Oxygen isotope model

During CO_2 degassing and $CaCO_3$ precipitation stable oxygen isotopes are – in analogy to carbon isotopes – fractionated. In contrast to carbon, oxygen can be found in almost any species contained in the solution layer. In particular the large reservoir of water has a significant influence on the isotopic composition of the precipitated calcite.

3.3.1 Fractionation under equilibrium conditions

Under equilibrium conditions the isotope ratios of bicarbonate and the water reservoir are in equilibrium and thus, the fractionation of oxygen during calcite precipitation can be written as:

$$\begin{aligned}
\delta^{18}O &= \left(\frac{\alpha^{18}_{HCO_3^- \rightarrow CaCO_3} R^{18}_{HCO_3^-}}{R_{std}} - 1 \right) \times 1000 \\
&= \left(\frac{\frac{\alpha^{18}_{HCO_3^- \rightarrow CaCO_3}}{\alpha^{18}_{HCO_3^- \rightarrow H_2O}} R^{18}_{H_2O}}{R_{std}} - 1 \right) \times 1000 \\
&= \left(\frac{\alpha^{18}_{H_2O \rightarrow CaCO_3} R^{18}_{H_2O}}{R_{std}} - 1 \right) \times 1000. \qquad (3.3.1)
\end{aligned}$$

The fractionation factors α_i^{18} are given in Table 2.4.2. Since $R^{18}_{H_2O}$ does not change with time, δ^{18}O depends on the temperature dependence of $\alpha^{18}_{H_2O \rightarrow CaCO_3}$ only. Again, this case occurs favourably in caves with low temperatures and small drip intervals. In contrast to ^{13}C the temperature dependence is reversed, i.e. δ^{18}O decreases with increasing temperatures.

3.3.2 Fractionation under disequilibrium conditions

The fractionation of oxygen isotopes under disequilibrium conditions is more complicated than that of carbon isotopes. Due to the large reservoir of water buffer reactions (see Eqs. 3.3.2 and 3.3.3) between bicarbonate and water occur, which might have a significant influence on the isotopic composition of δ^{18}O (Mickler et al., 2004):

Hydration

$$CO_2 + H_2O \rightleftharpoons HCO_3^- + H^+ \qquad (3.3.2)$$

Hydroxylation

$$CO_2 + OH^- \rightleftharpoons HCO_3^- \qquad (3.3.3)$$

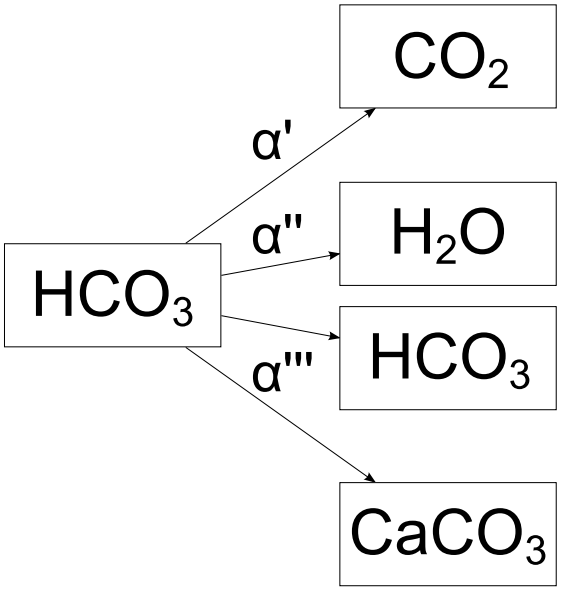

Figure 3.3.1: *The oxygen fractionation is described by a Rayleigh process between the species bicarbonate, carbon dioxide, calcium carbonate and water. The corresponding fractionation factors can be found in Table 2.4.2.*

The resulting fractionation of δ^{18}O in such a natural system lies in between two extreme cases: (i) the system is completely buffered and (ii) no buffer reactions occur in the system. In case (i) the H_2O reservoir buffers the isotopic composition of the bicarbonate in order that the isotope ratios of all species are in equilibrium. This is equivalent to fractionation under equilibrium conditions and can be calculated using Eq. 3.3.1. This results in the minimal possible enrichment of δ^{18}O .

In the second case (ii) the buffer reactions are neglected completely and the isotopic composition of the precipitated calcite can be determined in analogy to the fractionation of carbon by a Rayleigh fractionation process. However, compared to the fractionation of carbon the calculations must be extended by the fractionation between bicarbonate and water according to Eq. 1.2.8 (see Fig. 3.3.1). According to Mickler et al. (2004, 2006) the combined fractionation factor $\overline{\alpha^{18}}$ (compare $\overline{\alpha^{13}}$ in Eq. 3.2.7) is approximated according to the proportion of the oxygen amount of each product (see Eq. 1.2.8 and Fig 2.4.2): $\overline{\alpha^{18}} = \frac{2}{6}\alpha^{18}_{HCO_3^- \rightarrow CO_2^g} + \frac{3}{6}\alpha^{18}_{HCO_3^- \rightarrow CaCO_3} + \frac{1}{6}\alpha^{18}_{HCO_3^- \rightarrow H_2O}$. This results in a temperature dependent combined fractionation factor $\overline{\alpha^{18}}$.

To describe the influence of the buffer reactions in a mathematical way a buffer parameter b is adopted. Hereby a system, which is completely buffered, is described by a buffer parameter of $b = 1$, a system, where no buffer reactions occur, is described by a buffer parameter of $b = 0$. Thus, b determines the strength of the influence of the buffer

reactions. As a first approach b is included with a linear dependence[7]:

$$f_o(b) = b \cdot (f_o(b=1) - f_o(b=0)) + f_o(b=0), \tag{3.3.4}$$

Analogues to the calculation of f_c, a factor f_o for the oxygen system is determined. f_o is obtained by replacing the carbon fractionation factors by the oxygen fractionation factors in Eq. 3.2.7. For a system, which shows no buffering effects, the maximal value of $f_o(b=0)$ is obtained:

$$\begin{aligned} f_o(b=0) =& \alpha_2^{18} \frac{1}{\overline{\alpha^{18}}} \frac{\left(\frac{[HCO_3^-](n,d)}{[HCO_3^-](n,0)}\right)^{\overline{\alpha^{18}}} - 1}{\frac{[HCO_3^-](n,d)}{[HCO_3^-](n,0)} - 1} \\ & \times \left((1-\phi)^n \prod_{k=0}^{n-1} \left(\frac{[HCO_3^-](k,d)}{[HCO_3^-](k,0)}\right)^{\overline{\epsilon^{18}}} \right. \\ & \left. + \phi \sum_{k=0}^{n-1} (1-\phi)^k \prod_{m=n-k}^{n-1} \left(\frac{[HCO_3^-](m,d)}{[HCO_3^-](m,0)}\right)^{\overline{\epsilon^{18}}} \right). \end{aligned} \tag{3.3.5}$$

As shown for $\delta^{13}C$ (Eq. 3.2.8), fractionation under equilibrium conditions can be approximated by fractionation under disequilibrium conditions for short drip intervals. Thus, the value of $f_o(b=1)$ for a system, which is completely buffered, can also be approximated by $f_o(b=0)$ of a no buffer system for very short drip intervals:

$$f_o(b=1) = \lim_{d \to 0} f_o(b=0). \tag{3.3.6}$$

The resulting values of f_o for the two extreme cases confine the possible range of f_o in natural systems. The influence of the buffer reactions on f_o according to Eq. 3.3.4 is illustrated for an exemplary temperature of $T = 5°C$ and a mixing coefficient of $\phi = 0,5$ in Fig. 3.3.2. For $b = 1$, which represents a completely buffered system, f_o is described by the lowest curve with a constant value. With decreasing b f_o increases to the upper limit ($b = 0$), which represents a system, where no buffer reactions occur.

In analogy to the fractionation process of carbon this fractionation factor f_o includes mixing processes between the impinging drop and the existing solution layer, the averaged mean isotope ratio of the quasi equilibrium state as well as the fractionation between the solution and calcite. The relationship between the isotope ratio of the precipitated calcite and the isotope ratio of the drip water can be written as:

$$\delta^{18}O = \frac{f_o}{a}(\delta^{18}O_{drop} + 1000) - 1000, \tag{3.3.7}$$

[7]For reasons of clarity the dependence of f_o on d, T, ϕ and n is not mentioned here.

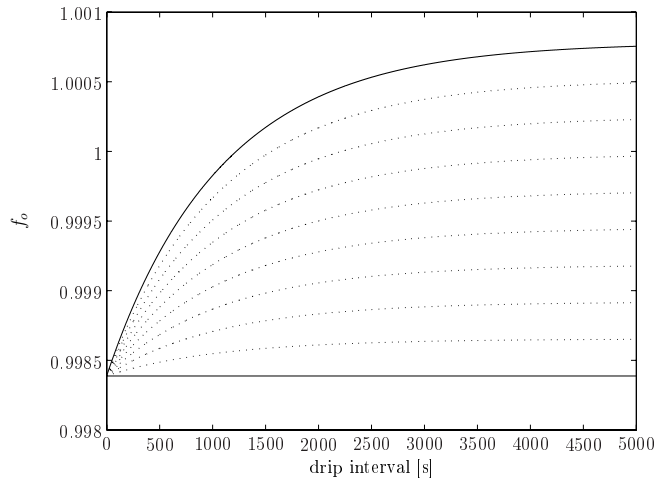

Figure 3.3.2: *The influence of the buffer parameter on f_o for T = 5°C and $\phi = 0.5$. As a first approach the influence of b on f_o is assumed linearly (see Eq. 3.3.4). The uppermost curve represents a buffer parameter of $b = 0$ (straight line). The subsequent curves to lower values of f_o result from an increasing buffer parameter in steps of 0,1 (dotted lines). The lowest curve represents a system which is completely buffered ($b = 1$, straight line). Since the buffer reactions do not have any influence on f_o for very short drip intervals, f_o of a buffered system can be approximated by $\lim_{\Delta T \to 0} f_o$ of a no buffer system.*

whereas a is the conversion factor between the isotope standards R_{VPDB} (δ^{18}O values of carbonates) and R_{VSMOW} (δ^{18}O values of water):

$$a = \frac{R_{VPDB}}{R_{VSMOW}}. \tag{3.3.8}$$

3.3.3 Results and discussion

The dependence of the upper limit of δ^{18}O (no buffering) on drip interval, temperature, mixing coefficient and soil p_{CO_2} is shown in Fig. 3.3.3. For very low mixing coefficients δ^{18}O shows a strong temperature dependence (see Fig. 3.3.3a). However, the temperature dependence changes with increasing drip intervals slightly. For $\lim_{d \to 0} \delta^{18}O$ the temperature characteristics becomes equal to the characteristics under equilibrium conditions. The influence of the drip interval on δ^{18}O varies and is minimal for low temperatures and increases with increasing temperatures. With increasing mixing coefficients these dependencies are attenuated, since low mixing coefficients extend the residence time of the solution on top of the stalagmite, whereas high mixing coefficients reduce this effect. If the soil p_{CO_2} is lowered from $p_{CO_2} = 10000ppm$ (Figs. 3.3.3a and 3.3.3d) to $p_{CO_2} = 1000ppm$ (Fig. 3.3.3e) the characteristics of δ^{18}O is similar to the characteristics at high mixing coefficients. However, the time needed to obtain a constant δ^{18}O value is reduced, since the p_{CO_2} pressure of solution is already close to equilibrium with the surrounding p_{CO_2} pressure of the cave.

T [°C]	$k_{avg}(10^{-3}\ \mathrm{min}^{-1})$	$t_{1/2}$ (min)	$t_{.99}$ (hr)
15	3,2	216	24
25	8,6	81	8,9
40	45	15	1,7

Table 3.3.1: *Exchange kinetics between bicarbonate and water according to Beck et al. (2005). $t_{1/2}$ gives the time needed to exchange 50% between the involved species, $t_{.99}$ the time needed to exchange 99%.*

A comparison of the dependencies of δ^{13}C and δ^{18}O on these parameters reveals that oxygen shows a more pronounced dependence on temperature than carbon. This is reasonable, since both isotopic values are calculated on the same basis (Eq. 3.2.7, 3.3.5). The only differences between the two isotopes are the fractionation factors and their dependence on temperatures. According to Table 2.4.2 the fractionation factors of oxygen show a stronger dependence on temperature than the fractionation factors of carbon. This results in the different temperature dependence of the δ^{13}C and δ^{18}O values of the precipitated calcite, whereas the influence of the other parameters on δ^{13}C and δ^{18}O is comparable.

Note
The influence of the buffering water reservoir on the isotopic composition of bicarbonate and especially the time constant of this process is unknown. However, some measurements can be found in recent literature (Beck et al., 2005). They measured the exchange kinetics between bicarbonate and water for different temperatures and determined the fraction of isotopic exchange F in δ^{18}O between these two compounds, which describes the degree of exchange with time:

$$F = \frac{\delta^{18}O(t) - \delta^{18}O(0)}{\delta^{18}O(\infty) - \delta^{18}O(0)}, \tag{3.3.9}$$

where $\delta^{18}O(t)$ is the isotopic composition of bicarbonate at the time t, $\delta^{18}O(0)$ the initial value of δ^{18}O and $\delta^{18}O(\infty) = \delta^{18}O_{eq}$ the value, which is obtained after reaching isotopic equilibrium. The dependence of F on time and temperature is according to Beck et al. (2005):

$$\ln(1 - F) = -k_{avg}t, \tag{3.3.10}$$

with the rate constant k_{avg} (Criss, 1999), which comprises many forward and backward reactions (Arrhenius law):

$$k_{avg} = A_0 e^{-\frac{E_a}{RT_k}}, \tag{3.3.11}$$

with $A_0 = 1,85 \times 10^{12} min^{-1}$, the apparent activation energy $E_a = 81,6 kJ/mol$, the ideal gas constant R and temperature in Kelvin. This yields that for typical cave temperatures of smaller than 20°C the isotopic exchange of oxygen between bicarbonate and water would have only a small influence on the isotopic composition of bicarbonate and the precipitated calcite respectively (see Table 3.3.1). This assumption will be confirmed in section 4.5 for natural data sets.

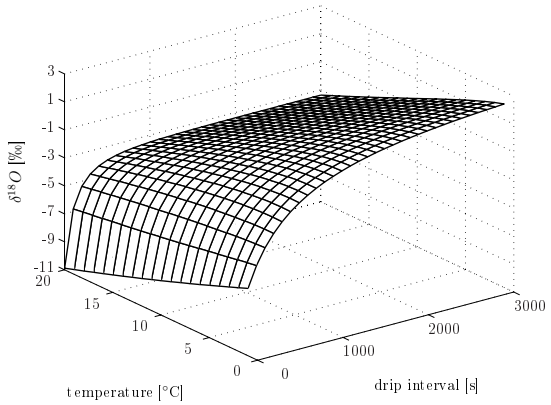

(a) $\phi = 0,1$

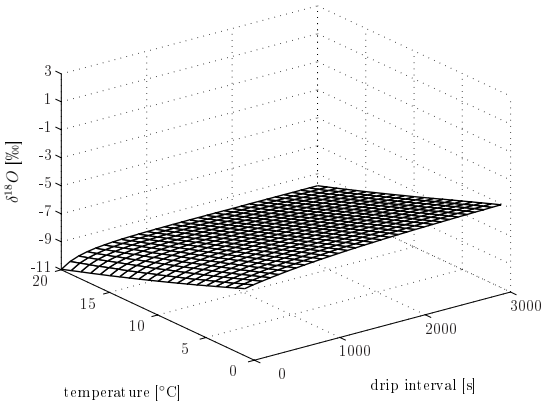

(b) $p_{CO_2} = 1000ppm$

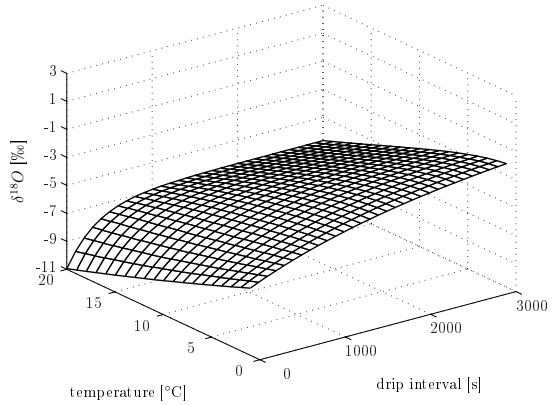

(c) $\phi = 0,5$

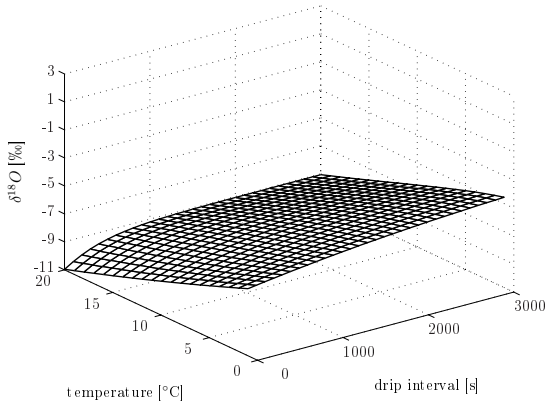

(d) $\phi = 1,0$

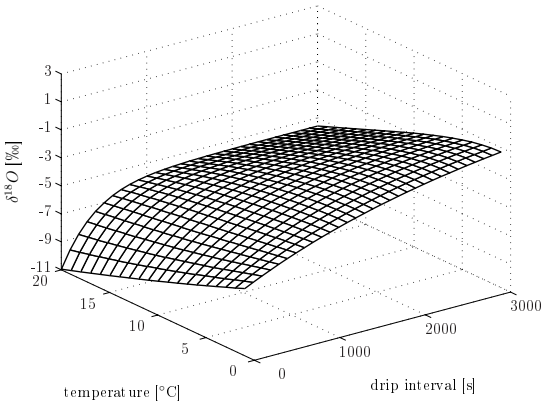

(e) $p_{CO_2} = 20000ppm$

Figure 3.3.3: *The figure shows the enrichment of $\delta^{18}O$ under varying boundary conditions. The figures on the left hand side ((a), (c) and (d)) show the enrichment for a change in the mixing coefficient for a p_{CO_2} value of the soil of 10000ppm. The figures on the right hand side ((b), (c) and (e)) are calculated for a fixed mixing coefficient of $\phi = 0,5$ and varying p_{CO_2} values. Lines are drawn every 100s and every degree centigrade.*

3.4 Multi-box-model

Until 2006 there was no appropriate model describing the temporal movement of the solution layer on top of the stalagmite. However, this is essential to determine the enrichment of stable isotopes along individual growth layers. To overcome the problem of the missing time-place link of the existing models a multi-box-model was developed (Mühlinghaus, 2006; Mühlinghaus et al., 2007). The multi-box-model is based on the decoupling of the movement of the solution from the chemical and physical processes occurring in the solution. This keeps the model in a general and all-purpose way. First the movement of the solution on top of the stalagmite is derived, whereas in the second part growth is described as a first application of the multi-box-model (see section 3.4.1).

Assuming a fixed size of the drop volume and the film thickness, one drop covers a specific area on the stalagmite. This area is defined as one box. Ideally, the surface of a stalagmite can be described by concentrical circles, whereas each annulus matches with the area covered by one drop. In a one-dimensional profile the difference of the radii of adjacent circles determines the box sizes (see Fig. 3.4.1). The radius of the circle with an area equivalent to the area covered by i drops is given by:

$$r_i = \sqrt{\frac{i\,V}{\pi\,\delta}}. \tag{3.4.1}$$

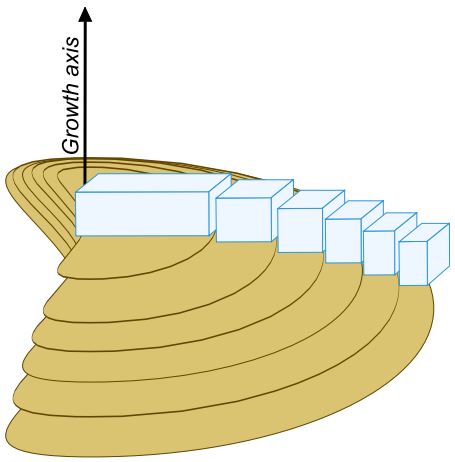

Figure 3.4.1: *Distribution of the boxes representing the solution layer on top of the stalagmite. Due to the rotational symmetry only one half of the stalagmite is shown. The annuli are equivalent to the area one drop would cover. Thus, the box sizes are defined by the volume of the drop and the film thickness of the solution layer. Their number is limited to the equilibrium radius of the stalagmite.*

Using this radius boxes are constructed to divide the solution layer into individual attached parts. The number of boxes is limited to the equilibrium radius of the stalagmite and does not exceed ten in our calculations. In analogy to section 2.3, mixing between

the falling drop and the innermost box is described by the mixing coefficient ϕ. In addition mixing between the individual boxes is allowed and described by individual mixing parameters ϕ_i (for box_i, $i \in [2,10]$). These ϕ_i describe, analogically to ϕ, the percentage of the solution in the inner adjacent box_{i-1} mixing with $(1-\phi_i)$ percent of the solution in box_i. Thus, high values of ϕ_i describe rather a substitution of the outer boxes by the inner ones. On the other hand, low values indicate splashing of the solution of the inner boxes to outer boxes or even apart the stalagmite. An exemplary mixing process between the drop and the two innermost boxes is illustrated in Fig. 3.4.2 with mixing coefficients $\phi = 0.8$ and $\phi_2 = 0.3$. The impinging drop contributes 80% (ϕ) of its solution to box_1, whereas its remaining 20% (i.e. $(1-\phi)$) splash or move further out without interacting with box_1. 20% of the solution in box_1 are kept and mix with 80% of the drop's solution. The remaining 80% of the solution in box_1 are pushed outwards. Now a simplification of the mixing process is made. The remaining 20% of the solution of the drop mix with the removed 80% of the solution of box_1. This might occur due to splashing effects. Thus, the mixed solution of box_1 is given as: $box_1^{mix} = (1-\phi)box_1 + \phi drop$. To fulfill the mass balance, the overflow of the mixing process between the drop and box_1 is defined as: $box_1^{overflow} = \phi box_1 + (1-\phi)drop$. In the example in Fig. 3.4.2, this mixed overflow solution contributes 30% (ϕ_2) to box_2, which keeps 70% (i.e. $(1-\phi_2)$) of its existing solution. The resulting overflow of this mixing process moves outwards to the next box and the process is continued. Under this assumption the mass balance of the mixing process is fulfilled and even splashing of solution parts of the drop or inner boxes to outer boxes can be explained by low mixing coefficients. Hereby, the mixing process is assumed to proceed in a short time, which can be neglected in comparison to natural drip intervals.

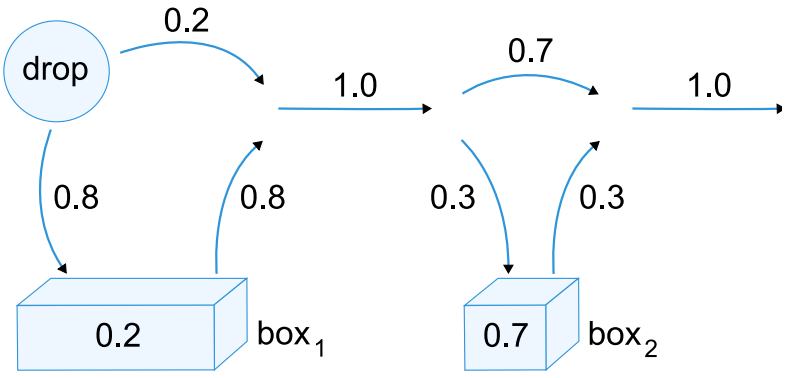

Figure 3.4.2: *Schematic illustration of the mixing process between the drop and the two innermost boxes. The numbers represent the mixing coefficients between the corresponding solutions, the arrows their flow directions. For a detailed description of the mixing process see text.*

Assuming a stagnant film, the solution moves only, if a new drop hits the innermost box. Therefore, the movement of the solution becomes dependent on drip interval and

thus on time. Due to the decoupling of the solution movement from inner (chemical or physical) processes of the solution, this box model is widely applicable. The mixing parameters ϕ_i depend on the equilibrium radius and therefore on temperature, drip interval and the mixing parameter ϕ. Since the additional mixing parameters ϕ_i raise the degrees of freedom of the model, they have to be calibrated.

3.4.1 Calibration of the multi box model

A crucial point of the multi-box-model are the values of the individual mixing coefficients ϕ_i. As described in section 3.4 these coefficients determine the mixing process between the individual boxes and are therefore essential for the calculation of growth or isotopic enrichment along a growth layer. However, their values are not known and thus a reference model is needed to calibrate the multi-box-model in order to obtain the values of ϕ_i. These values are not fixed and can vary depending on the shape of the stalagmite and thus on drip interval, temperature and mixing coefficient ϕ. The following calibration procedure is performed for both growth models, the one using an exponential and the one using a Gaussian ansatz.

The calibration of the different ϕ_i is realized by setting calcite precipitation as the inner process of the solution layer. In analogy to section 2.2, the temporal development of calcium excess is assumed to decrease according to:

$$[Ca^{2+}]_{ex} = [Ca^{2+}]^0_{ex} e^{-\frac{\alpha t}{\delta}}. \tag{3.4.2}$$

Using this equation for the solution in the boxes and applying the mixing process of the multi box model, the calcium excess concentration in each box can be determined. The direction of growth in each box must be orthogonal to the underlying surface and can be calculated according to section 3.1, whereas $[Ca^{2+}]^0_{ex}$ must be replaced by the concentration in the corresponding box. Since the position of the boxes is fixed (see equation 3.4.1), only the vertical component of the growth contributes to the growth in each box. Iterating these mixing and growth processes, the shape of the stalagmite is calculated until an equilibrium shape is established.

In order to optimize the mixing coefficients ϕ_i, the height in each box, calculated by the multi box model, is compared to the height at the corresponding radius computed by the stalagmite growth model (see Fig. 3.4.4). However, the mixing coefficients influence the calcium concentration in each box and so the shape of the stalagmite. Hence, the mixing coefficients need to be calculated iteratively starting with the inner coefficient ϕ_2, followed by ϕ_3 and so on. By this iterative adjustment of the box model to the growth model, the mixing parameters ϕ_i are optimized (see Fig. 3.4.5). This yields a database (see Appendix C.1) for the values of ϕ_i, which depends only on the equilibrium radius R_{mix} of the stalagmite and the mixing coefficient ϕ of the innermost box.
Comparing the multi box model to the exponential and Gaussian growth model yields values of ϕ_i, which decrease with increasing distance from centre and thus the outer boxes receive less overflow solution from the inner boxes (see Fig. 3.4.5). This is required to mimic the exponential or Gaussian decrease of the maximum growth used in the stalagmite growth model. For small radii growth can only be calculated in the inner boxes of the box model resulting in $\phi_i = 0$ for the outer boxes in these cases. To avoid conflicts during the calculation of ϕ at boxes near the radius, the number of calibrated boxes are restricted to 80% of the equilibrium radius. Values of ϕ_i are determined with a precision of $0,01$.

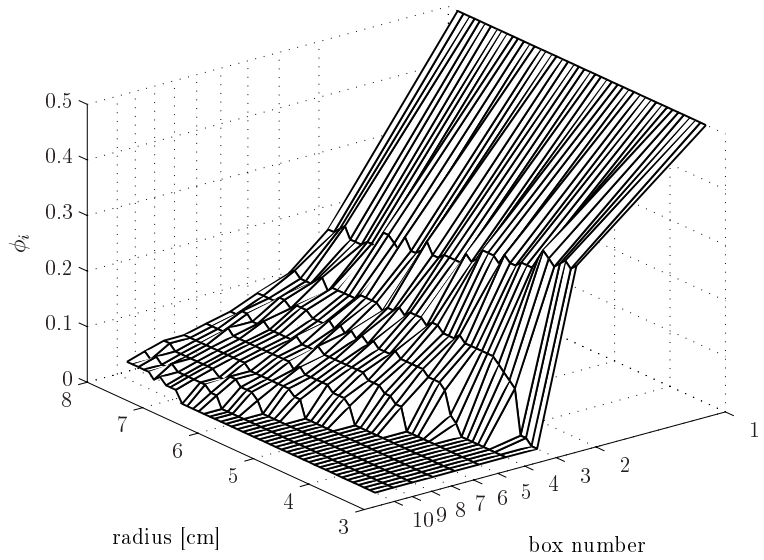

Figure 3.4.3: *Excerpt of the data base of ϕ_i for a mixing coefficient of $\phi = 0,5$ in dependence on the equilibrium radius for all boxes of the multi-box-model.*

The dependence of ϕ_i on the radius is exemplarily shown for a mixing coefficient of $\phi = 0,5$ calibrated to the exponential growth model (see Fig. 3.4.3). With increasing box numbers the ϕ_i decrease to mimic the exponential growth model. With decreasing radius due to a change in temperature or drip interval the number of boxes is reduced. The coefficients ϕ_i slightly increase for box 2, whereas for the outer boxes the coefficients are approximately at a constant value except for the outermost box, which approaches zero. The mixing coefficients of the outer boxes depend strongly on the mixing coefficient of the innermost box ϕ.

To determine values of ϕ_i at radii between two calibrated radii a linear interpolation of the adjacent ϕ_i values is used for the calibration with the exponential growth model (see Mühlinghaus et al. (2007). This interpolation procedure is used for two reasons: (i) the possibility of outlying ϕ_i due to computation accuracy is small and (ii) the approach of an exponential fit of the calculated ϕ_i in dependence on R represents the ϕ_i very well, but only in a specific range. If, however, ϕ_i approaches zero, the error made by the fitting process exceeds 100%, which is not useful for further model applications.

The calibration of the multi box model with the Gaussian growth model is restricted to values of ϕ smaller than 0,8. This can be explained by the shape of the stalagmite calculated with this model (see Figs 3.1.6). In comparison to the exponential growth model the shape of this model reveals a rather plane shape at the apex, which proceeds outwards. This requires that the multi box model yields an almost equal growth at the inner boxes. However, if the mixing coefficient of the innermost box approaches one, the overflow $(1 - \phi)$ to box 2 and the outer boxes approaches zero. This means that

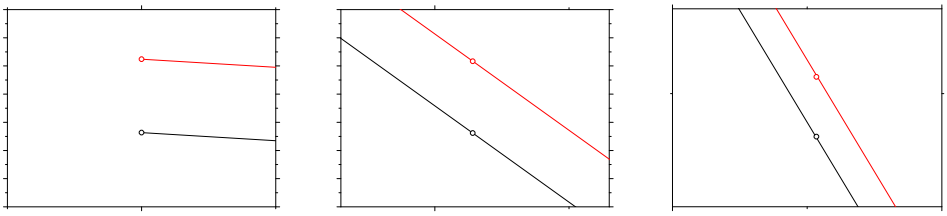

(a) *Box 1* **(b)** *Box 2* **(c)** *Box 8*

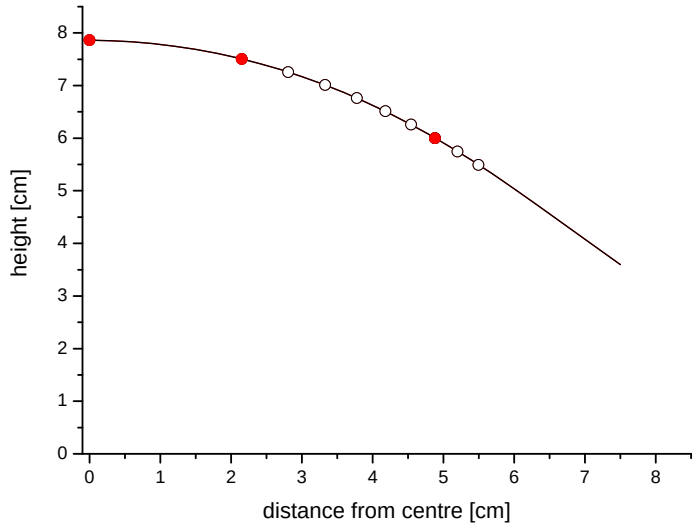

(d) *All Boxes*

Figure 3.4.4: *The growth model is run either with the exponential or the Gaussian ansatz until an equilibrium shape is obtained. The equilibrium shape of the growth model is obtained earlier at the location of the inner boxes and at the latest at the location of the outermost box. The criterion for an equilibrium shape is the comparison of the difference between two subsequent layers at box i with the difference at the apex (box 1). If the differences are equal, equilibrium is reached and the shape only gains on height without changing its form. The figure shows the shape of the stalagmite at the time, when it has reached the equilibrium shape at box 2 (Fig. (b)), whereas an outer box (box 8) is still not in equilibrium (Fig. (c)). (I.e. the differences of the layers shown in Figs. (a) and (b) are indentical, whereas the difference shown in Fig. (c) is still smaller than in Fig. (a)). Fig. (a), (b) and (c) have the same dimensions and can therefore be compared. The old layer is indicated by the black line, the new layer by the red one. The position of the boxes are circled. The layers represent the development of the shape after one drop. Thus, they can not be distinguished in Fig. (d).*

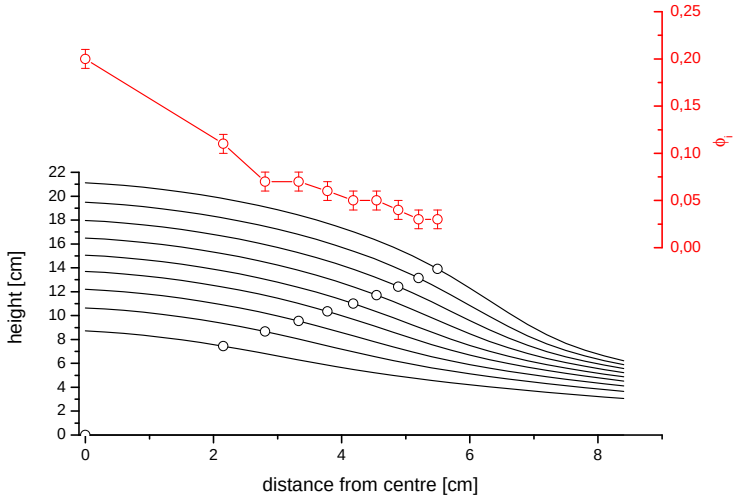

(a) *Exponential ansatz*

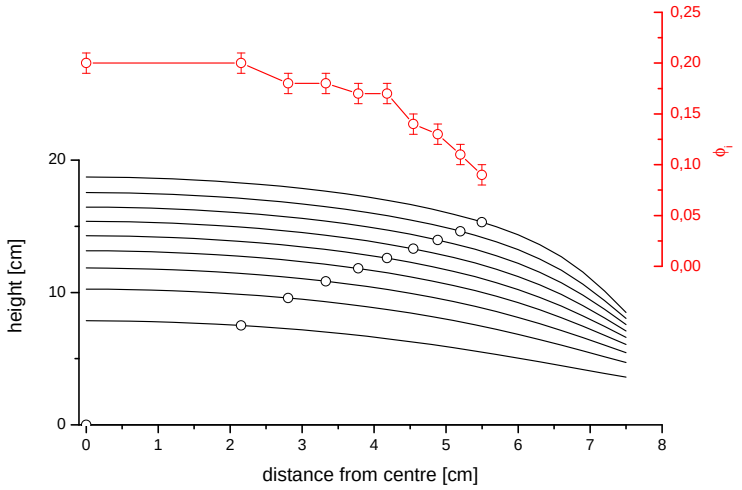

(b) *Gaussian ansatz*

Figure 3.4.5: *This figure exemplarily shows the calibration of the mixing coefficients ϕ_i for a given drip interval d = 100s, temperature T = 1°C, mixing coefficient ϕ = 0,2 and p_{CO_2} = 10000ppm. In this case, growth is calculated for ten boxes and, accordingly, ϕ_i can be adjusted for all boxes. The black lines represent the growth calculated by the stalagmite growth model with an exponential (Fig. (a)) and a Gaussian ansatz (Fig. (b)). To adjust the ϕ_i at box$_i$, an equilibrium shape at the corresponding box must have been established. Since the state of equilibrium is established earlier for the inner boxes, box$_2$ is calibrated first (represented by the lowest line), then, box$_3$ is calibrated (represented by the following line) and so on. The growth of the multi box model at the box centers calculated with the calibrated ϕ_i is illustrated by the black circles. The red line shows the values of the adjusted ϕ_i with increasing distance from centre for this particular calibration.*

box 1 receives most of the impinging drop and therefore most of the calcium, whereas the outer boxes lack of calcium. This results in a high growth at the inner box, but a diminished growth at all other boxes. Thus, the multi box model can not mimic the shape calculated by the Gaussian growth model for all values of the mixing coefficient ϕ.

Note
The growth of the stalagmite growth model by Dreybrodt (1999) and Kaufmann (2003) is slightly different to the growth of the multi-box model at box_1. This is due to the influence of λ on the calcium concentration in the solution layer. The growth model uses the equilibrated calcium excess concentration for growth calculation, whereas the multi box model uses the "real" calcium excess concentration. Thus, the equilibrium concentration of the box model must first be established, which takes up to 100 drops. This different starting condition results in a slightly increased growth calculated by the multi box model in comparison to the stalagmite growth model. However, after establishing an equilibrated calcium concentration in the box model the difference of the two models in growth is constant and does not change with time.

To reduce computation time the growth model is only calculated up to the equilibrium radius. Since the boundary conditions do not change during one calibration procedure the x-values of the polygon of the growth model can be fixed at equidistant points. This simplifies the calculations and accelerates the calibration. To check, if the shape has already reached an equilibrium state the differences between two adjacent layers or the growth at all boxes during one drip interval respectively is determined. The differences of the outer boxes is compared to the difference of the layers at the apex. At equilibrium the differences at all boxes are equal to the one at the apex (see Fig 3.4.4). This calculation is performed with an accuracy of $0,01\mu m$.

3.5 Isotopic profiles along individual growth layers

To calculate the isotopic composition of the calcite, which is precipitated along an individual growth layer, the principles of isotope fractionation of section 3.2 and 3.3 are applied to the multi-box-model. With increasing distance from centre the rare isotopes enrich due to the increased residence time and the ongoing degassing of light CO_2 from the solution on top of the stalagmite. To calculate the isotope ratios in the outer boxes and along the layer respectively, the database of ϕ_i is used. For a given drip interval, temperature and mixing coefficient of the inner box, the corresponding ϕ_i are extracted from this database. Note, that if the radius of the stalagmite changes due to a change in drip interval, temperature or mixing coefficient, the number of the calculated boxes changes as well.

3.5.1 Carbon profile

The influence of drip interval, temperature, CO_2 pressure of the soil and the mixing coefficient on the δ^{13}C value of the calcite is shown in Fig. 3.5.1. Thereby all parameters are fixed except the one which is varied. The fix values of these parameters are: $d = 100s$, $T = 10°$C, $\phi = 0,1$, p_{CO_2} = 10000ppm and $\delta^{13}C = -10‰$. The short drip interval is chosen in order to calculate δ^{13}C for as many boxes as possible. If an increased drip interval is used, the radius decreases, which leads to less boxes (see Fig. 3.5.1a).

The range of the parameters is chosen in order to obtain as many boxes as possible. This makes it easier to investigate the influence of these parameters on the enrichment of δ^{13}C . Most of the figures show an enrichment of δ^{13}C with a rather linear increase. This is due to the low mixing coefficient of $\phi = 0,1$, which can be seen in Fig. 3.5.1d. If the mixing coefficient is raised, the profile of δ^{13}C approaches the characteristics of a second order polynomial, whereas for low mixing coefficients the linear profile is maintained. Thus, the mixing coefficient seems to be the driving force for the profile of the enriched calcite. Since many measured profiles show a linear behaviour rather than a second order polynomial, the low mixing coefficient is chosen to investigate the influence of the other parameters on the enrichment of δ^{13}C .

To compare the slopes of the different results the innermost point (box 1) is neglected. This is due to the behaviour for high mixing coefficients. This is due to the fact that even for high values of ϕ the isotopic profile can be approximated linearly, if the innermost box is neglected.

Fig. 3.5.1a shows the influence of the drip interval on δ^{13}C . The slope changes slightly from short drip intervals ($\approx 0,10\ ‰/mm$) to long drip intervals ($\approx 0,04\ ‰/mm$). However, the overall change is small. Temperature has almost no influence on the enrichment of δ^{13}C as it can be seen in Fig. 3.5.1b. The slope changes from $\approx 0,07\ ‰/mm$ at low temperatures to $\approx 0,10\ ‰/mm$ at high temperatures. In contrast to these parameters the influence of the CO_2 content of the soil is notable. For low values of p_{CO_2} the

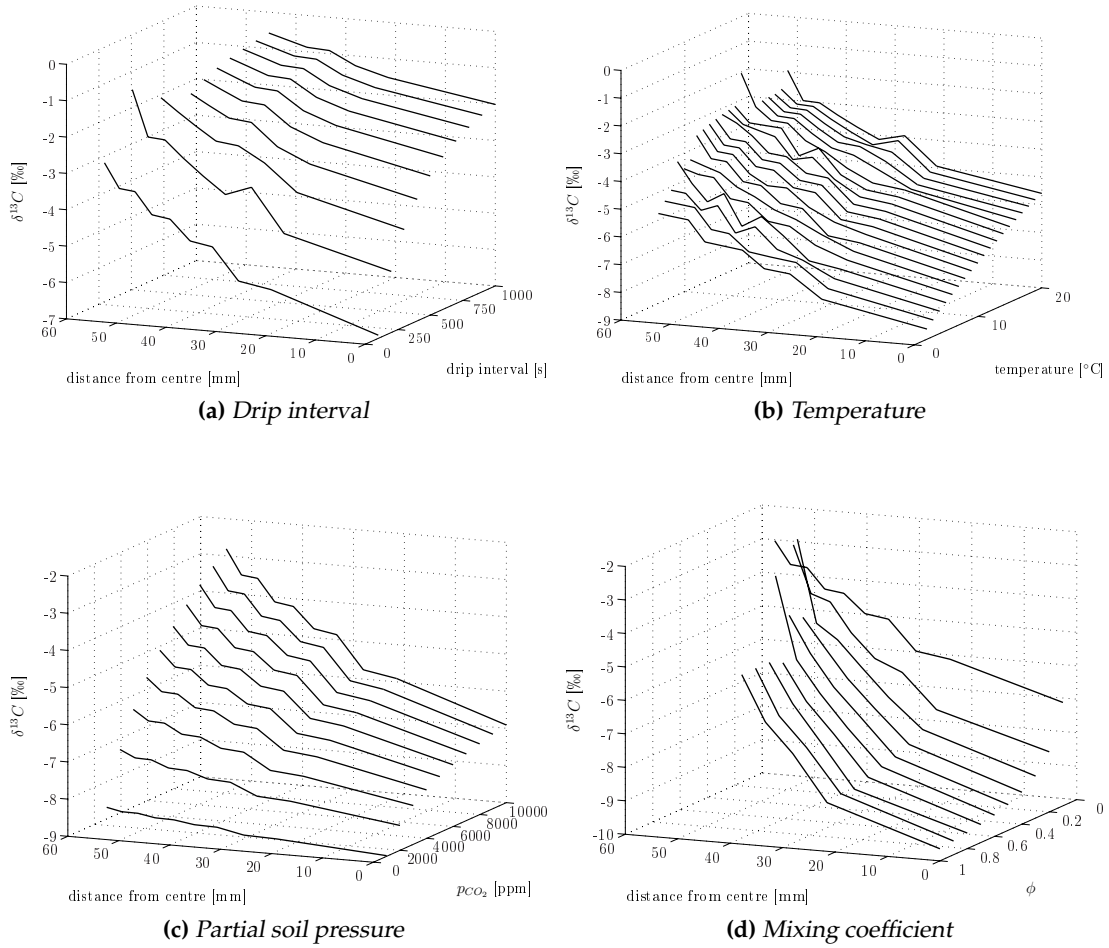

(a) *Drip interval* **(b)** *Temperature*

(c) *Partial soil pressure* **(d)** *Mixing coefficient*

Figure 3.5.1: *Enrichment of $\delta^{13}C$ along an individual growth layer. Values are calculated for $d = 100s$, $T = 10°C$, $\phi = 0,1$, $p_{CO_2} = 10000ppm$ and $\delta^{13}C = -10‰$.*

slope is $\approx 0{,}01$ ‰$/mm$ and increases for high values up to $\approx 0{,}09$ ‰$/mm$ (Fig. 3.5.1c). Fig. 3.5.1d finally shows the influence of the mixing coefficient on the slope, which is compared to the other parameters the most significant. For low mixing coefficients the slope is $\approx 0{,}09$ ‰$/mm$ and increases to $\approx 0{,}22$ ‰$/mm$ for high coefficients.

Please note, that the absolute values of these slopes change, if any boundary conditions are changed. These exemplified results shall give an understanding, which parameter might influence the slope and which might not. The jagged characteristic of some of the profiles is caused by the calibrated mixing coefficients ϕ_i. Since these coefficients are determined with an accuracy of 0,01, there might occur steps in their profile, which manifests in the modeled δ^{13}C values. This can be seen in Fig. 3.5.1b, where the radius changes due to a temperature variation. This leads to different ϕ_i data sets, which in turn explain the jagged δ^{13}C profile along the growth layer. However, this calibration uncertainty is averaged out, if the slope of the δ^{13}C enrichment is investigated.

3.5.2 Oxygen profile

The influence of drip interval, temperature, CO_2 pressure of the soil, buffer parameter and the mixing coefficient on the δ^{18}O value of the calcite is shown in Fig. 3.5.2. In analogy to carbon all parameters are fixed except the one which is varied. The fixed values of these parameters are: $d = 100s$, T = 10°C, $\phi = 0,1$, p_{CO_2} = 10000ppm, $b = 0,5$ and $\delta^{18}O = -10‰$. Again, the short drip interval is chosen in order to calculate δ^{13}C for as many boxes as possible.

In analogy to the enrichment of δ^{13}C the enrichment of δ^{18}O shows the same behaviour for the investigated parameters, however, the absolute values of the slopes change. In case of the drip interval the slope ranges between 0,045 – 0,020 ‰$/mm$, for temperature between 0,030 – 0,045 ‰$/mm$, for the p_{CO_2} of the soil between 0,005 – 0,040 ‰$/mm$ and for the mixing coefficient between 0,040 – 0,100 ‰$/mm$. The unique parameter of oxygen, the buffer parameter, shows also a change in the slope, which is not astonishing, since this parameter is based on a linear interpolation between two end members. This slope ranges between 0,085 – 0 ‰$/mm$. Again, the absolute values of these slopes are exemplarily and depend on the boundary conditions.

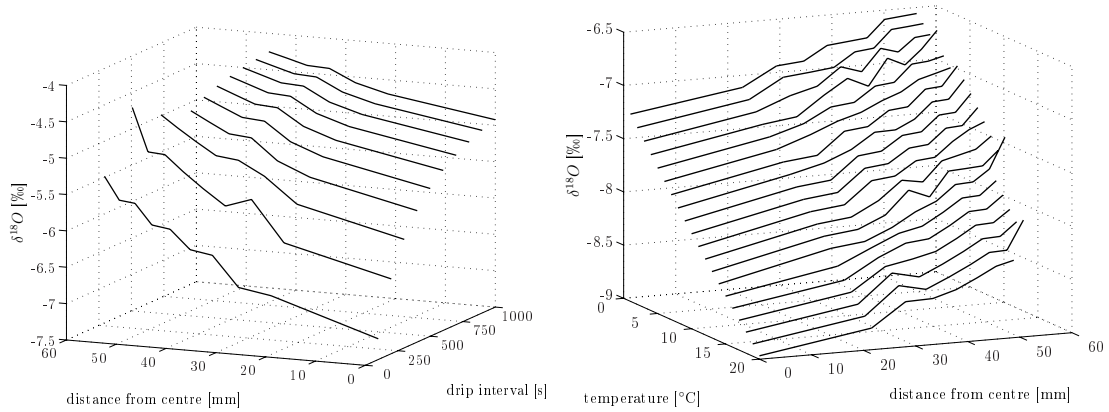

(a) *Drip interval* **(b)** *Temperature*

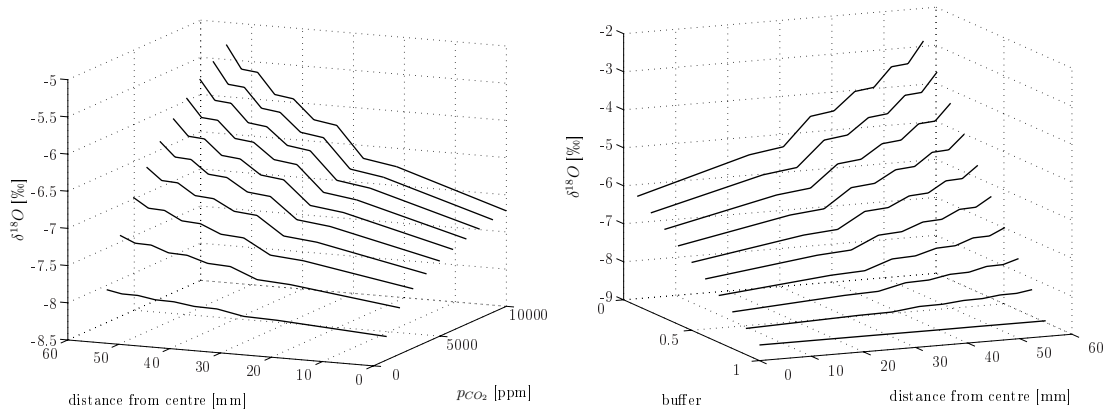

(c) *Partial soil pressure* **(d)** *Buffer parameter*

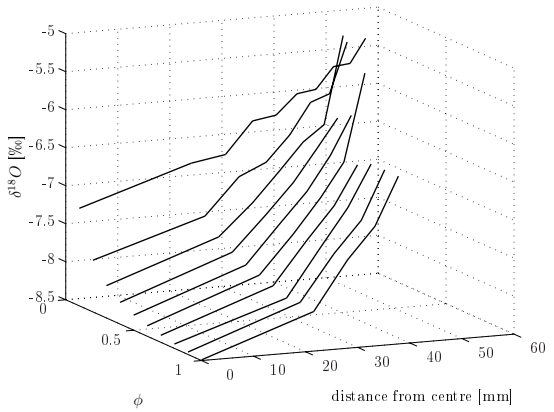

(e) *Mixing coefficient*

Figure 3.5.2: *Enrichment of $\delta^{18}O$ along an individual growth layer. Values are calculated for $d = 100s$, $T = 10°C$, $\phi = 0,1$, $p_{CO_2} = 10000ppm$, $b = 0,5$ and $\delta^{18}O = -10‰$.*

3.5.3 Hendy-Tests

To check, if isotope fractionation occurred under disequilibrium conditions, Hendy (1971) proposed the so called 'Hendy-Test' as an obligatory criterion. Thereby δ^{13}C and δ^{18}O of an individual growth layer must show (i) a simultaneous enrichment with increasing distance from the stalagmite's growth axis and (ii) should be correlated linearly in a δ^{18}O versus δ^{13}C plot. Using the multi-box-model the isotopic composition along individual growth layers are modelled. This allows to investigate the dependence of the slope of δ^{18}O versus δ^{13}C on the different parameters.

Fig. 3.5.4a shows the dependence of the slope on a varying drip interval ($d = 100s$ (circles) to $d = 1000s$ (crosses)). Long drip intervals increase the residence time of the solution on top of the stalagmite and result in more enriched δ^{13}C and δ^{18}O values, whereas short drip intervals reduce the residence time and the enrichment of δ^{13}C and δ^{18}O decreases. However, the slope between δ^{18}O and δ^{13}C does not change, because the enrichment of carbon and oxygen is affected to the same extent. The same holds for a varying mixing coefficient ϕ ($\phi = 0,1$ (circles) to $\phi = 1,0$ (crosses), Fig. 3.5.4b) and soil p_{CO_2} ($p^{soil}_{CO_2} = 1000ppm$ (circles) to $p^{soil}_{CO_2} = 11000ppm$ (crosses), 3.5.4c). Although the enrichment of δ^{13}C and δ^{18}O along an individual growth layer strongly depends on these parameters, the slope between δ^{13}C and δ^{18}O is constant. This constant slope is based on the underlying theory of fractionation and thus enrichment of δ^{13}C and δ^{18}O . The calculation of both isotopes is based upon the same theory. Hence, it is not astonishing that the influence of these parameters on the enrichment is the same.

The dependencies of the slope on a change of the isotopic composition of the drop is illustrated in Fig. 3.5.4d ($\delta^{13}C_{drop} = -10‰$, $\delta^{18}O_{drop} = -10‰$ (solid line), $\delta^{13}C_{drop} = -12‰$, $\delta^{18}O_{drop} = -10‰$ (dotted line), $\delta^{13}C_{drop} = -10‰$, $\delta^{18}O_{drop} = -12‰$ (dashed line)). A change of the drip water causes a shift of the resulting δ^{13}C and δ^{18}O values. However, the slope does not change.

Finally, Fig. 3.5.4e shows the influence of temperature on the slope ($T = 5°$C (solid line), $T = 10°$C (dotted line), $T = 15°$C (dashed line)). Due to the different temperature dependence of the fractionation factors of δ^{13}C and δ^{18}O (see Table 2.4.1 and 2.4.2) a temperature change results in a change of the slope. Higher temperatures increase the slope, while lower temperatures result in a decrease. The dependence of the slope on the buffer parameter is shown in Fig. 3.5.4f ($b = 0$ (solid line), $b = 0,5$ (dotted line), $b = 1$ (dashed line)). If no buffer reactions occur ($b = 0$), δ^{18}O shows a maximum enrichment and thus the slope is maximized. If on the other hand bicarbonate is completely buffered ($b = 1$), δ^{18}O shows no enrichment caused by kinetic fractionation effects and the slope is zero. Under natural conditions the influence of the buffer reactions is expected to be somewhere between these two boundary curves, i.e. $0 \leq b \leq 1$.

To summarise the effect of buffering as outlined in section 3.3, the slope of the δ^{18}O $/\delta^{13}$C relationship depends only on temperature and the degree of buffering, which is

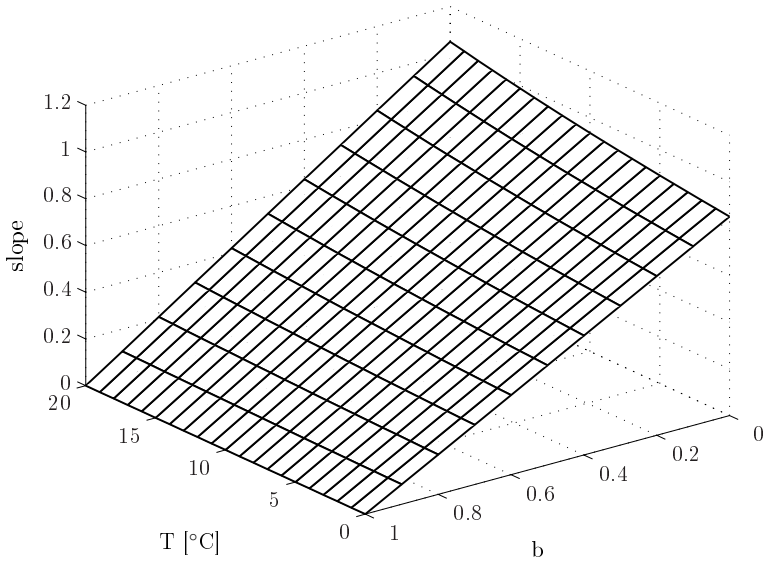

Figure 3.5.3: *The figure shows the dependence of the slope on temperature and the buffer parameter. If the system is completely buffered, the slope approaches zero. If no buffer reactions occur the slope strongly depends on temperature, with a maximum slope for high temperatures. According to section 3.3 the slopes for intermediate buffer values are obtained by linear interpolation.*

illustrated in Fig. 3.5.3. Whereas the boundary curves (i.e., $b = 0$ and $b = 1$, respectively) can be calculated, the slope for the intermediate buffer values are calculated by linear interpolation (compare Eq. 3.3.4 and Fig. 3.3.2). Dependencies of the buffering on temperature and the parameters are not included in this approach. However, if temperature is known, this simplified approach allows to estimate the degree of the buffering effect from Hendy-Tests of stalagmites, which grew under conditions of disequilibrium.

Thereby the degree of buffering does not include only the effect of buffering, but also other influences on the oxygen isotopes like evaporation, for instance. By investigating Hendy-Tests only the resulting enrichment of oxygen is examined and not the way this enrichment evolved. Hence, for natural data sets, the buffer parameter might not only describe the influence of the buffering water reservoir, but also other effects on the oxygen isotopes.

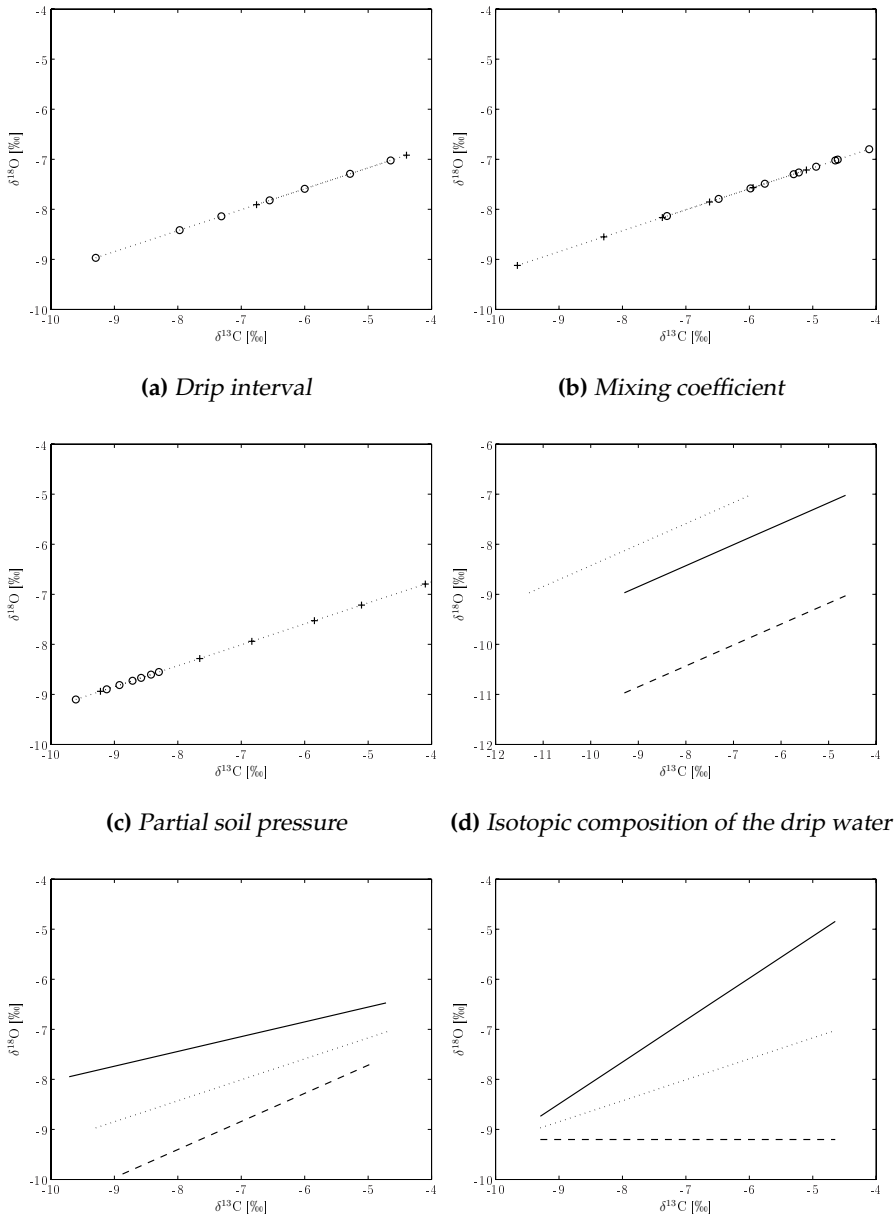

(a) *Drip interval* **(b)** *Mixing coefficient*

(c) *Partial soil pressure* **(d)** *Isotopic composition of the drip water*

(e) *Temperature* **(f)** *Buffer parameter*

Figure 3.5.4: *The figure shows the dependencies of the slope of $\delta^{13}C$ vs. $\delta^{18}O$ on mixing coefficient, soil p_{CO_2}, isotopic composition of the drip water, temperature and buffer parameter. See text for details.*

Chapter 4

Reverse Models

The forward models introduced in chapter 3 calculate stalagmite proxies like growth rate and the isotopic composition of precipitated calcite both along the growth axis and along individual growth layers in dependence on drip interval, temperature, CO_2 content of the soil, mixing coefficient, buffer parameter and the isotopic composition of the drip water. In order to obtain these parameters from data sets provided by natural stalagmites the models need to be reversed. However, since all forward models contain not only analytical but numerical operations this is a rather difficult issue. Thus, the inversion needs to be performed by a comparison of the measured data with the calculated values.

Except the growth model all other models are based on the assumption of a kinetic Rayleigh fractionation process during the degassing of CO_2 and the precipitation of calcite. Thus, the application of these models on data sets from natural stalagmites requires samples which show some kind of kinetic fractionation. In general, also samples developed under equilibrium conditions can be used, since equilibrium fractionation is a border case of disequilibrium fractionation. However, we focus on kinetically fractionated samples, which contain, beside the temperature signal, also information about varying drip intervals.

4.1 Stalagmites

A cave, which provides stalagmites grown under such disequilibrium conditions, is the small Marcelo Arevalo cave in Southern Chile. This cave is located 15km east of the climate divide of the Andes (52°41.7'S, 73°23.3'W, see Fig. 4.1.1) and is surrounded by dense rain forest and overlain by peaty soils. The cave is in contact with the atmosphere and thus its p_{CO_2} value is close to the atmospheric value of $p_{CO_2} = 380ppm$. For details see Kilian et al. (2006); Schimpf (2005) and an upcoming publication of Kilian et al. (in prep). The isotopic profiles of δ^{13}C and δ^{18}O were measured by C. Spötl at the Innsbruck University. Methods are similar as described in Vollweiler et al. (2006). Three stalagmites have been taken from this cave so far, all within a radius of only a few metres. This suggests that the stalagmites have been fed by the same or at least similar drip water. However, growth and isotopic profiles of these stalagmites differ, which is attributed to different drip rates and thus a different degree of kinetic fractionation during their formation.

For all three stalagmites there are growth rates and isotopic profiles of carbon and oxygen along the growth axis available. However, Hendy-Test have only be performed on stalagmite MA-1 (seven tests) and stalagmite MA-2 (five tests). Thus, only these two stalagmites will be used in the following (Fig. 4.1.2).

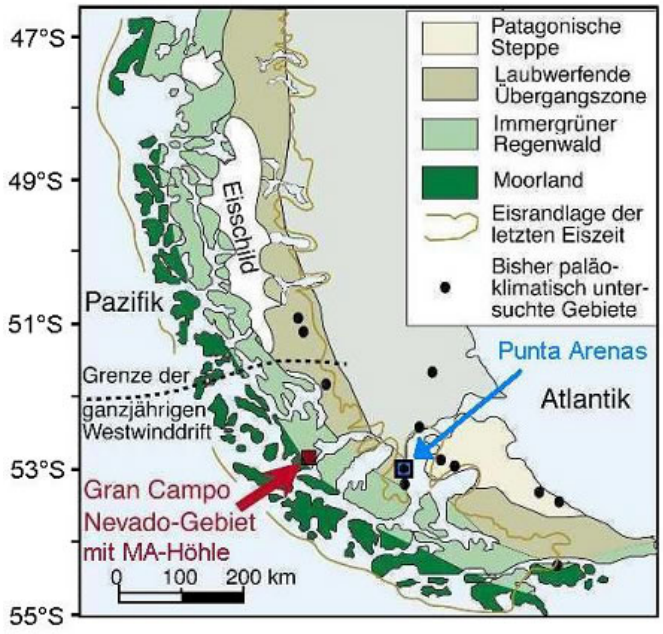

Figure 4.1.1: *Location of the Marcelo Arevalo (MA) cave in Southern Chile.*

4.1.1 Age-depth relation

To obtain the age-depth relation of a stalagmite several samples along the growth axis are taken. The ages of stalagmites MA-1 and MA-2 were determined by Schimpf (2005) using TIMS (Thermal Ionisation Mass Spectrometry) at the Heidelberg Academy of Sciences. This yields an age-depth relation along the growth axis, which is used to determine the growth rate of the stalagmite. Fig. 4.1.3 shows the ages versus depth and the growth rates of stalagmites MA-1 and MA-2. Both stalagmites span the time of approximately the last 5000 years, but show slightly different growth rates during this time, however, the order of magnitude is comparable.

The ages of stalagmite MA-1 are tuned to the ages of stalagmite MA-2, since MA-2 has the lowest detritus correction regarding the uranium thorium ages (Schimpf, pers. comment). The tuning is based upon the uranium profile of the stalagmites. These profiles show the same characteristics, but with a slight delay in age. The errors made by this tuning process are listed in the Appendix A.1.

To calculate the growth rate from the age depth relation, the distance between two sample points is divided by the difference of their ages. This yields a mean growth rate between these two samples. The temporal resolution of these growth rates is limited to the number of measured sample points. Mathematical fits of the age profile may

Figure 4.1.2: *Stalagmites MA-1 and MA-2 from Southern Chile.*

improve and increase the resolution of the growth rates (e.g. Akima (1970)), but also may raise errors and uncertainties. In the following I will focus on the measured data points to avoid errors made by the fitting procedure.

The growth rate W_{stal} and its error between two data points[1] (dft_1, age_1; dft_2, age_2) are calculated as follows:

$$W_{stal} = \frac{dft_2 - dft_1}{age_2 - age_1}. \tag{4.1.1}$$

Using error propagation yields for the error of the growth rate:

$$\Delta W_{stal} = \sqrt{\left(\frac{\sqrt{(\Delta dft_2)^2 + (\Delta dft_1)^2}}{age_2 - age_1}\right)^2 + \left(-\frac{(dft_2 - dft_1)\sqrt{(\Delta age_2)^2 + (\Delta age_1)^2}}{(age_2 - age_1)^2}\right)^2}. \tag{4.1.2}$$

This is shown in Fig. 4.1.3. The grey shaded area indicates the error of the growth rates, which are significant due to measurement and tuning uncertainties.

4.1.2 Isotopic profiles

Carbon and oxygen profiles have been taken along the growth axis for all three stalagmites and were measured by Christoph Spötl in Innsbruck. Although all three stalag-

[1] A data point contains information about its distance from top (dft) and its determined age (age).

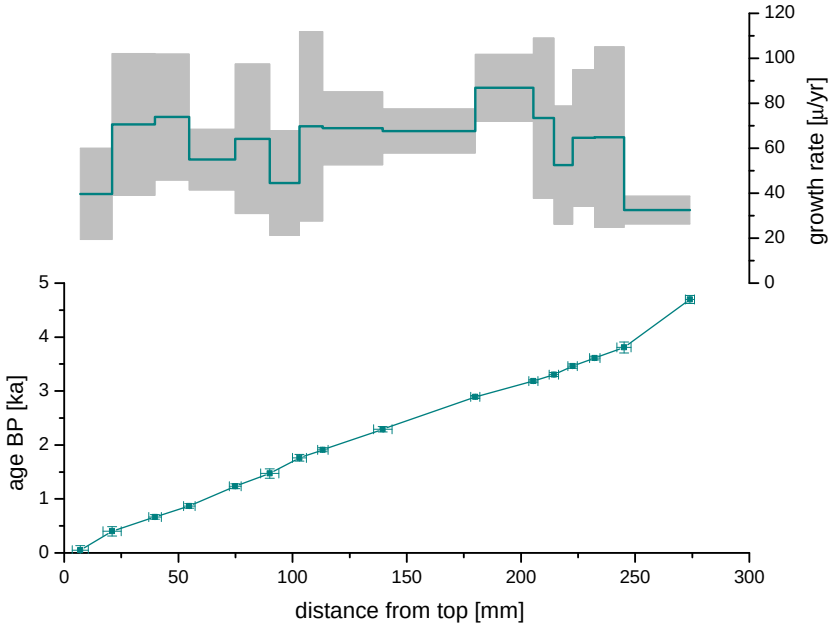

(a) *Age-depth relation and growth rate of stalagmite MA-1*

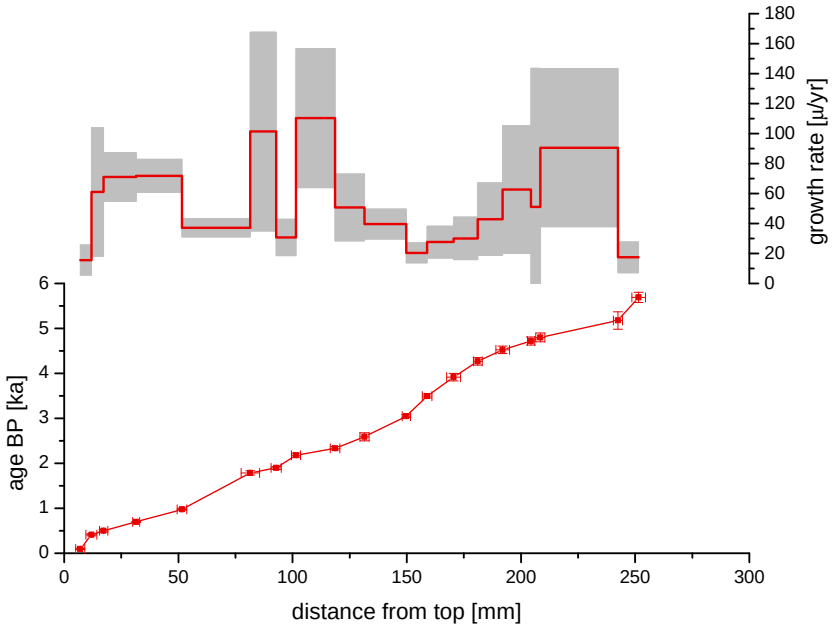

(b) *Age-depth relation and growth rate of stalagmite MA-2*

Figure 4.1.3: *Age-depth relations and growth rates of stalagmites MA-1 (cyan) and MA-2 (red) from Southern Chile. Stalagmites were analysed by Daniel Schimpf in Heidelberg. The errors of the growth rate (grey) are calculated using error propagation law (see text for details).*

mites were probably fed by the same drip water due to the close location to each other, the isotopic profiles differ. This might be due to kinetic fractionation processes during the degassing of CO_2 and the precipitation of calcite. Fig. 4.1.4 shows the isotopic profiles including the tuned ages.

There are also isotopic profiles along individual growth layers available, but only for stalagmite MA-1 and MA-2. Fig. 4.1.5 shows the enrichment of both carbon and oxygen with increasing distance from centre and the correlation between the enriched carbon and oxygen samples. According to Hendy and Wilson (1968); Hendy (1971) this indicates fractionation under disequilibrium. Here only two Hendy-Tests are shown exemplarily, the whole data set is shown in the Appendix A.1.

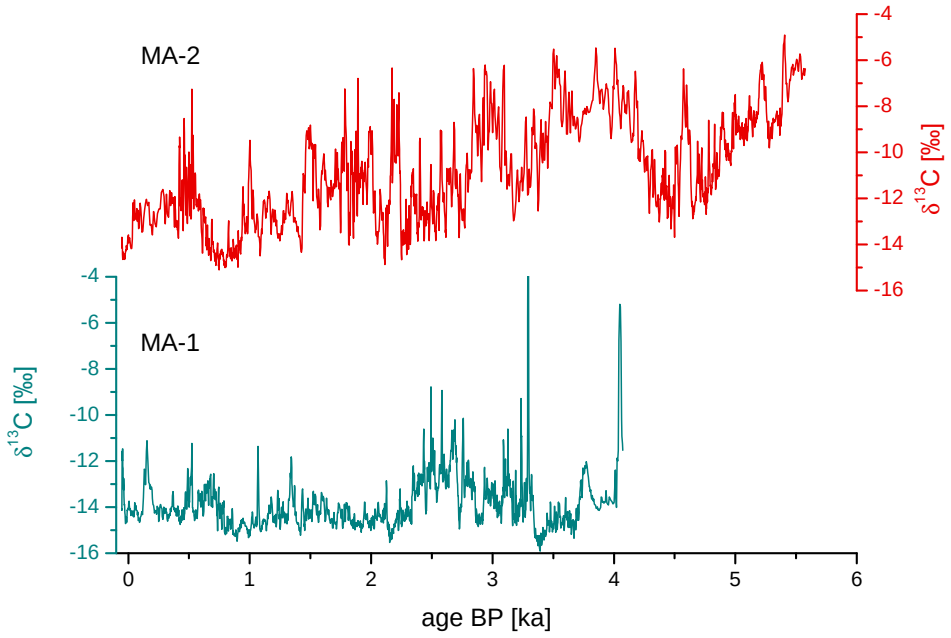

(a) *Carbon profile along the growth axis*

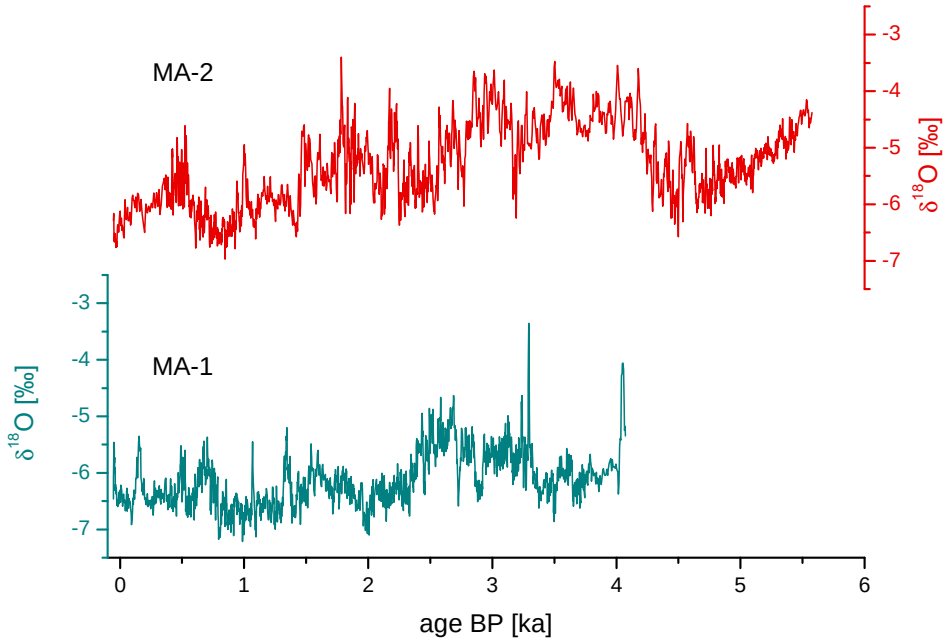

(b) *Oxygen profile along the growth axis*

Figure 4.1.4: *Isotopic profiles of stalagmites MA-1 (cyan) and MA-2 (red). Although both stalagmites were probably fed by the same drip water, the isotopic profiles differ. This might be due to kinetic fractionation processes during the degassing of CO_2 and the precipitation of calcite.*

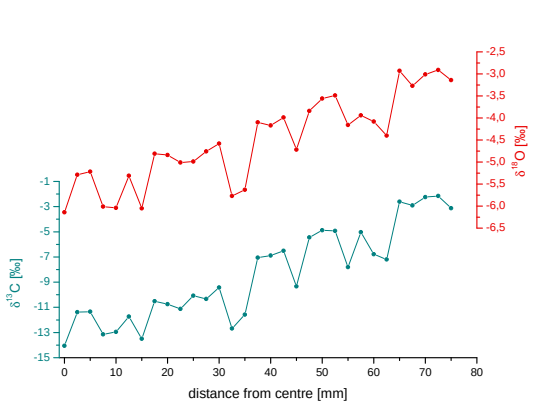

(a) *MA-1.b*

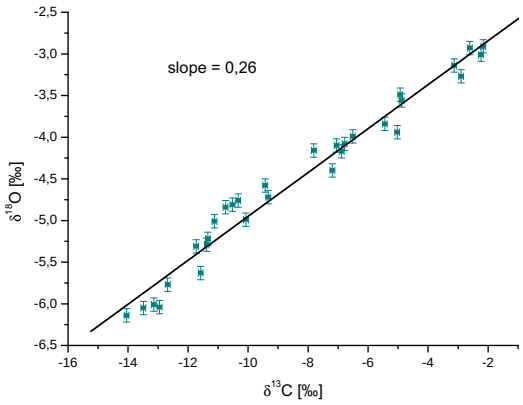

(b) *MA-1.b*

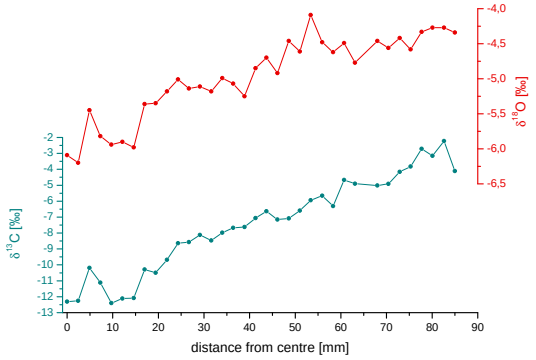

(c) *MA-2.a*

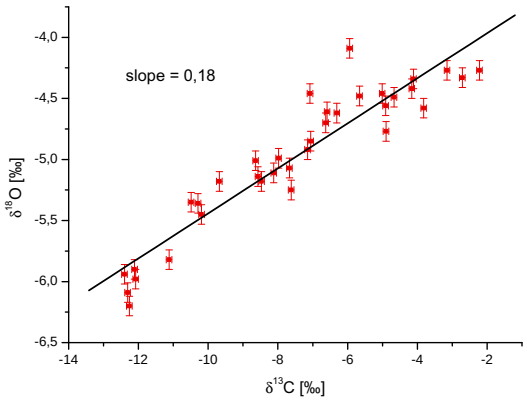

(d) *MA-2.a*

Figure 4.1.5: *Isotopic profiles and Hendy-Tests of stalagmites MA-1.b (a), (b) and MA-2.a (c), (d). Both Hendy-Tests show a linear correlation between carbon and oxygen, which indicates fractionation under disequilibrium conditions.*

4.2 AGE model

The AGE model is based on the inversion of the growth model. Thus, it depends on the same parameters as the growth model, which are drip interval, temperature, mixing coefficient and p_{CO_2} of the soil air. The intention of the model is to use the age-depth relation of a stalagmite in order to calculate the temporal development of one parameter in dependence on the others. Since the growth model contains not only analytical, but also numerical calculations, the inversion is performed by a comparison of the theoretical growth rates with the measured growth rates. Note, that this model is ambiguous.

4.2.1 Results and discussion

The AGE model is exemplarily applied to the data set of stalagmite MA-1. To determine one parameter from the age-depth relation all other parameters need to be fixed, i.e. the fixed parameters represent only mean values during the growth period of the stalagmite. In the following the results for all parameters will be shown in order to understand, to which amount one parameter must change to explain the temporal variation of the growth rates, while the other parameters are fixed.

The parameters are fixed at the following values: the drip interval is given as $d = 250s$, temperature is given as the recent mean value of approximately $T = 7°C$, the partial CO_2 pressure of the soil as $p_{CO_2} = 10000$ppm and the mixing coefficient as $\phi = 0,1$. The values of p_{CO_2} and ϕ are chosen to obtain more sensitive results according to Fig. 3.1.1. A higher mixing coefficient and lower p_{CO_2} would attenuate the sensitivity of the dependence of the growth rate on drip interval.

The grey shaded areas in Fig. 4.2.1 indicate the error due to tuning uncertainties of the age-depth relation. The error is calculated by Monte-Carlo method using 2000 runs. The significant error of the results can be explained by the error caused by tuning the ages of MA-1 to MA-2. This tuning error in combination with the uncertainty of the depth measurement can change the values of the growth rates significantly (see Fig. 4.1.3), resulting in varying results.

Under these assumptions the drip interval is determined (see Fig. 4.2.1a). The results show a contrary behaviour to the measured growth rates as expected. For fixed boundary conditions the drip interval must decrease, if the growth rate increases and vice versa. The significant error of the growth rates manifests in a high variability of the calculated drip interval ranging between 100 and 500s.
The behaviour of temperature is in contrast to the behaviour of the drip interval (see Fig. 4.2.1b). Fast growing stalagmites can either be explained by short drip interval or high temperatures and vice versa. If the drip interval is fixed, the temperature profile is consistent with the profile of the growth rate. To explain the growth rates of stalagmite MA-1 a temperature change of approximately 10°C is needed. If errors are included this range enlarges to about 13°C.

The change of p_{CO_2}, which is needed to explain the variations of the growth rate, ranges between 5000 and 20000ppm (see Fig. 4.2.1c). The p_{CO_2} profile follows in general the temperature profile, but reveals differences in its relative changes. If the p_{CO_2} content of the soil increases, more calcite is dissolved from the host rock, which leads to an increased calcite precipitation on top of the stalagmite and thus an increased growth. Including the error of the measured ages the values of the determined p_{CO_2} vary between 3000 and 21000ppm.
The mixing coefficient shows only a slight variation between 0,1 and 0,3 for the entire growth period (see Fig. 4.2.1d). This indicates the high sensitivity of the growth rate on a change of this parameter. However, if errors are included, the possible range of the mixing coefficient increases up to 0,7.

The variation of some parameters are in the range of their natural variability, even if the other parameters are kept fixed at the same time. This holds for the drip interval, for instance, which is in a reasonable range. Other parameters on the other hand would have to vary much more than under natural conditions. This holds for the variation of temperature and CO_2 content of the soil, which vary of more than 10°C and 15000ppm, respectively.
The variation of the mixing coefficient is hard to interpret, since it describes no natural condition, but may only reflect splashing processes of the impinging drop. However, if the surrounding physical environment of a stalagmite does not change (for example due to earthquakes or changes of the drip source location), this parameter is expected to be relatively constant during the growth period of a stalagmite.

In general the errors caused by the uncertainties of the age determination and tuning processes are significant. This and the rough temporal resolution of the age-depth relation make it difficult to use the AGE model for a quantitative determination of any parameter, assumed that the model is used individually.

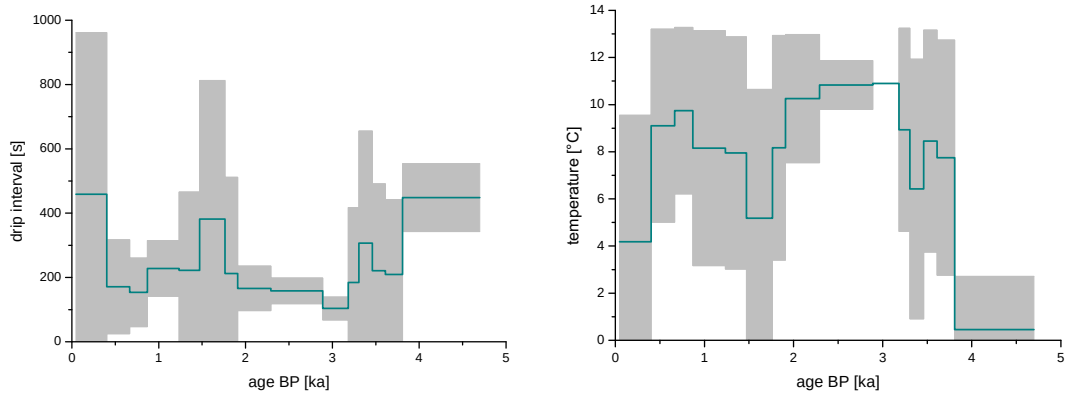

(a) *Drip interval*

(b) *Temperature*

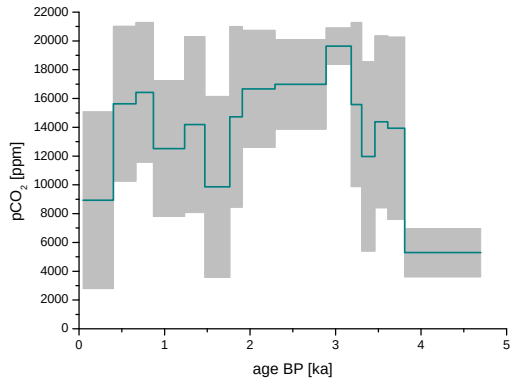

(c) *Partial soil pressure*

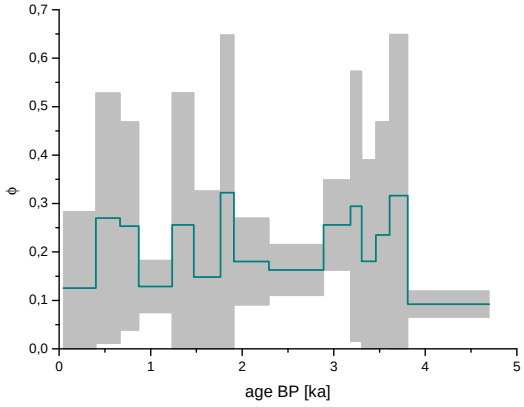

(d) *Mixing coefficient*

Figure 4.2.1: *Temporal variation of a parameter, which is needed to obtain the isotopic carbon profile along the growth axis, if all other parameters are fixed. Results are for* $d = 250s$, $T = 7°C$, $p_{CO_2} = 10000ppm$, *and* $\phi = 0,1$. *The grey shaded area indicates the error due to tuning uncertainties of the age-depth relation.*

4.3 AXIS model

The AXIS model is based on the inversion of the carbon and oxygen fractionation model. Thus, it depends on the same parameters, which are drip interval, temperature, mixing coefficient, p_{CO_2} of the soil and the isotopic composition of the drip water. The intention of the model is to use the isotopic profiles carbon and oxygen of a stalagmite in order to calculate the temporal development of one parameter in dependence on the others. Since the model describing the fractionation processes contains not only analytical, but also numerical calculations, the inversion is performed by a comparison of the theoretical enrichment of the precipitated calcite with the measured values of the samples. Note, that this model is ambiguous.

4.3.1 Carbon profile along the growth axis

The AXIS(C) model is exemplarily applied to the isotopic carbon profile of stalagmite MA-1. To determine one parameter all other parameters need to be fixed, i.e. the fixed parameters represent only mean values during the entire growth period of the stalagmite. In the following the results for all parameters are shown in order to understand, to which amount a parameter must change to explain the temporal variation of the carbon profile, while the other parameters are fixed. The following parameters are used: $d = 100s$, $T = 7°\mathrm{C}$, $p_{CO_2} = 10000ppm$, $\delta^{13}C_{drop} = -16‰$ and $\phi = 0,1$. All results are smoothed by a 20 point running mean.

The results (Fig. 4.3.1) show that in general it is possible to describe variations of the carbon profile by a variation of any parameter. Like the drip interval for instance, some of these variations lie within a range, which can be observed in natural caves, other parameters exceed the range of natural variability. However, in a natural environment a combination of the variations of different parameters will explain the δ^{13}C profile. The results are shown exemplarily for the chosen parameters. The variations will change, if any of these parameters is changed.

4.3.2 Oxygen profile along the growth axis

The AXIS(O) model is exemplarily applied to the isotopic oxygen profile of stalagmite MA-1. To determine one parameter all other parameters need to be fixed, i.e. the fixed parameters represent only mean values during the growth period of the stalagmite. In the following the results for all parameters are shown in order to understand, to which extent one parameter must change to explain the temporal variation of the oxygen profile, while the other parameters are fixed. The following parameters are used: $d = 100s$, $T = 7°\mathrm{C}$, $p_{CO_2} = 10000ppm$, $b = 0,5$, $\delta^{18}O_{drop} = -10‰$ and $\phi = 0,1$. All results are smoothed by a 20 point running mean.

The results show that in general variations of the oxygen profile can be described by a variation of any parameter. As already described for the carbon profile, some of these

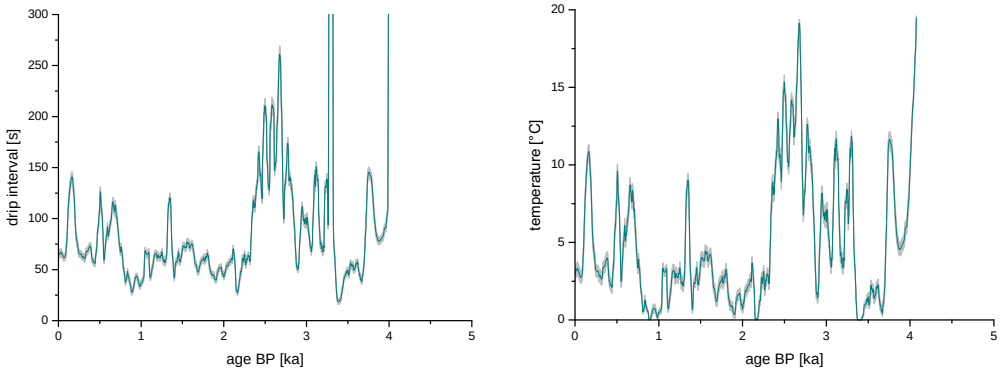

(a) *Drip interval*

(b) *Temperature*

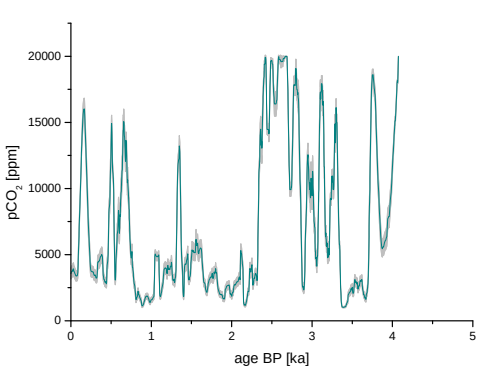

(c) *Partial soil pressure*

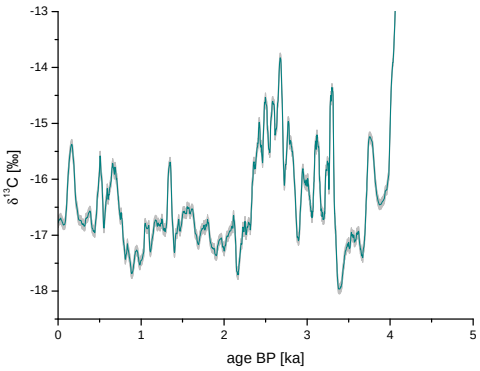

(d) $\delta^{13}C$ *of the drip water*

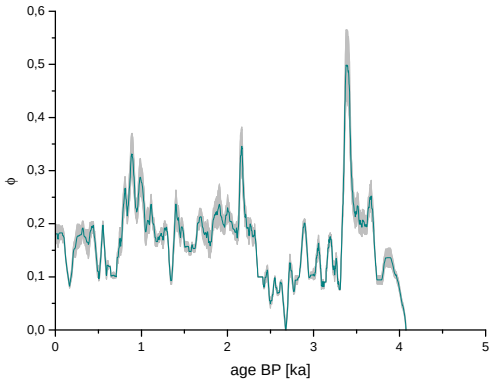

(e) *Mixing coefficient*

Figure 4.3.1: *Temporal variation of a parameter, which is needed to obtain the isotopic carbon profile along the growth axis, if all other parameters are fixed. Results are for* $d = 100s$, $T = 7°C$, $p_{CO_2} = 10000ppm$, $\delta^{13}C_{drop} = -16‰$ *and* $\phi = 0,1$. *The grey shaded area indicates the error due to the uncertainty of the measurement of* $\Delta\delta^{13}C = 0,08‰$. *The results are smoothed by a 20 point running mean.*

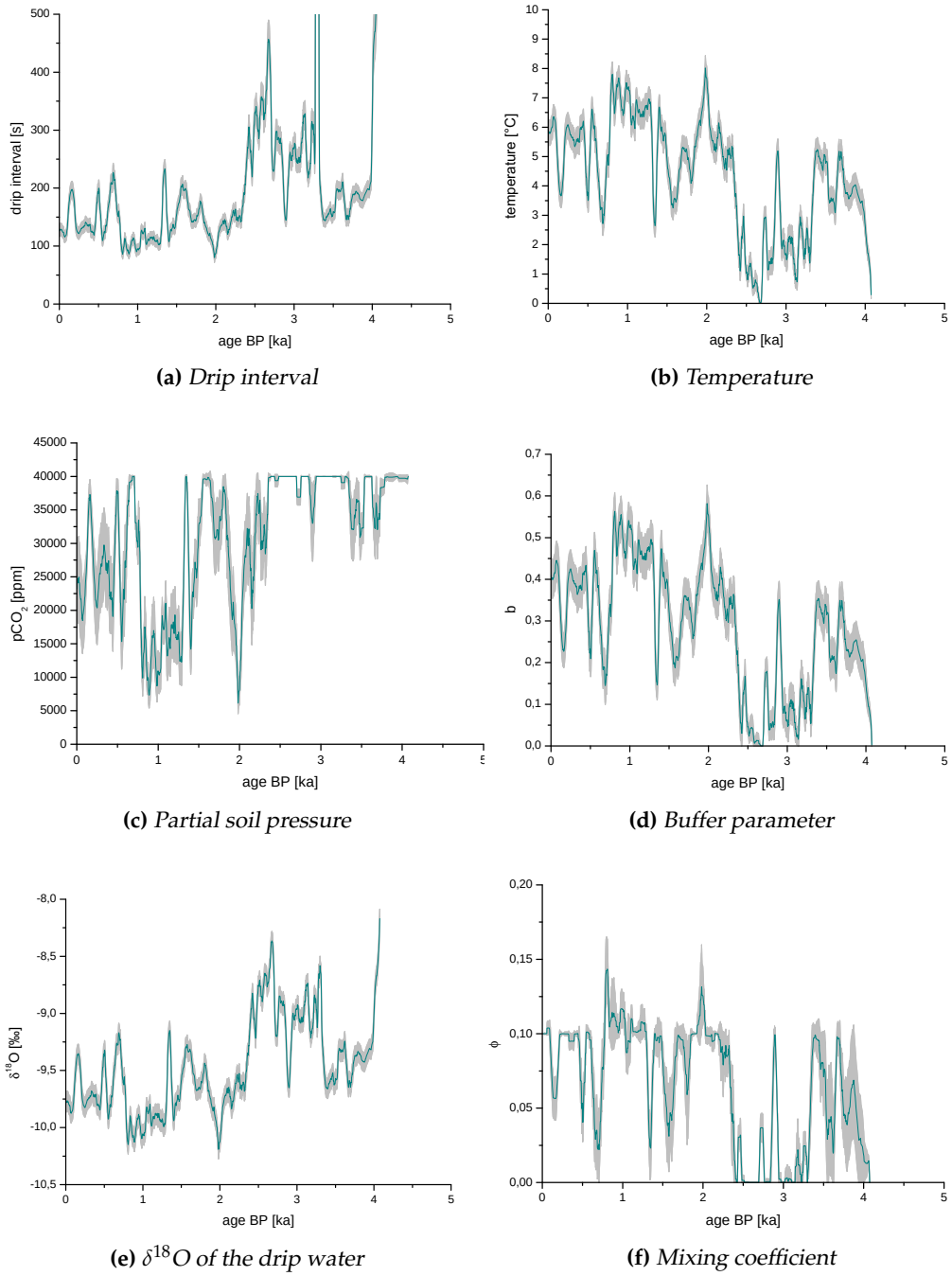

(a) *Drip interval*

(b) *Temperature*

(c) *Partial soil pressure*

(d) *Buffer parameter*

(e) $\delta^{18}O$ *of the drip water*

(f) *Mixing coefficient*

Figure 4.3.2: *Temporal variation of a parameter, which is needed to obtain the isotopic oxygen profile along the growth axis, if all other parameters are fixed. Results are for* $d = 100s$, $T = 7°C$, $p_{CO_2} = 10000ppm$, $b = 0,5$, $\delta^{18}O_{drop} = -10‰$ *and* $\phi = 0,1$. *The grey shaded area indicates the error due to the uncertainty of the measurement of* $\Delta\delta^{18}O = 0,08‰$. *The results are smoothed by a 20 point running mean.*

variations lie within a range, which can be observed in natural caves, like the drip interval, temperature or the δ^{18}O value of the drip water, others not. Again, if any of the chosen parameters is changed, the variations will change. In comparison to the variations needed to obtain the carbon profile, there are more parameters, whose variations can explain variations of the oxygen profile and lie within a natural range.

At first sight the main difference between the AGE and the AXIS model is the uncertainty of the resulting values. Whereas the error of the measured growth rates is significant due to measurement and tuning uncertainties, the accuracy of the measured isotopes is 0,08 ‰. This exact determination of the isotopic profile results in small errors of the determined values.

Examining the variation of the results of the AXIS(C) model only the drip interval seems to reflect natural variability. Temperature values range from 0 up to 20°C, which is not observed in nature. However, this range is reasonable, since the modelled δ^{13}C values only show a weak dependence on temperature and thus temperature must vary strongly to explain variations of the δ^{13}C value of the precipitated calcite. The results of p_{CO_2} and the δ^{13}C value of the drip water show a high variability, which could be attributed to significant changes in the soil system like changes of the vegetation type for instance. For rather constant conditions of the cave surroundings, the variations obtained for these parameters are too pronounced. The mixing coefficient shows only slight variations ranging around 0,2. In comparison to the AGE model all parameters except the mixing coefficient follow approximately the same trend. For an increased value of δ^{13}C of the isotopic profile, the corresponding parameter is also increased and vice versa. However, their relative change is different again.

For oxygen and the AXIS(O) model there are more parameters, whose temporal variations lie within a natural range. This is again the drip interval, which is reasonable, since it is included in the oxygen calculation in the same way as for the carbon calculation. Due to the higher sensitivity of δ^{18}O on temperature, the resulting temperature range is much smaller than for the carbon isotopes. However, almost 8°C variation is still too big for natural systems within this time frame, but might be explained by individual local features. Another parameter representing natural variability is the δ^{18}O value of the drip water. The obtained variations might be found in natural cave systems due to varying meteoric conditions or temperature changes outside the cave. In contrast the CO_2 content of the soil spans a range of almost 40000 ppm, which exceeds natural variability easily. This range would even be extended, if the upper limit of 40000 ppm would not have been fixed by the model.
The mixing coefficient shows small variations, which is expected for this parameter, and is in agreement with the results of the AGE model. This does not hold for the buffer parameter, which varies between 0 and 0,6. According to Hendy-Tests of natural stalagmites, which show rather constant values of the slope during the whole growth period, this parameter should not show a high temporal variability, if temperature changes are moderate. The general trends are not as clear as for the AXIS(C) model. The drip in-

terval, the partial soil pressure and the δ^{18}O value of the drip water show similar characteristics. The remaining parameters show also similar trends, but with an inverted profile in comparison to the other parameters.

4.4 LAYER model

The LAYER model is based on the isotopic enrichment along an individual growth layer described by the multi-box-model. The dependencies of the model introduced in section 3.5 are now investigated examplarily at Hendy-Test MA1.b from stalagmite MA-1 (see Appendix A.1). To obtain information from the measured isotope values along an individual growth layer the theoretical enrichment is compared to the measured. Since the enrichment shows most of the time a linear characteristic, the slopes of the enriched isotopes are compared. As shown in section 3.5 it can already be seen by eye, that if the measured values increase linearly, the mixing coefficient might be rather small than high. Otherwise the increase would be similar to a second order polynomial. However, to compare the theoretical to the measured slopes all mixing coefficients are considered. In analogy to section 3.5 only the slopes between the second and the outer boxes are investigated.

4.4.1 Carbon profile along individual growth layers

The carbon profile of MA1.b of stalagmite MA-1 shows a slope of 0,148 $‰/mm$. In analogy to the previous models the slope of the modelled values is calculated for a given set of parameters, whereas one parameter is varied and the others are fixed. The resulting slope is compared to the measured in dependence on the varying parameter. To take the number of boxes into account the deviation between the measured and the theoretical slope is normed to one box. Thus, the deviation can be written as:

$$dev = \frac{|slope_{theo} - slope_{sample}|}{\#_{boxes}}. \tag{4.4.1}$$

To determine the value of a parameter, which is needed to obtain the measured slope for fixed boundary conditions the following fixed values are chosen: $d = 100s$, $T = 10°\mathrm{C}$, $p_{CO_2} = 10000ppm$ and $\phi = 0,5$ respectively. The two parameters, which show the most important influence on the slope are the mixing coefficient and the partial pressure of the soil. The dependence of the slope on the partial pressure of the soil shows a clear minimum at 6000ppm (see Fig. 4.4.1a). The number of boxes is six, since the radius does not depend on the p_{Co_2} of the soil.
The characteristic of the mixing coefficient is not as smooth as the one of the p_{CO_2}, which is due to the dependence of the radius on ϕ (see Fig. 4.4.1b). Thus, the radius changes with varying ϕ, which yields a variation of the calibrated ϕ_i. This in turn leads to a jagged characteristics of the resulting profile. The number of boxes vary from ten to five in this case. However, a minimum can be found for $\phi = 0,2$.
Fig. 4.4.1c shows the result of the drip interval determination. For the given set of parameters the best fitting drip interval is obtained for $d = 70s$. Again, the changing radius allows no smooth characteristic of this profile due to changes of the calibrated ϕ_i. The number of boxes varies from ten to three.

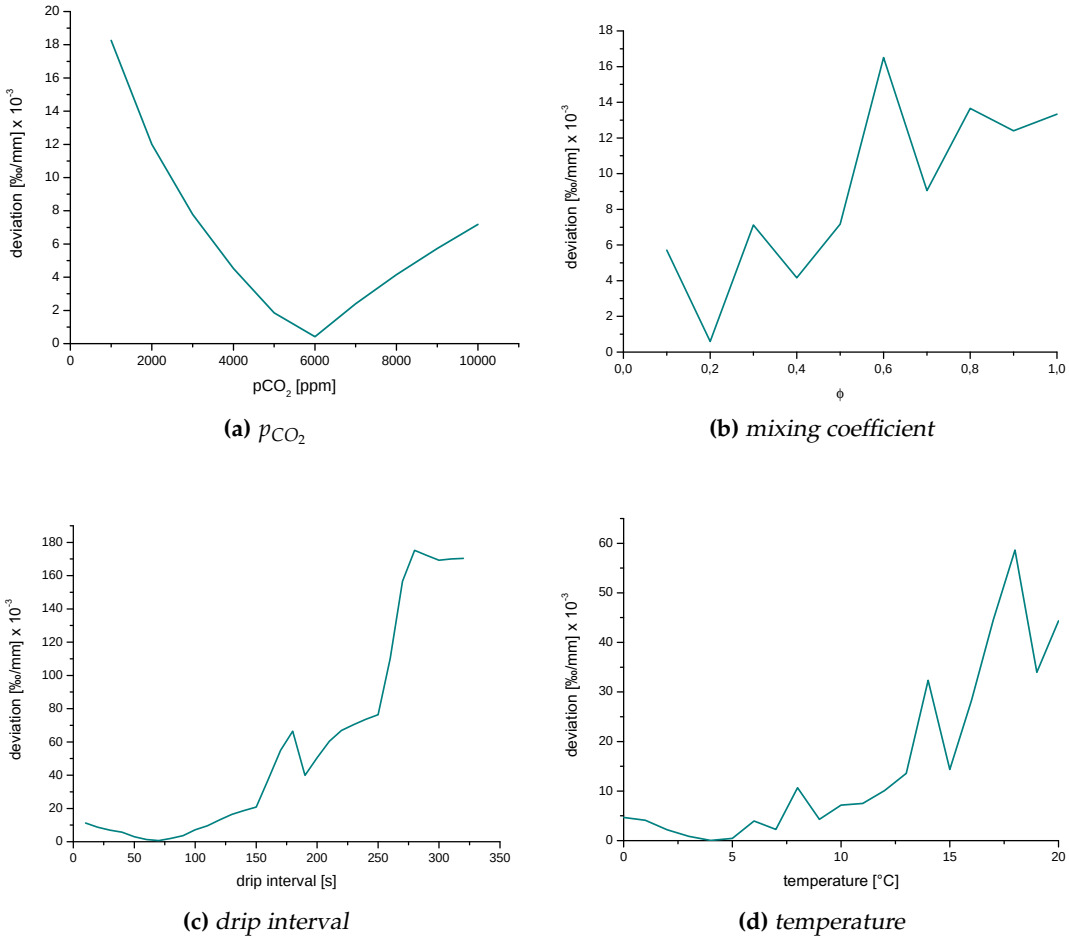

(a) p_{CO_2} **(b)** *mixing coefficient*

(c) *drip interval* **(d)** *temperature*

Figure 4.4.1: *Deviation of the theoretically calculated* $\delta^{13}C$ *values along a growth layer from the measured data. Not all resulting profiles show a clear minimum. Values are calculated for* $d = 100s$, $T = 10°C$, $p_{CO_2} = 10000ppm$ *and* $\phi = 0,5$.

The results for temperature is shown in Fig. 4.4.1d. The explanation of the profile is in analogy to the one of the drip interval. The determined temperature is $T = 4°$C and the number of boxes vary from ten to three.

In general it must be noted, that the data set of isotopic values along an individual growth layer need to be handled with care. Beside the problematic measurement to probe an individual growth layer, the dependencies of the slope on the different parameters are not always clear. Depending on the boundary conditions a determined profile can reveal several local minima, which are almost at the same level (see Fig. 4.4.1d). In such cases, the determination of a parameter is hardly possible.

4.4.2 Oxygen profile along individual growth layers

The oxygen profile of sample MA1.b shows a slope of 0,038 $‰/mm$. In analogy to carbon the same procedure to determine the individual parameters is applied including the buffer parameter b. The result for the partial pressure of the soil is shown in Fig. 4.4.2a. For the chosen set of parameters no minimum of p_{CO_2} is found, which lies at higher p_{CO_2} values. However, since the radius does not change, the characteristic of this profile is again smooth with an clear minimum, which lies beyond the given range. The profile of the mixing coefficient (Fig. 4.4.2b) is jagged in analogy to the one of the carbon profile, which is due to the changing number of boxes. In this case the solution is not clear, since two local minima can be found, one at 0,2 and one at 0,4. Even harder is the determination of the drip interval (Fig. 4.4.2c) and temperature (Fig. 4.4.2d). These results are ambiguous and show no clear minimum, which makes it impossible to determine a single value for these parameters for the given boundary conditions. However, in this specific case, the minima would lie at $d = 70s$ and $T = 4°\mathrm{C}$. The result of the buffer parameter is clear again, with a value of $b = 0,2$.

As already noted for the carbon profile, the determination of any parameter from the isotopic enrichment along individual growth layer is hard and needs to be handled with care, since many results are not unique and depend in addition on the boundary conditions. However, under certain boundary conditions, the partial pressure of the soil and the mixing coefficient can be determined. Even if the profile of the mixing coefficient reveals several local minima, there is an additional information, which can be used to confine the range of this value: the profile of the enrichment. In many cases, the isotopic enrichment of carbon and oxygen along an individual growth layer follows a linear trend. This kind of profile can only be reconstructed by the model, if the mixing coefficient is small. With this additional information, the mixing coefficient might be extracted from the enrichment of $\delta^{13}\mathrm{C}$ and $\delta^{18}\mathrm{O}$ under given boundary conditions.

The buffer parameter, which shows a clear result is determined in another way, which is more robust to boundary conditions (see section 4.5).

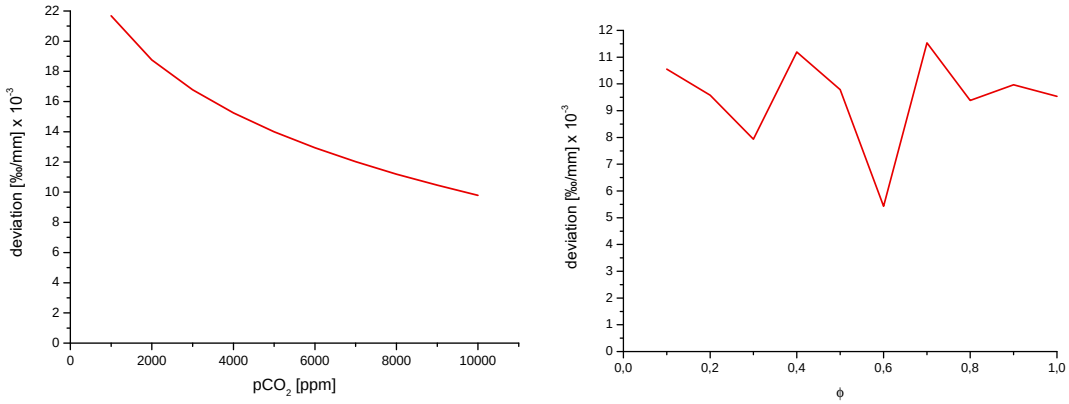

(a) p_{CO_2}

(b) *mixing coefficient*

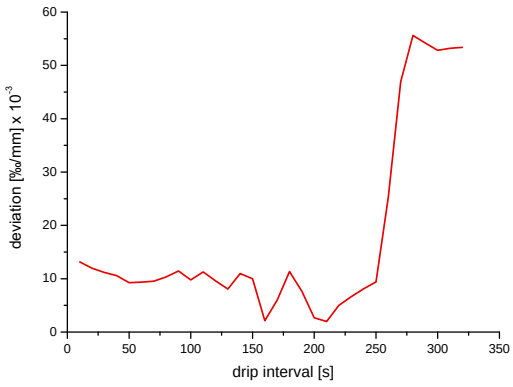

(c) *drip interval*

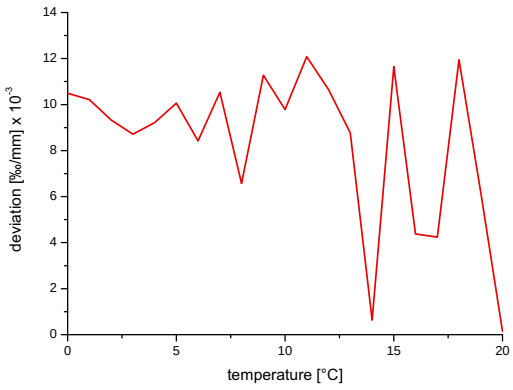

(d) *temperature*

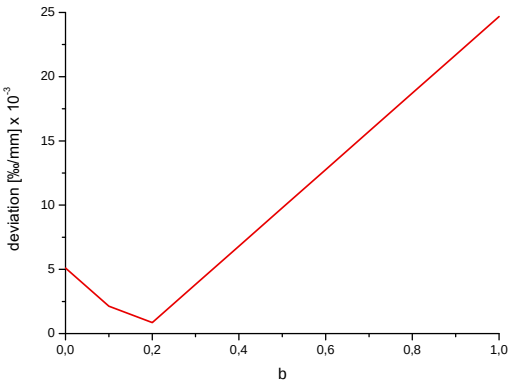

(e) *buffer parameter*

Figure 4.4.2: *Deviation of the theoretically calculated $\delta^{18}O$ values along a growth layer from the measured data. Not all resulting profiles show a clear minimum. Values are calculated for $d = 100s$, $T = 10°C$, $p_{CO_2} = 10000ppm$ and $\phi = 0,5$.*

4.5 BUFFER model

This model is based on the models of section 3.5.3 and the dependence of the slope of a δ^{13}C versus δ^{18}O plot on temperature and the buffer parameter. If no buffer reactions occur, the δ^{18}O in the precipitated calcite becomes maximal enriched resulting in a maximal value for the slope of 1,15. If the system is completely buffered the slope approaches zero, since the enrichment of δ^{18}O will not change with increasing distance from growth axis. Under natural conditions the influence of the buffer reactions is expected to be somewhere between the boundary limits, i.e. $0 \leq b \leq 1$.

The degree of buffering is calculated for seven Hendy-Tests of stalagmite MA-1 and five Hendy-Tests of stalagmite MA-2. The slopes of these Hendy-Test are listed in Table 4.5.1 and range between 0,18 and 0,35. To determine the buffer parameter at the time the investigated calcite was precipitated a temperature must be estimated. Therefore the recent cave temperature of $T_{rec} = 6,5°C$ is used allowing an error of $\pm 3°C$ to take temperature variations during the last 3000 years into account. Using the temperature uncertainty the minimal and maximal buffer parameter can be read off Fig. 3.5.3. Therefore the buffer dependent slope is determined for the given temperature range $T \in [3.5, 9.5]°C$. Since the slope increases with increasing temperature ($b > 0$) and decreases with increasing buffer parameter a maximal and minimal value of b can be determined. b^{min} can be obtained at the intersection of the minimal value of the slope and the maximal temperature, whereas b^{max} is determined at the intersection of the maximal slope and the minimal temperature. In this way a range of the buffer parameter is determined, which is given in Table 4.5.1. The resulting values of b range between 0,20 and 0,39 and centre around $b = 0,29$ for stalagmite MA-1 and $b = 0,27$ for stalagmite MA-2. It is remarkable that the slopes of the Hendy-Tests and thus the buffer parameter shows only slight variations during the whole growth period of almost 3000 years. This implies that the influence of the buffer reactions might have only small temporal variability.

Using the measurements of Beck (2004) (see section 3.3) the time needed to obtain such a degree of buffering can be estimated. According to Eq. 3.3.10 and 3.3.11 the time can be calculated:

$$t = -\frac{\ln(1-F)}{A_0 e^{-\frac{E_a}{RT_k}}}. \tag{4.5.1}$$

Replacing the fraction F describing the amount of buffering by the mean values of b yields a time of $t \approx 320s$ for stalagmite MA-1 and $t \approx 300s$ for stalagmite MA-2. These values are comparable to the drip intervals determined by the CSM model (section 4.6). The mean drip interval around the investigated Hendy-Tests is $\overline{d_{Hendy}} = 270s$ for stalagmite MA-1, whereas the mean drip interval over the whole growth period is given as $\overline{d} = 290s$. For stalagmite MA-2 the mean drip interval around the Hendy-Tests

Sample	[a]DFT [mm]	MA-1 Age [ka]	Slope	Buffer
MA-1.a	194,55	3,062	$0,21 \pm 0,01$	$0,23 \pm 0,03$
MA-1.b	169,95	2,730	$0,26 \pm 0,01$	$0,29 \pm 0,03$
MA-1.c	127,80	2,154	$0,25 \pm 0,01$	$0,28 \pm 0,03$
MA-1.d	91,35	1,496	$0,29 \pm 0,01$	$0,32 \pm 0,03$
MA-1.e	77,55	1,280	$0,35 \pm 0,02$	$0,39 \pm 0,05$
MA-1.f	47,25	0,765	$0,22 \pm 0,01$	$0,24 \pm 0,03$
MA-1.g	20,70	0,396	$0,26 \pm 0,01$	$0,29 \pm 0,03$
Mean value			$0,26 \pm 0,05$	$0,29 \pm 0,05$

Sample	[a]DFT [mm]	MA-2 Age [ka]	Slope	Buffer
MA-2.a	26,40	0,616	$0,18 \pm 0,01$	$0,20 \pm 0,02$
MA-2.b	56,70	1,082	$0,30 \pm 0,01$	$0,33 \pm 0,03$
MA-2.c	69,15	1,460	$0,24 \pm 0,01$	$0,27 \pm 0,03$
MA-2.d	107,10	2,208	$0,30 \pm 0,01$	$0,33 \pm 0,03$
MA-2.e	132,15	2,595	$0,21 \pm 0,01$	$0,23 \pm 0,03$
Mean value			$0,25 \pm 0,04$	$0,27 \pm 0,06$

Table 4.5.1: *Slopes of Hendy-Tests of MA-1 and MA-2 and the corresponding buffer parameters. Calculations are performed for a temperature of $T = 6,5 \pm 3,0°C$. The errors of the mean values are determined by standard deviation.*

[a] *Distance from top.*

is given by $\overline{d_{Hendy}} = 160s$ and over the whole growth period by $\overline{d} = 350s$[2]. Even if the absolute values do not fit exactly, they are in the same order of magnitude and in addition the trend of the drip intervals agree. For MA-1 the drip intervals calculated around the Hendy-Tests are larger in comparison to the drip intervals of MA-2, which is obtained for both calculations, the Beck (2004) approach and the CSM (section 4.6). However, the mean values of the drip interval over the whole growth period do not reflect this trend as it can be seen in the results of the CSM.

An explanation for the deviation of the calculated drip intervals of the Beck (2004) approach and the CSM might be the following. According to section 3.5.3 the buffer parameter obtained from natural data sets may contain additional influences like evaporation effects. Since the MA cave is rather open to the atmosphere, evaporation must be taken into account in this case. If the resulting values of b include both, the effect of

[2]Note, that for the CSM only Hendy-Tests MA-2.a, MA-2.b, MA-2.d and MA-2.e have been used for stalagmite MA-2.

buffering and evaporation, the actual degree of buffering is smaller than the obtained value of b depending on the degree of evaporation. This suggests that the times calculated by the Beck (2004) approach ($t = 320s$/MA-1 and $t = 300s$/MA-2, see above) are longer than the actual times needed to explain the corresponding degree of buffering. This is in agreement with the results obtained by the CSM ($t = 270s$/MA-1 and $t = 160s$/MA-2, see above).

4.6 Combined Stalagmite Model – CSM

All reverse models, which have been introduced in the previous sections are more or less ambiguous and thus, no exact information about climatic boundary conditions can be obtained from these theoretical constructs. However, a combination of the models enables the determination of absolute values of two very important climate parameters: the drip interval and temperature.

The idea of the combined model is based on the different dependencies of δ^{13}C and δ^{18}O on temperature and drip interval. Whereas both proxies show a similar dependence on the drip interval, the carbon isotopes show a rather weak dependence on temperature, whereas the dependence of oxygen on temperature is strong. This is used to extract a drip interval record from the carbon profile along the growth axis, which is then used to correct the oxygen profile in order to obtain a pure temperature signal.

If a new model is set up, the general intention is to use as less input parameters as possible in order to obtain as many output parameters as possible. In this CSM the following data sets and input parameters are used:

Data sets The stalagmite data, which include age, distance from top, δ^{13}C and δ^{18}O values along the growth axis and as many Hendy-Tests as available.

$\boldsymbol{\delta^{13}C_{drop}}$ An estimation of the mean δ^{13}C value of the drop.

Estimated temperature The cave temperature at any point of time during the growth period of the stalagmite needs to be known or estimated.

In addition an internal starting temperature between 0 and 20°C must be provided. This value can be chosen arbitrarily, since it influences only the number of runs, but not the results.

Running the CSM with these input data and parameters yields a temperature and drip interval record in a high temporal resolution. For the other parameters like CO_2 partial pressure of the soil, mixing coefficient, buffer parameter and the isotopic oxygen composition of the drop mean values are obtained, which represent the most likely values of the corresponding parameters during the growth period of the stalagmite. For these parameters no temporal variations can be obtained with the current model version. This is a simplification for parameters like the isotopic composition of the drip water, which indeed shows temporal variations due to its correlation to temperature and other climatic changes. For other parameters like the buffer or mixing coefficient this approximation may only disguise small temporal variations, which can be neglected in this first approach.

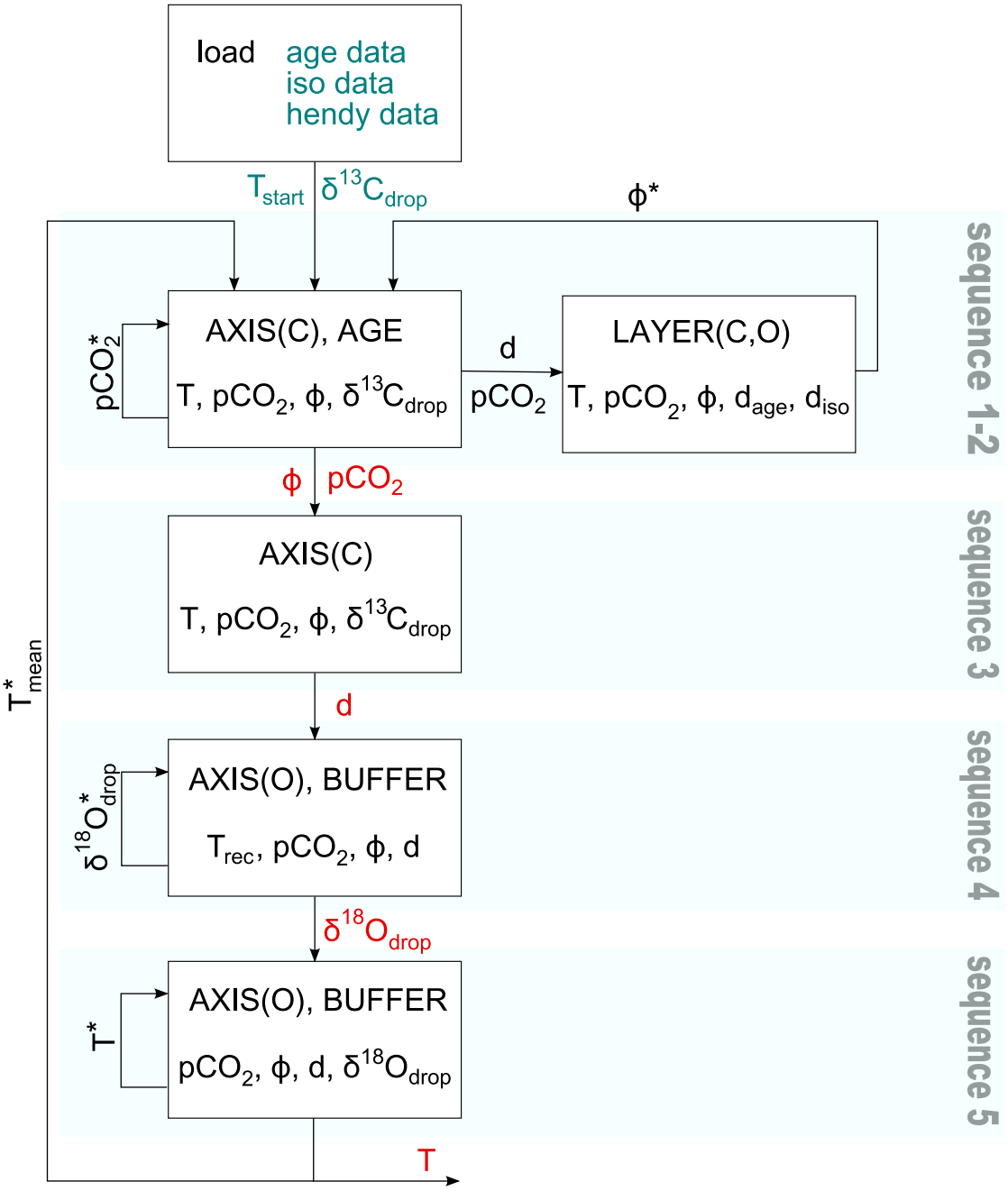

Figure 4.6.1: *Setup of CSM. The input data and parameters are marked blue, the output parameters red. The running parameters, which are determined in the corresponding sequences, are marked by a star.*

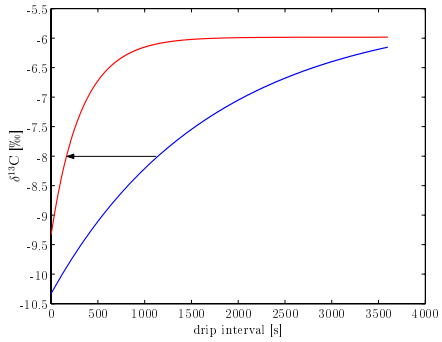

(a) *Dependence of $\delta^{13}C$ on T*

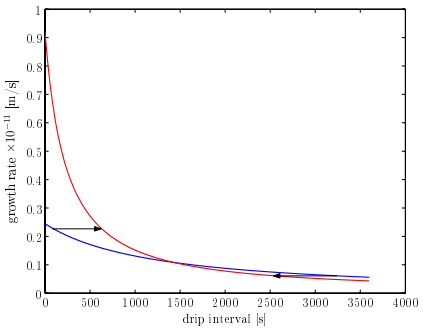

(b) *Dependence of growth rate on T*

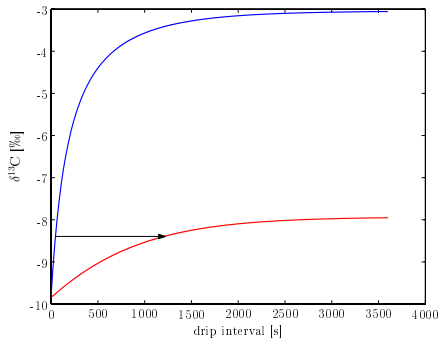

(c) *Dependence of $\delta^{13}C$ on ϕ*

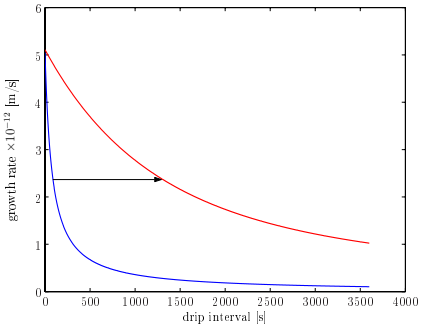

(d) *Dependence of growth rate on ϕ*

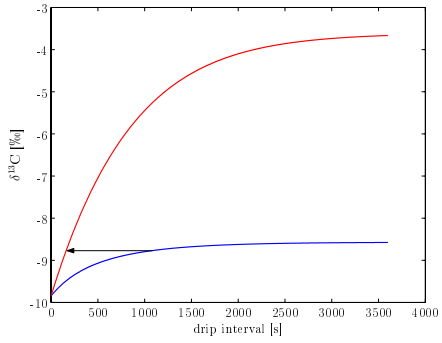

(e) *Dependence of $\delta^{13}C$ on p_{CO_2}*

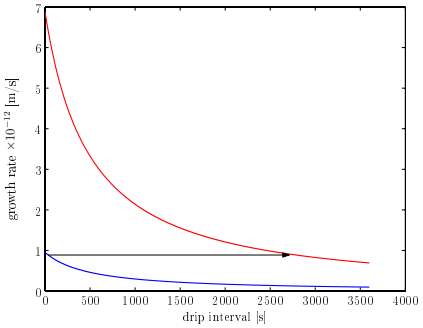

(f) *Dependence of growth rate on p_{CO_2}*

Figure 4.6.2: *Dependence of $\delta^{13}C$ and growth rate on temperature, mixing coefficient and p_{CO_2} of the soil. Values are calculated for fixed boundary conditions ($b = 0$, $\delta^{13}C_{drop} = -10‰$). Parameters, which are changed range from $T \in [1;20]°C$, $\phi \in [0,1;1,0]$ and $p_{CO_2} \in [1000;20000]ppm$. All parameters, which are not varied are kept at the mean values of their ranges. The blue lines indicate the lower value of the varying parameter, the red line the higher value. Arrows indicate the change of the drip interval caused by a variation of the relevant parameter. These dependencies are summarised in table 4.6.1. Note the ambiguous dependence of the growth rate on temperature.*

Parameter	δ^{13}C	Growth rate
Temperature $T \uparrow$	$d \uparrow\downarrow$	$d \uparrow$
Mixing coefficient $\phi \uparrow$	$d \uparrow$	$d \uparrow$
Partial pressure $p_{CO_2} \uparrow$	$d \downarrow$	$d \uparrow$

Table 4.6.1: *Dependencies of the models on temperature, mixing coefficient and CO_2 partial pressure of the soil.*

4.6.1 Detailed description

The combined model consists of five sequences, whereas in each sequence one parameter is determined (see Fig. 4.6.1). The most important and difficult step is the start of the combined model, since all individual models itself are ambiguous. This is overcome by looking at the dependencies of the individual models on temperature, drip interval, mixing coefficient and CO_2 partial pressure. As shown in Fig. 4.6.2 the AGE and the AXIS(C) models react differently and even contrarily on a change of external parameters. To compare the influence of these parameters on the models the drip interval is calculated for each model using a specific set of parameters. By varying one parameter of this set the reaction of the drip interval on this change is investigated. This gives the direction, in which the drip interval needs to change, if the same output value (δ^{13}C and growth rate) wants to be obtained (see arrows in Fig. 4.6.2).

By comparing the reaction of the drip interval on different parameters for different models, a starting point of the combined model can be found. According to Fig. 4.6.2 the AGE and the AXIS(C) model react contrarily only for a change of the partial CO_2 pressure of the soil. If the p_{CO_2} raises the drip interval calculated by the AGE model increases, whereas the drip interval calculated by the AXIS(C) model decreases. This enables the determination of p_{CO_2} via a comparison of the mean drip intervals calculated by theses models. All other parameters show either the same influence on the models (ϕ) or no clear result (T)[3].

In the following the individual sequences are listed and results are exemplarily shown for stalagmite MA-1.

Sequence 1: determination of p_{CO_2} To determine the p_{CO_2} the drip intervals of both, the AGE model and the AXIS(C) model are calculated for the provided temperature and δ^{13}C value of the drop and any mixing coefficient[4]. The results are compared in the following way: since the AGE model is based on only a few measured ages the temporal resolution of the result is rough. Thus, the result of the AXIS(C)

[3]The AXIS(O) is not investigated for this starting procedure due to its additional dependence on the buffer parameter. This complicates and even disables calculations, since the parameter is not known at this point of time.

[4]This determination is performed for every mixing coefficient, since sequence 1 is embedded in sequence 2 of the model (see Fig. 4.6.1.)

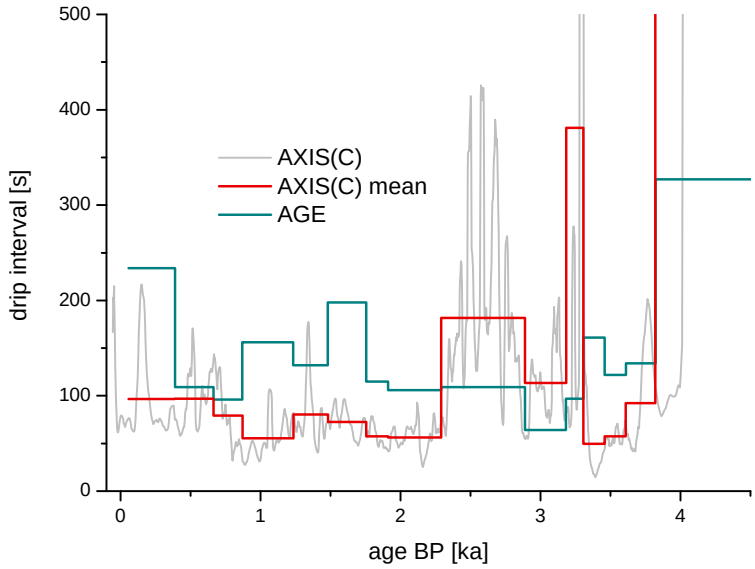

Figure 4.6.3: *Sequence 1: Determination of p_{CO_2} for T = 6,5°C, $\delta^{13}C_{drop} = -16‰$ and $\phi = 0,1$. The cyan line represents the drip interval calculated by the AGE model. The red line represents the mean drip interval at every section of the AGE model calculated by the AXIS(C) model (grey line). For reasons of clarity the result of the drip interval (grey line) is smoothed by a 20 point running mean. In the model the original data set is used.*

model, which has a rather high temporal resolution, is divided according to the sections of the AGE model and the mean value of the drip interval calculated by the AXIS(C) model is determined for each section (see Fig. 4.6.3). These mean values are compared to the drip intervals calculated by the AGE model at every section. Due to the contrary response of the drip interval calculated by the two models on a change of the partial CO_2 soil pressure, a value of p_{CO_2} must exist, where the deviation of the drip intervals of both models is smallest. This is determined using a mean square error fit. In this way the p_{CO_2} of the soil for a given temperature, mixing coefficient and $\delta^{13}C$ value of the drop can be determined. The partial pressure of the soil is determined with an accuracy of 1000 ppm.

Obviously the choice of the input parameters such as temperature and $\delta^{13}C$ of the drop seems to influence the resulting p_{CO_2}. This is true for the $\delta^{13}C$ value of the drip water, since an increase in $\delta^{13}C_{drop}$ causes a decrease of the drip interval and thus of p_{CO_2}. However, for temperature, this influence is less critical, since the algorithm of the whole model is repeated, whereas the resulting mean temperature of sequence 5 acts as the new input temperature, until the mean temperature converges. Thus, the input value of temperature can be chosen arbitrarily.

Sequence 2: determination of ϕ To determine the mixing coefficient the Hendy-Test

data sets are used. This is reasonable since the LAYER model shows an increased sensitivity to a change of the mixing coefficient compared to the AXIS(C) model. Therefore the values of the drip intervals are determined by the AGE and the AXIS(C) models at the ages, where Hendy-Tests were taken. To include uncertainties of the age measurements of the Hendy-Test data and to average out single events in the drip interval profile, mean drip intervals were calculated for the range of $\pm$250 years around the actual Hendy-Test age (Fig. 4.6.4a). These drip intervals plus the determined p_{CO_2} of sequence 1 are put into the LAYER(C, O) models and the theoretical enrichment along the growth layer for both carbon and oxygen is determined for varying mixing coefficients. In the next step these theoretical enrichments are fitted linearly, which gives values of the resulting slopes in dependence on the varying mixing coefficient. These slopes are compared to the slope of the measured Hendy-Test values in order to obtain the mixing coefficient for which the theoretical slope shows the smallest deviation to the measured slope.

This determination of ϕ is performed for both input values, the drip interval calculated by the AGE model and the drip interval calculated by the AXIS(C) model and is additionally applied to two LAYER(C, O) models using the carbon and oxygen enrichment along individual growth layers. This yields four results of ϕ for each Hendy-Test, which is shown in Fig. 4.6.4b. The mixing coefficients determined by the LAYER(C, O) models using the drip interval calculated by the AGE model are equal. The coefficients obtained for the drip interval calculated by the AXIS(C) model differ at only one Hendy-Test. Thus, all results show the same characteristics. However, to simplify calculations only the mean value of ϕ is used for the next sequence of the model. The mixing coefficient is determined with an accuracy of 0,1.

Sequence 3: determination of *d* In the third sequence the drip interval is determined using the AXIS(C) model and the calculated input values of ϕ and p_{CO_2}. This straightforward calculation has already been performed in sequence 1 and is repeated here. Since the calculation of the drip interval is fast, it is not necessary to store the results of the drip interval of sequence 1.

Sequence 4: determination $\delta^{18}O_{drop}$ In the fourth sequence the oxygen composition of the drip water is calculated. Therefore temperature must be known at any point of time during the growth period of the stalagmite. Using this temperature and the slope of the Hendy-Test, which is, regarding to the age, closest to this point of time, the buffer parameter b is determined. With the results from the earlier sequences the theoretical enrichment of δ^{18}O for varying values of the drip water is determined for the time frame, where temperature is known or estimated (Fig. 4.6.6). By comparing the theoretical values (grey lines) with the measured data (red line) the δ^{18}O value of the drip water can be obtained at every sample point of the oxygen record within this time frame. The resulting values are averaged

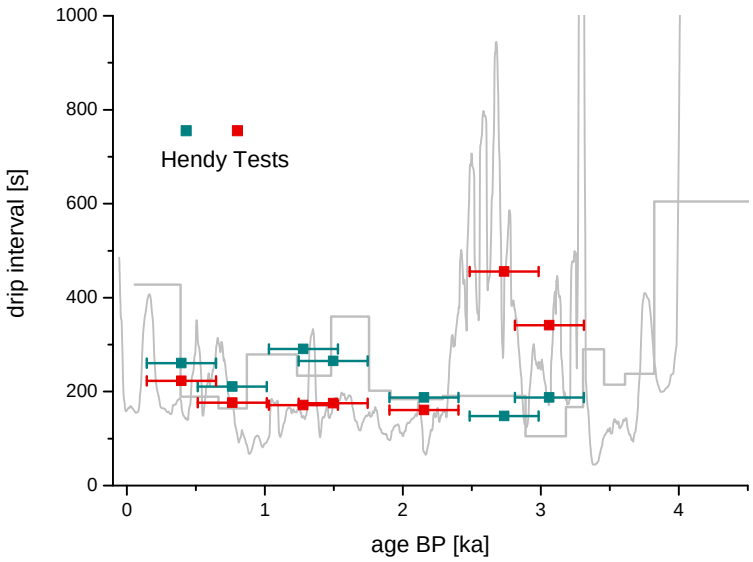

(a) *Hendy-Tests location*

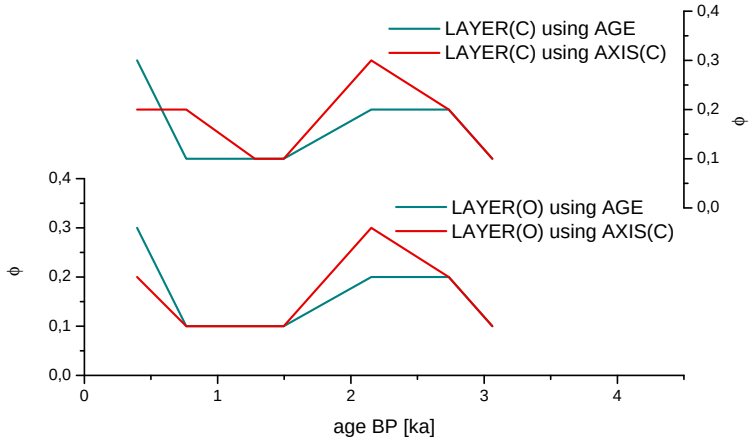

(b) *Results of ϕ*

Figure 4.6.4: *Sequence 2: Determination of ϕ. Fig. (a) shows the drip interval used for the LAYER(C,O) model and the location of the Hendy-Tests within the stalagmite. The red dots represent the drip interval obtained from the AXIS(C) model results, whereas the cyan dots are obtained from the AGE model results. The bars indicate the range, in which the drip interval of these results are averaged ($\pm$250 years). Fig. (b) shows the results of the ϕ determination for both drip intervals and both LAYER models. The characteristics of all four lines show a good agreement.*

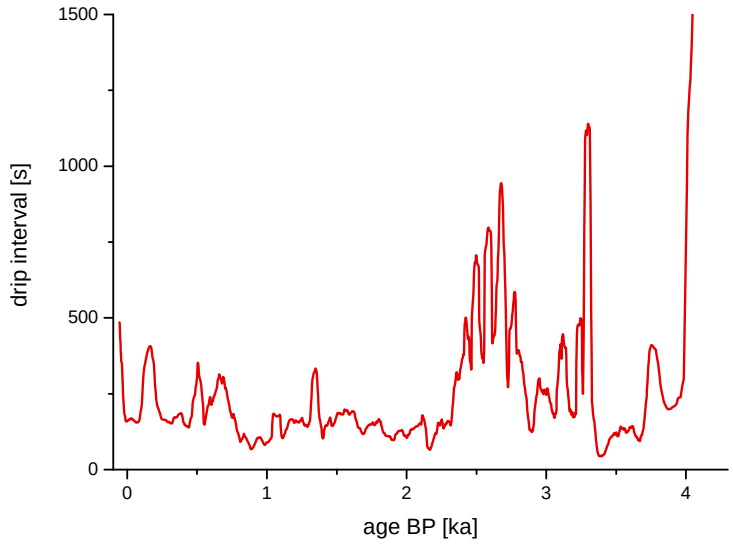

Figure 4.6.5: *Sequence 3: Determination of the drip interval. Using the mixing coefficient and p_{CO_2} from the previous sequences and the starting temperature the drip interval can be determined using the AXIS(C) model. For reasons of clarity the result of the drip interval is smoothed by a 20 point running mean. In the model the original data set is used.*

and yield an approximation of the δ^{18}O value of the drip water for the investigated time. In the following it is assumed that this δ^{18}O value of the drop was constant during the growth period of the stalagmite. This is not realistic for natural stalagmites, but reasonable for this first model approximation. In the example (see Fig. 4.6.6) the recent temperature is known and thus approximately the last 100 years are investigated. The δ^{18}O value of the drip water is determined with an accuracy of 0,01 ‰.

Sequence 5: determination of *T* In the last sequence temperature variations during the growth period of the stalagmite are determined. First, the starting temperature is used to calculate a mean buffer parameter from the available Hendy-Tests using the BUFFER model. With this value of the buffer parameter, the determined mixing coefficient, the δ^{18}O value of the drip water and the drip interval record, the theoretical enrichment of δ^{18}O for varying temperatures is calculated for the whole δ^{18}O record using the AXIS(O) model. This is illustrated in Fig. 4.6.7, where the grey lines represent the theoretical δ^{18}O values for varying temperatures and the red line the measured δ^{18}O values. These two values are compared at every sample point of the δ^{18}O record in order to determine temperature at every point. Temperature is determined with an accuracy of 0,1°C.

Until now a starting temperature was used to determine all these parameters. To over-

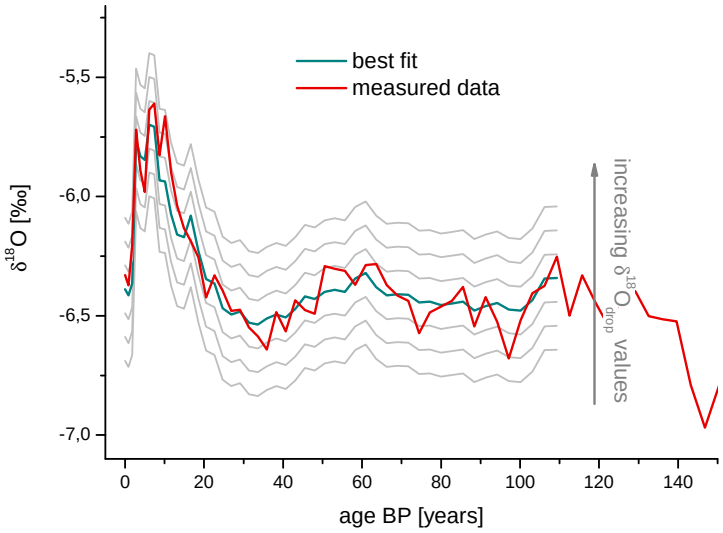

Figure 4.6.6: *Sequence 4: Determination of $\delta^{18}O$ of the drip water for stalagmite MA-1. Since the recent temperature of the cave is known approximately the last 100 years are used to determine the value of the drip water. The grey lines indicate the theoretical values, the red lines the measured data and the cyan line the $\delta^{18}O$ values, which are obtained using the determined $\delta^{18}O$ value of the drop. Therefore the BUFFER and AXIS(O) models are used. For reasons of clarity the results of $\delta^{18}O$ (grey and red lines) are smoothed by a 20 point running mean. In the model the original data set is used.*

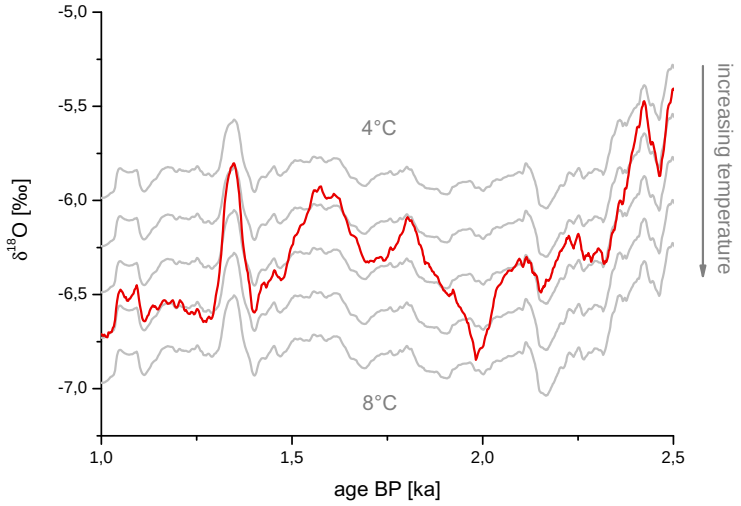

Figure 4.6.7: *Sequence 5: Determination of temperature. The grey lines represent the theoretical values, the red line the measured $\delta^{18}O$ data. At every sample point of the $\delta^{18}O$ record these values are compared in order to determine temperature at this point. For reasons of clarity only the time frame between 1 and 2,5 ka is shown. By eye it can be seen that between 1 and 1,3 ka the temperature is around 7°C, whereas it ranges between 5 and 6°C during the time between 1,3 and 1,7 ka and so on. For this determination the BUFFER and AXIS(O) models are used.*

come this starting problem of the algorithm, the obtained temperature record of sequence 5 is averaged over the growth period. The mean value of the resulting temperature record is then used as the new starting temperature and the process is repeated until the resulting mean temperature converges[5]. Depending on the starting temperature the model converges in general after at most five runs. If the input temperature is estimated close to the resulting value ($\pm$ 1°C) the model needs only two runs to converge[6].

4.6.2 Results and discussion

The CSM model is applied to stalagmites MA-1 and MA-2 from Southern Chile, which provide an accurate age-depth relation, isotopic profiles along the growth axis in a high temporal resolution and enough Hendy-Tests to indicate kinetic fractionation during the whole growth period. In addition the stalagmites were growing recently at the time of cutting, so a temperature, which needs to be estimated for the model, was measured directly in the cave. A crucial point of the model is the estimation of the $\delta^{13}C$ value of the drip water. How this and other uncertainties influence the resulting temperature

[5]The model breaks, if the first decimal place of the resulting temperature stops changing.

[6]Using a personal computer with an AMD 4000+ CPU and 2GB RAM this calculation takes between 1 and 5 minutes.

and drip interval record will be shown in the following.

The recent cave temperature was measured to $T_{rec} = 6,5 \pm 0,5°C$ and the $\delta^{13}C$ value of the drip water was estimated as $\delta^{13}C_{drop} = -15,5 \pm 1,0‰$. To determine the error of the resulting temperature and drip interval record a Monte-Carlo method was used. This is needed, since the model contains not only analytical, but also numerical calculations.

The set up of the Monte-Carlo run varies the input parameter within its error using a Gaussian distribution. This yields distributions of the resulting values of temperature, drip interval, $\delta^{18}O$ of the drip water, p_{CO_2} of the soil and ϕ. For the temporal records of temperature and drip interval, the mean values and the standard deviation are determined at every sample point, whereas for the other parameters only one mean value and standard deviation need to be determined.

Beside the simplifications made for the model, the uncertainty of the results depends on the uncertainty of the data sets (age-depth relation, isotopic profiles) and the input parameters (T_{rec}, $\delta^{13}C_{drop}$). To investigate the influence of these uncertainties and in order to determine, which parameter causes the main error, the model is run four times allowing in each run only the uncertainty of one parameter. This is used to investigate the influence of one varying parameter exemplarily on the results of stalagmite MA-1. For all calculations the Monte-Carlo method was run at least 1000 times.

Uncertainty of the recent temperature The recent temperature is varied within an estimated error of $T_{rec} = 6,5 \pm 0,5°C$. The results are shown in Table 4.6.2. As expected the recent temperature does not have a significant influence on the drip interval, which can be seen at the resulting standard deviation of the drip interval of only 9s. This is due to the weak dependence of $\delta^{13}C$ on temperature. The same holds for the mixing coefficient and the partial pressure of the soil, whose errors approach zero. By contrast the error of the resulting temperature is 0,45°C. This is close to the error estimated for the recent temperature. Due to the relatively small number of Monte-Carlo runs (1000), the actual resulting error of the recent temperature is 0,46°C instead of the presumed value of 0,50°C[7]. Thus, the error of the input data seems to be completely copied to the resulting temperature. This also explains the error of the $\delta^{18}O$ value of the drip water, which is approximately 0,11 ‰. If temperature changes by half a degree centigrade, the isotopic composition of the drip water must balance this change in order to obtain the measured $\delta^{18}O$ profile. Following in a first approach the temperature dependence of oxygen fractionation under equilibrium of -0,23 ‰/°C the error of the resulting $\delta^{18}O$ value of the drip water can be attributed to the error of the resulting temperature.

Uncertainty of the $\delta^{13}C$ drip water value The estimation of the $\delta^{13}C$ value of the drip water is a crucial point of the model, since there are no direct measurements.

[7] If the number of Monte-Carlo runs is increased, the actual error approaches the presumed error. Due to limited computational resources this result is acceptable.

Thus, this is an arbitrary guess in order to obtain results in a reasonable range. The value is estimated as $\delta^{13}C_{drop} = -15,5 \pm 1,0‰$ resulting in an actual value of $\delta^{13}C_{drop} = -15,54 \pm 0,95‰$ due to the small number of Monte-Carlo runs. Since the δ^{13}C value of the drop is directly used to determine the drip interval from the carbon record along the growth axis, the resulting error of the drip interval is not astonishing. This uncertainty of the drip interval also influences the uncertainties of the other parameters like the partial CO_2 pressure, the mixing coefficient and the δ^{18}O value of the drop. The calculations of these parameters are directly related to the drip interval, which explains their significant errors. Temperature, however, is not affected in the same manner as the other parameters. Thereby the effect of a changing drip interval on the temperature reconstruction from the δ^{18}O record is balanced out by variations of the other parameters. Thus, temperature shows only slight variations.

Uncertainty of the isotopic profiles Isotopic profiles were measured by C. Spötl at the Innsbruck University with an accuracy of $\pm 0,08‰$. These exact measurements allow an exact determination of most of the parameters and so the results show only a small variability. This holds for the mean value of the drip interval, the δ^{18}O value of the drop, the partial pressure of the soil and the mixing coefficient, which all show a small variation, which even approaches zero in some cases. However, the temperature record shows an increased variability. This variability is not caused by uncertainties of the other parameters, but by the uncertainty of the measured δ^{18}O profile of 0,08 ‰. In analogy to the argument used to explain the influence of the uncertainty of the recent temperature, this error of temperature can be deduced from the error of δ^{18}O assuming the conversion factor of equilibrium fractionation of -0,23 ‰/°C. Thus, an error of 0,08 ‰ would result in an error of approximately 1/3rd centigrade degree. This is in the range of the temperature error obtained from the Monte-Carlo run.

Uncertainty of the age-depth relation The ages of stalagmite MA-1 were determined by D. Schimpf at the Heidelberg Academy of Sciences / Heidelberg University. However, stalagmite MA-1 shows a high amount of detritus and so the ages of MA-1 were tuned to the ages of stalagmite MA-2 using the uranium profile of these stalagmites. This increases the uncertainties of the measured ages slightly, resulting in an increased variability of the drip interval. This in turn increases the error of the partial pressure of the soil and the mixing coefficient. Although the drip interval shows an error, which is in the same range as the error caused by $\delta^{13}C_{drop}$ variations, the resulting uncertainties of the other parameters are small. This is due to the increased mean value of the drip interval. At larger drip intervals the sensitivity of this parameter is attenuated resulting in a weaker influence on the other parameters. Thus, the partial pressure of the soil as well as the mixing coefficients show smaller variations than in the case of a varying $\delta^{13}C_{drop}$ value. This also results in a small variation of the δ^{18}O value of the drop and the resulting temperature.

[a]Error of	$\overline{T}$ [°C]	$\overline{d}$ [s]	$\delta^{18}O_{drop}$ [‰]	p_{CO_2} [ppm]	ϕ
T_{rec}	$5,47 \pm 0,45$	224 ± 9	$-9,13 \pm 0,11$	5984 ± 125	$0,20 \pm 0,00$
$\delta^{13}C_{drop}$	$5,50 \pm 0,16$	206 ± 81	$-9,15 \pm 0,26$	6277 ± 2378	$0,22 \pm 0,12$
[b]ds-i	$5,48 \pm 0,35$	229 ± 17	$-9,14 \pm 0,01$	6000 ± 0	$0,20 \pm 0,00$
[c]ds-a	$5,50 \pm 0,09$	282 ± 80	$-9,12 \pm 0,04$	4788 ± 1025	$0,22 \pm 0,04$

Table 4.6.2: *Results of the Monte-Carlo runs using the uncertainty of only one parameter (index (a)). The error of the recent temperature is estimated as $T_{rec} = 6,49 \pm 0,46°C$, the $\delta^{13}C$ value of the drip water as $\delta^{13}C_{drop} = -15,54 \pm 0,95‰$. The indices (b) and (c) indicate the different data sets ((b): isotopic profiles, (c): age-depth relation) The errors of the age-depth data are given in the Appendix A.1, the error of the isotopic profile as $\pm 0,08‰$.*

The results show, that some parameters respond to changes of the input data with a change of their mean values, some only with a change of their errors and other with changes in both values.
The resulting mean temperature values of all Monte-Carlo runs are at a almost constant level no matter which input parameter is changed. This is a big advantage of the CSM. However, the influence on the uncertainty of temperature is different. The recent temperature as well as the error of the isotopic profiles show a significant influence on temperature, whereas the errors of the δ^{13}C value of the drop and the age-depth relation show only a small influence.
The mean values of the drip interval also agree within their errors, however, their deviation is significant. The errors of the recent temperature, δ^{13}C value of the drop and the isotopic profiles cause rather short drip intervals, whereas the drip intervals resulting from the age-depth uncertainty are enlarged. The errors of these values are contrarily to the errors of temperature. The recent temperature as well as the isotope error result in small variations of the drip interval, whereas the error of the δ^{13}C value of the drop and the age-depth relation yield larger errors of the drip interval.
Another parameter, which shows almost no variation of its mean value is the δ^{18}O value of the drop. This parameter is robust against all different uncertainties and reveals only in- or decreased errors, if the input uncertainties are changed. Thereby the error of the δ^{13}C value of the drop has the largest influence on the error, followed by the recent temperature. The uncertainties of the data sets have almost no influence on the error of this parameter.
The partial pressure of the soil is the only parameter, which does not agree within its errors for changing input parameters. However, only the result of the age-depth error is slightly smaller than the others and thus not in their 1σ error range. This is due to the enlarged drip intervals of this Monte-Carlo run. The errors of this parameter are largest for uncertainties of the δ^{13}C value of the drop and the age-depth relation. For the other input data the error of p_{CO_2} even approaches zero.
The influence of the input uncertainties on the mixing coefficient is rather weak. All results agree within their errors and only the error of the resulting mixing coefficient due to $\delta^{13}C_{drop}$ uncertainties is increased in comparison to the other results. This is

Stalagmite	$\overline{T}$ [°C]	$\overline{d}$ [s]	$\delta^{18}O_{drop}$ [‰]	p_{CO_2} [ppm]	ϕ
MA-1	$5,53 \pm 0,62$	277 ± 133	$-9,13 \pm 0,29$	5114 ± 2254	$0,24 \pm 0,10$
MA-2	$5,47 \pm 0,69$	360 ± 111	$-9,08 \pm 0,24$	11517 ± 2832	$0,10 \pm 0,01$

Table 4.6.3: *Results of CSM model for stalagmites MA-1 and MA-2 using 7797 (MA-1) and 6396 (MA-2) Monte-Carlo runs. The input parameters of MA-1 are* $T_{rec} = 6,52 \pm 0,49°C$ *and* $\delta^{13}C_{drop} = -15,51 \pm 1,01‰$ *and the input parameters of MA-2 are* $T_{rec} = 6,51 \pm 0,51°C$ *and* $\delta^{13}C_{drop} = -15,52 \pm 0,99‰$.

caused by the increased errors of p_{CO_2} and the drip interval of this run.

The results show, that the uncertainties of all input parameters and data sets need to be taken into account, if a temperature and drip interval record wants to be extracted from stalagmites.

To calculate temperatures and drip intervals from stalagmites MA-1 and MA-2 the recent temperature is estimated as $T_{rec} = 6,5 \pm 0,5°C$ and the $\delta^{13}C$ value of the drip water as $\delta^{13}C_{drop} = -15,5 \pm 1,0‰$. Using 7797 (MA-1) and 6396 (MA-2) Monte-Carlo runs the distribution of the input parameters is shown in Fig. 4.6.8a, 4.6.8b and Fig. 4.6.9a, 4.6.9b. The results of the constant parameters for stalagmite MA-1 are shown in Figs. Figs. 4.6.8c to 4.6.8e, for MA-2 in Figs. Figs. 4.6.9c to 4.6.9e and the resulting drip interval and temperature records in Figs. 4.6.10 and 4.6.11.

Note, that both model runs for stalagmites MA-1 and MA-2 are completely independent from each other and use only the same input parameters of the recent temperature and the estimated $\delta^{13}C$ drip water value. This is reasonable since both stalagmites grew in a distance of approximately a metre.

The resulting mean values of the $\delta^{18}O$ value of the drip water of both runs agree well within the errors (MA-1: -9,13 ‰, MA-2: -9,08 ‰). However, temporal variations of this parameter are neglected, which is not realistic, but reasonable in a first order approach, which is made here.
The mixing coefficient determined for MA-1 is slightly higher than the value obtained for MA-2 (MA-1: 0,24, MA-2: 0,10). Since this parameter describes the mixing between the impinging drop and the existing solution layer, this difference might be explained by a different splashing behaviour of the drip water. This might be due to different heights of fall of the drop or surface properties of the top of the stalagmite. However, the order of magnitude agree.
The calculated partial pressure of the soil shows the greatest deviation for the two stalagmites (MA-1: 5114 ppm, MA-2: 11517 ppm). However, this still can be explained, if the two stalagmites were fed by drip water coming from sources, which have taken different water tracks throughout the soil. This might result in an uptake of CO_2 under different boundary conditions (open/closed systems), which easily can describe a devi-

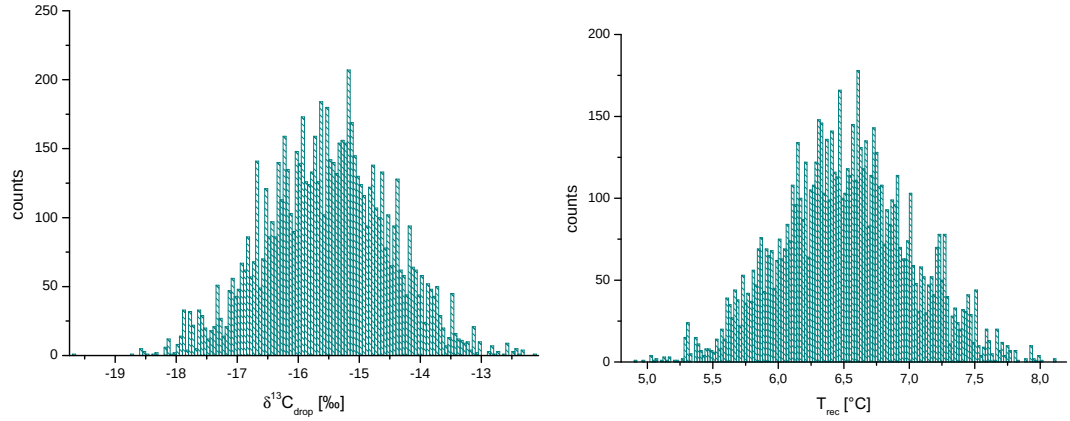

(a) $\delta^{13}C_{drop}$

(b) T_{rec}

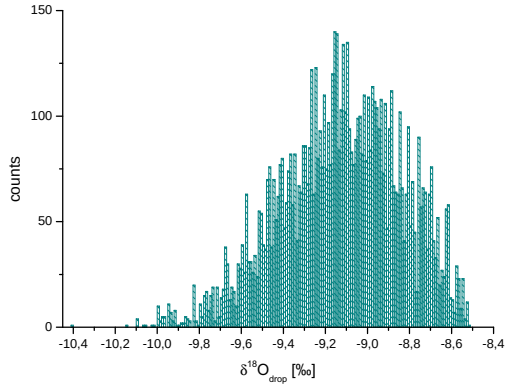

(c) $\delta^{18}O_{drop}$

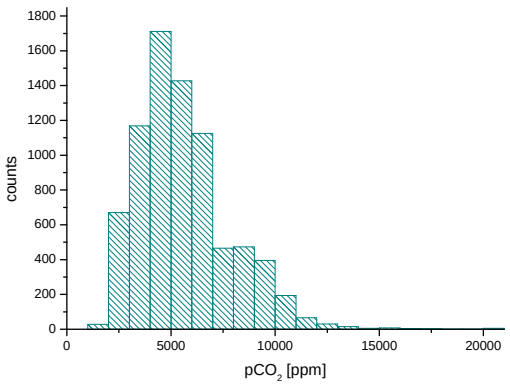

(d) p_{CO_2}

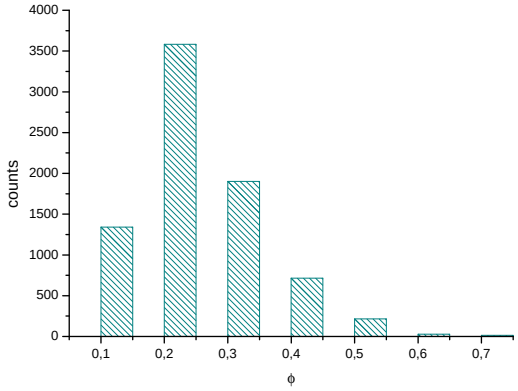

(e) ϕ

Figure 4.6.8: *Input and output parameters of CSM for stalagmite MA-1 using 7797 Monte-Carlo runs. Mean values and their standard deviation are listed in Table 4.6.3.*

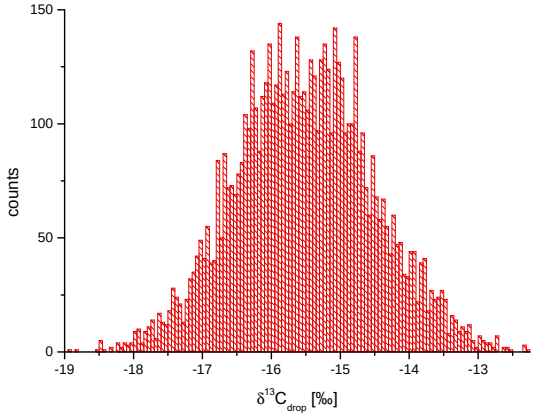

(a) $\delta^{13}C_{drop}$

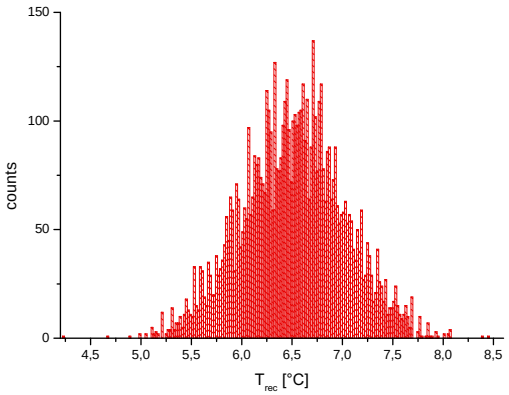

(b) T_{rec}

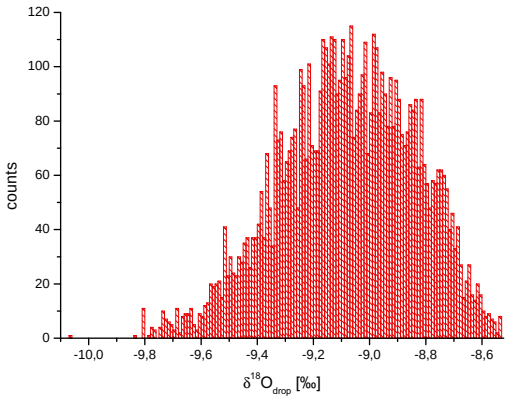

(c) $\delta^{18}O_{drop}$

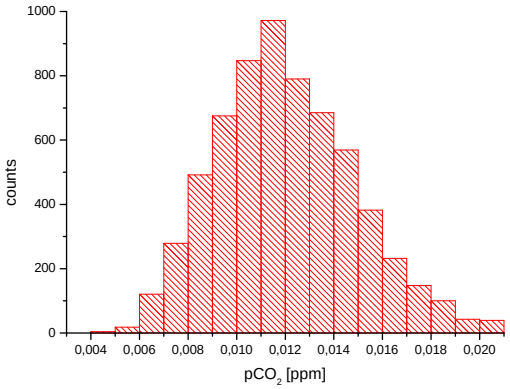

(d) p_{CO_2}

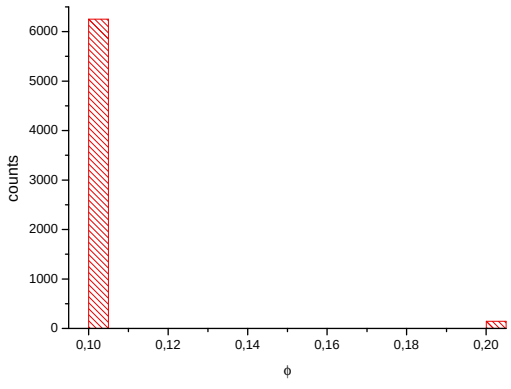

(e) ϕ

Figure 4.6.9: *Input and output parameters of CSM for stalagmite MA-2 using 6396 Monte-Carlo runs. Mean values and their standard deviation are listed in Table 4.6.3.*

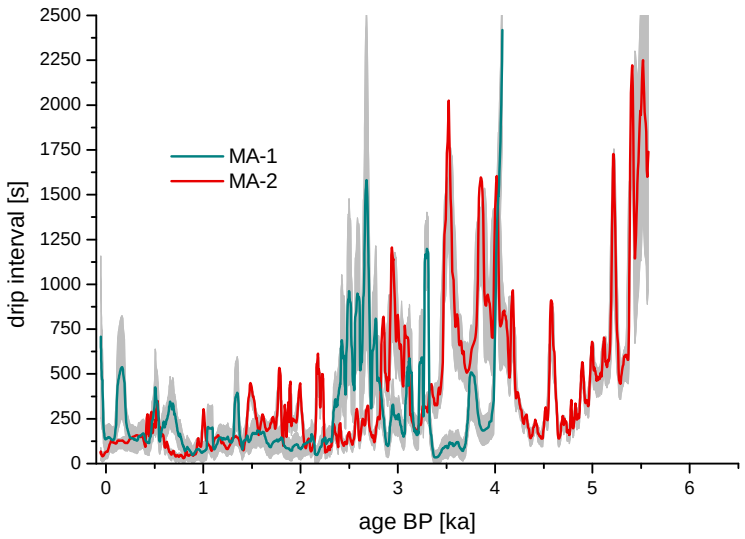

Figure 4.6.10: *Drip interval record calculated by CSM using the data sets of stalagmites MA-1 and MA-2. The grey shaded area indicates the range of the error. The record is smoothed by a 20 point running mean.*

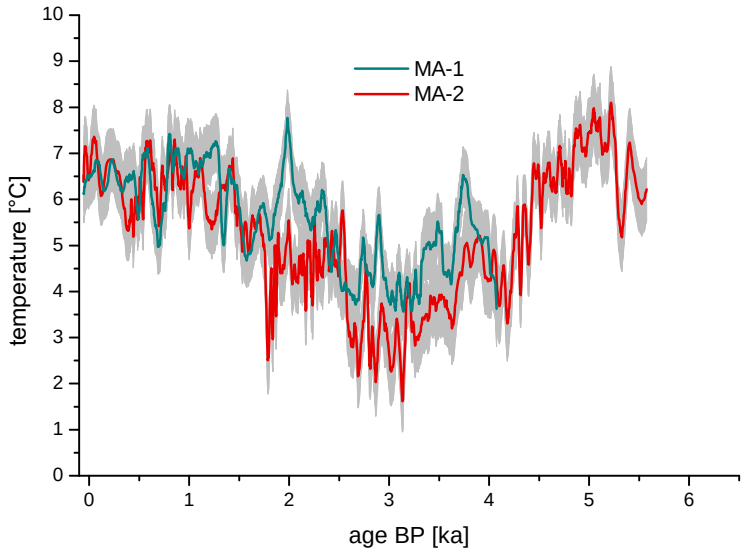

Figure 4.6.11: *Temperature record calculated by CSM using the data sets of stalagmites MA-1 and MA-2. The grey shaded area indicates the range of the error. The record is smoothed by a 20 point running mean.*

ation in this order of magnitude. However, this would be in contrast to the assumption that the drip water of both stalagmites has the same $\delta^{13}C$ value. Another explanation might be prior calcite precipitation of one of the solutions, since the determined value of p_{CO_2} reflects the amount of dissolved calcite of the solution. If one of the solutions precipitates calcite before hitting the stalagmite, the calcium concentration and the CO_2 content of the solution is decreased. This might occur, if stalagmite MA-1 developed beneath a stalactite, where calcite has already been precipitated from the solution.

The drip interval record of the stalagmites show no correlation, which is not remarkable, since both stalagmites show a different degree of kinetic fractionation, which is attributed to different drip intervals (see Fig. 4.6.10). This difference in drip interval might also support the explanation for the partial pressure of the soil, that the stalagmite were fed by drip water from different sources. In this case, stalagmite MA-1 is characterized by short drip intervals, whereas the drip water feeding stalagmite MA-2 seemed to be limited due to a smaller water reservoir for instance. However, the general trend of both records show, that water supply was higher during the last 2500 years BP in comparison to the water supply between 2500 and 6000 years BP, which is characterized by low drip intervals.

In contrast to the differences of the drip intervals of the two stalagmites the calculated temperature records show a rather high correlation of $R^2 = 0,76$. This is remarkable, since the correlation of the used $\delta^{18}O$ profile, from which the temperature is extracted show only a correlation of $R^2 = 0,51$. This suggests, that the CSM model is really able to extract temperatures from the given data sets and does not only copy the existing correlations. The calculated temperature agree well within the last 1600 years. Between 1600 and 4000 years the two profiles reveal an offset of approximately one centigrade degree, which shifts MA-2 to lower values than MA-1. However, the trend and even the main peaks of the two records still show a good agreement.

The absolute values of the results need to be handled with care, though. Stalagmite MA-1 shows a temperature variability of approximately 3–4°C and stalagmite MA-2 a variability of almost 5–6°C. This is huge compared to a global scale, but might occur locally. However, the reason for this variability lies probably in the assumption of a fixed $\delta^{18}O$ value of the drip water. This value will change with temperature, changing wind/rain trajectories like a shift of the Westerlies or due to the amount effect. If, for instance, the $\delta^{18}O$ value of the drip water would increase between 2000 and 4000 years, the decreasing temperature records would be attenuated and the variability damped. Thus, this temperature record might still include information about the $\delta^{18}O$ value of the drip water.

Note
The calculation of the theoretical $\delta^{18}O$ values for varying temperatures, mixing coefficients, partial pressures of the soil and $\delta^{18}O$ values of the drip water of sequence 5 is computationally very intensive. It slows down the algorithm especially in sequence five, where temperature is determined using the $\delta^{18}O$ record. However, the influence of the drip water value on the $\delta^{18}O$

in calcite can almost be described in a linear way for a large range of $\delta^{18}O_{drop}$. The deviation of the precipitated calcite in dependence on drip interval for two extreme values of the drip water is shown in Fig. 4.6.12. It shows the dependence of the deviation of δ^{18}O on drip interval for $\delta^{18}O_{drop} = -20‰$ and $\delta^{18}O_{drop} = -10‰$. For the extreme case of very long drip intervals, low temperatures, low mixing coefficients and a system, which is not buffered, the deviation of the calculated from the approximated δ^{13}C and δ^{18}O values does not exceed 0,1 and 0,13 ‰ respectively. Both values are close to the measurement uncertainty of 0,08 ‰. However, in general these extreme cases are not used in the model.

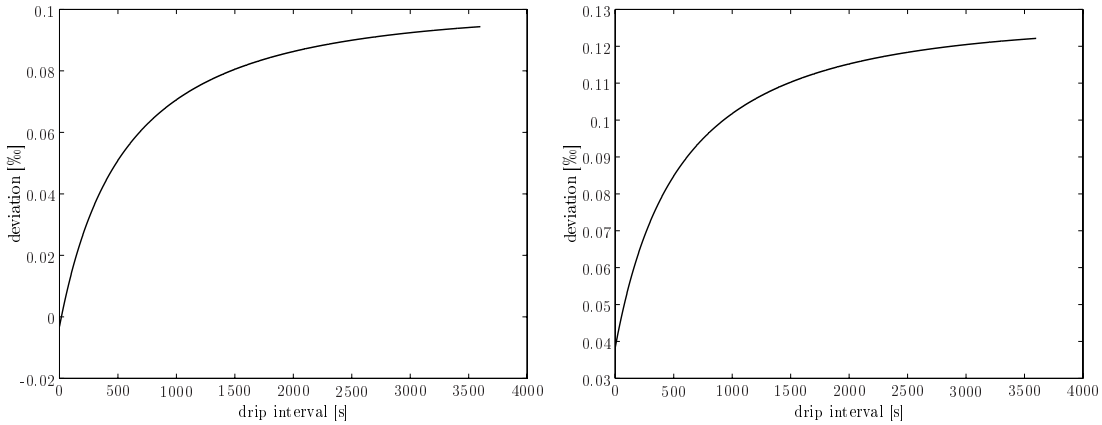

(a) *Influence of drip water on $\delta^{13}C$*

(b) *Influence of drip water on $\delta^{18}O$*

Figure 4.6.12: *Dependence of $\delta^{13}C$ and $\delta^{18}O$ on the isotopic composition of the drip water. The figure shows the deviation of two isotope calculations for varying values of the drip water ($\delta^{13}C_{drop}$, $\delta^{18}O_{drop}$ -20 ‰ to -10 ‰ (carbon with respect to VPDB, oxygen to VSMOW)). The difference are expected to be greatest for low temperatures, small mixing coefficients and no buffer effects. Thus the parameters are chosen as $pCO2 = 10000ppm$, $\phi_1 = 0.1$, $b = 0$ and $T = 1°C$. This gives the maximal deviation, which lies in the range of the accuracy of the isotope measurements (0,08 ‰).*

Due to the approximately linear response of δ^{18}O on the value of the drip water external data bases are created. These contain values of δ^{18}O in dependence on drip interval and temperature for different values of ϕ and p_{CO_2} for a given value of the drip water of $\delta^{18}O_{drop} = -10‰$. Since the calculated drip water values range around -9 ‰ the expected deviation between the real and approximated values is small.

Chapter 5

Summary and future prospects

5.1 Summary

In this study the underlying mechanisms of stalagmite growth and fractionation processes, in particular the fractionation under disequilibrium conditions, occurring during calcite precipitation are investigated. The theoretical framework of these processes is implemented in analytical and numerical models to understand the dependencies of growth and enrichment of $\delta^{13}C$ and $\delta^{18}O$ on climate related parameters like temperature, drip interval, partial CO_2 pressure of the soil zone and isotopic composition of the drip water. In addition two model parameters are adopted: the mixing coefficient and the buffer parameter. The mixing coefficient takes mixing effects into account between the impinging drop and the existing solution layer on top of the stalagmite. The buffer parameter describes buffering processes in the solution layer occurring between the huge water reservoir and the dissolved bicarbonate. These two parameters are idealized model parameters, which approximate natural processes in a simple way.

The intention of this work is to extract a temporal record of climate related parameters from data sets of natural stalagmites. In particular information about variations of temperature and drip interval want to be obtained. To overcome this challenge forward models are developed in a first step. These models calculate climate proxies like growth and isotopic profiles both along the growth axis and individual growth layers in dependence on the mentioned parameters in order to understand and quantify the influences of these parameters on stalagmite proxies.
In a second step the forward models are reversed to determine climate related parameters from the provided stalagmite data sets. However, the reversed individual models are ambiguous and do not reveal clear results for these parameters.

To overcome this ambiguity the reversed models are combined in a final step. This CSM (combined stalagmite model) utilises the different strength of influence of the different parameters on the reversed individual models and enables the extraction of a temperature and drip interval record from stalagmites. In addition mean values of the partial CO_2 pressure of the soil, the $\delta^{18}O$ value of the drip water and the mixing coefficient during the growth period of the stalagmite are obtained. Therefore commonly provided stalagmite data sets like the age-depth relation, isotopic profiles both along the growth axis and individual growth layers need be to provided as well as an estimation of the average $\delta^{13}C$ value of the drip water and a temperature at any time during the growth period of the stalagmite.

The advantages of the CSM are: (i) the model can be applied to kinetically grown stalagmites, (ii) only commonly measured data sets are needed, (iii) only two input parameters must be provided yielding a temporal record of temperature and drip interval as well as mean values of the $\delta^{18}O$ value of the drip water and the partial CO_2 pressure of the soil.
The disadvantages of the current version are: (i) the CSM is based on the simplification that all parameters except temperature and drip interval are at a fixed averaged

value during the entire growth period, (ii) a temperature at any time during the growth period as well as a mean $\delta^{13}C$ value of the drip water need to be estimated.

The CSM is a first approach to extract information about climate related parameters from stalagmites, even if they show fractionation under disequilibrium conditions. In particular the reconstruction of the amount of drip water can not be performed on stalagmites grown under equilibrium conditions. This is an improvement in comparison to existing growth and fractionation models and a further step toward understanding and extraction of climate signals from these kind of stalagmites.

The model was applied to two stalagmites from Southern Chile, which exhibit isotopic fractionation under kinetic conditions. The resulting temperature records of both stalagmites show a good correlation during the whole growth period, although the measured isotopic profiles differ due to different kinetic influences. Additionally the results of this first stalagmite are robust against variations of the input parameters, which gives confidence in the algorithm of the model.

A crucial point of all models dealing with fractionation processes of carbon and oxygen isotopes is the choice of the right fractionation factors. Depending on the kind of transition some of these factors are measured and some are calculated theoretically. Especially for carbon some factors describing the same temperature dependence of a transition between two species vary significantly. This results in a different enrichment of $\delta^{13}C$ and can even lead to different interpretation of the measured signals. For this study the fractionation factors are chosen regarding their temperature range, their date of determination or regarding earlier publications of the daphne Forschergruppe.

5.2 Future prospects

The existing model delivers promising first results of a temperature and drip interval record from two kinetically grown stalagmites. As a future prospect, the model might be enhanced to include also temporal variations of all parameters and in particular variations of the isotopic composition of the drip water, which are surely related to temperature. However, this calculation is computationally intensive. This might be a step to extract a pure temperature record from stalagmites, which have developed under disequilibrium conditions.

Another aspect is the implementation of buffer effects on the oxygen isotopes based on the measurements of Beck (2004). The current approach of the enrichment of oxygen interpolates the intermediate states between the two border cases of fractionation under equilibrium and disequilibrium in a linear way and can not distinguish, if the enrichment is caused by buffering or evaporation effects. Applying the results of Beck (2004) to the multi-box-model and thus on the fractionation of oxygen might enable the separation of buffering effects of the water reservoir from other effects like evaporation processes. Thus, the actual degree of buffering and evaporation could be determined

by this method. However, this implementation does not have an effect on the temperature and drip interval records obtained by CSM, where only the resulting enrichment of oxygen is investigated irrespective of its origin.

Until now the CSM only takes only processes into account, which occur within the cave system. By coupling this stalagmite model to an atmospheric and soil model the complete isotopic circle might be tracked, starting with evaporation at the ocean, followed by rainfall on the continent, penetration of the rain water into the soil and finally precipitation of calcite on the stalagmite. This might improve the understanding of regional or even global effects on stalagmites and will take place during the second phase of the daphne Forschergruppe based in Heidelberg.

List of Figures

List of Tables

Bibliography

Akima, H., 1970. A New Method of Interpolation and Smooth Fitting Based on Local Procedures. Journal of the Association for Computing Machinery 17/4, 589 – 602.

Baker, A., Genty, D., Dreybrodt, W., Barnes, W., Mockler, N., Grapes, J., 1998. Testing theoretically predicted stalagmite growth rate with Recent annually laminated samples: Implications for past stalagmite deposition. Geochimica et Cosmochimica Acta 62 (3), 393 – 404.

Baker, A., Smart, P., 1995. Recent flowstone growth rates: field measurements in comparison to theoretical prediction. Chemical Geology 122, 121 – 128.

Bar-Matthews, M., Ayalon, A., Kaufman, A., 2000. Timing and hydrological conditions of Sapropel events in the Eastern Mediterranean, as evident from speleothems, Soreq cave, Israel. Chemical Geology 169, 145 – 156.

Beck, W., 2004. Experimental studies of oxygen isotope frasctionation in the carbonic acid system at 15°, 25° and 40°C. Master's thesis, Texas A&M University.

Beck, W., Grossman, E., Morse, J., 2005. Experimental studies of oxygen isotope fractionation in the carbonic acid system at 15°, 25° and 40°C. Geochimica et Cosmochimica Acta 69, 3493 – 3503.

Bottinga, Y., 1968. Calculation Of Fractionation Factors For Carbon And Oxygen Isotopic Exchange In The System Calcite-Carbon Dioxide-Water. The Journal Of Physical Chemistry 72, 800 – 808.

Brenninkmeijer, C., Kraft, P., Mook, W., 1983. Oxygen isotope fractionation between CO_2 and H_2O. Isotope Geoscience 1, 181 – 190.

Buhmann, D., Dreybrodt, W., 1985a. The kinetics of calcite dissolution and precipitation in geologically relevant situations of karst areas - Closed system. Chemical Geology 53, 109 – 124.

Buhmann, D., Dreybrodt, W., 1985b. The kinetics of calcite dissolution and precipitation in geologically relevant situations of karst areas - Open system. Chemical Geology 48, 189 – 211.

Burns, S., Fleitmann, D., Matter, A., Neff, U., Mangini, A., 2001. Speleothem evidence from Oman for continental pluvial events during interglacial periods. Geology 29, 623 – 626.

Constantin, S., 2008. Chronology of the second termination and the paleoclimatic during MIS 5 based on the study of a stalagmite from Closani cave (SW Romania). In: daphne - 2nd workshop.

Criss, R., 1999. Principles of stable isotope distribution. Oxford University Press, New York.

Deines, P., Langmuir, D., Harmon, R., 1974. Stable carbon isotope ratios and the existence of a gas phase in the evolution of carbonate ground waters. Geochimica et Cosmochimica Acta 38, 1147 – 1164.

Desmarchelier, J., Goede, A., Ayliffe, L., McCulloch, M., Moriarty, K., 2000. Stable isotope record and its palaeoenvironmental interpretation for a late Middle Pleistocene speleothem from Victoria Fossil Cave, Naracoorte, South Australia. Quaternary Science Reviews 19, 763 – 774.

Dreybrodt, W., 1988. Processes in Karst Systems. Physics, Chemistry and Geology. Springer Series in Physical Environment 4. Springer, Berlin/Heidelberg/New York.

Dreybrodt, W., 1999. Chemical kinetics, speleothem growth and climate. Boreas 28, 347 – 356.

Dreybrodt, W., Eisenlohr, L., Madry, B., Ringer, S., 1997. Precipitation kinetics of calcite in the system $CaCO_3 - CO_2 - H_2O$: The conversion to CO2 by the slow preocess $CO_2 + H_2O \rightleftharpoons H^+ + HCO_3^-$ as a rate limiting step. Geochimica et Cosmochimica Acta 61, 3897 – 3904.

Dreybrodt, W., Lauckner, J., Zaihua, L., Svensson, U., Buhmann, D., 1996. The kinetics of the reaction $CO_2 + H_2O \rightleftharpoons H^+ + HCO_3^-$ as one of the rate limiting steps for the dissolution of calcite in the system $H_2O - CO_2 - CaCO_3$. Geochimica et Cosmochimica Acta 60, 3375 – 3381.

Emrich, K., Ehhalt, D., Vogel, J., 1970. Carbon isotope fractionation during the precipitation of calcium carbonate. Earth and Planetary Science Letters 8, 363 – 371.

Fantidis, J., Ehhalt, D., 1970. Variations of the carbon and oxygen isotopic composition in stalagmites: evidence of non-equilibrium isotopic fractionation. Earth and Planetary Science Letters 10, 136 – 144.

Friedman, I., O'Neil, J., 1977. Compilation of stable isotope fractionation factors of geochemical interest. Data of Geochemistry, 440–KK.

Garrels, M., Christ, C., 1965. Solutions, minerals and equilibria. Harper and Row, New York.

Goede, A., 1994. Continuous Early Last Glacial Palaeoenvironmental Record From A Tasmanian Speleothem Based On Stable Isotope And Minor Element Variations. Quaternary Science Reviews 13, 283 – 291.

Halas, S., Wolacewicz, W., 1982. The experimental srudy of oxygeb isotope exchange reaction between dissolved bicarbonate and water. J. Chem. Phys. 76, 5470 –5472.

Harmon, R., Schwarcz, H., Gascoyne, M., Hess, J., Ford, D., 2004. Studies of cave sediments. Physical and chemical records of palaeoclimate. Kluwer Academic, Ch. Palaeoclimate Information From Speleothems: The Present As A Guide To The Past, pp. 199 – 226.

Harmon, R., Schwarcz, H., O'Neil, J., 1979. D/H Ratios in speleothem fluid inclusions: A guide to variations in the isotopic composition of meteoric precipitation. Earth and Planetary Science Letters 42, 254 – 266.

Harmon, R., Thompson, P., Schwarcz, H., Ford, D., 1978. Late Pleistocene paleoclimates of North America as inferred from stable isotope studies of speleothems. Quaternary Research 9, 54 – 70.

Hendy, C., 1971. The isotopic geochemistry of speleothems - I. The calculation of the effects of different modes of formation on the isotopic composition of speleothems and their applicability as palaeoclimatic indicators. Geochimica et Cosmochimica Acta 35, 801 – 824.

Hendy, C., Wilson, A., 1968. Palaeoclimatic Data from Speleothems. Nature 219, 48 – 51.

Kaufmann, G., 2003. Stalagmite growth and palaeo-climate: the numerical perspective. Earth and Planetary Science Letters 214, 251 – 266.

Kempe, S., 1997. Welt voller Geheimnisse: Höhlen. HB Bildatlas, Sonderausgabe 17, Hamburg.

Kilian, R., Biester, H., Behrmann, J., Baeza, O., Fesq-Martin, M., Hohner, M., Schimpf, D., Friedmann, A., Mangini, A., 2006. Millennium-scale volcanic impact on a superhumid and pristine ecosystem, Geology (Boulder). Geological Society of America 34, 8, 609 – 612.

Kilian, R., Schimpf, D., Mangini, A., Spötl, C., Kronz, A., Arz, H., in prep. Strong coupling of both hemisphere westerly zones and the tropics the during past millennia.

Kim, S.-T., O'Neil, J., 1997. Equilibrium and nonequilibrium oxygen isotope effects in synthetic carbonates. Geochimica et Cosmochimica Acta 61, 3461 – 3475.

Lesniak, P., Sakai, H., 1989. Carbon isotope fractionation between dissolved carbonate (CO_3^{2-}) and CO_2(g) at 25° and 40°C. Earth and Planetary Science Letters 95, 297 – 301.

McDermott, F., 2004. Palaeo-climate reconstruction from stable isotope variations in speleothems: a review. Quaternary Science Reviews 23, 901 – 918.

Mickler, P., Banner, J., Stern, L., Asmerom, Y., Edwards, R., Ito, E., 2004. Stable isotope variations in modern tropical speleothems: Evaluating equilibrium vs. kinetic isotope effects. Geochimica et Cosmochimica Acta 68 (21), 4381 – 4393.

Mickler, P., Stern, L., Banner, J., 2006. Large kinetic isotope effects in modern speleothems. Geological Society of America 118 (1/2), 65 – 81.

Mook, W., Bommerson, J., Staverman, W., 1974. Carbon isotope fractionation between dissolved bicarbonate and gaseous carbon dioxide. Earth and Planetary Science Letters 22, 169 – 176.

Mook, W., de Vriess, J., 2000. Environmental Isotopes in the Hydrological Cycle. Principles and Applications. IAEA, Ch. Volume 1: Introduction - Theory, Methods, Review.

Mühlinghaus, C., 2006. Modellierung paläoklimatischer Parameter anhand Wachstum und Isotopiekorrelationen von Stalagmiten. Master's thesis, Ruprecht-Karls-University, Heidelberg.

Mühlinghaus, C., Scholz, D., Mangini, A., 2007. Modelling stalagmite growth and $\delta^{13}C$ as a function of drip interval and temperature. Geochimica et Cosmochimica Acta 71, 2780 – 2790.

Neff, U., Burns, S., Mangini, A., Mudelsee, M., Fleitmann, D., Matter, A., 2001. Strong coherence between solar variability and the monsoon in Oman between 9 and 6 kyr ago. Nature 411, 290 – 293.

O'Neil, J., Adami, L., 1969. The oxygen isotope partition function ratio of water and the structure of liquid water. The Journal of Physical Chemistry 73, 1553 – 1558.

O'Neil, J., Clayton, R., Mayeda, T., 1969. Oxygen isotope fractionation in divalent metal carbonates. The Journal of Chemical Physics 51, 5547 – 5558.

Plummer, L., Mackenzie, F., 1974. Predicting mineral solubility from rate data: application to the dissolution of magnesian calcites. American Journal of Science 274, 61 – 83.

Plummer, L., Wigley, T., Parkhurst, D., 1978. The kinetics of calcite dissolution in CO_2 water systems at 5 °C to 60 °C nad 0,0 to 1,0 atm CO_2. American Journal of Science 278, 179 – 216.

Romanek, C., Grossman, E., Morse, J., 1992. Carbon isotopic fractionation in synthetic aragonite and calcite: Effects of temperature and precipitation rate. Geochimica et Cosmochimica Acta 56, 419 – 430.

Romanov, C., Kaufmann, G., Dreybrodt, W., 2008. Modeling stalagmite growth by first principles of chemistry and physics of calcite precipitation. Geochimica et Cosmochimica Acta 72, 423 – 437.

Rubinson, M., Clayton, R., 1969. Carbon-13 fractionation between aragonite and calcite. Geochimica et Cosmochimica Acta 38, 997 – 1002.

Salomons, W., Mook, W., 1986. Handbook of Environmental Isotope Geochemistry, Volume 2, The Terrestrial Environment. Vol. 2. B. Elsevier, Amsterdam, Ch. Isotope geochemistry of carbonates in the weathering zone, pp. 239–270.

Schimpf, D., 2005. Datierung und Interpretation der Kohlenstoff- und Sauerstoffisotopie zweier holozäner Stalagmiten aus dem Süden Chiles (Patagonien). Master's thesis, Ruprecht-Karls-University, Heidelberg.

Spötl, C., Mangini, A., 2002. Stalagmite from the Austrian Alps reveals Dansgaard-Oeschger events during isotope stage 3: Implications for the absolute chronology of Greenlandice cores. Earth and Planetary Science Letters 203, 507 – 518.

Thorstenson, D., Parkhurst, D., 2004. Calculation of individual equilibrium constants for geochemical reactions. Geochimica et Cosmochimica Acta 68, 2449 – 2465.

Turner, J., 1982. Kinetic fractionation of carbon-13 during calcium carbonate precipitation. Geochimica et Cosmochimica Acta 46, 1183 – 1191.

Usdowski, E., 1982. Reactions and equilibria in the systems $CO_2 - H_2O$ and $CaCO_3 - CO_2 - H_2O$. A review. In: Neues Jahrbuch fuer Mineralogie, Abhandlungen. Vol. 144. pp. 148 – 171.

Usdowski, E., Hoefs, J., 1993. Oxygen isotope exchange between carbonic acid, bicarbonate, carbonate and water: A re-examination of the data of McCrea (1950) and an expression for the overall partitioning of oxygen isotopes between the carbonate species and water. Geochimica et Cosmochimica Acta 57, 3815 – 3818.

Usdowski, E., Hoefs, J., Menschel, G., 1979. Relationship between ^{13}C and ^{18}O fractionation and changes in major element composition in a recent calcite-depositing spring - A model of chemical variations with inorganic $CaCO_3$ precipitation. Earth and Planetary Science Letters 42, 267 – 276.

Vogel, J., Grootes, P., Mook, W., 1970. Isotopic fractionation between gaseous and dissolved carbon dioxide. Zeitschrift für Physik A Hadrons and Nuclei 230, 225 – 238.

Vollweiler, N., Scholz, D., Mühlinghaus, C., Mangini, A., Spötl, C., 2006. A precisely dated climate record for the last 9 kyr from three high alpine stalagmites, Spannagel Cave, Austria. Geophysical Research Letters 33, L20703.

Wiedner, E., Scholz, D., Mangini, A., Polag, D., Mühlinghaus, C., Segl, M., 2007. Investigation of the stable isotope fractionation in speleothems with laboratory experiments. Quaternary International In Press.

Zhang, J., Quay, P., Wilbur, D., 1995. Carbon isotope fractionation during gas-water exchange and dissolution of CO_2. Geochimica et Cosmochimica Acta 59, 107 – 114.

Acknowledgement

First I like to thank my supervisor Augusto Mangini for giving me the opportunity to continue the work of my diploma thesis on kinetically grown stalagmites in form of this PhD thesis, for his time, whenever problems occurred, for his good ideas, whenever work got stuck and for having me in his awesome research team.

Thanks to Werner Aeschbach-Hertig, who agreed without hesitating to revise this thesis as second referee (although he was warned of the subject, since he has already revised my diploma thesis).

Thanks to Iring Bender and Karlheinz Meier for their agreement to join the committee of my oral examination.

Thanks to Christoph Spötl for isotope analysis and Daniel Schimpf, who determined the ages of the investigated stalagmites and explored the MA cave in a cold, windy and rainy Chile.

Thanks to the proof-readers Andrea, Anne, Monika and Klaus for their thorough corrections both in form and content. That helped a lot.

Thanks to the modelling and isotope guys Anne, Daniela, Denis and Jens for bug detections, new ideas and scientific chats that helped on.

Thanks to the whole research group, who made the last three years passing by too quickly. I really enjoyed the casual and fertile atmosphere of work, which really exceeds scientific level.

Thanks to the beach volleyball team of our institute for providing the best beach outside Australia.

And last but not least, thanks to my family and my girlfriend Uschi, who supported me and my work at any time. The boy is grown up...

Appendix A

Stalagmite data sets

MA-1		MA-2	
DFT [mm]	age BP [ka]	DFT [mm]	age BP [ka]
7,00 ± 3,50	0,0481 ± 0,0840	7,00 ± 2,00	0,0964 ± 0,0150
21,00 ± 4,00	0,4010 ± 0,0873	11,90 ± 2,40	0,4105 ± 0,0228
39,75 ± 2,75	0,6665 ± 0,0415	17,25 ± 1,80	0,4981 ± 0,0291
54,75 ± 2,50	0,8695 ± 0,0411	31,50 ± 1,50	0,6985 ± 0,0125
74,90 ± 2,60	1,2360 ± 0,0458	51,60 ± 2,10	0,9783 ± 0,0202
90,00 ± 4,00	1,4712 ± 0,0851	81,50 ± 4,00	1,7849 ± 0,0471
103,00 ± 3,00	1,7631 ± 0,0599	92,80 ± 2,20	1,8963 ± 0,0329
113,25 ± 2,25	1,9100 ± 0,0372	101,50 ± 2,00	2,1792 ± 0,0450
139,50 ± 4,00	2,2910 ± 0,0480	118,60 ± 2,10	2,3342 ± 0,0392
180,00 ± 2,00	2,8896 ± 0,0290	131,50 ± 2,00	2,5887 ± 0,0880
205,40 ± 2,00	3,1821 ± 0,0251	149,80 ± 1,80	3,0503 ± 0,0321
214,40 ± 2,10	3,3047 ± 0,0369	158,90 ± 2,10	3,4958 ± 0,0446
222,60 ± 2,10	3,4609 ± 0,0394	170,50 ± 3,00	3,9159 ± 0,0819
232,30 ± 2,30	3,6111 ± 0,0335	181,10 ± 1,90	4,2684 ± 0,0827
245,10 ± 3,10	3,8083 ± 0,1012	192,00 ± 3,00	4,5223 ± 0,0824
274,00 ± 2,00	4,6972 ± 0,0754	204,40 ± 1,60	4,7201 ± 0,0920
		208,50 ± 2,00	4,8003 ± 0,1004
		242,50 ± 2,00	5,1757 ± 0,1918
		251,50 ± 3,00	5,6912 ± 0,1118

Table A.1.1: *Age-depth relations of stalagmites MA-1 and MA-2. Note, that MA-1 is tuned to MA-2 via their uranium profiles. Note, that the errors of MA-1 are slightly increased due to the tuning process.*

A.1 Stalagmites MA-1 and MA-2

Stalagmite MA-1 and MA-2 provide an accurate age-depth relation (Schimpf, 2005) as well as isotopic profiles in a high temporal resolution both along the growth axis as well as along individual growth layers (measured by C. Spötl at Innsbruck University).

The ages of stalagmite MA-1 are tuned to stalagmite MA-2, which has the lowest detritus correction of the uranium thorium ages (Schimpf, pers. comment). The tuning was performed on the uranium profile of the stalagmites. These profiles show the same characteristics, but with a slightly delay in age (see Table A.1.1). This yields in increased errors of the ages of stalagmite MA-1.

The isotopic carbon and oxygen profiles contain 1665 (MA-1) and 1669 (MA-2) data points respectively and are therefore not listed here explicitly.

Hendy-Tests of stalagmites MA-1 and MA-2 are used to make sure that both stalagmites developed under disequilibrium conditions. All data sets show an enrichment of both

carbon and oxygen along the corresponding growth layer and a linear correlation. This is according to Hendy (1971) an indication for fractionation and precipitation under disequilibrium conditions. The slopes of the δ^{13}C vs. δ^{18}O plots range between 0,18 and 0,35.

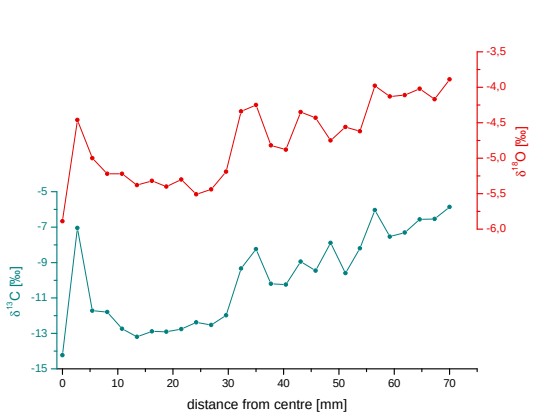

(a) *MA-1.a*

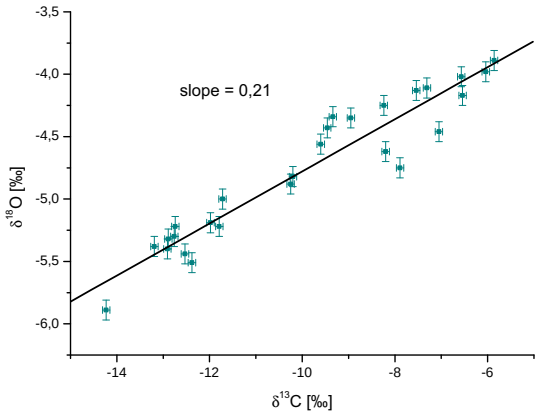

(b) *MA-1.a*

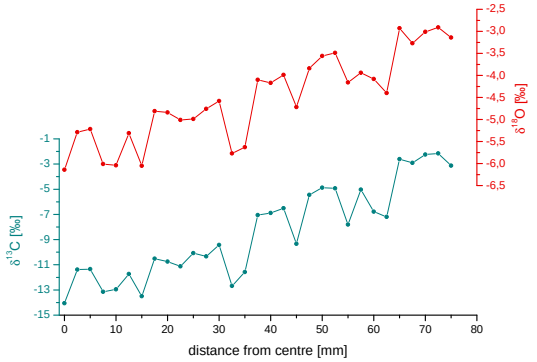

(c) *MA-1.b*

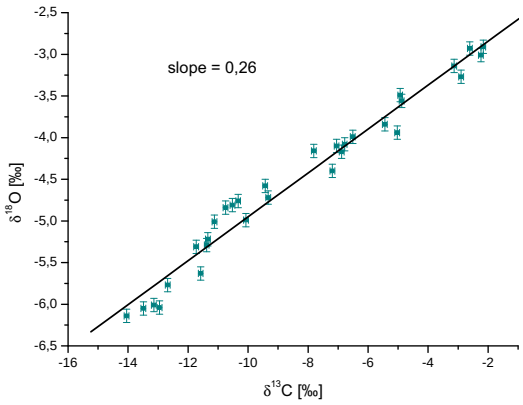

(d) *MA-1.b*

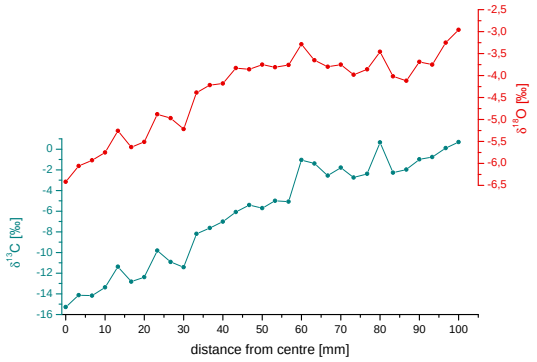

(e) *MA-1.c*

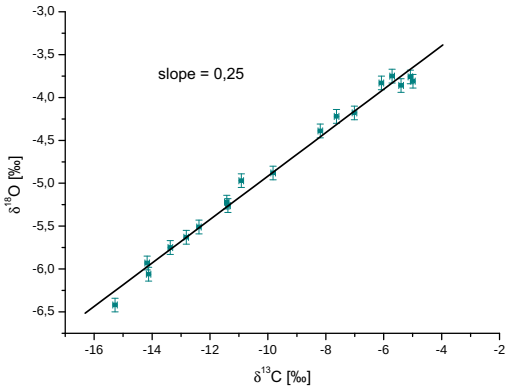

(f) *MA-1.c*

Figure A.1.1: *Hendy-Tests MA-1.a–c of stalagmite MA-1. All tests show a linear correlation between carbon and oxygen, which indicates fractionation under disequilibrium conditions.*

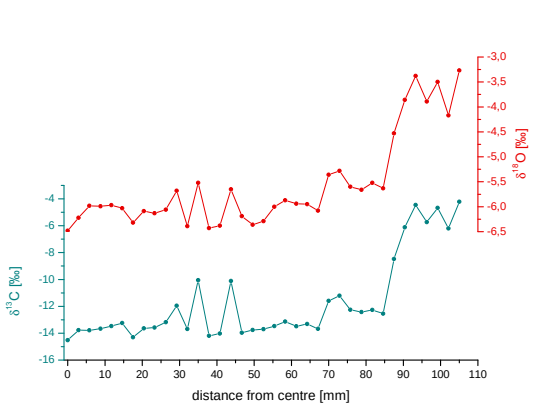

(a) *MA-1.d*

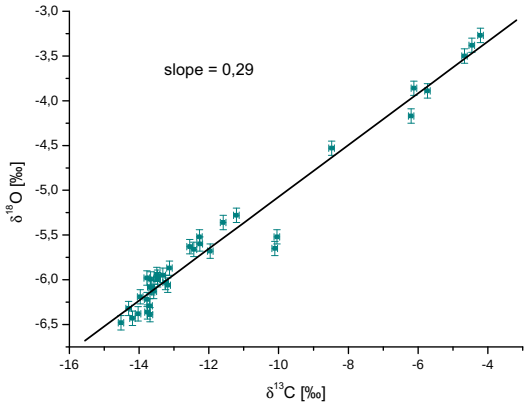

(b) *MA-1.d*

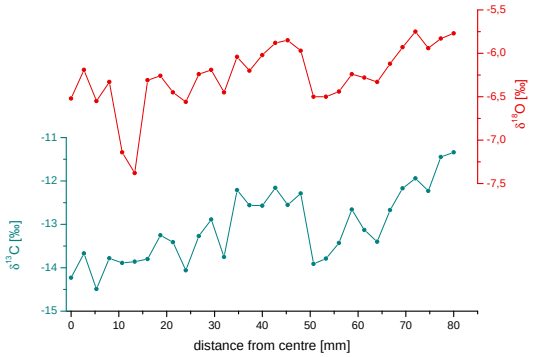

(c) *MA-1.e*

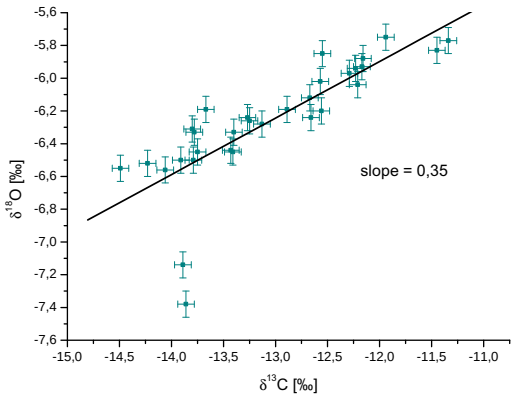

(d) *MA-1.e*

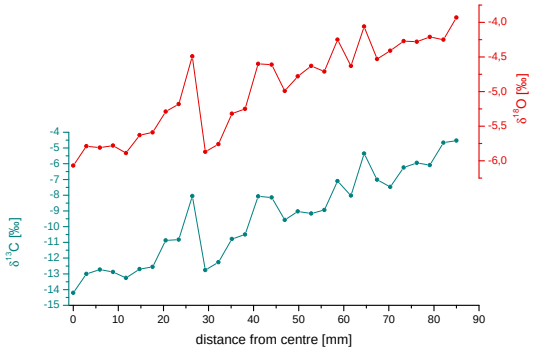

(e) *MA-1.f*

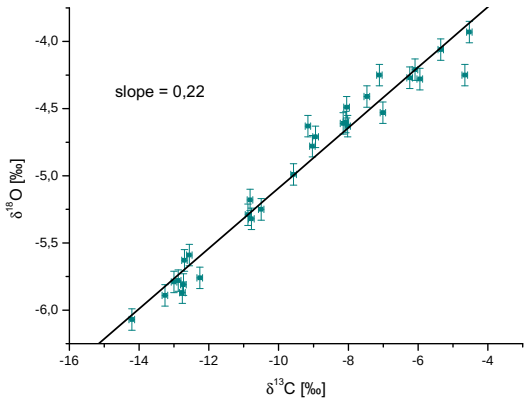

(f) *MA-1.f*

Figure A.1.2: *Hendy-Tests MA-1.d–f of stalagmite MA-1. All tests show a linear correlation between carbon and oxygen, which indicates fractionation under disequilibrium conditions.*

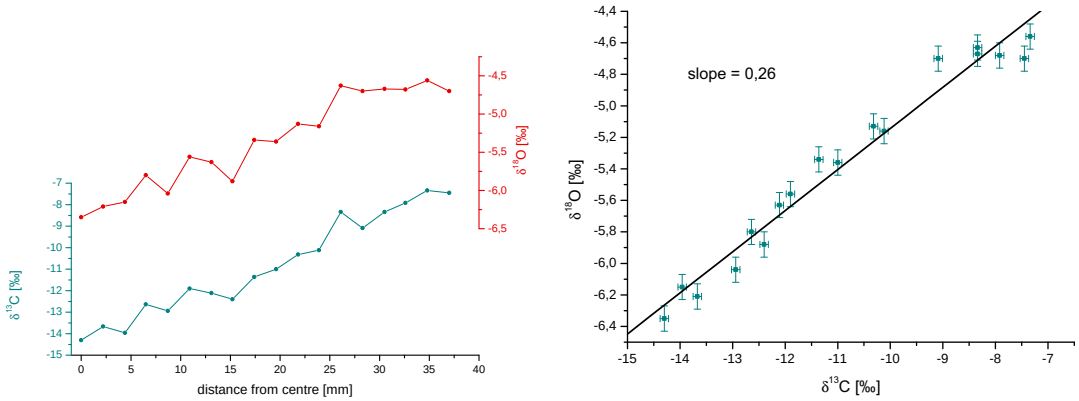

(a) *MA-1.g* **(b)** *MA-1.g*

Figure A.1.3: *Hendy-Test MA-1.g of stalagmite MA-1. The test shows a linear correlation between carbon and oxygen, which indicates fractionation under disequilibrium conditions.*

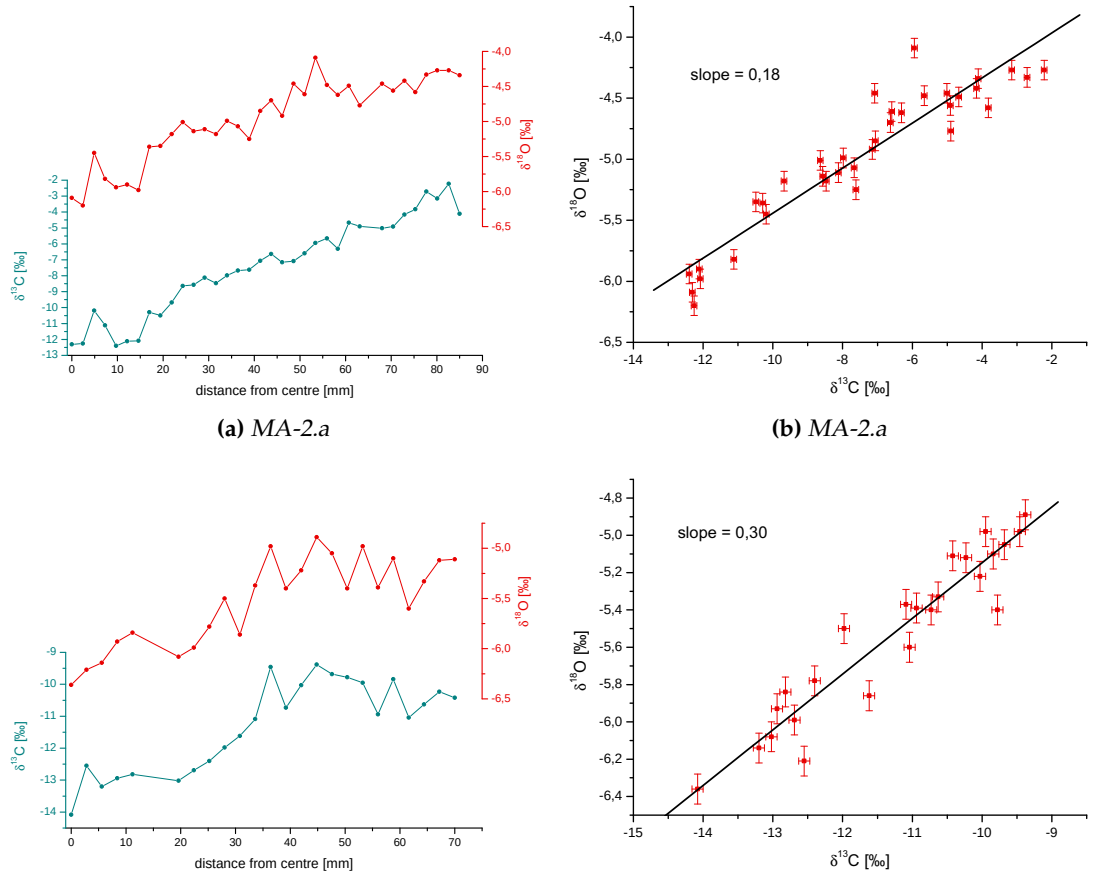

(a) *MA-2.a* **(b)** *MA-2.a*

(c) *MA-2.b* **(d)** *MA-2.b*

Figure A.1.4: *Hendy-Tests MA-2.a–b of stalagmite MA-2. All tests show a linear correlation between carbon and oxygen, which indicates fractionation under disequilibrium conditions.*

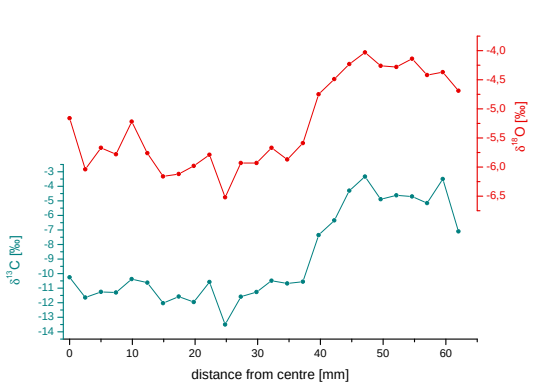

(a) *MA-2.c*

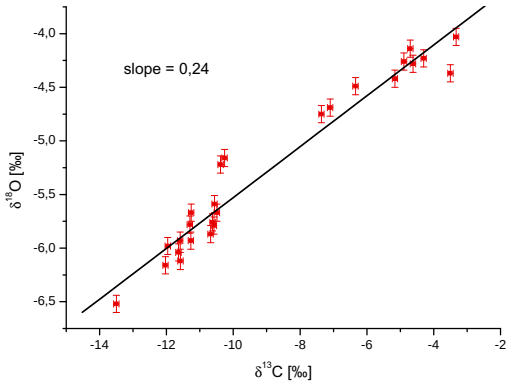

(b) *MA-2.c*

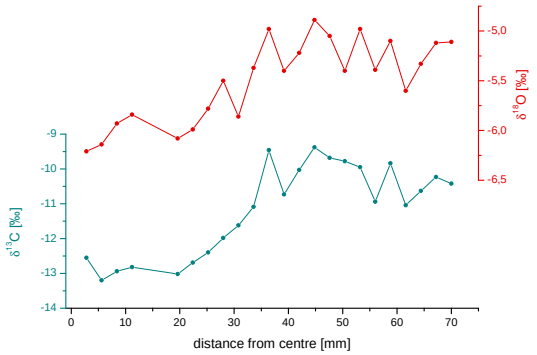

(c) *MA-2.d*

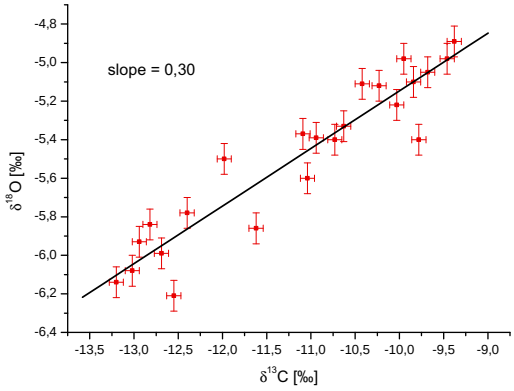

(d) *MA-2.d*

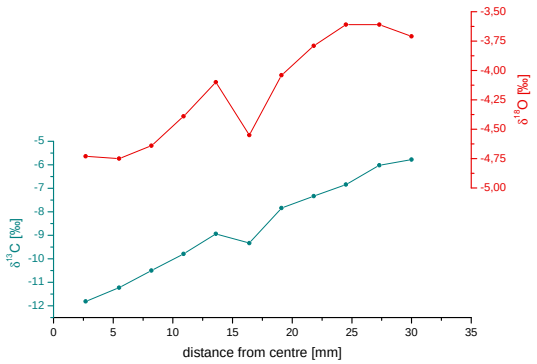

(e) *MA-2.e*

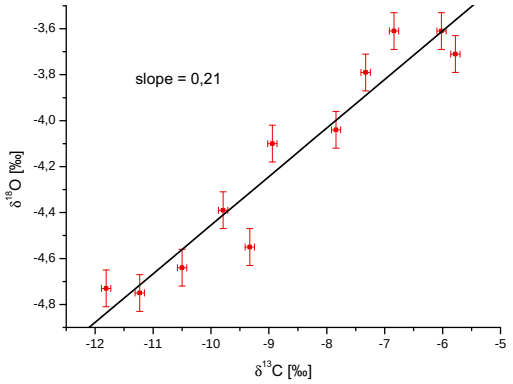

(f) *MA-2.e*

Figure A.1.5: *Hendy-Test MA-2.c–e of stalagmite MA-2. All tests show a linear correlation between carbon and oxygen, which indicates fractionation under disequilibrium conditions.*

Appendix B

Mathematical proofs

B.1 Proofs

B.1.1 Proof of the mixing process of bicarbonate concentrations

This proof is performed by complete induction.
The temporal development of a solution with a initial bicarbonate concentration of $[HCO_3^-]_{soil}$ is:

$$[HCO_3^-](t) = A + (B - A)e^{-\frac{\alpha t}{\delta}}, \tag{B.1.1}$$

with $A = [HCO_3^-]_{cave}$, $B = [HCO_3^-]_{soil}$. For $n = 1$ (one new drop) and $x = \frac{\alpha \Delta T}{\delta}$ the mixed concentration is:

$$\begin{aligned}
[HCO_3^-](1,t) &= A + \left[(1-\phi)\left(A + (B-A)e^{-x}\right) + \phi B - A\right] e^{-\frac{\alpha t}{\delta}} \\
&= A + \left[(1-\phi)A + (1-\phi)(B-A)e^{-x} + \phi(B-A+A) - A\right] e^{-\frac{\alpha t}{\delta}} \\
&= A + (B-A)\left((1-\phi)e^{-x} + \phi\right) e^{-\frac{\alpha t}{\delta}}
\end{aligned} \tag{B.1.2}$$

From Eq. 2.3.7 follows:

$$[HCO_3^-](1,t) = A + (B-A)\left((1-\phi)e^{-x} + \phi\right) e^{-\frac{\alpha t}{\delta}} \tag{B.1.3}$$

Thus, Eq. 2.3.7 is true for $n = 1$. This can be shown for all drop numbers n. In the following it is proven that the equation is true for $n + 1$:

$$\begin{aligned}
[HCO_3^-](n+1,t) &= A + \left[(1-\phi)[HCO_3^-](n,\Delta T) + \phi B - A\right] e^{-\frac{\alpha t}{\delta}} \\
&= A + \left[(1-\phi)\left(A + (B-A)e^{-x}\left(\left((1-\phi)e^{-x}\right)^n + \phi \sum_{k=0}^{n-1}\left((1-\phi)e^{-x}\right)^k\right)\right) + \phi B - A\right] e^{-\frac{\alpha t}{\delta}} \\
&= A + (B-A) \\
&\times \left((1-\phi)e^{-x}\left(\left((1-\phi)e^{-x}\right)^n + \phi \sum_{k=0}^{n-1}\left((1-\phi)e^{-x}\right)^k\right) + \phi\right) e^{-\frac{\alpha t}{\delta}} \\
&= A + (B-A)\left(\left((1-\phi)e^{-x}\right)^{n+1} + \phi \sum_{k=1}^{n}\left((1-\phi)e^{-x}\right)^k + \phi\right) e^{-\frac{\alpha t}{\delta}} \\
&= A + (B-A)\left(\left((1-\phi)e^{-x}\right)^{n+1} + \phi \sum_{k=0}^{n}\left((1-\phi)e^{-x}\right)^k\right) e^{-\frac{\alpha t}{\delta}}
\end{aligned} \tag{B.1.4}$$

qed.

B.1.2 Proof of the mixing process of bicarbonate ratios

This proof is performed by complete induction.
The temporal development of the isotope ratio of a solution with an initial isotope ratio of $R_{drop} = R(0)$ is:

$$R_{HCO_3^-}(t) = R(0)\left(\frac{[HCO_3^-](0,t)}{[HCO_3^-](0,0)}\right)^{\overline{\epsilon}}. \tag{B.1.5}$$

After one drop ($n = 1$) the initial isotope ratio R_{drop} of the solution changes to:

$$\begin{aligned} R(1) &= (1-\phi)R_{drop}\left(\frac{[HCO_3^-](0,\Delta T)}{[HCO_3^-](0,0)}\right)^{\overline{\epsilon}} + \phi R_{drop} \\ &= \left((1-\phi)\left(\frac{[HCO_3^-](0,\Delta T)}{[HCO_3^-](0,0)}\right)^{\overline{\epsilon}} + \phi\right) R_{drop} \end{aligned} \tag{B.1.6}$$

From Eqs. 3.2.4 and 3.2.5 follow for $n = 1$:

$$R(1) = \left((1-\phi)\left(\frac{[HCO_3^-](0,\Delta T)}{[HCO_3^-](0,0)}\right)^{\overline{\epsilon}} + \phi\right) R_{drop} \tag{B.1.7}$$

Thus, Eq. 3.2.4 is true for $n = 1$. This can be shown for all drop numbers n. It is now proven that the equation is true for $n + 1$:

$$R(n+1) = (1-\phi)R(n)\left(\frac{[HCO_3^-](n,\Delta T)}{[HCO_3^-](n,0)}\right)^{\overline{\epsilon}} + \phi R_{drop}. \tag{B.1.8}$$

With

$$A(i) = \left(\frac{[HCO_3^-](i,\Delta T)}{[HCO_3^-](i,0)}\right)^{\overline{\epsilon}} \tag{B.1.9}$$

it follows:

$$\begin{aligned} R(n+1) &= \left[(1-\phi)\left((1-\phi)^n \prod_{k=0}^{n-1} A(k) + \phi \sum_{k=0}^{n-1}(1-\phi)^k \prod_{m=n-k}^{n-1} A(m)\right) A(n) + \phi\right] R_{drop} \\ &= \left[(1-\phi)^{n+1} \prod_{k=0}^{n} A(k) + \phi(1-\phi)A(n) \sum_{k=0}^{n-1}(1-\phi)^k \prod_{m=n-k}^{n-1} A(m) + \phi\right] R_{drop} \\ &= \left[(1-\phi)^{n+1} \prod_{k=0}^{n} A(k) + \phi \sum_{k=0}^{n}(1-\phi)^k \prod_{m=n-k}^{n} A(m)\right] R_{drop} \end{aligned} \tag{B.1.10}$$

qed.

B.1.3 Proof of the limit of λ

If the mixing factor λ includes a function in the form of $\lim_{x\to 0} f(x) \to 1$, it can be approximated for $x \to 0$ as the following:

$$\begin{aligned}\lambda(n) &= ((1-\phi)f(x))^n + \phi \sum_{k=0}^{n-1} ((1-\phi)f(x))^k \\ &\approx (1-\phi)^n + \phi \sum_{k=0}^{n-1} (1-\phi)^k \\ &= 1.\end{aligned} \tag{B.1.11}$$

This is shown by complete induction.
For $x \to 0$ and $n = 1$ λ is:

$$\begin{aligned}\lambda(1) &= (1-\phi)^1 + \phi \sum_{k=0}^{0} (1-\phi)^k \\ &= 1 - \phi + 1 \\ &= 1.\end{aligned} \tag{B.1.12}$$

This can be shown for all n. In the following it is shown that the equation is true for $n+1$:

$$\begin{aligned}\lambda(n+1) &= (1-\phi)\lambda(n) + \phi \\ &= (1-\phi)\left((1-\phi)^n + \phi \sum_{k=0}^{n-1} (1-\phi)^k\right) + \phi \\ &= (1-\phi)^{n+1} + \phi \sum_{k=1}^{n} (1-\phi)^k + \phi \\ &= (1-\phi)^{n+1} + \phi \sum_{k=0}^{n} (1-\phi)^k\end{aligned} \tag{B.1.13}$$

qed.

B.1.4 Proof of the limit of disequilibrium fractionation

The proof that the isotopic composition occurring under equilibrium conditions is equal to the isotopic composition occurring under disequilibrium conditions for short drip intervals ($\lim_{\Delta T\to 0} \delta^{13}C_{de} = \delta^{13}C_{eq}$) is exemplarily shown for δ^{13}C and can be performed analogously for δ^{18}O .
Under equilibrium conditions δ^{13}C can be calculated after Eq. 3.2.1:

$$\delta^{13}C_{eq} = \alpha_1^{13}(\delta^{13}C_{drop} + 1000) - 1000. \tag{B.1.14}$$

under disequilibrium conditions Eq. 3.2.6 is needed:

$$\delta^{13}C_{de} = f_c(\delta^{13}C_{drop} + 1000) - 1000. \tag{B.1.15}$$

with

$$\begin{aligned} f_c =& \alpha_1^{13} \frac{1}{\overline{\alpha^{13}}} \frac{\left(\frac{[HCO_3^-](n,\Delta T)}{[HCO_3^-](n,0)}\right)^{\overline{\alpha^{13}}} - 1}{\frac{[HCO_3^-](n,\Delta T)}{[HCO_3^-](n,0)} - 1} \\ & \times \left((1-\phi)^n \prod_{k=0}^{n-1} \left(\frac{[HCO_3^-](k,\Delta T)}{[HCO_3^-](k,0)} \right)^{\overline{\epsilon}} \right. \\ & \left. + \phi \sum_{k=0}^{n-1} (1-\phi)^k \prod_{m=n-k}^{n-1} \left(\frac{[HCO_3^-](m,\Delta T)}{[HCO_3^-](m,0)} \right)^{\overline{\epsilon}} \right). \end{aligned} \tag{B.1.16}$$

For short drip intervals $\Delta T \to 0$ Eq. 3.2.6 and f_c in particular can be approximated by a Taylor series as follows. Again $x = \frac{\alpha \Delta T}{\delta}$ is used. The concentration of bicarbonate can be approximated as:

$$[HCO_3^-](n,\Delta T) \approx [HCO_3^-]_{cave} + \left([HCO_3^-]_{soil} - [HCO_3^-]_{cave}\right)\left(1 - \frac{\alpha \Delta T}{\delta}\right). \tag{B.1.17}$$

From this follows:

$$\begin{aligned} \frac{[HCO_3^-](n,\Delta T)}{[HCO_3^-](n,0)} &\approx \frac{[HCO_3^-]_{cave} + \left([HCO_3^-]_{soil} - [HCO_3^-]_{cave}\right)\left(1 - \frac{\alpha \Delta T}{\delta}\right)}{[HCO_3^-]_{cave} + \left([HCO_3^-]_{soil} - [HCO_3^-]_{cave}\right)} \\ &= 1 - \frac{\left([HCO_3^-]_{soil} - [HCO_3^-]_{cave}\right)\frac{\alpha \Delta T}{\delta}}{[HCO_3^-]_{soil}} \\ &= (1 - A). \end{aligned} \tag{B.1.18}$$

With

$$(1-A)^{\overline{\alpha^{13}}} \approx 1 - \overline{\alpha^{13}} A \tag{B.1.19}$$

yields for f_c:

$$
\begin{aligned}
f_c \approx & \alpha_1^{13} \frac{1}{\overline{\alpha^{13}}} \frac{1-\overline{\alpha^{13}}A-1}{1-A-1} \\
& \times \left((1-\phi)^n \underbrace{\prod_{k=0}^{n-1} (1-A)^{\overline{\epsilon}}}_{\approx 1} + \phi \sum_{k=0}^{n-1} (1-\phi)^k \underbrace{\prod_{m=n-k}^{n-1} (1-A)^{\overline{\epsilon}}}_{\approx 1} \right) \\
& \approx \alpha_1^{13}.
\end{aligned}
\tag{B.1.20}
$$

The isotopic composition of the precipitated calcite is after Eq. 3.2.6:

$$
\begin{aligned}
\delta^{13}C_{de} &= f_c \left(\delta^{13}C_{drop} + 1000 \right) - 1000 \\
&\approx \alpha_1^{13} \left(\delta^{13}C_{drop} + 1000 \right) - 1000 \\
&= \delta^{13}C_{eq}.
\end{aligned}
\tag{B.1.21}
$$

qed.

Appendix C

Databases

C.1 Calibrated mixing parameters

The multi-box-model is calibrated by a comparison to the exponential and the Gaussian growth model. As described in section 3.4.1 of the thesis the adjustment to the Gaussian model failures at high mixing coefficients. Thus, the calibration can only be performed for mixing coefficients up to $\phi = 0,7$. (Table C.1.2)
As described in section 3.1 the exponential growth model seems to mimic the natural shape of stalagmites in a more realistic way than the Gaussian model. Hence, the exponential calibration is used to determine the ϕ database (Table C.1.1).

The calibrated mixing parameters depend on the radius of the stalagmite and the chosen mixing coefficient ϕ, which describes the mixing between the impinging drop and the innermost box of the solution layer (see section 3.4). The following tables are arranged in ascending order of the mixing coefficient ϕ and the equilibrium radius. Mixing parameters of boxes, which can not be calculated due to small radii, have a value of zero.

C.1.1 Exponential calibration

Radius [mm]	ϕ	ϕ_2	ϕ_3	ϕ_4	ϕ_5	ϕ_6	ϕ_7	ϕ_8	ϕ_9	ϕ_{10}
60,5	0,10	0,08	0,07	0,05	0,05	0,04	0,03	0,00	0,00	0,00
61,5	0,10	0,08	0,06	0,05	0,05	0,04	0,03	0,02	0,00	0,00
62,5	0,10	0,08	0,06	0,05	0,05	0,04	0,03	0,02	0,00	0,00
63,5	0,10	0,08	0,06	0,05	0,05	0,04	0,03	0,02	0,00	0,00
64,5	0,10	0,08	0,05	0,06	0,05	0,04	0,03	0,03	0,00	0,00
65,5	0,10	0,08	0,05	0,06	0,05	0,04	0,03	0,03	0,02	0,00
66,5	0,10	0,08	0,06	0,05	0,05	0,04	0,03	0,03	0,02	0,00
67,5	0,10	0,08	0,06	0,05	0,05	0,04	0,03	0,03	0,02	0,00
68,5	0,10	0,07	0,07	0,06	0,05	0,04	0,03	0,03	0,02	0,00
69,5	0,10	0,07	0,07	0,06	0,04	0,05	0,03	0,03	0,03	0,02
70,5	0,10	0,07	0,07	0,06	0,04	0,05	0,03	0,03	0,03	0,02
71,5	0,10	0,07	0,07	0,05	0,05	0,04	0,04	0,03	0,02	0,02
72,5	0,10	0,07	0,07	0,05	0,05	0,04	0,04	0,03	0,03	0,02
73,4	0,10	0,07	0,07	0,05	0,05	0,04	0,04	0,03	0,03	0,02
74,4	0,10	0,07	0,07	0,05	0,05	0,04	0,04	0,03	0,03	0,02
75,5	0,10	0,07	0,06	0,06	0,04	0,05	0,04	0,03	0,03	0,02
76,4	0,10	0,07	0,07	0,05	0,05	0,04	0,04	0,03	0,03	0,02
77,5	0,10	0,07	0,07	0,05	0,05	0,04	0,04	0,03	0,03	0,02
78,4	0,10	0,07	0,06	0,06	0,04	0,05	0,03	0,04	0,03	0,02
79,5	0,10	0,07	0,06	0,05	0,05	0,04	0,04	0,03	0,03	0,03
80,5	0,10	0,07	0,07	0,05	0,05	0,04	0,04	0,03	0,03	0,02
81,4	0,10	0,07	0,06	0,05	0,05	0,04	0,04	0,03	0,03	0,03
82,4	0,10	0,07	0,06	0,05	0,05	0,04	0,04	0,03	0,03	0,03
83,4	0,10	0,07	0,07	0,05	0,04	0,05	0,03	0,04	0,03	0,02
84,4	0,10	0,07	0,06	0,05	0,04	0,05	0,04	0,03	0,03	0,03
85,5	0,10	0,07	0,05	0,06	0,04	0,04	0,04	0,03	0,03	0,03
86,5	0,10	0,07	0,06	0,05	0,04	0,05	0,03	0,04	0,03	0,03
87,3	0,10	0,07	0,05	0,05	0,05	0,04	0,04	0,03	0,03	0,03

Radius [mm]	ϕ	ϕ_2	ϕ_3	ϕ_4	ϕ_5	ϕ_6	ϕ_7	ϕ_8	ϕ_9	ϕ_{10}
88,4	0,10	0,07	0,06	0,05	0,04	0,04	0,04	0,03	0,03	0,03
89,4	0,10	0,07	0,05	0,05	0,05	0,04	0,04	0,03	0,03	0,03
90,4	0,10	0,07	0,06	0,05	0,04	0,04	0,04	0,03	0,03	0,03
91,4	0,10	0,07	0,05	0,05	0,04	0,04	0,04	0,03	0,04	0,03
92,3	0,10	0,07	0,05	0,05	0,05	0,04	0,04	0,03	0,03	0,03
93,2	0,10	0,07	0,05	0,05	0,04	0,04	0,04	0,03	0,03	0,03
119,7	0,10	0,06	0,05	0,04	0,04	0,04	0,03	0,04	0,03	0,03
45,5	0,20	0,15	0,09	0,06	0,00	0,00	0,00	0,00	0,00	0,00
46,5	0,20	0,15	0,10	0,06	0,00	0,00	0,00	0,00	0,00	0,00
47,5	0,20	0,14	0,10	0,07	0,03	0,00	0,00	0,00	0,00	0,00
48,5	0,20	0,15	0,09	0,07	0,04	0,00	0,00	0,00	0,00	0,00
49,5	0,20	0,14	0,10	0,07	0,04	0,00	0,00	0,00	0,00	0,00
50,5	0,20	0,15	0,09	0,07	0,04	0,00	0,00	0,00	0,00	0,00
51,5	0,20	0,14	0,10	0,07	0,05	0,00	0,00	0,00	0,00	0,00
52,5	0,20	0,14	0,09	0,07	0,05	0,03	0,00	0,00	0,00	0,00
53,5	0,20	0,14	0,10	0,07	0,05	0,03	0,00	0,00	0,00	0,00
54,5	0,20	0,13	0,10	0,08	0,05	0,04	0,00	0,00	0,00	0,00
55,5	0,20	0,13	0,10	0,08	0,05	0,04	0,00	0,00	0,00	0,00
56,5	0,20	0,13	0,10	0,08	0,05	0,04	0,00	0,00	0,00	0,00
57,5	0,20	0,13	0,10	0,07	0,06	0,04	0,03	0,00	0,00	0,00
58,5	0,20	0,13	0,10	0,07	0,06	0,04	0,03	0,00	0,00	0,00
59,5	0,20	0,13	0,09	0,08	0,06	0,04	0,03	0,00	0,00	0,00
60,4	0,20	0,14	0,08	0,08	0,06	0,04	0,03	0,00	0,00	0,00
61,5	0,20	0,13	0,09	0,08	0,06	0,04	0,04	0,02	0,00	0,00
62,5	0,20	0,12	0,10	0,08	0,06	0,05	0,04	0,02	0,00	0,00
63,5	0,20	0,13	0,09	0,07	0,06	0,05	0,04	0,03	0,00	0,00
64,4	0,20	0,14	0,08	0,08	0,06	0,05	0,03	0,03	0,00	0,00
65,5	0,20	0,12	0,10	0,07	0,06	0,05	0,04	0,03	0,02	0,00
66,4	0,20	0,12	0,10	0,07	0,06	0,05	0,04	0,03	0,02	0,00
67,4	0,20	0,13	0,08	0,08	0,06	0,05	0,04	0,03	0,02	0,00
68,4	0,20	0,12	0,09	0,07	0,06	0,05	0,04	0,04	0,02	0,00
69,4	0,20	0,12	0,08	0,08	0,06	0,05	0,04	0,04	0,03	0,02
70,5	0,20	0,12	0,08	0,08	0,06	0,05	0,04	0,04	0,03	0,02
71,5	0,20	0,12	0,08	0,07	0,06	0,06	0,04	0,04	0,03	0,02
72,5	0,20	0,12	0,08	0,07	0,06	0,05	0,05	0,03	0,03	0,03
73,4	0,20	0,11	0,09	0,08	0,06	0,05	0,05	0,03	0,03	0,03
74,4	0,20	0,11	0,09	0,07	0,06	0,06	0,04	0,04	0,03	0,03
75,4	0,20	0,13	0,08	0,07	0,06	0,05	0,04	0,04	0,03	0,03
76,5	0,20	0,12	0,09	0,07	0,06	0,05	0,04	0,04	0,03	0,03
77,4	0,20	0,11	0,09	0,08	0,06	0,05	0,04	0,04	0,03	0,03
78,4	0,20	0,11	0,09	0,07	0,06	0,05	0,05	0,04	0,03	0,03
79,4	0,20	0,11	0,08	0,07	0,06	0,05	0,05	0,04	0,03	0,03
80,2	0,20	0,11	0,09	0,07	0,06	0,05	0,05	0,04	0,03	0,03
81,4	0,20	0,11	0,08	0,07	0,06	0,05	0,05	0,04	0,03	0,03
82,3	0,20	0,11	0,07	0,08	0,06	0,05	0,05	0,04	0,03	0,03
83,2	0,20	0,11	0,09	0,07	0,06	0,05	0,04	0,04	0,04	0,03
84,2	0,20	0,11	0,07	0,07	0,06	0,05	0,05	0,04	0,03	0,03
112,9	0,20	0,10	0,07	0,06	0,05	0,05	0,04	0,04	0,03	0,04
38,5	0,30	0,21	0,09	0,00	0,00	0,00	0,00	0,00	0,00	0,00
39,5	0,30	0,20	0,10	0,00	0,00	0,00	0,00	0,00	0,00	0,00
40,5	0,30	0,21	0,10	0,00	0,00	0,00	0,00	0,00	0,00	0,00

Radius [mm]	ϕ	ϕ_2	ϕ_3	ϕ_4	ϕ_5	ϕ_6	ϕ_7	ϕ_8	ϕ_9	ϕ_{10}
41,5	0,30	0,20	0,11	0,00	0,00	0,00	0,00	0,00	0,00	0,00
42,5	0,30	0,20	0,11	0,02	0,00	0,00	0,00	0,00	0,00	0,00
43,5	0,30	0,20	0,11	0,03	0,00	0,00	0,00	0,00	0,00	0,00
44,5	0,30	0,19	0,12	0,06	0,00	0,00	0,00	0,00	0,00	0,00
45,5	0,30	0,19	0,12	0,07	0,00	0,00	0,00	0,00	0,00	0,00
46,5	0,30	0,21	0,11	0,07	0,00	0,00	0,00	0,00	0,00	0,00
47,5	0,30	0,19	0,11	0,08	0,03	0,00	0,00	0,00	0,00	0,00
48,5	0,30	0,19	0,12	0,08	0,04	0,00	0,00	0,00	0,00	0,00
49,5	0,30	0,20	0,11	0,08	0,04	0,00	0,00	0,00	0,00	0,00
50,5	0,30	0,18	0,11	0,08	0,05	0,00	0,00	0,00	0,00	0,00
51,5	0,30	0,19	0,11	0,08	0,05	0,00	0,00	0,00	0,00	0,00
52,5	0,30	0,18	0,11	0,08	0,06	0,03	0,00	0,00	0,00	0,00
53,5	0,30	0,19	0,11	0,08	0,06	0,03	0,00	0,00	0,00	0,00
54,5	0,30	0,17	0,12	0,08	0,06	0,04	0,00	0,00	0,00	0,00
55,5	0,30	0,17	0,12	0,08	0,06	0,04	0,00	0,00	0,00	0,00
56,4	0,30	0,17	0,12	0,08	0,06	0,05	0,00	0,00	0,00	0,00
57,5	0,30	0,17	0,11	0,09	0,06	0,05	0,03	0,00	0,00	0,00
58,5	0,30	0,17	0,11	0,08	0,07	0,05	0,03	0,00	0,00	0,00
59,5	0,30	0,16	0,12	0,08	0,07	0,05	0,03	0,00	0,00	0,00
60,4	0,30	0,17	0,11	0,09	0,06	0,05	0,03	0,00	0,00	0,00
61,4	0,30	0,16	0,12	0,08	0,07	0,05	0,04	0,02	0,00	0,00
62,4	0,30	0,16	0,10	0,09	0,07	0,05	0,04	0,03	0,00	0,00
63,5	0,30	0,16	0,11	0,09	0,06	0,06	0,04	0,03	0,00	0,00
64,4	0,30	0,18	0,10	0,08	0,07	0,05	0,04	0,03	0,00	0,00
65,5	0,30	0,16	0,10	0,08	0,07	0,05	0,05	0,03	0,02	0,00
66,5	0,30	0,16	0,10	0,09	0,06	0,06	0,04	0,03	0,03	0,00
67,5	0,30	0,16	0,11	0,08	0,07	0,05	0,05	0,03	0,03	0,00
68,4	0,30	0,16	0,11	0,08	0,07	0,05	0,05	0,03	0,03	0,00
69,5	0,30	0,15	0,10	0,08	0,07	0,06	0,04	0,04	0,03	0,02
70,3	0,30	0,14	0,11	0,09	0,07	0,05	0,05	0,04	0,03	0,02
71,4	0,30	0,14	0,11	0,08	0,07	0,06	0,05	0,04	0,03	0,02
72,5	0,30	0,14	0,11	0,08	0,07	0,06	0,05	0,04	0,03	0,02
73,4	0,30	0,14	0,10	0,09	0,07	0,05	0,05	0,04	0,03	0,03
74,4	0,30	0,14	0,10	0,08	0,07	0,06	0,05	0,04	0,03	0,03
75,5	0,30	0,14	0,09	0,09	0,07	0,05	0,05	0,04	0,03	0,03
76,3	0,30	0,15	0,09	0,08	0,07	0,06	0,04	0,04	0,04	0,03
77,4	0,30	0,14	0,10	0,08	0,07	0,06	0,05	0,04	0,03	0,03
78,3	0,30	0,14	0,09	0,08	0,07	0,06	0,05	0,04	0,03	0,03
79,3	0,30	0,13	0,10	0,08	0,07	0,06	0,05	0,04	0,04	0,03
80,3	0,30	0,14	0,10	0,08	0,07	0,05	0,05	0,04	0,04	0,03
80,3	0,30	0,14	0,10	0,08	0,07	0,05	0,05	0,04	0,04	0,03
81,0	0,30	0,13	0,10	0,08	0,07	0,05	0,05	0,05	0,03	0,03
81,0	0,30	0,13	0,10	0,08	0,07	0,05	0,05	0,05	0,03	0,03
35,5	0,40	0,27	0,01	0,00	0,00	0,00	0,00	0,00	0,00	0,00
36,5	0,40	0,26	0,01	0,00	0,00	0,00	0,00	0,00	0,00	0,00
37,5	0,40	0,27	0,02	0,00	0,00	0,00	0,00	0,00	0,00	0,00
38,5	0,40	0,26	0,10	0,00	0,00	0,00	0,00	0,00	0,00	0,00
39,5	0,40	0,26	0,11	0,00	0,00	0,00	0,00	0,00	0,00	0,00
40,5	0,40	0,25	0,12	0,00	0,00	0,00	0,00	0,00	0,00	0,00
41,5	0,40	0,24	0,12	0,00	0,00	0,00	0,00	0,00	0,00	0,00
42,5	0,40	0,24	0,12	0,02	0,00	0,00	0,00	0,00	0,00	0,00

Radius [mm]	ϕ	ϕ_2	ϕ_3	ϕ_4	ϕ_5	ϕ_6	ϕ_7	ϕ_8	ϕ_9	ϕ_{10}
43,5	0,40	0,24	0,12	0,03	0,00	0,00	0,00	0,00	0,00	0,00
44,5	0,40	0,23	0,13	0,07	0,00	0,00	0,00	0,00	0,00	0,00
45,5	0,40	0,23	0,12	0,08	0,00	0,00	0,00	0,00	0,00	0,00
46,5	0,40	0,25	0,12	0,07	0,00	0,00	0,00	0,00	0,00	0,00
47,5	0,40	0,23	0,12	0,08	0,04	0,00	0,00	0,00	0,00	0,00
48,5	0,40	0,23	0,13	0,08	0,04	0,00	0,00	0,00	0,00	0,00
49,5	0,40	0,24	0,12	0,08	0,05	0,00	0,00	0,00	0,00	0,00
50,4	0,40	0,23	0,12	0,09	0,05	0,00	0,00	0,00	0,00	0,00
51,4	0,40	0,22	0,12	0,09	0,05	0,00	0,00	0,00	0,00	0,00
52,4	0,40	0,21	0,12	0,09	0,06	0,03	0,00	0,00	0,00	0,00
53,5	0,40	0,22	0,12	0,09	0,06	0,04	0,00	0,00	0,00	0,00
54,5	0,40	0,20	0,13	0,09	0,06	0,04	0,00	0,00	0,00	0,00
55,5	0,40	0,20	0,13	0,09	0,06	0,04	0,00	0,00	0,00	0,00
56,5	0,40	0,20	0,13	0,09	0,06	0,05	0,00	0,00	0,00	0,00
57,5	0,40	0,20	0,12	0,09	0,07	0,05	0,03	0,00	0,00	0,00
58,4	0,40	0,19	0,13	0,09	0,07	0,05	0,03	0,00	0,00	0,00
59,5	0,40	0,19	0,12	0,09	0,07	0,05	0,03	0,00	0,00	0,00
60,4	0,40	0,20	0,12	0,09	0,07	0,05	0,04	0,00	0,00	0,00
61,5	0,40	0,19	0,12	0,09	0,07	0,05	0,04	0,02	0,00	0,00
62,4	0,40	0,21	0,11	0,09	0,07	0,05	0,04	0,03	0,00	0,00
63,4	0,40	0,19	0,11	0,09	0,07	0,06	0,04	0,03	0,00	0,00
64,4	0,40	0,20	0,12	0,09	0,07	0,05	0,04	0,03	0,00	0,00
65,5	0,40	0,18	0,11	0,09	0,07	0,06	0,04	0,03	0,02	0,00
66,4	0,40	0,18	0,12	0,09	0,07	0,06	0,04	0,04	0,02	0,00
67,4	0,40	0,18	0,12	0,09	0,07	0,06	0,04	0,04	0,02	0,00
68,4	0,40	0,20	0,11	0,09	0,07	0,06	0,04	0,04	0,02	0,00
69,5	0,40	0,17	0,11	0,09	0,07	0,06	0,05	0,04	0,03	0,02
70,4	0,40	0,16	0,12	0,09	0,07	0,06	0,05	0,04	0,03	0,02
71,3	0,40	0,16	0,12	0,09	0,07	0,06	0,05	0,04	0,03	0,02
72,4	0,40	0,16	0,11	0,09	0,07	0,06	0,05	0,04	0,03	0,03
73,4	0,40	0,16	0,11	0,09	0,07	0,06	0,05	0,04	0,03	0,03
74,2	0,40	0,18	0,11	0,09	0,07	0,06	0,05	0,04	0,03	0,03
75,4	0,40	0,19	0,10	0,09	0,07	0,06	0,05	0,04	0,03	0,03
76,3	0,40	0,17	0,10	0,09	0,07	0,06	0,05	0,04	0,03	0,03
77,3	0,40	0,16	0,10	0,09	0,07	0,06	0,05	0,04	0,04	0,03
78,3	0,40	0,15	0,11	0,09	0,07	0,06	0,05	0,04	0,04	0,03
79,3	0,40	0,15	0,10	0,09	0,07	0,06	0,05	0,04	0,04	0,03
33,5	0,50	0,31	0,00	0,00	0,00	0,00	0,00	0,00	0,00	0,00
34,5	0,50	0,30	0,00	0,00	0,00	0,00	0,00	0,00	0,00	0,00
35,5	0,50	0,31	0,01	0,00	0,00	0,00	0,00	0,00	0,00	0,00
36,5	0,50	0,30	0,01	0,00	0,00	0,00	0,00	0,00	0,00	0,00
37,5	0,50	0,29	0,09	0,00	0,00	0,00	0,00	0,00	0,00	0,00
38,5	0,50	0,30	0,10	0,00	0,00	0,00	0,00	0,00	0,00	0,00
39,5	0,50	0,31	0,11	0,00	0,00	0,00	0,00	0,00	0,00	0,00
40,5	0,50	0,29	0,12	0,00	0,00	0,00	0,00	0,00	0,00	0,00
41,5	0,50	0,27	0,13	0,00	0,00	0,00	0,00	0,00	0,00	0,00
42,5	0,50	0,27	0,13	0,02	0,00	0,00	0,00	0,00	0,00	0,00
43,5	0,50	0,27	0,13	0,03	0,00	0,00	0,00	0,00	0,00	0,00
44,5	0,50	0,26	0,13	0,07	0,00	0,00	0,00	0,00	0,00	0,00
45,5	0,50	0,26	0,13	0,08	0,00	0,00	0,00	0,00	0,00	0,00
46,5	0,50	0,27	0,13	0,08	0,00	0,00	0,00	0,00	0,00	0,00

Radius [mm]	ϕ	ϕ_2	ϕ_3	ϕ_4	ϕ_5	ϕ_6	ϕ_7	ϕ_8	ϕ_9	ϕ_{10}
47,5	0,50	0,25	0,14	0,08	0,04	0,00	0,00	0,00	0,00	0,00
48,5	0,50	0,26	0,13	0,09	0,04	0,00	0,00	0,00	0,00	0,00
49,4	0,50	0,26	0,13	0,09	0,05	0,00	0,00	0,00	0,00	0,00
50,4	0,50	0,26	0,13	0,09	0,05	0,00	0,00	0,00	0,00	0,00
51,5	0,50	0,24	0,14	0,09	0,06	0,00	0,00	0,00	0,00	0,00
52,5	0,50	0,23	0,14	0,09	0,06	0,03	0,00	0,00	0,00	0,00
53,4	0,50	0,24	0,13	0,10	0,06	0,04	0,00	0,00	0,00	0,00
54,4	0,50	0,22	0,14	0,09	0,07	0,04	0,00	0,00	0,00	0,00
55,4	0,50	0,22	0,14	0,09	0,07	0,04	0,00	0,00	0,00	0,00
56,4	0,50	0,22	0,14	0,09	0,07	0,05	0,00	0,00	0,00	0,00
57,4	0,50	0,22	0,13	0,10	0,07	0,05	0,03	0,00	0,00	0,00
58,4	0,50	0,21	0,14	0,09	0,07	0,05	0,03	0,00	0,00	0,00
59,5	0,50	0,21	0,13	0,10	0,07	0,05	0,04	0,00	0,00	0,00
60,5	0,50	0,23	0,13	0,09	0,07	0,05	0,04	0,00	0,00	0,00
61,4	0,50	0,21	0,12	0,10	0,07	0,06	0,04	0,02	0,00	0,00
62,5	0,50	0,20	0,13	0,09	0,08	0,05	0,04	0,03	0,00	0,00
63,4	0,50	0,20	0,13	0,10	0,07	0,06	0,04	0,03	0,00	0,00
64,4	0,50	0,22	0,13	0,09	0,07	0,06	0,04	0,03	0,00	0,00
65,4	0,50	0,19	0,13	0,10	0,07	0,06	0,04	0,04	0,02	0,00
66,4	0,50	0,20	0,12	0,09	0,08	0,06	0,04	0,04	0,02	0,00
67,4	0,50	0,21	0,12	0,09	0,07	0,06	0,05	0,03	0,03	0,00
68,3	0,50	0,21	0,12	0,09	0,07	0,06	0,05	0,03	0,03	0,00
69,5	0,50	0,18	0,12	0,10	0,07	0,06	0,05	0,04	0,03	0,02
70,5	0,50	0,18	0,12	0,10	0,07	0,06	0,05	0,04	0,03	0,02
71,2	0,50	0,18	0,11	0,10	0,07	0,06	0,05	0,04	0,03	0,02
72,3	0,50	0,17	0,13	0,09	0,08	0,06	0,05	0,04	0,03	0,03
73,5	0,50	0,17	0,12	0,10	0,07	0,06	0,05	0,04	0,04	0,02
74,3	0,50	0,17	0,11	0,10	0,07	0,07	0,05	0,04	0,03	0,03
75,3	0,50	0,19	0,11	0,09	0,08	0,06	0,05	0,04	0,03	0,03
76,2	0,50	0,18	0,11	0,09	0,08	0,06	0,05	0,04	0,04	0,03
77,2	0,50	0,17	0,12	0,09	0,07	0,06	0,05	0,05	0,03	0,03
78,3	0,50	0,17	0,11	0,09	0,07	0,06	0,05	0,05	0,04	0,03
38,5	0,60	0,33	0,11	0,00	0,00	0,00	0,00	0,00	0,00	0,00
39,5	0,60	0,33	0,12	0,00	0,00	0,00	0,00	0,00	0,00	0,00
40,5	0,60	0,32	0,12	0,00	0,00	0,00	0,00	0,00	0,00	0,00
41,5	0,60	0,30	0,13	0,00	0,00	0,00	0,00	0,00	0,00	0,00
42,5	0,60	0,29	0,14	0,02	0,00	0,00	0,00	0,00	0,00	0,00
43,5	0,60	0,30	0,14	0,03	0,00	0,00	0,00	0,00	0,00	0,00
44,5	0,60	0,28	0,14	0,07	0,00	0,00	0,00	0,00	0,00	0,00
45,5	0,60	0,28	0,14	0,08	0,00	0,00	0,00	0,00	0,00	0,00
46,5	0,60	0,30	0,14	0,08	0,00	0,00	0,00	0,00	0,00	0,00
47,5	0,60	0,28	0,14	0,09	0,04	0,00	0,00	0,00	0,00	0,00
48,5	0,60	0,29	0,14	0,09	0,04	0,00	0,00	0,00	0,00	0,00
49,5	0,60	0,29	0,14	0,09	0,05	0,00	0,00	0,00	0,00	0,00
50,5	0,60	0,30	0,13	0,09	0,05	0,00	0,00	0,00	0,00	0,00
51,4	0,60	0,26	0,15	0,09	0,06	0,00	0,00	0,00	0,00	0,00
52,4	0,60	0,25	0,14	0,10	0,06	0,03	0,00	0,00	0,00	0,00
53,4	0,60	0,26	0,14	0,10	0,06	0,04	0,00	0,00	0,00	0,00
54,5	0,60	0,24	0,14	0,10	0,07	0,04	0,00	0,00	0,00	0,00
55,5	0,60	0,24	0,14	0,10	0,07	0,04	0,00	0,00	0,00	0,00
56,5	0,60	0,24	0,14	0,10	0,07	0,05	0,00	0,00	0,00	0,00

Radius [mm]	ϕ	ϕ_2	ϕ_3	ϕ_4	ϕ_5	ϕ_6	ϕ_7	ϕ_8	ϕ_9	ϕ_{10}
57,5	0,60	0,24	0,14	0,10	0,07	0,05	0,03	0,00	0,00	0,00
58,4	0,60	0,23	0,14	0,10	0,07	0,05	0,03	0,00	0,00	0,00
59,4	0,60	0,22	0,14	0,10	0,07	0,06	0,03	0,00	0,00	0,00
60,5	0,60	0,27	0,13	0,10	0,07	0,05	0,04	0,00	0,00	0,00
61,5	0,60	0,23	0,13	0,10	0,07	0,06	0,04	0,02	0,00	0,00
62,3	0,60	0,24	0,13	0,10	0,07	0,06	0,04	0,03	0,00	0,00
63,4	0,60	0,22	0,13	0,10	0,07	0,06	0,04	0,03	0,00	0,00
64,4	0,60	0,23	0,13	0,10	0,07	0,06	0,04	0,03	0,00	0,00
65,4	0,60	0,21	0,13	0,10	0,07	0,06	0,05	0,03	0,02	0,00
66,4	0,60	0,21	0,13	0,10	0,08	0,06	0,04	0,04	0,02	0,00
67,3	0,60	0,21	0,13	0,10	0,08	0,06	0,05	0,03	0,03	0,00
68,5	0,60	0,19	0,13	0,10	0,08	0,06	0,05	0,04	0,03	0,00
69,5	0,60	0,19	0,13	0,10	0,08	0,06	0,05	0,04	0,03	0,02
70,5	0,60	0,19	0,13	0,10	0,08	0,06	0,05	0,04	0,03	0,02
71,3	0,60	0,19	0,12	0,10	0,08	0,06	0,05	0,04	0,03	0,02
72,4	0,60	0,19	0,12	0,10	0,07	0,07	0,05	0,04	0,03	0,03
73,3	0,60	0,18	0,13	0,09	0,08	0,06	0,05	0,04	0,04	0,03
74,2	0,60	0,22	0,11	0,10	0,07	0,06	0,05	0,04	0,04	0,02
75,2	0,60	0,20	0,12	0,09	0,08	0,06	0,05	0,04	0,04	0,03
76,2	0,60	0,19	0,12	0,09	0,08	0,06	0,05	0,04	0,04	0,03
77,3	0,60	0,18	0,12	0,09	0,08	0,06	0,05	0,05	0,03	0,03
77,6	0,60	0,19	0,12	0,09	0,08	0,06	0,05	0,05	0,03	0,03
30,5	0,70	0,04	0,00	0,00	0,00	0,00	0,00	0,00	0,00	0,00
31,5	0,70	0,37	0,00	0,00	0,00	0,00	0,00	0,00	0,00	0,00
32,5	0,70	0,38	0,00	0,00	0,00	0,00	0,00	0,00	0,00	0,00
33,5	0,70	0,38	0,00	0,00	0,00	0,00	0,00	0,00	0,00	0,00
34,5	0,70	0,37	0,00	0,00	0,00	0,00	0,00	0,00	0,00	0,00
35,5	0,70	0,37	0,01	0,00	0,00	0,00	0,00	0,00	0,00	0,00
36,5	0,70	0,37	0,01	0,00	0,00	0,00	0,00	0,00	0,00	0,00
37,5	0,70	0,37	0,02	0,00	0,00	0,00	0,00	0,00	0,00	0,00
38,5	0,70	0,35	0,11	0,00	0,00	0,00	0,00	0,00	0,00	0,00
39,5	0,70	0,36	0,12	0,00	0,00	0,00	0,00	0,00	0,00	0,00
40,5	0,70	0,34	0,13	0,00	0,00	0,00	0,00	0,00	0,00	0,00
41,5	0,70	0,32	0,14	0,00	0,00	0,00	0,00	0,00	0,00	0,00
42,5	0,70	0,32	0,14	0,02	0,00	0,00	0,00	0,00	0,00	0,00
43,5	0,70	0,32	0,14	0,03	0,00	0,00	0,00	0,00	0,00	0,00
44,5	0,70	0,30	0,15	0,07	0,00	0,00	0,00	0,00	0,00	0,00
45,5	0,70	0,30	0,15	0,08	0,00	0,00	0,00	0,00	0,00	0,00
46,5	0,70	0,32	0,14	0,08	0,00	0,00	0,00	0,00	0,00	0,00
47,5	0,70	0,30	0,15	0,09	0,04	0,00	0,00	0,00	0,00	0,00
48,5	0,70	0,30	0,15	0,09	0,04	0,00	0,00	0,00	0,00	0,00
49,5	0,70	0,28	0,15	0,09	0,05	0,00	0,00	0,00	0,00	0,00
50,4	0,70	0,30	0,14	0,09	0,05	0,00	0,00	0,00	0,00	0,00
51,4	0,70	0,28	0,15	0,10	0,06	0,00	0,00	0,00	0,00	0,00
52,4	0,70	0,27	0,14	0,10	0,06	0,03	0,00	0,00	0,00	0,00
53,5	0,70	0,28	0,14	0,10	0,06	0,04	0,00	0,00	0,00	0,00
54,5	0,70	0,26	0,14	0,10	0,07	0,04	0,00	0,00	0,00	0,00
55,4	0,70	0,26	0,14	0,10	0,07	0,04	0,00	0,00	0,00	0,00
56,4	0,70	0,25	0,15	0,10	0,07	0,05	0,00	0,00	0,00	0,00
57,5	0,70	0,25	0,15	0,10	0,07	0,05	0,03	0,00	0,00	0,00
58,5	0,70	0,25	0,14	0,10	0,07	0,05	0,03	0,00	0,00	0,00

Radius [mm]	ϕ	ϕ_2	ϕ_3	ϕ_4	ϕ_5	ϕ_6	ϕ_7	ϕ_8	ϕ_9	ϕ_{10}
59,4	0,70	0,24	0,14	0,10	0,07	0,06	0,03	0,00	0,00	0,00
60,4	0,70	0,25	0,14	0,10	0,07	0,06	0,04	0,00	0,00	0,00
61,4	0,70	0,23	0,14	0,11	0,07	0,06	0,04	0,02	0,00	0,00
62,4	0,70	0,22	0,14	0,10	0,08	0,06	0,04	0,03	0,00	0,00
63,4	0,70	0,23	0,14	0,10	0,08	0,06	0,04	0,03	0,00	0,00
64,4	0,70	0,25	0,13	0,10	0,08	0,06	0,04	0,03	0,00	0,00
65,4	0,70	0,22	0,13	0,10	0,08	0,06	0,05	0,03	0,02	0,00
66,3	0,70	0,22	0,13	0,10	0,08	0,06	0,05	0,03	0,03	0,00
67,4	0,70	0,23	0,13	0,10	0,08	0,06	0,05	0,03	0,03	0,00
68,4	0,70	0,26	0,13	0,09	0,08	0,06	0,05	0,03	0,03	0,00
69,4	0,70	0,20	0,13	0,10	0,08	0,06	0,05	0,04	0,03	0,02
70,5	0,70	0,20	0,13	0,10	0,08	0,06	0,05	0,04	0,03	0,02
71,3	0,70	0,20	0,12	0,10	0,08	0,06	0,05	0,04	0,03	0,03
72,5	0,70	0,20	0,12	0,10	0,08	0,06	0,05	0,04	0,04	0,02
73,4	0,70	0,19	0,13	0,10	0,08	0,06	0,05	0,05	0,03	0,03
74,4	0,70	0,19	0,12	0,10	0,08	0,06	0,06	0,04	0,03	0,03
75,4	0,70	0,22	0,13	0,09	0,08	0,06	0,05	0,04	0,04	0,03
76,4	0,70	0,21	0,12	0,09	0,08	0,06	0,05	0,05	0,03	0,03
77,1	0,70	0,19	0,12	0,09	0,08	0,06	0,06	0,04	0,04	0,03
29,5	0,80	0,03	0,00	0,00	0,00	0,00	0,00	0,00	0,00	0,00
30,5	0,80	0,04	0,00	0,00	0,00	0,00	0,00	0,00	0,00	0,00
31,5	0,80	0,40	0,00	0,00	0,00	0,00	0,00	0,00	0,00	0,00
32,5	0,80	0,40	0,00	0,00	0,00	0,00	0,00	0,00	0,00	0,00
33,5	0,80	0,41	0,00	0,00	0,00	0,00	0,00	0,00	0,00	0,00
34,5	0,80	0,39	0,00	0,00	0,00	0,00	0,00	0,00	0,00	0,00
35,5	0,80	0,40	0,01	0,00	0,00	0,00	0,00	0,00	0,00	0,00
36,5	0,80	0,39	0,01	0,00	0,00	0,00	0,00	0,00	0,00	0,00
37,5	0,80	0,39	0,02	0,00	0,00	0,00	0,00	0,00	0,00	0,00
38,5	0,80	0,38	0,11	0,00	0,00	0,00	0,00	0,00	0,00	0,00
39,5	0,80	0,40	0,12	0,00	0,00	0,00	0,00	0,00	0,00	0,00
40,5	0,80	0,36	0,13	0,00	0,00	0,00	0,00	0,00	0,00	0,00
41,5	0,80	0,34	0,14	0,00	0,00	0,00	0,00	0,00	0,00	0,00
42,5	0,80	0,34	0,14	0,02	0,00	0,00	0,00	0,00	0,00	0,00
43,5	0,80	0,35	0,14	0,03	0,00	0,00	0,00	0,00	0,00	0,00
44,5	0,80	0,32	0,15	0,08	0,00	0,00	0,00	0,00	0,00	0,00
45,5	0,80	0,32	0,15	0,08	0,00	0,00	0,00	0,00	0,00	0,00
46,5	0,80	0,34	0,15	0,08	0,00	0,00	0,00	0,00	0,00	0,00
47,5	0,80	0,32	0,15	0,09	0,04	0,00	0,00	0,00	0,00	0,00
48,5	0,80	0,33	0,15	0,09	0,04	0,00	0,00	0,00	0,00	0,00
49,4	0,80	0,32	0,15	0,09	0,05	0,00	0,00	0,00	0,00	0,00
50,5	0,80	0,34	0,15	0,09	0,05	0,00	0,00	0,00	0,00	0,00
51,5	0,80	0,30	0,15	0,10	0,06	0,00	0,00	0,00	0,00	0,00
52,5	0,80	0,28	0,15	0,10	0,06	0,04	0,00	0,00	0,00	0,00
53,5	0,80	0,30	0,15	0,10	0,06	0,04	0,00	0,00	0,00	0,00
54,4	0,80	0,27	0,15	0,10	0,07	0,04	0,00	0,00	0,00	0,00
55,4	0,80	0,27	0,14	0,11	0,07	0,04	0,00	0,00	0,00	0,00
56,4	0,80	0,27	0,14	0,11	0,07	0,05	0,00	0,00	0,00	0,00
57,4	0,80	0,26	0,15	0,10	0,07	0,05	0,03	0,00	0,00	0,00
58,5	0,80	0,26	0,14	0,10	0,08	0,05	0,03	0,00	0,00	0,00
59,4	0,80	0,25	0,14	0,10	0,08	0,05	0,04	0,00	0,00	0,00
60,4	0,80	0,27	0,14	0,10	0,08	0,05	0,04	0,00	0,00	0,00

Radius [mm]	ϕ	ϕ_2	ϕ_3	ϕ_4	ϕ_5	ϕ_6	ϕ_7	ϕ_8	ϕ_9	ϕ_{10}
61,4	0,80	0,25	0,14	0,10	0,08	0,06	0,04	0,02	0,00	0,00
62,4	0,80	0,28	0,13	0,10	0,08	0,06	0,04	0,03	0,00	0,00
63,3	0,80	0,24	0,14	0,10	0,08	0,06	0,04	0,03	0,00	0,00
64,3	0,80	0,25	0,14	0,10	0,08	0,06	0,04	0,03	0,00	0,00
65,4	0,80	0,23	0,13	0,11	0,08	0,06	0,05	0,03	0,02	0,00
66,3	0,80	0,23	0,13	0,11	0,08	0,06	0,05	0,03	0,03	0,00
67,5	0,80	0,25	0,13	0,10	0,08	0,06	0,05	0,03	0,03	0,00
68,5	0,80	0,21	0,14	0,10	0,08	0,06	0,05	0,04	0,03	0,00
69,3	0,80	0,26	0,13	0,10	0,08	0,06	0,05	0,04	0,03	0,02
70,4	0,80	0,21	0,13	0,10	0,08	0,06	0,05	0,04	0,03	0,02
71,2	0,80	0,20	0,13	0,11	0,08	0,06	0,05	0,04	0,03	0,03
72,4	0,80	0,20	0,13	0,10	0,08	0,07	0,05	0,04	0,03	0,03
73,3	0,80	0,20	0,13	0,10	0,08	0,06	0,06	0,04	0,03	0,03
74,3	0,80	0,19	0,13	0,10	0,08	0,07	0,05	0,04	0,04	0,03
75,3	0,80	0,23	0,12	0,10	0,08	0,06	0,05	0,04	0,04	0,03
76,4	0,80	0,21	0,13	0,10	0,07	0,07	0,05	0,05	0,03	0,03
76,8	0,80	0,19	0,12	0,10	0,08	0,06	0,06	0,04	0,04	0,03
28,5	0,90	0,03	0,00	0,00	0,00	0,00	0,00	0,00	0,00	0,00
29,5	0,90	0,03	0,00	0,00	0,00	0,00	0,00	0,00	0,00	0,00
30,5	0,90	0,04	0,00	0,00	0,00	0,00	0,00	0,00	0,00	0,00
31,5	0,90	0,42	0,00	0,00	0,00	0,00	0,00	0,00	0,00	0,00
32,5	0,90	0,43	0,00	0,00	0,00	0,00	0,00	0,00	0,00	0,00
33,5	0,90	0,43	0,00	0,00	0,00	0,00	0,00	0,00	0,00	0,00
34,5	0,90	0,41	0,00	0,00	0,00	0,00	0,00	0,00	0,00	0,00
35,5	0,90	0,42	0,01	0,00	0,00	0,00	0,00	0,00	0,00	0,00
36,5	0,90	0,41	0,01	0,00	0,00	0,00	0,00	0,00	0,00	0,00
37,5	0,90	0,42	0,02	0,00	0,00	0,00	0,00	0,00	0,00	0,00
38,5	0,90	0,40	0,12	0,00	0,00	0,00	0,00	0,00	0,00	0,00
39,5	0,90	0,42	0,12	0,00	0,00	0,00	0,00	0,00	0,00	0,00
40,5	0,90	0,39	0,13	0,00	0,00	0,00	0,00	0,00	0,00	0,00
41,5	0,90	0,42	0,13	0,00	0,00	0,00	0,00	0,00	0,00	0,00
42,5	0,90	0,35	0,15	0,02	0,00	0,00	0,00	0,00	0,00	0,00
43,5	0,90	0,37	0,15	0,03	0,00	0,00	0,00	0,00	0,00	0,00
44,5	0,90	0,39	0,14	0,07	0,00	0,00	0,00	0,00	0,00	0,00
45,4	0,90	0,38	0,14	0,08	0,00	0,00	0,00	0,00	0,00	0,00
46,5	0,90	0,37	0,15	0,08	0,00	0,00	0,00	0,00	0,00	0,00
47,5	0,90	0,33	0,15	0,09	0,04	0,00	0,00	0,00	0,00	0,00
48,5	0,90	0,34	0,15	0,09	0,04	0,00	0,00	0,00	0,00	0,00
49,5	0,90	0,31	0,15	0,10	0,05	0,00	0,00	0,00	0,00	0,00
50,4	0,90	0,33	0,15	0,10	0,05	0,00	0,00	0,00	0,00	0,00
51,4	0,90	0,31	0,15	0,10	0,06	0,00	0,00	0,00	0,00	0,00
52,5	0,90	0,30	0,15	0,10	0,06	0,04	0,00	0,00	0,00	0,00
53,4	0,90	0,30	0,15	0,10	0,07	0,04	0,00	0,00	0,00	0,00
54,5	0,90	0,28	0,15	0,11	0,07	0,04	0,00	0,00	0,00	0,00
55,4	0,90	0,28	0,15	0,10	0,07	0,05	0,00	0,00	0,00	0,00
56,5	0,90	0,28	0,15	0,10	0,07	0,05	0,00	0,00	0,00	0,00
57,5	0,90	0,28	0,14	0,11	0,07	0,05	0,03	0,00	0,00	0,00
58,4	0,90	0,26	0,15	0,11	0,07	0,05	0,03	0,00	0,00	0,00
59,4	0,90	0,25	0,15	0,11	0,07	0,06	0,03	0,00	0,00	0,00
60,4	0,90	0,27	0,15	0,10	0,08	0,05	0,04	0,00	0,00	0,00
61,4	0,90	0,26	0,14	0,11	0,07	0,06	0,04	0,03	0,00	0,00

Radius [mm]	ϕ	ϕ_2	ϕ_3	ϕ_4	ϕ_5	ϕ_6	ϕ_7	ϕ_8	ϕ_9	ϕ_{10}
62,4	0,90	0,31	0,13	0,11	0,07	0,06	0,04	0,03	0,00	0,00
63,4	0,90	0,25	0,14	0,10	0,08	0,06	0,04	0,03	0,00	0,00
64,4	0,90	0,28	0,14	0,10	0,08	0,06	0,04	0,03	0,00	0,00
65,3	0,90	0,23	0,14	0,11	0,08	0,06	0,05	0,03	0,02	0,00
66,4	0,90	0,24	0,14	0,10	0,08	0,06	0,05	0,03	0,03	0,00
67,4	0,90	0,25	0,14	0,10	0,08	0,06	0,05	0,04	0,02	0,00
68,4	0,90	0,22	0,13	0,11	0,08	0,06	0,05	0,04	0,03	0,00
69,5	0,90	0,22	0,13	0,11	0,08	0,06	0,05	0,04	0,03	0,02
70,3	0,90	0,21	0,14	0,10	0,08	0,07	0,05	0,04	0,03	0,02
71,5	0,90	0,21	0,14	0,10	0,08	0,07	0,05	0,04	0,03	0,03
72,4	0,90	0,21	0,13	0,10	0,08	0,07	0,05	0,04	0,03	0,03
73,4	0,90	0,20	0,14	0,10	0,08	0,07	0,05	0,04	0,04	0,03
74,4	0,90	0,20	0,13	0,10	0,08	0,07	0,05	0,04	0,04	0,03
75,4	0,90	0,25	0,12	0,10	0,08	0,06	0,05	0,05	0,03	0,03
76,5	0,90	0,23	0,12	0,10	0,08	0,06	0,06	0,04	0,04	0,03
27,5	1,00	0,00	0,00	0,00	0,00	0,00	0,00	0,00	0,00	0,00
28,5	1,00	0,03	0,00	0,00	0,00	0,00	0,00	0,00	0,00	0,00
29,5	1,00	0,04	0,00	0,00	0,00	0,00	0,00	0,00	0,00	0,00
30,5	1,00	0,04	0,00	0,00	0,00	0,00	0,00	0,00	0,00	0,00
31,5	1,00	0,44	0,00	0,00	0,00	0,00	0,00	0,00	0,00	0,00
32,5	1,00	0,45	0,00	0,00	0,00	0,00	0,00	0,00	0,00	0,00
33,5	1,00	0,45	0,00	0,00	0,00	0,00	0,00	0,00	0,00	0,00
34,5	1,00	0,43	0,00	0,00	0,00	0,00	0,00	0,00	0,00	0,00
35,5	1,00	0,45	0,01	0,00	0,00	0,00	0,00	0,00	0,00	0,00
36,5	1,00	0,44	0,01	0,00	0,00	0,00	0,00	0,00	0,00	0,00
37,5	1,00	0,45	0,02	0,00	0,00	0,00	0,00	0,00	0,00	0,00
38,5	1,00	0,42	0,12	0,00	0,00	0,00	0,00	0,00	0,00	0,00
39,5	1,00	0,42	0,13	0,00	0,00	0,00	0,00	0,00	0,00	0,00
40,5	1,00	0,40	0,14	0,00	0,00	0,00	0,00	0,00	0,00	0,00
41,5	1,00	0,38	0,14	0,00	0,00	0,00	0,00	0,00	0,00	0,00
42,5	1,00	0,41	0,14	0,02	0,00	0,00	0,00	0,00	0,00	0,00
43,4	1,00	0,37	0,15	0,03	0,00	0,00	0,00	0,00	0,00	0,00
44,5	1,00	0,39	0,15	0,07	0,00	0,00	0,00	0,00	0,00	0,00
45,5	1,00	0,34	0,16	0,08	0,00	0,00	0,00	0,00	0,00	0,00
46,5	1,00	0,38	0,15	0,08	0,00	0,00	0,00	0,00	0,00	0,00
47,4	1,00	0,34	0,15	0,09	0,04	0,00	0,00	0,00	0,00	0,00
48,4	1,00	0,34	0,16	0,09	0,04	0,00	0,00	0,00	0,00	0,00
49,4	1,00	0,35	0,15	0,10	0,05	0,00	0,00	0,00	0,00	0,00
50,5	1,00	0,36	0,15	0,10	0,05	0,00	0,00	0,00	0,00	0,00
51,4	1,00	0,32	0,15	0,10	0,06	0,00	0,00	0,00	0,00	0,00
52,5	1,00	0,31	0,15	0,10	0,06	0,04	0,00	0,00	0,00	0,00
53,4	1,00	0,32	0,15	0,10	0,07	0,04	0,00	0,00	0,00	0,00
54,4	1,00	0,29	0,15	0,11	0,07	0,04	0,00	0,00	0,00	0,00
55,5	1,00	0,29	0,15	0,11	0,07	0,05	0,00	0,00	0,00	0,00
56,4	1,00	0,29	0,15	0,11	0,07	0,05	0,00	0,00	0,00	0,00
57,5	1,00	0,28	0,15	0,11	0,07	0,05	0,03	0,00	0,00	0,00
58,4	1,00	0,27	0,15	0,11	0,07	0,06	0,03	0,00	0,00	0,00
59,4	1,00	0,26	0,15	0,11	0,08	0,05	0,04	0,00	0,00	0,00
60,4	1,00	0,29	0,15	0,10	0,08	0,05	0,04	0,00	0,00	0,00
61,3	1,00	0,26	0,15	0,11	0,08	0,06	0,04	0,02	0,00	0,00
62,5	1,00	0,25	0,15	0,10	0,08	0,06	0,04	0,03	0,00	0,00

Radius [mm]	ϕ	ϕ_2	ϕ_3	ϕ_4	ϕ_5	ϕ_6	ϕ_7	ϕ_8	ϕ_9	ϕ_{10}
63,3	1,00	0,25	0,15	0,10	0,08	0,06	0,04	0,03	0,00	0,00
64,4	1,00	0,27	0,15	0,10	0,08	0,06	0,04	0,03	0,00	0,00
65,5	1,00	0,24	0,15	0,10	0,08	0,06	0,05	0,03	0,02	0,00
66,4	1,00	0,25	0,14	0,10	0,08	0,06	0,05	0,03	0,03	0,00
67,4	1,00	0,26	0,13	0,11	0,08	0,06	0,05	0,04	0,02	0,00
68,4	1,00	0,22	0,14	0,11	0,08	0,06	0,05	0,04	0,03	0,00
69,2	1,00	0,27	0,13	0,10	0,08	0,06	0,05	0,04	0,03	0,02
70,4	1,00	0,22	0,13	0,11	0,08	0,07	0,05	0,04	0,03	0,02
71,3	1,00	0,21	0,14	0,10	0,09	0,06	0,05	0,04	0,03	0,03
72,5	1,00	0,21	0,14	0,10	0,08	0,07	0,05	0,04	0,04	0,02
73,5	1,00	0,21	0,13	0,10	0,08	0,07	0,05	0,05	0,03	0,03
74,5	1,00	0,20	0,14	0,10	0,08	0,07	0,05	0,05	0,03	0,03
75,2	1,00	0,23	0,12	0,10	0,08	0,07	0,05	0,04	0,04	0,03
76,2	1,00	0,22	0,13	0,10	0,08	0,06	0,06	0,04	0,04	0,03

Table C.1.1: *Database of the mixing parameters ϕ_i obtained by calibration with the exponential growth model. This database is used in the models.*

C.1.2 Gaussian calibration

Radius [mm]	ϕ	ϕ_2	ϕ_3	ϕ_4	ϕ_5	ϕ_6	ϕ_7	ϕ_8	ϕ_9	ϕ_{10}
84,1	0,10	0,09	0,10	0,09	0,08	0,09	0,08	0,08	0,07	0,06
82,5	0,10	0,10	0,09	0,09	0,08	0,09	0,07	0,08	0,06	0,06
81,5	0,10	0,10	0,08	0,10	0,08	0,08	0,08	0,07	0,07	0,06
80,1	0,10	0,10	0,10	0,09	0,08	0,08	0,08	0,07	0,06	0,06
79,2	0,10	0,10	0,08	0,10	0,08	0,08	0,08	0,07	0,06	0,05
78,0	0,10	0,09	0,10	0,08	0,09	0,08	0,08	0,07	0,06	0,06
76,7	0,10	0,10	0,09	0,08	0,09	0,08	0,07	0,06	0,06	0,05
75,6	0,10	0,10	0,08	0,09	0,08	0,08	0,07	0,07	0,06	0,05
74,8	0,10	0,09	0,10	0,08	0,09	0,08	0,07	0,06	0,06	0,05
74,1	0,10	0,10	0,09	0,08	0,08	0,08	0,07	0,06	0,06	0,04
73,0	0,10	0,10	0,08	0,09	0,08	0,07	0,07	0,06	0,06	0,04
71,7	0,10	0,10	0,09	0,08	0,08	0,08	0,06	0,06	0,05	0,04
70,4	0,10	0,10	0,08	0,08	0,08	0,08	0,06	0,06	0,05	0,04
69,2	0,10	0,10	0,09	0,08	0,08	0,07	0,06	0,06	0,04	0,04
67,8	0,10	0,09	0,10	0,08	0,08	0,07	0,07	0,05	0,05	0,00
66,7	0,10	0,10	0,08	0,09	0,07	0,07	0,06	0,05	0,04	0,00
65,4	0,10	0,09	0,10	0,08	0,07	0,07	0,06	0,05	0,04	0,00
64,0	0,10	0,10	0,08	0,08	0,07	0,06	0,06	0,04	0,00	0,00
62,7	0,10	0,10	0,09	0,07	0,08	0,06	0,05	0,04	0,00	0,00
61,4	0,10	0,09	0,10	0,08	0,07	0,06	0,05	0,04	0,00	0,00
60,0	0,10	0,10	0,07	0,08	0,07	0,06	0,05	0,00	0,00	0,00
58,7	0,10	0,10	0,08	0,08	0,07	0,05	0,04	0,00	0,00	0,00
57,3	0,10	0,09	0,09	0,09	0,06	0,06	0,04	0,00	0,00	0,00
55,9	0,10	0,09	0,10	0,07	0,07	0,05	0,00	0,00	0,00	0,00
54,5	0,10	0,10	0,07	0,07	0,06	0,05	0,00	0,00	0,00	0,00
53,0	0,10	0,10	0,07	0,07	0,06	0,04	0,00	0,00	0,00	0,00
51,6	0,10	0,09	0,09	0,07	0,05	0,00	0,00	0,00	0,00	0,00
50,1	0,10	0,09	0,09	0,07	0,05	0,00	0,00	0,00	0,00	0,00
48,6	0,10	0,09	0,09	0,06	0,05	0,00	0,00	0,00	0,00	0,00

Radius [mm]	ϕ	ϕ_2	ϕ_3	ϕ_4	ϕ_5	ϕ_6	ϕ_7	ϕ_8	ϕ_9	ϕ_{10}
47,2	0,10	0,09	0,08	0,07	0,00	0,00	0,00	0,00	0,00	0,00
45,6	0,10	0,09	0,08	0,06	0,00	0,00	0,00	0,00	0,00	0,00
44,0	0,10	0,09	0,08	0,05	0,00	0,00	0,00	0,00	0,00	0,00
42,4	0,10	0,09	0,07	0,05	0,00	0,00	0,00	0,00	0,00	0,00
40,8	0,10	0,09	0,07	0,00	0,00	0,00	0,00	0,00	0,00	0,00
39,0	0,10	0,09	0,07	0,00	0,00	0,00	0,00	0,00	0,00	0,00
37,3	0,10	0,09	0,06	0,00	0,00	0,00	0,00	0,00	0,00	0,00
35,5	0,10	0,09	0,04	0,00	0,00	0,00	0,00	0,00	0,00	0,00
33,6	0,10	0,08	0,00	0,00	0,00	0,00	0,00	0,00	0,00	0,00
31,6	0,10	0,08	0,00	0,00	0,00	0,00	0,00	0,00	0,00	0,00
29,5	0,10	0,08	0,00	0,00	0,00	0,00	0,00	0,00	0,00	0,00
27,3	0,10	0,02	0,00	0,00	0,00	0,00	0,00	0,00	0,00	0,00
75,2	0,20	0,20	0,18	0,18	0,17	0,17	0,14	0,13	0,11	0,09
74,1	0,20	0,20	0,21	0,18	0,17	0,15	0,14	0,12	0,11	0,08
73,0	0,20	0,19	0,20	0,18	0,17	0,16	0,14	0,12	0,10	0,09
72,0	0,20	0,20	0,19	0,17	0,17	0,15	0,14	0,11	0,10	0,08
70,7	0,20	0,20	0,20	0,18	0,17	0,15	0,13	0,11	0,09	0,07
69,8	0,20	0,19	0,20	0,17	0,17	0,15	0,13	0,11	0,09	0,07
68,6	0,20	0,20	0,18	0,17	0,16	0,15	0,12	0,10	0,09	0,00
67,5	0,20	0,20	0,19	0,17	0,16	0,14	0,12	0,10	0,08	0,00
66,5	0,20	0,21	0,18	0,17	0,15	0,14	0,11	0,09	0,07	0,00
65,7	0,20	0,20	0,17	0,18	0,15	0,14	0,11	0,09	0,07	0,00
65,2	0,20	0,22	0,16	0,17	0,15	0,13	0,11	0,08	0,06	0,00
64,0	0,20	0,19	0,19	0,17	0,16	0,13	0,11	0,08	0,00	0,00
62,9	0,20	0,19	0,19	0,18	0,15	0,13	0,10	0,08	0,00	0,00
61,8	0,20	0,20	0,17	0,16	0,15	0,12	0,10	0,07	0,00	0,00
61,5	0,20	0,20	0,19	0,16	0,14	0,13	0,09	0,07	0,00	0,00
60,6	0,20	0,20	0,17	0,16	0,14	0,12	0,09	0,00	0,00	0,00
59,4	0,20	0,20	0,17	0,16	0,13	0,12	0,08	0,00	0,00	0,00
58,2	0,20	0,19	0,19	0,16	0,13	0,11	0,08	0,00	0,00	0,00
57,0	0,20	0,19	0,19	0,15	0,13	0,11	0,07	0,00	0,00	0,00
55,7	0,20	0,20	0,19	0,15	0,12	0,10	0,00	0,00	0,00	0,00
54,5	0,20	0,20	0,17	0,15	0,12	0,09	0,00	0,00	0,00	0,00
53,4	0,20	0,20	0,16	0,15	0,11	0,08	0,00	0,00	0,00	0,00
52,1	0,20	0,21	0,18	0,14	0,10	0,00	0,00	0,00	0,00	0,00
50,9	0,20	0,20	0,16	0,14	0,10	0,00	0,00	0,00	0,00	0,00
49,7	0,20	0,19	0,17	0,14	0,09	0,00	0,00	0,00	0,00	0,00
48,4	0,20	0,20	0,16	0,12	0,08	0,00	0,00	0,00	0,00	0,00
47,1	0,20	0,21	0,14	0,12	0,00	0,00	0,00	0,00	0,00	0,00
45,8	0,20	0,19	0,16	0,12	0,00	0,00	0,00	0,00	0,00	0,00
44,5	0,20	0,20	0,14	0,10	0,00	0,00	0,00	0,00	0,00	0,00
43,2	0,20	0,20	0,13	0,10	0,00	0,00	0,00	0,00	0,00	0,00
41,8	0,20	0,19	0,15	0,09	0,00	0,00	0,00	0,00	0,00	0,00
40,5	0,20	0,19	0,14	0,00	0,00	0,00	0,00	0,00	0,00	0,00
39,1	0,20	0,19	0,12	0,00	0,00	0,00	0,00	0,00	0,00	0,00
37,7	0,20	0,20	0,11	0,00	0,00	0,00	0,00	0,00	0,00	0,00
36,3	0,20	0,19	0,10	0,00	0,00	0,00	0,00	0,00	0,00	0,00
34,8	0,20	0,19	0,00	0,00	0,00	0,00	0,00	0,00	0,00	0,00
33,3	0,20	0,19	0,00	0,00	0,00	0,00	0,00	0,00	0,00	0,00
31,8	0,20	0,18	0,00	0,00	0,00	0,00	0,00	0,00	0,00	0,00
30,2	0,20	0,18	0,00	0,00	0,00	0,00	0,00	0,00	0,00	0,00

Radius [mm]	ϕ	ϕ_2	ϕ_3	ϕ_4	ϕ_5	ϕ_6	ϕ_7	ϕ_8	ϕ_9	ϕ_{10}
28,5	0,20	0,03	0,00	0,00	0,00	0,00	0,00	0,00	0,00	0,00
75,2	0,30	0,30	0,28	0,29	0,27	0,25	0,22	0,19	0,16	0,13
74,4	0,30	0,32	0,29	0,28	0,27	0,24	0,21	0,18	0,15	0,12
73,4	0,30	0,29	0,30	0,28	0,27	0,25	0,21	0,18	0,15	0,12
72,3	0,30	0,30	0,29	0,29	0,26	0,24	0,20	0,17	0,14	0,11
71,4	0,30	0,31	0,30	0,27	0,26	0,23	0,20	0,16	0,13	0,10
70,1	0,30	0,31	0,31	0,28	0,25	0,22	0,19	0,16	0,12	0,09
69,2	0,30	0,29	0,30	0,27	0,26	0,23	0,19	0,16	0,12	0,09
68,1	0,30	0,29	0,30	0,28	0,25	0,22	0,19	0,15	0,11	0,00
67,0	0,30	0,30	0,28	0,27	0,25	0,21	0,18	0,14	0,10	0,00
65,9	0,30	0,30	0,29	0,27	0,24	0,21	0,17	0,13	0,09	0,00
64,7	0,30	0,30	0,28	0,27	0,23	0,20	0,16	0,12	0,00	0,00
63,5	0,30	0,30	0,28	0,26	0,23	0,19	0,16	0,11	0,00	0,00
62,7	0,30	0,30	0,28	0,27	0,22	0,19	0,15	0,10	0,00	0,00
61,4	0,30	0,34	0,26	0,25	0,20	0,18	0,13	0,09	0,00	0,00
60,4	0,30	0,33	0,27	0,25	0,20	0,17	0,12	0,00	0,00	0,00
59,3	0,30	0,31	0,29	0,25	0,20	0,17	0,11	0,00	0,00	0,00
58,2	0,30	0,31	0,26	0,25	0,20	0,16	0,11	0,00	0,00	0,00
57,0	0,30	0,35	0,25	0,23	0,18	0,14	0,09	0,00	0,00	0,00
55,9	0,30	0,31	0,28	0,23	0,19	0,14	0,00	0,00	0,00	0,00
54,7	0,30	0,30	0,27	0,23	0,18	0,13	0,00	0,00	0,00	0,00
53,6	0,30	0,31	0,27	0,22	0,17	0,12	0,00	0,00	0,00	0,00
52,4	0,30	0,33	0,24	0,21	0,15	0,11	0,00	0,00	0,00	0,00
51,3	0,30	0,30	0,27	0,21	0,15	0,00	0,00	0,00	0,00	0,00
50,1	0,30	0,31	0,25	0,20	0,14	0,00	0,00	0,00	0,00	0,00
48,9	0,30	0,31	0,25	0,19	0,13	0,00	0,00	0,00	0,00	0,00
47,7	0,30	0,31	0,24	0,19	0,11	0,00	0,00	0,00	0,00	0,00
46,6	0,30	0,31	0,24	0,17	0,00	0,00	0,00	0,00	0,00	0,00
45,4	0,30	0,30	0,24	0,17	0,00	0,00	0,00	0,00	0,00	0,00
44,2	0,30	0,33	0,21	0,15	0,00	0,00	0,00	0,00	0,00	0,00
43,0	0,30	0,31	0,21	0,14	0,00	0,00	0,00	0,00	0,00	0,00
41,8	0,30	0,32	0,20	0,12	0,00	0,00	0,00	0,00	0,00	0,00
40,5	0,30	0,30	0,20	0,00	0,00	0,00	0,00	0,00	0,00	0,00
39,2	0,30	0,33	0,17	0,00	0,00	0,00	0,00	0,00	0,00	0,00
38,0	0,30	0,31	0,18	0,00	0,00	0,00	0,00	0,00	0,00	0,00
36,7	0,30	0,30	0,16	0,00	0,00	0,00	0,00	0,00	0,00	0,00
35,4	0,30	0,32	0,01	0,00	0,00	0,00	0,00	0,00	0,00	0,00
34,1	0,30	0,29	0,00	0,00	0,00	0,00	0,00	0,00	0,00	0,00
32,7	0,30	0,28	0,00	0,00	0,00	0,00	0,00	0,00	0,00	0,00
31,3	0,30	0,29	0,00	0,00	0,00	0,00	0,00	0,00	0,00	0,00
29,9	0,30	0,27	0,00	0,00	0,00	0,00	0,00	0,00	0,00	0,00
28,5	0,30	0,03	0,00	0,00	0,00	0,00	0,00	0,00	0,00	0,00
27,0	0,30	0,03	0,00	0,00	0,00	0,00	0,00	0,00	0,00	0,00
75,2	0,40	0,39	0,41	0,40	0,38	0,35	0,31	0,25	0,21	0,16
74,1	0,40	0,40	0,41	0,40	0,37	0,35	0,29	0,24	0,19	0,15
73,0	0,40	0,42	0,39	0,40	0,36	0,33	0,27	0,23	0,18	0,14
72,0	0,40	0,44	0,39	0,39	0,35	0,31	0,27	0,21	0,17	0,13
71,0	0,40	0,49	0,41	0,38	0,33	0,31	0,24	0,20	0,15	0,12
69,8	0,40	0,48	0,39	0,37	0,33	0,30	0,24	0,19	0,14	0,11
68,9	0,40	0,40	0,41	0,38	0,35	0,31	0,25	0,19	0,15	0,10
67,8	0,40	0,40	0,41	0,38	0,34	0,30	0,24	0,18	0,14	0,00

Radius [mm]	ϕ	ϕ_2	ϕ_3	ϕ_4	ϕ_5	ϕ_6	ϕ_7	ϕ_8	ϕ_9	ϕ_{10}
66,7	0,40	0,41	0,38	0,38	0,33	0,29	0,23	0,17	0,12	0,00
65,7	0,40	0,41	0,39	0,37	0,32	0,28	0,22	0,16	0,11	0,00
64,7	0,40	0,41	0,39	0,37	0,31	0,28	0,21	0,15	0,00	0,00
63,5	0,40	0,49	0,37	0,34	0,29	0,25	0,18	0,13	0,00	0,00
63,5	0,40	0,45	0,37	0,35	0,29	0,24	0,18	0,12	0,00	0,00
61,4	0,40	0,43	0,38	0,35	0,29	0,24	0,17	0,11	0,00	0,00
60,4	0,40	0,42	0,39	0,34	0,29	0,23	0,16	0,00	0,00	0,00
59,3	0,40	0,48	0,37	0,33	0,27	0,20	0,14	0,00	0,00	0,00
58,2	0,40	0,43	0,39	0,33	0,26	0,21	0,13	0,00	0,00	0,00
57,0	0,40	0,48	0,36	0,32	0,24	0,19	0,11	0,00	0,00	0,00
56,0	0,40	0,44	0,36	0,31	0,25	0,18	0,00	0,00	0,00	0,00
54,8	0,40	0,45	0,38	0,30	0,23	0,16	0,00	0,00	0,00	0,00
53,8	0,40	0,42	0,37	0,31	0,22	0,16	0,00	0,00	0,00	0,00
52,6	0,40	0,43	0,34	0,30	0,21	0,14	0,00	0,00	0,00	0,00
51,6	0,40	0,44	0,35	0,28	0,20	0,00	0,00	0,00	0,00	0,00
50,5	0,40	0,43	0,36	0,28	0,18	0,00	0,00	0,00	0,00	0,00
49,4	0,40	0,43	0,35	0,26	0,17	0,00	0,00	0,00	0,00	0,00
48,2	0,40	0,42	0,35	0,25	0,16	0,00	0,00	0,00	0,00	0,00
47,1	0,40	0,46	0,31	0,23	0,00	0,00	0,00	0,00	0,00	0,00
45,9	0,40	0,43	0,31	0,23	0,00	0,00	0,00	0,00	0,00	0,00
44,8	0,40	0,44	0,31	0,21	0,00	0,00	0,00	0,00	0,00	0,00
43,6	0,40	0,46	0,29	0,19	0,00	0,00	0,00	0,00	0,00	0,00
42,5	0,40	0,47	0,29	0,16	0,00	0,00	0,00	0,00	0,00	0,00
41,3	0,40	0,45	0,28	0,00	0,00	0,00	0,00	0,00	0,00	0,00
40,1	0,40	0,43	0,27	0,00	0,00	0,00	0,00	0,00	0,00	0,00
39,0	0,40	0,47	0,24	0,00	0,00	0,00	0,00	0,00	0,00	0,00
37,8	0,40	0,42	0,23	0,00	0,00	0,00	0,00	0,00	0,00	0,00
36,6	0,40	0,42	0,21	0,00	0,00	0,00	0,00	0,00	0,00	0,00
75,2	0,50	0,51	0,53	0,53	0,48	0,45	0,38	0,31	0,24	0,19
74,1	0,50	0,53	0,52	0,52	0,48	0,43	0,36	0,29	0,23	0,17
73,0	0,50	0,55	0,54	0,51	0,45	0,42	0,34	0,27	0,22	0,16
72,0	0,50	0,59	0,53	0,50	0,44	0,40	0,33	0,25	0,20	0,14
71,0	0,50	0,50	0,52	0,51	0,47	0,42	0,33	0,27	0,20	0,14
70,1	0,50	0,51	0,53	0,51	0,45	0,41	0,32	0,25	0,18	0,14
68,9	0,50	0,51	0,52	0,50	0,45	0,39	0,31	0,23	0,17	0,12
67,8	0,50	0,51	0,51	0,50	0,44	0,38	0,29	0,22	0,16	0,00
67,0	0,50	0,52	0,53	0,48	0,43	0,37	0,28	0,21	0,15	0,00
65,9	0,50	0,52	0,52	0,48	0,42	0,36	0,27	0,19	0,14	0,00
64,7	0,50	0,61	0,50	0,46	0,38	0,33	0,24	0,17	0,00	0,00
63,8	0,50	0,60	0,49	0,46	0,37	0,32	0,23	0,16	0,00	0,00
62,7	0,50	0,56	0,48	0,46	0,38	0,31	0,22	0,15	0,00	0,00
61,6	0,50	0,53	0,51	0,46	0,37	0,31	0,21	0,14	0,00	0,00
60,6	0,50	0,65	0,47	0,42	0,34	0,27	0,18	0,00	0,00	0,00
59,4	0,50	0,55	0,50	0,43	0,35	0,27	0,18	0,00	0,00	0,00
58,5	0,50	0,54	0,48	0,43	0,34	0,26	0,17	0,00	0,00	0,00
57,3	0,50	0,56	0,47	0,41	0,32	0,24	0,15	0,00	0,00	0,00
56,4	0,50	0,64	0,45	0,40	0,29	0,22	0,00	0,00	0,00	0,00
55,3	0,50	0,55	0,46	0,40	0,30	0,21	0,00	0,00	0,00	0,00
54,1	0,50	0,55	0,47	0,39	0,28	0,19	0,00	0,00	0,00	0,00
53,0	0,50	0,56	0,46	0,38	0,26	0,17	0,00	0,00	0,00	0,00
52,0	0,50	0,57	0,45	0,36	0,25	0,00	0,00	0,00	0,00	0,00

Radius [mm]	ϕ	ϕ_2	ϕ_3	ϕ_4	ϕ_5	ϕ_6	ϕ_7	ϕ_8	ϕ_9	ϕ_{10}
50,9	0,50	0,56	0,45	0,36	0,23	0,00	0,00	0,00	0,00	0,00
49,8	0,50	0,55	0,43	0,35	0,22	0,00	0,00	0,00	0,00	0,00
48,7	0,50	0,60	0,43	0,32	0,19	0,00	0,00	0,00	0,00	0,00
47,6	0,50	0,56	0,43	0,31	0,17	0,00	0,00	0,00	0,00	0,00
46,5	0,50	0,59	0,41	0,29	0,00	0,00	0,00	0,00	0,00	0,00
45,4	0,50	0,62	0,38	0,27	0,00	0,00	0,00	0,00	0,00	0,00
44,3	0,50	0,62	0,38	0,24	0,00	0,00	0,00	0,00	0,00	0,00
43,2	0,50	0,60	0,37	0,23	0,00	0,00	0,00	0,00	0,00	0,00
42,1	0,50	0,58	0,36	0,20	0,00	0,00	0,00	0,00	0,00	0,00
41,0	0,50	0,62	0,34	0,00	0,00	0,00	0,00	0,00	0,00	0,00
39,8	0,50	0,55	0,34	0,00	0,00	0,00	0,00	0,00	0,00	0,00
38,7	0,50	0,55	0,32	0,00	0,00	0,00	0,00	0,00	0,00	0,00
37,5	0,50	0,58	0,28	0,00	0,00	0,00	0,00	0,00	0,00	0,00
36,3	0,50	0,55	0,26	0,00	0,00	0,00	0,00	0,00	0,00	0,00
35,2	0,50	0,55	0,01	0,00	0,00	0,00	0,00	0,00	0,00	0,00
34,0	0,50	0,57	0,00	0,00	0,00	0,00	0,00	0,00	0,00	0,00
32,8	0,50	0,60	0,00	0,00	0,00	0,00	0,00	0,00	0,00	0,00
31,5	0,50	0,55	0,00	0,00	0,00	0,00	0,00	0,00	0,00	0,00
30,3	0,50	0,51	0,00	0,00	0,00	0,00	0,00	0,00	0,00	0,00
29,0	0,50	0,03	0,00	0,00	0,00	0,00	0,00	0,00	0,00	0,00
27,8	0,50	0,03	0,00	0,00	0,00	0,00	0,00	0,00	0,00	0,00
75,2	0,60	0,72	0,64	0,65	0,58	0,53	0,43	0,35	0,27	0,20
74,8	0,60	0,65	0,66	0,65	0,59	0,55	0,44	0,35	0,28	0,20
73,7	0,60	0,68	0,65	0,65	0,57	0,53	0,42	0,33	0,25	0,19
72,7	0,60	0,72	0,66	0,63	0,56	0,50	0,40	0,31	0,23	0,17
71,7	0,60	0,82	0,62	0,62	0,53	0,48	0,37	0,28	0,22	0,15
70,7	0,60	0,62	0,63	0,65	0,56	0,51	0,40	0,30	0,22	0,16
69,8	0,60	0,63	0,66	0,63	0,55	0,49	0,38	0,28	0,21	0,14
68,6	0,60	0,63	0,63	0,62	0,55	0,48	0,36	0,27	0,19	0,00
67,8	0,60	0,65	0,62	0,62	0,53	0,46	0,34	0,25	0,18	0,00
66,7	0,60	0,64	0,63	0,61	0,52	0,44	0,33	0,24	0,16	0,00
65,7	0,60	0,63	0,64	0,60	0,52	0,43	0,31	0,22	0,15	0,00
64,5	0,60	0,71	0,64	0,58	0,47	0,40	0,28	0,19	0,00	0,00
63,5	0,60	0,70	0,62	0,57	0,47	0,38	0,27	0,18	0,00	0,00
62,4	0,60	0,66	0,61	0,58	0,46	0,38	0,25	0,17	0,00	0,00
61,4	0,60	0,78	0,59	0,54	0,43	0,34	0,22	0,14	0,00	0,00
60,4	0,60	0,70	0,60	0,55	0,43	0,33	0,22	0,00	0,00	0,00
59,3	0,60	0,80	0,60	0,52	0,39	0,30	0,19	0,00	0,00	0,00
58,4	0,60	0,71	0,61	0,52	0,40	0,30	0,18	0,00	0,00	0,00
57,3	0,60	0,90	0,56	0,49	0,36	0,26	0,15	0,00	0,00	0,00
56,2	0,60	0,67	0,60	0,51	0,38	0,26	0,00	0,00	0,00	0,00
55,1	0,60	0,69	0,59	0,50	0,35	0,24	0,00	0,00	0,00	0,00
54,1	0,60	0,72	0,57	0,48	0,33	0,22	0,00	0,00	0,00	0,00
53,0	0,60	0,72	0,56	0,46	0,31	0,20	0,00	0,00	0,00	0,00
52,0	0,60	0,72	0,55	0,45	0,29	0,00	0,00	0,00	0,00	0,00
50,9	0,60	0,70	0,54	0,43	0,28	0,00	0,00	0,00	0,00	0,00
49,8	0,60	0,76	0,54	0,40	0,24	0,00	0,00	0,00	0,00	0,00
48,7	0,60	0,71	0,53	0,39	0,23	0,00	0,00	0,00	0,00	0,00
47,6	0,60	0,75	0,51	0,37	0,19	0,00	0,00	0,00	0,00	0,00
46,6	0,60	0,86	0,49	0,33	0,00	0,00	0,00	0,00	0,00	0,00
45,5	0,60	0,82	0,48	0,31	0,00	0,00	0,00	0,00	0,00	0,00

Radius [mm]	ϕ	ϕ_2	ϕ_3	ϕ_4	ϕ_5	ϕ_6	ϕ_7	ϕ_8	ϕ_9	ϕ_{10}
44,5	0,60	0,81	0,47	0,29	0,00	0,00	0,00	0,00	0,00	0,00
43,3	0,60	0,74	0,46	0,27	0,00	0,00	0,00	0,00	0,00	0,00
42,2	0,60	0,80	0,44	0,23	0,00	0,00	0,00	0,00	0,00	0,00
41,1	0,60	0,71	0,44	0,00	0,00	0,00	0,00	0,00	0,00	0,00
40,0	0,60	0,71	0,41	0,00	0,00	0,00	0,00	0,00	0,00	0,00
38,9	0,60	0,75	0,38	0,00	0,00	0,00	0,00	0,00	0,00	0,00
37,8	0,60	0,71	0,36	0,00	0,00	0,00	0,00	0,00	0,00	0,00
36,6	0,60	0,70	0,33	0,00	0,00	0,00	0,00	0,00	0,00	0,00
35,5	0,60	0,76	0,00	0,00	0,00	0,00	0,00	0,00	0,00	0,00
75,2	0,70	0,76	0,78	0,80	0,73	0,68	0,53	0,42	0,32	0,23
74,4	0,70	0,89	0,78	0,78	0,69	0,63	0,49	0,38	0,29	0,21
73,4	0,70	1,01	0,78	0,75	0,66	0,60	0,45	0,35	0,26	0,19
72,3	0,70	0,72	0,78	0,79	0,72	0,64	0,50	0,38	0,27	0,20
71,4	0,70	0,74	0,78	0,78	0,70	0,62	0,47	0,35	0,26	0,18
70,4	0,70	0,76	0,79	0,77	0,67	0,60	0,45	0,33	0,24	0,16
69,2	0,70	0,75	0,76	0,77	0,67	0,58	0,42	0,31	0,22	0,15
68,3	0,70	0,77	0,77	0,75	0,65	0,55	0,41	0,29	0,20	0,00
67,2	0,70	0,75	0,78	0,75	0,64	0,54	0,39	0,27	0,19	0,00
66,2	0,70	1,14	0,75	0,68	0,56	0,46	0,32	0,23	0,15	0,00
65,2	0,70	0,94	0,74	0,69	0,56	0,47	0,32	0,22	0,14	0,00
64,0	0,70	0,81	0,77	0,70	0,57	0,46	0,32	0,21	0,00	0,00
63,1	0,70	0,80	0,74	0,70	0,56	0,45	0,30	0,19	0,00	0,00
62,0	0,70	0,97	0,73	0,66	0,51	0,40	0,26	0,17	0,00	0,00
61,0	0,70	0,84	0,73	0,67	0,52	0,39	0,26	0,00	0,00	0,00
60,0	0,70	0,79	0,73	0,66	0,51	0,39	0,24	0,00	0,00	0,00
58,9	0,70	0,84	0,72	0,64	0,48	0,35	0,22	0,00	0,00	0,00
57,8	0,70	0,93	0,69	0,62	0,44	0,32	0,19	0,00	0,00	0,00
56,8	0,70	0,81	0,71	0,62	0,45	0,31	0,18	0,00	0,00	0,00
55,9	0,70	0,86	0,71	0,60	0,42	0,29	0,00	0,00	0,00	0,00
54,8	0,70	0,89	0,69	0,57	0,39	0,26	0,00	0,00	0,00	0,00
53,7	0,70	0,87	0,67	0,56	0,37	0,24	0,00	0,00	0,00	0,00
52,6	0,70	0,85	0,68	0,55	0,35	0,21	0,00	0,00	0,00	0,00
51,6	0,70	0,84	0,68	0,53	0,33	0,00	0,00	0,00	0,00	0,00
50,6	0,70	0,97	0,64	0,48	0,29	0,00	0,00	0,00	0,00	0,00
49,5	0,70	0,86	0,64	0,48	0,28	0,00	0,00	0,00	0,00	0,00
48,4	0,70	0,92	0,63	0,45	0,24	0,00	0,00	0,00	0,00	0,00
47,4	0,70	0,98	0,60	0,42	0,20	0,00	0,00	0,00	0,00	0,00
46,4	0,70	0,85	0,62	0,41	0,00	0,00	0,00	0,00	0,00	0,00
45,3	0,70	0,97	0,58	0,36	0,00	0,00	0,00	0,00	0,00	0,00
44,2	0,70	0,93	0,56	0,34	0,00	0,00	0,00	0,00	0,00	0,00
43,1	0,70	1,02	0,54	0,29	0,00	0,00	0,00	0,00	0,00	0,00
42,0	0,70	0,87	0,54	0,28	0,00	0,00	0,00	0,00	0,00	0,00
41,0	0,70	0,88	0,51	0,00	0,00	0,00	0,00	0,00	0,00	0,00
39,8	0,70	0,95	0,47	0,00	0,00	0,00	0,00	0,00	0,00	0,00
38,8	0,70	0,88	0,46	0,00	0,00	0,00	0,00	0,00	0,00	0,00
37,7	0,70	0,89	0,42	0,00	0,00	0,00	0,00	0,00	0,00	0,00
36,6	0,70	0,94	0,36	0,00	0,00	0,00	0,00	0,00	0,00	0,00
35,4	0,70	0,98	0,01	0,00	0,00	0,00	0,00	0,00	0,00	0,00
34,3	0,70	0,93	0,00	0,00	0,00	0,00	0,00	0,00	0,00	0,00
33,2	0,70	0,97	0,00	0,00	0,00	0,00	0,00	0,00	0,00	0,00
32,1	0,70	0,90	0,00	0,00	0,00	0,00	0,00	0,00	0,00	0,00

Radius [mm]	ϕ	ϕ_2	ϕ_3	ϕ_4	ϕ_5	ϕ_6	ϕ_7	ϕ_8	ϕ_9	ϕ_{10}
30,9	0,70	0,88	0,00	0,00	0,00	0,00	0,00	0,00	0,00	0,00
29,7	0,70	0,82	0,00	0,00	0,00	0,00	0,00	0,00	0,00	0,00
28,6	0,70	0,03	0,00	0,00	0,00	0,00	0,00	0,00	0,00	0,00
27,4	0,70	0,03	0,00	0,00	0,00	0,00	0,00	0,00	0,00	0,00
75,2	0,80	0,82	0,94	0,97	0,91	0,83	0,64	0,49	0,37	0,26

Table C.1.2: *Database of the mixing parameters ϕ_i obtained by calibration with the Gaussian growth model. For mixing coefficients higher than 0,8 the multi-box-model can not be adjusted to the Gaussian growth model.*